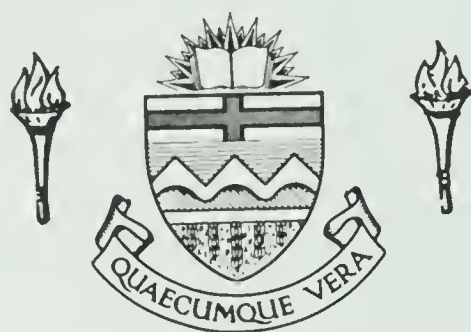


For Reference

NOT TO BE TAKEN FROM THIS ROOM

Ex libris
UNIVERSITATIS
ALBERTAENSIS





Digitized by the Internet Archive
in 2019 with funding from
University of Alberta Libraries

<https://archive.org/details/Sprenke1982>

THE UNIVERSITY OF ALBERTA

RELEASE FORM

NAME OF AUTHOR KENNETH FREDRICK SPRENKE

TITLE OF THESIS POTENTIAL FIELD INVERSION

DEGREE FOR WHICH THESIS WAS PRESENTED DOCTOR OF PHILOSOPHY

YEAR THIS DEGREE GRANTED FALL 1982

Permission is hereby granted to THE UNIVERSITY OF ALBERTA LIBRARY to reproduce single copies of this thesis and to lend or sell such copies for private, scholarly or scientific research purposes only.

The author reserves other publication rights, and neither the thesis nor extensive extracts from it may be printed or otherwise reproduced without the author's written permission.



THE UNIVERSITY OF ALBERTA

POTENTIAL FIELD INVERSION

by



KENNETH FREDRICK SPRENKE

A THESIS

SUBMITTED TO THE FACULTY OF GRADUATE STUDIES AND RESEARCH
IN PARTIAL FULFILMENT OF THE REQUIREMENTS FOR THE DEGREE
OF DOCTOR OF PHILOSOPHY

IN

PHYSICS

DEPARTMENT OF PHYSICS

EDMONTON, ALBERTA

FALL 1982

THE UNIVERSITY OF ALBERTA
FACULTY OF GRADUATE STUDIES AND RESEARCH

The undersigned certify that they have read, and recommend to the Faculty of Graduate Studies and Research, for acceptance, a thesis entitled POTENTIAL FIELD INVERSION submitted by KENNETH FREDRICK SPRENKE in partial fulfilment of the requirements for the degree of DOCTOR OF PHILOSOPHY in PHYSICS.

ABSTRACT

In this thesis, the inversion of large potential field data sets in combination with other geological information is investigated. The chief tool for this study is the Parker algorithm which allows for series expansion of potential fields in terms of Fourier transforms. Modifications of the Parker algorithm are derived to allow for variation of crustal parameters. The algorithms are coded for use on an AP-190L Array Processor. Generally, potential field calculations using the Parker algorithm are found to be at least an order of magnitude faster than calculations by other methods. The largest errors using the the algorithm are associated with the grid parameters chosen during the sampling process.

The first application of the method is to a regional gravity study of western Canada. The inverse algorithm is seen to be useful in the determination of crustal parameters under various assumptions on the nature of intermediate crustal layers. A further use of the algorithm is in the rapid calculation of isostatic anomalies. The isostatic anomalies are calculated, sorted on the basis of wavelength, and interpreted in terms of known geological information. The inverse algorithm is also used in combination with known seismic data to produce a crustal thickness map for western Canada. In essence, seismically determined crustal profiles in the region are assumed correct, and the gravity field is

used to interpolate the crustal thickness over the entire map area. Multilayered crustal models for the southern plains of western Canada are presented. A reformulation of the Parker-Oldenburg algorithm is developed to produce a multilayered crustal model over the southern plains of western Canada.

The second major application of the algorithm is in a detailed geophysical study of the exposed shield in northeastern Alberta. Here the inverse algorithm as applied to the magnetic field with ground control on magnetic susceptibility is found to be a useful tool in mapping the Curie isotherm. A further inverse procedure utilizing the algorithm on the gravity data in combination with ground control on density provides evidence that the major geological structures present are large crustal units extending to the top of the lower crust.

ACKNOWLEDGEMENTS

I wish to thank Dr. E. R. Kanasewich for his guidance, advice, and patience during the course of this study.

I would also like to acknowledge the help of Dr. John D. Godfrey of the Research Council of Alberta who provided both the data and the encouragement for Chapter 5 of this thesis.

Computer funds for this work were provided by National Research Council grants. The field work in northeastern Alberta was supported by the Research Council of Alberta.

Table of Contents

Chapter	Page
ABSTRACT	iv
ACKNOWLEDGEMENTS	vi
LIST OF TABLES	x
LIST OF FIGURES	xi
1. INTRODUCTION	1
2. METHOD	4
2.1 THEORY	4
2.1.1 THE PARKER ALGORITHM	4
2.1.2 AN ALGORITHM FOR PARALLEL LAYERS	8
2.1.3 THE INVERSE ALGORITHM	12
2.1.4 THEORY OF GRAVITY INVERSION	13
2.1.5 GENERAL MULTILAYERED GRAVITY INVERSION	14
2.1.6 GENERAL INVERSION FOR DENSITY	20
2.1.7 THE FORWARD MAGNETIC PROBLEM	20
2.1.8 THEORY OF MAGNETIC INVERSION	28
2.1.9 PREFILTERING	31
2.2 TESTS OF THE ALGORITHM	35
3. A REGIONAL STUDY OF THE GRAVITY FIELD IN WESTERN CANADA	37
3.1 INTRODUCTION	37
3.1.1 STUDY AREA	38
3.1.2 BOUGUER GRAVITY DATA	40
3.1.3 CORRECTION FOR SEDIMENTARY ROCK	47
3.1.4 FINAL CORRECTED GRAVITY MAP	53
3.1.5 SIMPLE INVERSIONS	57

3.1.6	RESIDUAL GRAVITY	59
3.2	GRAVITY INVERSION AND ISOSTASY	62
3.2.1	MASS COMPENSATION	62
3.2.2	LONG WAVELENGTH AIRY ANOMALY	67
3.2.3	MIDDLE WAVELENGTH REGIONAL AIRY ANOMALIES ...	73
3.2.4	SHORT WAVELENGTH REGIONAL AIRY ANOMALIES	85
3.3	COMPARISON OF GRAVITY AND SEISMIC RESULTS IN WESTERN CANADA	94
3.3.1	INTRODUCTION	94
3.3.2	VELOCITY MODEL	96
3.3.3	PROCEDURE	101
3.3.4	DISCUSSION OF RESULTS	101
4.	MULTILAYERED GRAVITY MODELLING ON THE SOUTHERN PLAINS	104
4.1	INTRODUCTION	104
4.1.1	GEOLOGICAL BACKGROUND	107
4.1.2	MAGNETIC INFORMATION	109
4.1.3	SEISMIC STUDIES IN THE AREA	111
4.2	INVERSION PROCEDURE	115
4.2.1	MODEL PARAMETERS	120
4.2.2	MULTILAYERED MODELLING PROCEDURE	132
4.2.3	DENSITY INVERSION	142
4.2.4	MANTLE DENSITY CONSIDERATIONS	149
4.3	DISCUSSION OF RESULTS	150
4.3.1	THE SUPERIOR PROVINCE	150
4.3.2	THE NELSON FRONT	153
4.3.3	THE COVERED CHURCHILL PROVINCE	161
4.4	CONCLUSIONS	164

5. A DETAILED STUDY OF POTENTIAL FIELD DATA IN NORTHEASTERN ALBERTA	167
5.1 INTRODUCTION	167
5.1.1 NORTHEASTERN ALBERTA MAP-AREA	167
5.1.2 DIGITAL SAMPLING OF POTENTIAL FIELD DATA ...	170
5.2 PHYSICAL ROCK PROPERTIES	173
5.2.1 RELATION OF PHYSICAL ROCK PROPERTIES AND STRUCTURE	181
5.2.2 FIELD MEASUREMENTS OF SUSCEPTIBILITY	186
5.3 THE CURIE ISOTHERM IN NORTHEASTERN ALBERTA	193
5.4 GRAVITY INVERSION IN NORTHEASTERN ALBERTA	203
5.5 COMBINED GRAVITY AND MAGNETIC ANALYSIS	209
5.6 CONCLUSIONS	214
6. DISCUSSION	217
BIBLIOGRAPHY	223
APPENDIX A: TESTS OF THE ALGORITHM	231
APPENDIX B: SIMPLE GRAVITY INVERSIONS	254
APPENDIX C: DERIVATION OF THE PARKER ALGORITHM	270
APPENDIX D: COMPUTER PROGRAMS	273

LIST OF TABLES

TABLE		PAGE
1	Effect of filter on convergence	34
2	Standard crust	90
3	Seismic profiles	96

LIST OF FIGURES

FIGURE		PAGE
2.1	The coordinate system	5
2.2	Parallel multilayered scheme	9
2.3	General multilayered scheme	16
2.4	Flowchart	19
3.1	Base map of area	39
3.2	Smooth Bouguer gravity	41
3.3	Density function	50
3.4	Cover thickness	51
3.5	Smooth gravity	54
3.6	Highly smoothed gravity	56
3.7	Residual gravity	60
3.8	Airy anomaly	64
3.9	Pratt Anomaly	61
3.10	Long wavelength Moho surface	69
3.11	Middle wavelength Airy anomaly	74
3.12	Geologic zones	77
3.13	Geologic zones and gravity	78
3.14	NE-SW profile	79
3.15	Walcott's model	86
3.16	Short wave Airy anomaly	88
3.17	Density variation	91
3.18	Moho relief	92
3.19	Seismic profile locations	95
3.20	Velocity function	97

3.21	Crustal model for western Canada	99
3.22	Seismic and gravity disagreement	102
4.1	Base-map for the multilayered modelling study	105
4.2	Refraction lines shot by Co-crust, 1977	113
4.3	Refraction lines shot by Co-crust, 1980	114
4.4	Bouguer gravity anomaly of the southern plains	117
4.5	The station correction for the southern plains	119
4.6	Velocity models for manitoba	123
4.7	Velocity of upper crust	124
4.8	Thickness of the lower crust	125
4.9	Velocity of the lower crust	126
4.10	Velocity of the upper mantle	128
4.11	East-west velocity profiles	129
4.12	Compiled aeromagnetic anomaly.	130
4.13	Long wavelength gravity profiles	134
4.14	Crustal thickness map	138
4.15	Thickness of the upper crust	139
4.16	Cross-sections of the crust	141
4.17	Residual gravity profiles	143
4.18	Density of the upper crust	144
4.19	Profiles of upper crustal density	146
4.20	Density of the upper mantle	147
4.21	Gravity profiles with Nelson Front.	155
4.22	Crustal thickness in North America.	159
5.1	Northeastern Alberta Map-Area	168
5.2	Magnetic Field	171
5.3	Density Distribution	174

	PAGE
5.4	Susceptibility Distribution 176
5.5	Rock Densities 178
5.6	Rock Susceptibilities 179
5.7	General Rock Densities 180
5.8	General Rock Susceptibilities 181
5.9	Geologic Structure Map 182
5.10	Density Distributions and Structure 184
5.11	Mylonite Zone Susceptibility Distribution 185
5.12	Base Map 187
5.13	Typical Outcrop 189
5.14	Outcrop Profiles 190
5.15	Outcrop Susceptibility Distribution 191
5.16	Curie Isotherm Map 195
5.17	Curie Depth Determination 200
5.18	Curie Depth Determination From Outcrops 201
5.19	Slab Depth Determination 203
5.20	Bouguer Anomaly Map 204
5.21	Density Distribution Comparison 207
5.22	Density Distribution Comparison 208
5.23	Pseudo-Magnetic Map 210
5.24	Coherency and Ratio Plot 212
5.25	Ratio Distribution 216
A.1	Pyramid test structure 232
A.2	Profile of pyramid structure 233
A.3	Gravity anomaly for pyramid model 234
A.4	Talwani vs Parker profiles 236
A.5	Parker vs exact profiles 238

	PAGE
A.6	Oval Model 240
A.7	Oval inverse model 241
A.8	Error in structure 242
A.9	Error in gravity 243
A.10	Filter response 244
A.11	Radial spectrum 245
A.12	Gravity anomaly for cylinder 247
A.13	Radial spectrum for cylinder 250
A.14	Cylinder inverse 251
A.15	Magnetic test 253
B.1	Crustal density 255
B.2	Mantle density 258
B.3	Crustal model types 259
B.4	Radial spectral amplitude 260
B.5	Type 3 Moho 261
B.6	Type 2 Moho 262
B.7	Type 4 Moho 263
B.8	Type 1 Moho 264
B.9	Gravity profiles 265

1. INTRODUCTION

This thesis is concerned with the problem of direct three dimensional inversion of large gravity and magnetic data sets. An attempt will be made to integrate potential field data with other geological and geophysical data in the interior of western Canada as a regional study and in the Precambrian shield area of northeast Alberta as a more detailed study.

The significance of the problem dealt with in this thesis may be garnered from the recent 50th anniversary issue of GEOPHYSICS as published by the Society of Exploration Geophysicists, November, 1980. Therein, in a review of the history of the gravity method, Lefehr (1980) states:

Although several contributions on the subject of gravity inversions have been published, none deals with the practical problems of anomaly separation, seismic, well log, and magnetic integration, and practical solutions for handling large data sets.

Further, in a review of the history of the magnetic method, Reford (1980) restates a much quoted saying of Zietz and Bhattacharyya (1975):

Although aeromagnetic data has been collected all over the world for the past 30 years at a total astronomical cost, it is safe to say that practically nothing is known of the physical characteristics of the rocks that produce the magnetic anomaly. The unpredictability of observed magnetic field over rocks where geology is "known" reinforces the observation. In our opinion, one of the most significant studies that ought to be made in the immediate future is the relationship between mineralogy and petrology, rock magnetism and aeromagnetic studies.

Clearly, the inversion of large gravity and magnetic data sets and their integration with other geological and geophysical information is thought to be a topic of some importance to modern geophysical research.

By "inversion" is meant a method of potential field interpretation in which one attempts to derive subsurface models of varying geometry which are physically capable of producing the variations or "anomalies" in the potential field as measured on or above the ground surface. Such modelling procedures rarely produce unique results; that is, many shapes of anomalous material in the subsurface are generally capable of producing the observed variations in the potential field. Usually information from additional geological or geophysical methods is required to produce an adequate potential field interpretation.

In some instances, given sufficient control on the parameters of a possible function which models the subsurface, "direct" inversion of the potential field can be attempted. For direct interpretation, one starts with the observed data, specifies certain parameters, and performs prescribed mathematical manipulations to arrive at a unique result for the parameters specified. The only practical method of direct inversion of extensive amounts of potential field data currently available is based on the Parker algorithm which utilizes a series expansion of the potential field in terms of Fourier transforms.

Previously published examples of the use of the Parker algorithm have been two dimensional, that is, the resultant models are assumed to be of infinite strike length. The advantage of such analyses is that one only has to consider one dimensional profiles of the potential field data. The disadvantage is that geological structures are not generally infinite in strike length. In this thesis, the potential fields are to be analyzed in the form of two dimensional maps. While this procedure results in an increase in the amount of computation required, it results in more satisfying three dimensional geological models.

2. METHOD

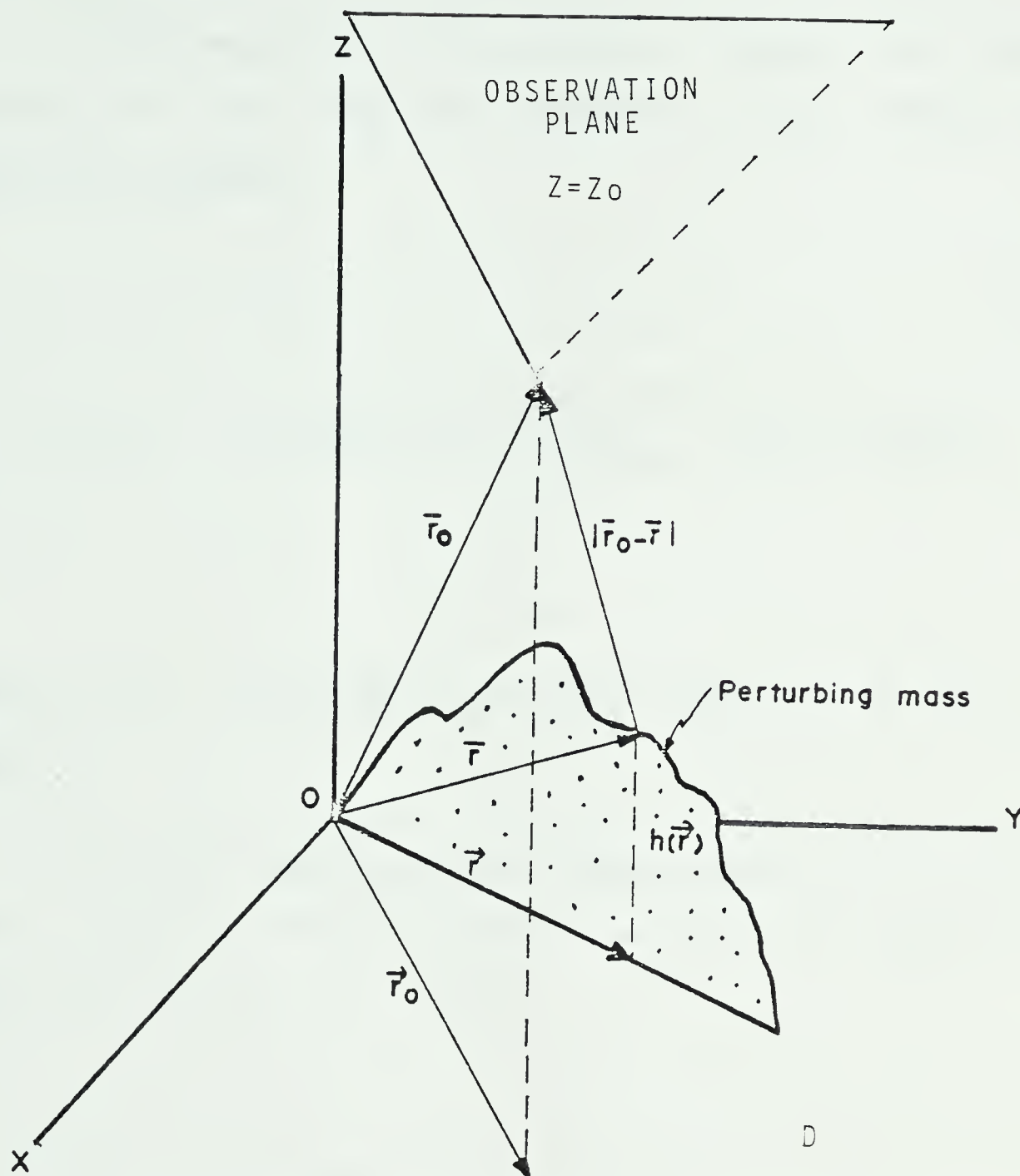
2.1 THEORY

2.1.1 THE PARKER ALGORITHM

Parker's (1973) algorithm for the calculation of the gravitational anomaly due to an uneven layer of material of constant density contrast, d , where the lower and upper boundaries of the layer are given by $z = 0$ and $z = h(x,y)$, respectively is

$$F\{g(x,y)\} = -2\pi G \quad d \exp(-|\vec{k}| Z_0) \sum_{n=1}^{\infty} \frac{|\vec{k}|^{n-1}}{n!} F\{h^n(x,y)\} \quad [1]$$

where F signifies that a two dimensional Fourier transform is to be taken of the quantity in brackets, $g(x,y)$ is the gravity anomaly, G is the universal gravitational constant, \vec{k} is the wavenumber vector in the spatial frequency domain, and Z_0 is the height of the observation plane ($z = Z_0$) above the reference plane ($z = 0$). A Cartesian coordinate system with z positive upwards is being used (Figure 2.1). The function $h(x,y)$ is known as the inversion surface. A brief outline of the derivation of the Parker algorithm is given



The observations are made on the $z=Z_0$ plane.. All radius vectors with an arrow are restricted to the $x-y$ plane. All vectors with a bar are three dimensional. The perturbing mass with base at $z=0$ and top at $z=h(r)$ is restricted to a finite domain D . The location of an element of mass is given by \vec{r} , and its projection in the $x-y$ plane, by \vec{r} . The observation location is represented by \vec{r}_0 , and its projection on the $x-y$ plane by \vec{r}_0 .

Figure 2.1. The coordinate system used in the present study.

in the appendix.

If the density of the material below the inversion surface is not constant laterally, then Parker's basic algorithm becomes

$$F\{g(x,y)\} = -2\pi G \exp(-|\vec{k}|Z_0) \sum_{n=1}^{\infty} \frac{|\vec{k}|^{n-1}}{n!} F\{D(x,y) h^n(x,y)\} \quad [2]$$

where $D(x,y)$ is the density of the material in the lower medium.

The above equation can be used to arrive at a formula for a slab of variable density material with upper surface constant at $h(x,y)=H$. Since

$$\sum_{n=1}^{\infty} \frac{|\vec{k}|^{n-1}}{n!} F\{D(x,y) H^n\} = \frac{\exp(-|\vec{k}|H)-1}{|\vec{k}|} F\{D(x,y)\} \quad [3]$$

it follows that

$$F\{g(x,y)\} = -2\pi G \left\{ \frac{\exp(\frac{|\vec{k}|H)-1}{|\vec{k}|}} \right\} F\{D(x,y)\} \exp(-|\vec{k}|Z_0) \quad [4]$$

If the density of the material in the medium above the inversion surface is not constant laterally, then the gravity effect of such an upper medium can be calculated by subtracting a result using (2) from a result using (4) with $H=Z_0$ in the latter.

Parker (1973) demonstrated that the summations in the above type of formulae converge most rapidly if $h(x,y)$ is measured relative to a level which is median to the two extreme values of the topography on the inversion surface. This is merely a computational problem which can be overcome as follows

$$F\{g(x,y)\} = F\{S(x,y)\} - 2\pi G \exp(-|\vec{k}|(Z_0-M)) \cdot \sum_{n=1}^{\infty} \frac{|\vec{k}|^{n-1}}{n!} F\{D(x,y)(h(x,y)-M)^n\} \quad [5]$$

where $S(x,y)$ is the gravity effect due to a slab of density $D(x,y)$ and of height M . $S(x,y)$ can be determined by setting $H=M$ in equation (4). Hence the necessary summations can be calculated in equivalent forms which yield optimum

convergence.

2.1.2 AN ALGORITHM FOR PARALLEL LAYERS

If many layers parallel to and above the inversion surface are present as shown in Figure 2.2, and if the density contrasts between the successive layers do not vary with x or y , then the gravity anomaly of the multilayered system can be calculated in terms of the lowermost interface (which is called the inversion surface) by

$$F\{g(x,y)\} = -2\pi G d \frac{\exp(-|\vec{k}|Z_0)}{R(\vec{k})} \sum_{n=1}^{\infty} \frac{|\vec{k}|^{n-1}}{n!} F\{h^n(x,y)\} \quad [6]$$

where $R(\vec{k})$ is that fraction of the gravity anomaly due only to topography, $h(x,y)$, on the lowermost interface and where d is now a constant density contrast at the inversion surface. Here, density contrast is defined as the difference between the densities immediately above and below the interface being considered. The function $R(\vec{k})$ can be calculated for discrete layers using the downward continuation operator, $\exp(-|\vec{k}|z)$, in the following manner.

By definition:

$$R(\vec{k}) = \frac{F\{g_I(x,y)\}}{F\{g_I(x,y)\} + \sum_{L=1}^m F\{g_L(x,y)\}} \quad [7]$$

where m is the number of interfaces above the inversion surface, $g_I(x,y)$ is the gravity anomaly due only to the inversion surface, and $g_L(x,y)$ is the gravity anomaly due to the L' th interface above the inversion surface. Then

$$F\{g_L(x,y)\} = \frac{d_L}{d} \exp(|\vec{k}| z_L) F\{g_I(x,y)\} \quad [8]$$

where d_L is the density contrast at the L' th interface above the inversion surface, and z_L is the vertical distance between the L' th interface and the inversion surface. By substitution of (8) into (7), one obtains

$$R(\vec{k}) = \frac{d}{d + \sum_{L=1}^m d_L \exp(|\vec{k}| z_L)} \quad [9]$$

This function determines, in the wave number domain, that

fraction of the total gravity anomaly which is due only to the inversion surface.

If there are many thin layers parallel to the inversion surface and if, at any given x-y location, density is a linear function of depth such that the density contrast between successive layers is constant, then the sum in (9) becomes

$$\sum_{L=1}^{\infty} A \exp(|\vec{k}|z) \Delta z = \int_{z=0}^T A \exp(|\vec{k}|z) \delta z = \frac{A}{|\vec{k}|} (\exp(|\vec{k}|T) - 1) \quad [10]$$

where A is the constant density contrast between successive layers and where T is the total thickness of all the layers above the inversion surface. Hence, for a system of parallel laminae whose densities vary linearly with depth, the fraction of the total anomaly due only to the inversion surface becomes

$$R(k) = \frac{d}{d + \frac{A}{|\vec{k}|} (\exp(|\vec{k}|T) - 1)} \quad [11]$$

where d is the density contrast at the inversion surface, " Δ " is the constant rate of change of density with depth.

2.1.3 THE INVERSE ALGORITHM

The traditional method of potential field inversion involves the comparison of theoretical anomalies produced by crustal models with actual observations. Such indirect methods involve an extraordinary amount of computing time if one is dealing with large data sets. This situation was considerably improved with the advent of direct iterative schemes based on Parker's algorithm. By separating the first term of the series in (2) from the remainder of the equation, iterative equations for subsurface topography, bed thickness or density can be obtained. This has been accomplished by Oldenburg (1974), and the following algorithm results.

$$F\{D(x,y) h(x,y)\} = \frac{-F\{\Delta g(x,y)\} \exp(|\vec{k}| Z_0)}{2 \pi G} \quad [12]$$

$$- \sum_{n=2}^{\infty} \frac{|\vec{k}|^{n-1}}{n!} F\{D(x,y) h^n(x,y)\}$$

where $D(x,y)$, the density of the material in the lower medium, is variable with respect to x and y . The convergence of the iterative scheme is not assured and some

filtering of the data is always required to remove short wavelength noise. Nonetheless, this procedure constitutes a very practical direct inverse method for gravity field data.

2.1.4 THEORY OF GRAVITY INVERSION

The simplest type of crustal model to be considered in the next chapter will be based on the following assumptions:

- 1) The gravity anomaly is due only to subsurface topographical variations.
- 2) All densities are constant with respect to x and y .
- 3) Any intermediate layers are parallel to the Moho.

The forward algorithm for this type of model is given by (6), and the iterative formula is:

$$F\{h(x,y)\} = \frac{F\{\Delta q(x,y)\} \exp(|\vec{k}|Z_0) R(\vec{k})}{-2\pi G d} \quad [13]$$

$$- \sum_{n=2}^{\infty} \frac{|\vec{k}|^{n-1}}{n!} F\{h^n(x,y)\}$$

where d in this case is a constant density contrast at the base of the crust.

Another type of simplified crustal model to be used later uses the following assumptions:

- 1) The gravity anomalies are due only to lateral variation in crustal density.

2) All interfaces are horizontal

The algorithm for such slabs of material is given by equation (4) and the inversion formula for density is as follows:

$$F\{D(x,y)\} = \frac{P}{-2\pi G} F\{g(x,y)\} \quad [14]$$

where

$$P = \frac{|\vec{k}| \exp(|\vec{k}|Z_0)}{1 - \exp(-|\vec{k}|H)} \quad [15]$$

2.1.5 GENERAL MULTILAYERED GRAVITY INVERSION

The Parker algorithm in its most basic form involves the premise that the gravity anomaly is due only to the topography on a single subsurface interface of constant density contrast (Figure 2.1). This assumption is not suitable for most geologic models which generally presume the lithosphere to be composed of many different layers.

In this section, the Oldenburg (1974) inversion scheme will be extended to allow for a multilayered medium under the following conditions:

1. The thickness and density of each layer, as known from limited seismic information, must vary smoothly across the map-area.
2. Each interface must be altered in order to suit the gravity anomaly in the same manner as the bottom-most interface, which is called the inversion surface.

Lee(1977) accomplished this extension for the two-dimensional case. Here, his method is extended to three dimensional situations. To calculate the gravity anomaly due to a multilayered medium, such as that shown in Figure 2.3, the Parker algorithm becomes

$$F[g(\text{total})] = -2\pi G \sum_{j=1}^{j=M} \exp(-|\vec{k}|Z_j) \sum_{n=1}^{\infty} (|\vec{k}|^{n-1}/n!) F[d_j(x,y)h_j^n(x,y)] \quad [16]$$

where Z_j is the reference level for the j' th interface, $d_j(x,y)$ is the density contrast at the j' th interface, $h_j(x,y)$ is the topography on the j' th interface, and M is the number of layers present. The gravity anomaly of only the inversion surface is called $g(\text{inv})$ and the gravity

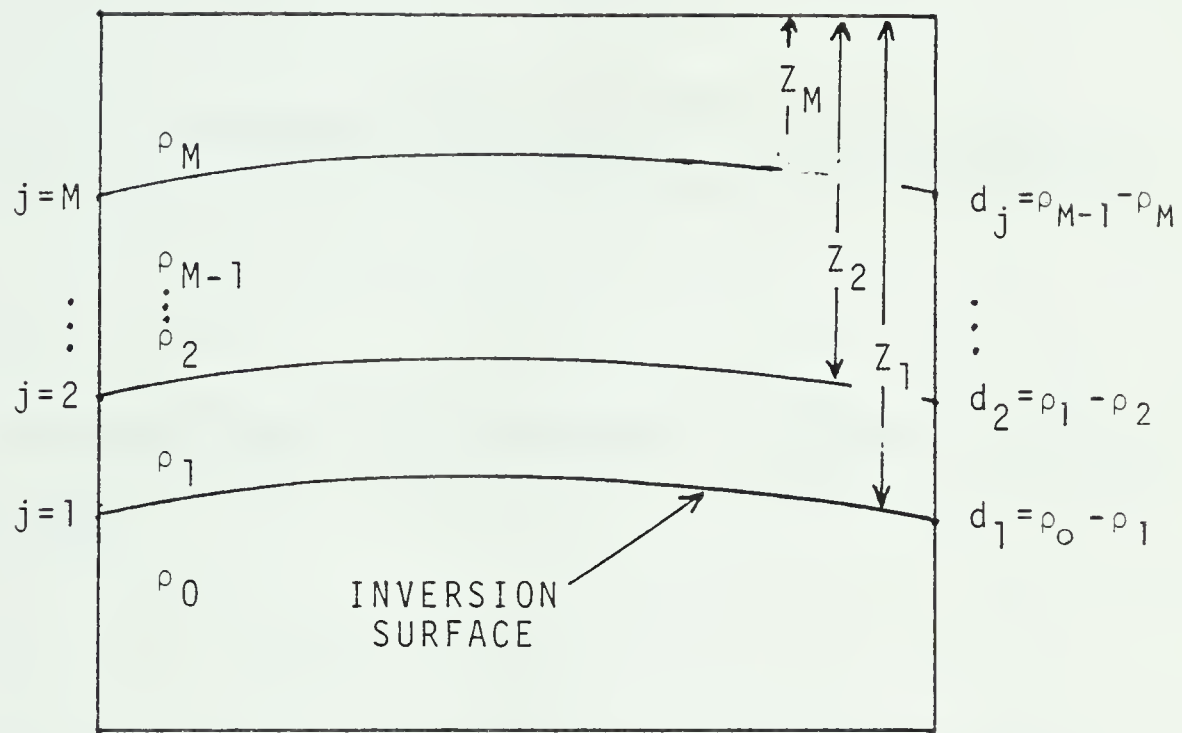


Figure 2.3. The general multilayered scheme for which equation (16) is derived. The density contrast, d_j , at each interface is equal to the difference in densities of the layers immediately above and below the L' th interface.

anomaly due to the remainder of the system is referred to as $g(\text{sum})$. The summation of $g(\text{sum})$ and $g(\text{inv})$ is termed $g(\text{total})$. To evaluate $g(\text{inv})$, M is set to 1 in the above equation, such that

$$F[\Delta g(\text{inv})] = -2\pi G \exp(-|\vec{k}|Z_1) \sum_{n=1}^{\infty} (|\vec{k}|^{n-1}/n!) F[d_1(x,y)h_1^n(x,y)] \quad [17]$$

Upon transposition, an inversion procedure is accomplished as follows:

$$F[d_1(x,y)h_1(x,y)] = -F\{[g(\text{total}) - g(\text{sum})] / 2\pi G\} \exp(|\vec{k}|Z_1) - \sum_{n=2}^{\infty} (|\vec{k}|^{n-1}/n!) F[d_1(x,y)h_1^n(x,y)] \quad [18]$$

where

$$F[g(\text{sum})] = -2\pi G \sum_{j=2}^{j=M} \exp(-|\vec{k}|Z_j) \sum_{n=1}^{\infty} (|\vec{k}|^{n-1}/n!) F[d_j(x,y)h_j^n(x,y)] \quad [19]$$

Since densities are known, the most recent value of $h(x,y)$ is multiplied by $d(x,y)$ and the infinite sum calculated to yield a new value of $h(x,y)$. This value is then substituted back in as part of an iterative procedure. The process is repeated until convergence criteria are met. The method of inversion is outlined by the flowchart in Figure 2.4.

Only a portion of the observed gravity is used in the first inversion since the inversion surface itself accounts for only a fraction of the gravity anomaly, the rest being due to density, thickness and topographic variations in the other layers. Lee (1977) more or less guessed at the initial fraction. Here, the parallel multilayered system fraction, $R(\vec{k})$, as discussed earlier, is applied in the spatial frequency domain to yield a higher quality initial estimate of $g(inv)$.

The gravity anomaly due to all the layers other than the inversion surface is calculated as $g(sum)$. The difference between the initial gravity, $g(total)$ and $g(sum)$ then yields a new value of $g(inv)$ for subsequent iterations. In practice, the mean of the new $g(inv)$, called $g(res)$ and the old $g(inv)$ is used to improve convergence.

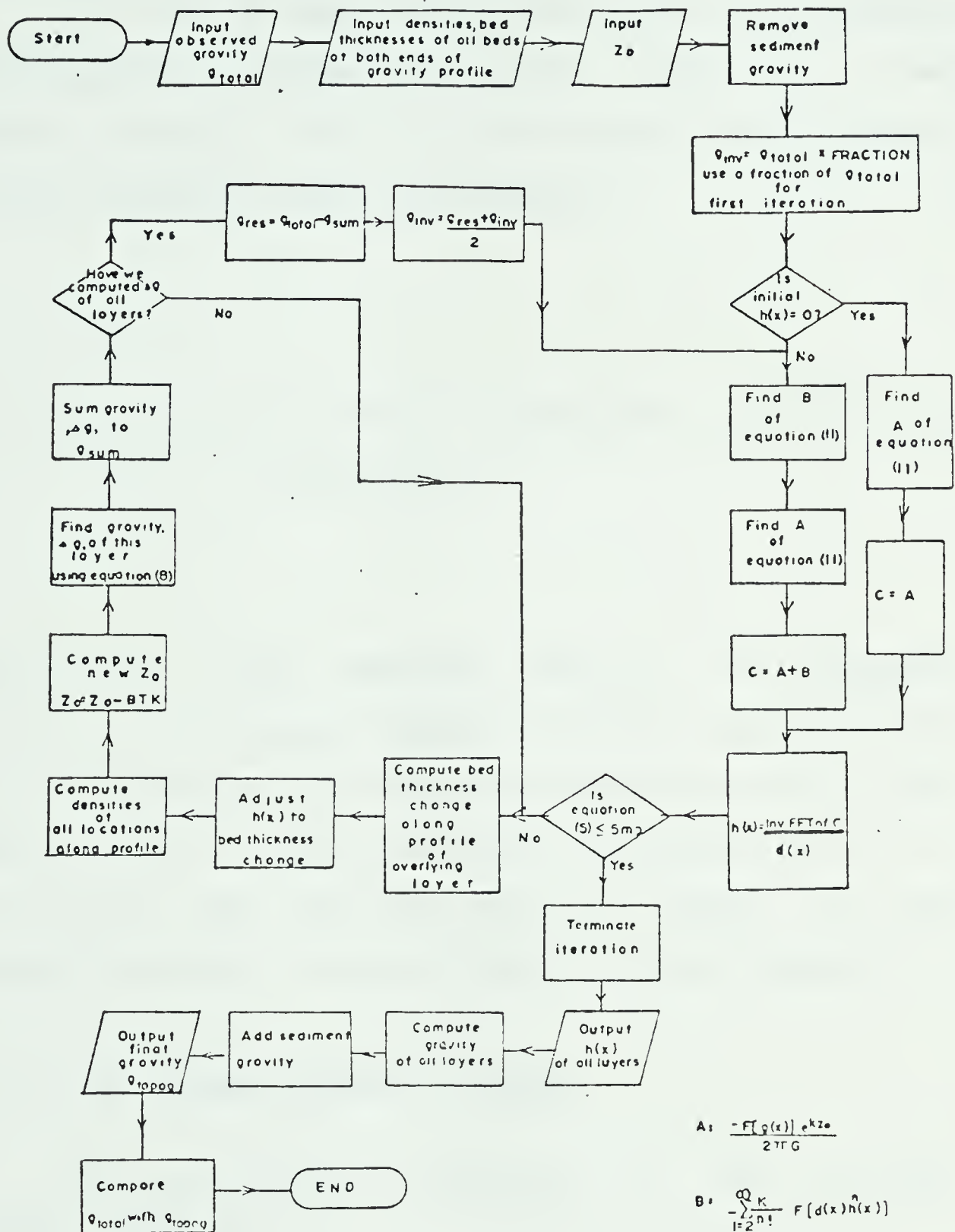


Figure 2.4. A flowchart of the multilayered modelling procedure. (After Lee, 1977).

2.1.6 GENERAL INVERSION FOR DENSITY

If a slab of known varied thickness but unknown density distribution is assumed to be the source of a residual gravity anomaly, then the following reformulation of the Parker-Oldenburg algorithm is useful:

$$F\{d(x,y)h(x,y)\} = -(F\{g(\text{res})\} / 2\pi G) \exp(|\vec{k}|Z) - \sum_{n=2}^{\infty} (|\vec{k}|^{n-1} / n!) F\{d(x,y)h^n(x,y)\} \quad [20]$$

where $g(\text{res})$ is the residual gravity. The procedure is similar to the usual iterative process, except in this case $h(x)$ is known and the iterative scheme is used to find the density at the various locations along the profile. If $h(x)$ is constant, then the above algorithm reduces to the much simpler equation (14) for a slab of variable density.

2.1.7 THE FORWARD MAGNETIC PROBLEM

The gravitational potential, U , was derived by Parker (1973) as

$$F\{U\} = 2\pi G \exp(-|\vec{k}|Z_0) \cdot \sum_{n=1}^{\infty} \frac{|\vec{k}|^{n-2}}{n!} F\{h^n(x,y) D(x,y)\} \quad [21]$$

By definition

$$\vec{\nabla}U = - G \int_V D(x,y) \vec{\nabla}(1/r) \delta V \quad [22]$$

where $r=|\vec{r}_0-\vec{r}|$.

If the ratio of density to susceptibility is a constant value, Q , such that

$$Q = \frac{D(x,y)}{X(x,y)} \quad [23]$$

and if there is no remanent magnetization and the ambient field is constant, (22) becomes

$$\vec{\nabla}U = -G Q \int_V X(x,y) \vec{\nabla}(1/r) \delta V \quad [24]$$

By definition, the magnetic potential, W , is given by

$$W = \frac{\vec{H}_0 \cdot}{\mu_0} \int \chi(x,y) \vec{\nabla}(1/r) \delta V \quad [25]$$

where \vec{H}_0 is the ambient field.

Therefore, by combining (24) and (25)

$$\frac{\vec{\nabla} U}{-G Q} = \frac{\mu_0 W}{\vec{H}_0} \quad [26]$$

or

$$W = - \frac{\vec{H}_0 \cdot \vec{\nabla} U}{Q \mu_0 G} \quad [27]$$

This is a generalization of Poisson's relation (Garland, 1951) between the magnetic potential and the gravitational field. It holds only under the restrictions mentioned above.

In the spatial frequency domain

$$F\{W\} = - \frac{\vec{H}_0 \cdot F\{\vec{\nabla} U\}}{\mu_0 G Q} \quad [28]$$

but

$$F\{\nabla U\} = \{ik_x, ik_y, -|k|\} F\{U\} \quad [29]$$

so

$$F\{W\} = - \frac{\vec{H}_0 \cdot \{ik_x, ik_y, |\vec{k}|\} F\{U\}}{G \mu_0 Q} \quad [30]$$

The magnetic field anomaly, \vec{A} , is given by

$$\vec{A} = -\nabla W \quad [31]$$

or, upon taking the Fourier transform

$$F\{\vec{A}\} = - F\{\vec{\nabla}W\} \quad [32]$$

so

$$F\{\vec{A}\} = - \{ik_x, ik_y, -|\vec{k}|\} F\{W\} \quad [33]$$

Let

$$\vec{V} = \{ik_x, ik_y, -|\vec{k}|\} \quad [34]$$

then by substituting (34) and (30) into (33)

$$F\{\vec{A}\} = \frac{\vec{V} \cdot \vec{V} \cdot \vec{H}_0 F\{U\}}{\mu_0 G Q} \quad [35]$$

The total field magnetic anomaly is usually approximated by the component of the true anomaly, \vec{A} , in the direction of the ambient field, \vec{H}_0 ,

$$|\Delta A| = \frac{\vec{A} \cdot \vec{H}_0}{|\vec{H}_0|} \quad [36]$$

or, in the spatial frequency domain

$$F\{|\Delta \vec{A}|\} = \frac{F\{\vec{A} \cdot \vec{H}_0\}}{|\vec{H}_0|} = \frac{\vec{H}_0}{|\vec{H}_0|} \cdot F\{\vec{A}\} \quad [37]$$

After substitution of (35) and (21) into (37) using (23), one obtains

$$F\{|\Delta\vec{A}\} = \frac{2\pi [\vec{H}_0 \cdot \vec{V}]^2 \exp(-|\vec{k}| Z_0)}{\mu_0 |\vec{H}_0|} \quad [38]$$

$$\sum_{n=1}^{\infty} \frac{|\vec{k}|^{n-2}}{n!} F\{h^n(x,y) X(x,y)\}$$

To simplify the algorithm, the ambient field direction can be absorbed by a dimensionless vector, $N(\vec{k})$, defined in the following manner as a function of declination, D , and inclination, I .

$$N(\vec{k}) = \frac{(i k_x \cos D \cos I - i k_y \sin D \cos I + |\vec{k}| \sin I)^2}{|\vec{k}|^2} \quad [39]$$

Then

$$\frac{(\vec{V} \cdot \vec{H}_0)^2}{|\vec{H}_0|} = N(\vec{k}) |\vec{k}|^2 |\vec{H}_0| \quad [40]$$

By removing one wave number factor from the summation of (38) and by substituting (40) into (38), one obtains

$$F\{|\Delta\vec{A}|\} = \frac{2\pi N(\vec{k}) |\vec{k}| |\vec{H}_0| \exp(-|\vec{k}|Z_0)}{\mu_0} \quad [41]$$

$$\sum_{n=1}^{\infty} \frac{|\vec{k}|^{n-1}}{n!} F\{X(x,y)h^n(x,y)\}$$

The above equation is the forward algorithm for the magnetic problem.

To obtain an algorithm for a magnetized slab of constant thickness, T , a series expansion is used.

$$\sum_{n=1}^{\infty} \frac{|\vec{k}|^{n-1}}{n!} F\{T^n(x,y) X(x,y)\} = \frac{\exp(|\vec{k}|T)-1}{|\vec{k}|} F\{X(x,y)\} \quad [42]$$

By substitution of (42) into (41), the magnetic anomaly for the slab is

$$F\{|\Delta\vec{A}|\} = \frac{2\pi |\vec{H}_0| N(\vec{k}) [\exp(|\vec{k}|T) - 1] \exp(-|\vec{k}|Z_0) F\{X(x,y)\}}{\mu_0} \quad [43]$$

2.1.8 THEORY OF MAGNETIC INVERSION

Parker and Huestis (1974) directly inverted magnetic anomalies measured at sea in terms of a two dimensional irregular layer of magnetized material of constant thickness. In a present study, the similar algorithm will be used to invert directly continental magnetic anomalies in terms of three dimensional layered models.

The types of crustal models used in magnetic inversion are considerably different from those used in gravity studies. The temperature gradient in the crust is roughly $30^{\circ}\text{C}/\text{km}$, hence at a depth of about 20 km, the Curie point for magnetite, about 580°C , is exceeded. Therefore, all magnetic anomalies due to crustal variations have their source in the upper 20 km or so of the crust. The level at which the ferromagnetic properties of the rocks cease to occur is called the Curie isotherm. The absence of anomalies in the geomagnetic field on a wavelength intermediate between local ones of origin above the Curie isotherm and those of origin within the earth's core is well known. The shape of the Curie isotherm is a worthy target for magnetic inversion in that it is of interest to heat flow studies. This deepest objective of aeromagnetic studies is not necessarily a geological discontinuity at all, but rather a temperature surface.

Inversion of magnetic anomalies for continental crustal structure is essentially different from inversion for the sea floor case. For continental studies, the magnetization of the rocks is generally assumed to be due to the rock's magnetic susceptibility within the present geomagnetic field. For marine studies, on the other hand, the magnetization of the rocks is generally taken to be mostly due to remanence, that is, permanent magnetization.

In this study, considerable ground control is available on the susceptibilities of the surface rocks, hence an attempt will be made to invert the magnetic field to yield susceptibilities of surface slabs of varied magnetization and thickness using equation (43). These models should prove useful for petrological studies of the crustal rocks.

For the case of crustal models with uniform magnetization, the magnetic anomaly due to a slab of constant thickness is zero as is clear from equation (43). For non-uniform magnetization, a slab results in positive anomalies in the total field over areas of higher magnetization.

For the Curie isotherm type of model, on the other hand, the top surface of the crust (surface topography) is assumed to be flat, and the lower surface is the unknown "topography" to be found by the inversion process. The susceptibility is in this case constant. For convenience,

the origin is placed at the mean level of the base of the magnetic crust. Z_0 is then the distance from the mean base of the magnetic crust to the flight height, A_0 , above the ground surface and $T_0 = Z_0 - A_0$ is the mean thickness assumed for that part of the crust above the Curie isotherm. Under these conditions, equation (41) becomes

$$F\{|\Delta\vec{A}|\} = -(2\pi/\mu_0) N(\vec{k}) |\vec{k}| |\vec{H}_0| \chi \exp(-|\vec{k}|Z_0) \cdot \sum_{n=1}^{\infty} \frac{|\vec{k}|^{n-1}}{n!} F\{h^n(x,y)\} \quad [44]$$

where χ is now a constant susceptibility. The negative sign in the above formula is due to the fact that the anomalous material is now above rather than below the $z=h(x,y)$ surface.

The factor $N(\vec{k})$ is equal to unity for the case of a vertical magnetic field. In Canada, the field is so close to vertical that this factor is not very important. For the map-area to be considered in Chapter 5, for example, I varies from 80.5° to 81.5° and D varies from 26° to $27^\circ E$. For the highest wave number utilized (about 1.57 radians/km), the value of $N(k)$ as determined by (39) is $(1.95+0.21i) \pm (0.01+0.01i)$. Hence the gradual variation of this factor across the map-area can be ignored.

To develop an inversion scheme, the first term in the series of (44) is transposed and the equation is rearranged to yield

$$F\{h(x,y)\} = \frac{-\mu_0 F\{|\Delta\vec{A}|\} \exp(|\vec{k}|Z_0)}{2\pi N(\vec{k}) |\vec{k}| |\vec{H}_0| x} \quad [45]$$

$$\sum_{n=2}^{\infty} \frac{|\vec{k}|^{n-1}}{n!} F\{h^n(x,y)\}$$

Since the constant susceptibility is known, one begins with an estimate for $h(x,y)$ and uses (45) iteratively. After each iteration, the origin is readjusted such that it lies at the chosen depth, T_0 , beneath the surface, thus insuring rapid convergence of the series.

2.1.9 PREFILTERING

It is necessary to prefilter the gravity anomaly in order to achieve convergence using the inverse Parker-Oldenburg algorithm. In this study, filtering is performed in the spatial frequency domain with a simple two dimensional low pass filter symmetric with respect to all axes in order to ensure a real output in the space domain. The filter response is tapered between the chosen high pass and high cut spatial frequencies with a two dimensional cosine bell function. The spatial frequency response of such a filter is shown in Figure A.10 (Appendix A); this

particular one with a high pass at 0.25 cycles per data interval and a high cut at 0.375 cycles per data interval.

The proper choice of the high pass and high cut frequencies is critical to the success of the Oldenburg algorithm. If too much high frequency noise is allowed in, the algorithm will diverge or give geologically absurd results. If filtering is too severe, the resulting model will be unnecessarily smoothed with useful information lost. In previous studies (Oldenburg, 1974; Lee, 1977), the choice of filter parameters was more or less arbitrary. In this study, the amplitude spectrum of the equivalent stratum at the reference depth will be utilized as a guide toward proper choice of the filter parameters.

To obtain the equivalent stratum, the observed field is continued down to the reference depth and multiplied by the appropriate factor. The first term on the right hand side of the Parker-Oldenburg algorithm is the equivalent stratum if the first guess at the subsurface topography is uniformly zero for all x and y . The effect of the exponential downward continuation operator increases severely with both wavenumber and reference level depth. If the logarithm of the amplitude spectrum of the equivalent stratum is considered, one finds that downward continuation of white noise tends to add a quantity whose slope is 2.3 times the reference depth on a semi-log plot of spectral amplitude versus wavenumber. Hence by searching the amplitude

spectrum of the equivalent stratum for such a strong positive slope, one can estimate the wavenumber or spatial frequency at which filtering should commence.

It is awkward to analyse spectra in two dimensions for linear slopes, hence the average radial spectral amplitude was utilized instead. This spectrum is obtained by averaging the spectral amplitudes encountered in rings of increasing radii about the origin. This method seems reasonable since the filter to be designed is to be symmetrical with respect to all axes.

The average radial spectral amplitude of the equivalent stratum for a test structure is shown in Figure A.11 of Appendix A. The reference depth is only 1 km for this test, hence the positive slope on the semi-log plot does not appear until about 0.5 cycles per data interval. Accordingly, this frequency was chosen as the most efficient high cut parameter for this particular problem. The high pass frequency was set arbitrarily at 0.75 of the high cut spatial frequency in order to ensure a smooth filter free from Gibb's effect.

That the above choice of filter parameters was, in fact, efficient can be seen in some results tabulated in Table 1. The *rms* difference between successive values of $h(x,y)$ is utilized as the criteria of convergence of the Oldenburg algorithm. Table 1 shows how the *rms* difference

<u>FILTER:</u>	0.50-0.70	0.38-0.50	0.25-0.37
<u>ITERATION</u>			
1	173m	173m	173m
2	23.1m	21.7m	21.1m
3	8.30m	4.91m	2.98m
4	3.68m	1.58m	0.88m
5	3.07m	0.65m	0.32m
6	3.39m	0.33m	0.13m

Table 1. Effect of filter on convergence.

changed with each iteration for three different filter settings. When the *rms* difference between successive estimates of $h(x,y)$ is less than half a metre, the algorithm is considered to have converged (Oldenburg, 1974). As is evident from Table 1, the inversion diverged for the 0.5-0.7 filter, converged after six iterations for the 0.38-0.50 filter, and converged even faster for the 0.25-0.375 filter. Hence, the most efficient filter was the 0.38-0.5 filter as predicted from the spectrum of the equivalent stratum. It allowed the most information in without losing convergence. The 0.25-0.375 filter, while it converged quickly, no doubt eliminated some information by oversmoothing.

2.2 TESTS OF THE ALGORITHM

In order to test the computer programs developed for this study, various tests were devised for the forward and reverse algorithms. The results of these tests are given and discussed in Appendix A. The more fundamental computer programs used in this study are listed in Appendix D. Some of the more important conclusions were as follows:

1. The forward Parker algorithm requires less than one tenth the computing time of integration methods such as that of Talwani and Ewing (1960) for a 4096 point grid.
2. The largest errors associated with the Parker algorithm occur near the edges of the grid. These errors are due to the cyclic properties of the Fourier transform and

can be minimized by adding additional zeros around the structure to be modelled.

3. Other possible errors with the algorithm occur near sharp edges of the structural models. These errors are due to sampling too coarsely for the model being considered. It is therefore imperative that the structural models used with the Parker algorithm be sampled finely enough to avoid this type of error.
4. The choice of filter parameters is vital to the success of the inverse procedure. Too little filtering leads to divergence and too much filtering produces a loss of detail in the results.
5. The most efficient filter to apply is best determined by inspection of the amplitude spectrum of the field continued down to the reference depth.

3. A REGIONAL STUDY OF THE GRAVITY FIELD IN WESTERN CANADA

3.1 INTRODUCTION

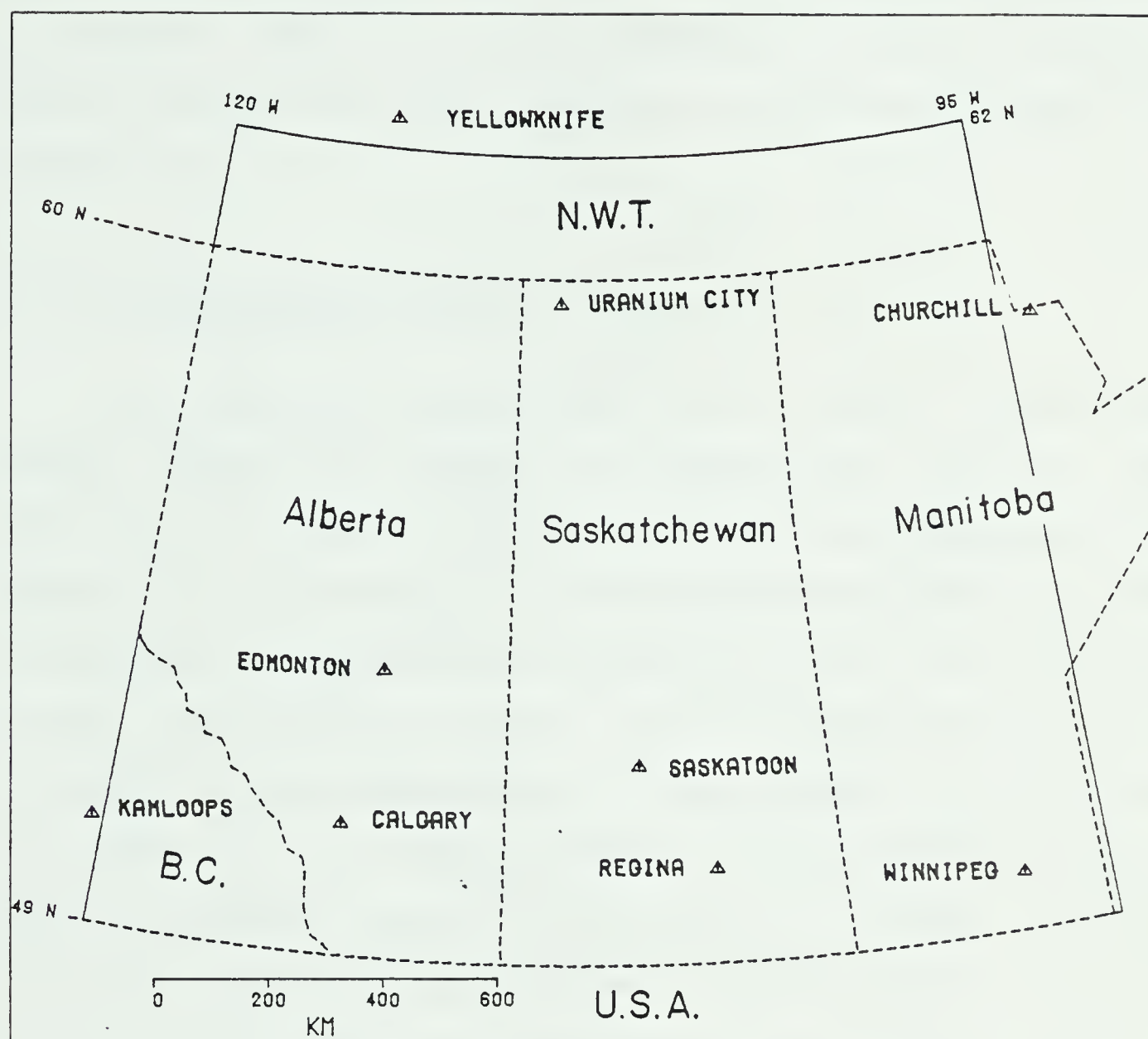
Current knowledge of the structure of the lithosphere in western Canada is quite sparse. Most of the available information is the result of various seismological studies which have utilized refraction, reflection, and earthquake data. The gravitational field in western Canada is, on the other hand, well established in a regional sense and it provides an alternative source of deep structural information. The most difficult problem with using gravity information is the lack of uniqueness inherent in its analysis. Nevertheless, Oldenburg (1974) while extending an algorithm of Parker (1973) suggested a method of gravity inversion in terms of a single subsurface layer for which the nonuniqueness of the problem is controlled by only two parameters, namely, the depth to the layer and the density contrast across the layer. Lee (1977) extended this idea to invert a profile of gravity data from the southern plains region of Canada in terms of several subsurface crustal layers with seismic data used to control the free parameters. In the present study, the gravity field over much of western Canada is analyzed using various reformulations of the Parker algorithm. Seismic, geologic, and geodetic data are utilized to maintain reasonable bounds on the free parameters involved.

3.1.1 STUDY AREA

A base map showing the location of the study area is given in Figure 3.1. The map-area is bounded on the south by the 49th parallel which is the international boundary and on the north by the 60th parallel which passes just south of Yellowknife, N.W.T. The western limit is the 118°W meridian which passes nearly through Kelowna, B.C. and the eastern limit is the 95°W meridian which passes east of the city of Winnipeg, Manitoba.

The map-area is not square but tapers toward the north. At the southern boundary, the map-area is about 1600 km wide while at the northern limit, the map-area width is only about 1150 km. In a north-south direction, the map-area spans about 1450 km. The overall area considered is just over 2,000,000 km².

The maps presented for this map-area are all plotted on a Lambert Conformal Conic projection with standard parallels at 49°N and 77°N which is the usual one utilized by the G.S.C. for small scale maps. The Lambert Conformal projection is one in which all meridians are straight lines that meet at a common point beyond the limits of the map area, and all the parallels are concentric circles whose center is at the point of intersection of the meridians. This projection tends to preserve angular relationships and lengths of linear elements with minimal scale errors. A



Interior of WESTERN CANADA

Figure 3.1. The map-area for which gravity data were available for this study.

review of the theory of the Lambert Conformal projection is given by Bhattacharyya and Clay (1966). A computer program to convert from a latitude-longitude location to a grid location using the Lambert Conformal projection is given in Appendix D.

3.1.2 BOUGUER GRAVITY DATA

The smoothed Bouguer gravity for the interior of western Canada is mapped in Figures 3.2a. and 3.2b. The map-area is the same as that shown on the base map given in Figure 3.1. The data for this map were obtained from some 26,000 gravity observations recorded by the Earth Physics Branch, Department of Energy, Mines, and Resources, Canada. To enable further computations, it was decided to reformat this data onto a square 256 by 256 point grid with about eight kilometres between grid points. Since gravity stations are generally about ten kilometres apart, aliasing problems which might have occurred with a larger sampling interval were avoided. Frequency filtering was then used to produce smoother maps with grid sizes 128 by 128 and 64 by 64.

In order to reformat the data to a square grid, it was necessary to use some form of automatic interpolation. Crain and Bhattacharyya (1967) have discussed various methods of computing values of an observed variable at equidistant points along two orthogonal directions from an

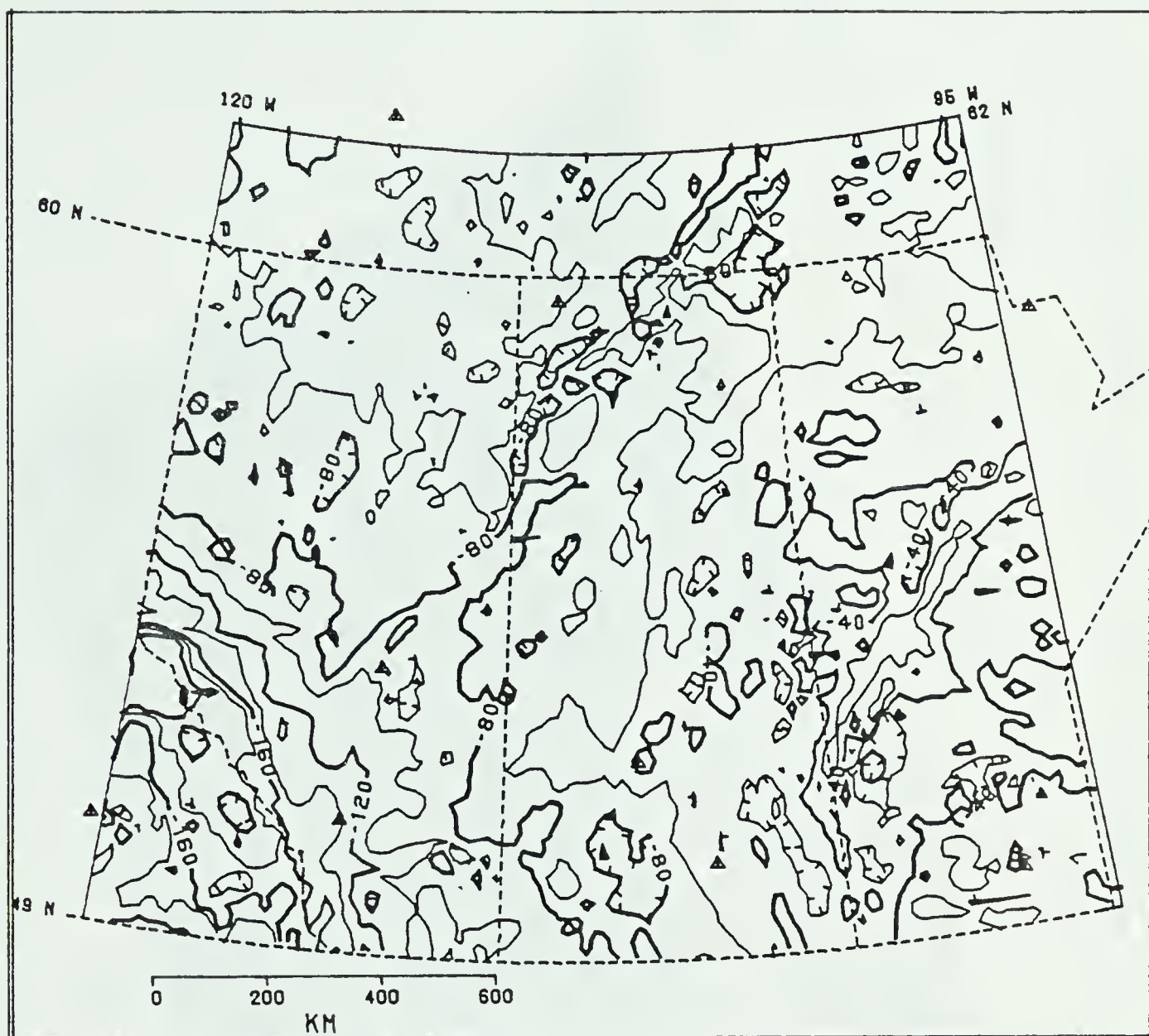


Figure 3.2a. Bouguer gravity anomaly for the interior of western Canada. Wavelengths shorter than about 15 km have been removed. The contour interval is 20 milligal.

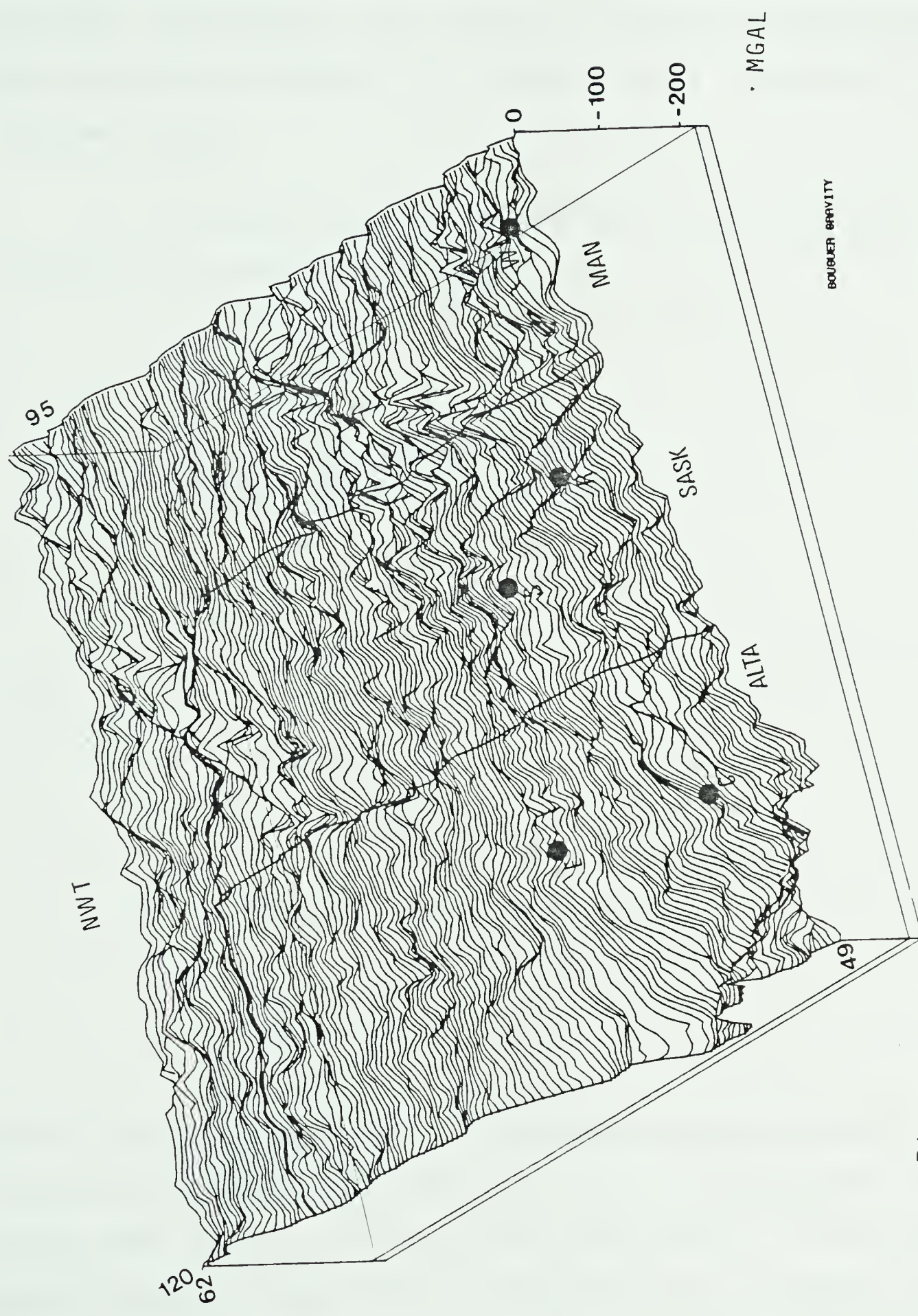


Figure 3.2b. A perspective view of the Bouguer gravity anomaly for the interior of western Canada.

irregularly distributed data set. Of the simpler and faster methods considered, the quadratic weighted average method was found to be adequate for quantitative analysis on a regional basis.

For the quadratic weighted method, the interpolation function is written as follows

$$f(x,y) = \frac{\sum_{i=1}^N w_i(x,y) G_i(x_i,y_i)}{\sum_{i=1}^N w_i(x,y)} \quad [46]$$

where

$$w_i(x,y) = \frac{1}{x_i^2 + y_i^2} \quad [47]$$

and x_i, y_i are original data locations relative to point x, y ; x, y are grid point locations, $g(x_i, y_i)$ is the original data set; and $f(x, y)$ is the interpolated result. This widely used method (McDougal, 1976) is based on the premises that the value at the grid point should not be greatly different

from values at nearby data points and that more consideration should be given to nearby points than to remote ones.

For most of the map area, a routine simply searched for the five nearest stations to each grid point, and then interpolated a value for the grid point taking into account the distances to and the values of the surrounding five points. Some special cases did occur at various locations on the grid which required special handling, however. At unusually well surveyed areas where two or more stations occurred closer than 3.9 km (one half the sampling interval) to the grid point, the values and locations of these stations were averaged together prior to interpolation. This procedure eliminated potential aliasing errors. Also, for unusually sparsely surveyed areas, such as in the mountains and across unsurveyed lakes, the stations utilized in the interpolation were carefully chosen to insure that the grid point was adequately surrounded by sufficient data on all sides to yield a reasonable interpolated value. For grid points outside the map area, a cosine taper was applied to reduce the gravity values smoothly and gradually to zero at the edges of the grid. This procedure insured that no short wavelength noise was artificially introduced at the boundaries of the map area.

In order to check for errors, line printer maps were produced on a scale of 1:500,000 for every 2° by 2°

subdivision of the map area showing both original stations and interpolated values at grid points. These maps were then compared visually with published contoured gravity maps of the 1:500,000 Gravity Map Series produced by the Dominion Observatory and more recently by the Earth Physics Branch. Some care must be exercised in comparing gravity data on the new absolute system (as used in this study and on all Canadian government maps since 1974) with pre-1974 maps on the old National Gravity Net since a latitude dependent shift has taken place. For the map area of this study, this shift is from 6 to 8 mgal in amplitude.

In order to produce smaller grid sizes for computational purposes over the map area, it was necessary to prefilter out short wavelengths to avoid aliasing errors. The impulse response of the radially symmetric low pass filter used for this purpose is as follows

$$f(r) = \int_{k=-k_H}^{k_H} \exp(-ikr) \delta k = 2 k_H \frac{\sin(r k_H)}{r k_H} \quad [48]$$

where k_H is the cut off wave number and r is the radial distance from the origin of the filter response. The above impulse response is real and even, as is its frequency

response. In order to produce a practical filter, the impulse response was shortened by a cosine taper of the form

$$C(r) = 0.5 [1 + \cos(\pi r/R_{\max})]$$

$$C(r) = 0 \quad r > R_{\max}$$
[49]

where R_{\max} is the desired maximum length of the filter (Fuller, 1966).

For the gravity data, it was desired to repeatably reduce the size of the gravity grid by two. Hence the cut off wave number was set at 1.57 data interval (equivalent to a spatial frequency of 0.25 cycles per data interval which is one half of the Nyquist frequency). The filter length was set at 7 data intervals. A computer program which calculates the filter coefficients, and simultaneously applies the filter and reduces the data using a two dimensional convolution is shown in Appendix D. Alternately and equivalently, filtering could have been accomplished in the wave number domain.

It is interesting to compare the smoothed Bouguer map of this study (Figure 3.2) with the western portion of the Bouguer Anomaly Map of Canada (Department of Energy, Mines, and Resources, 1974). Both of the maps have been smoothed

to the same degree, but by different techniques. The similarity in anomaly pattern is expected in that both maps are based on precisely the same data. The source of any difference lies in processing technique only. In this study, processing involved quadratic weighting interpolation, Fourier filtering and SURFACE II contouring, whereas different smoothing packages were used for the published map.

The anomalies apparent in Figure 3.2 are related to gradual lateral variations in subsurface density structure. However, these regional anomalies are not necessarily of deep seated origin. As will be shown later, for example, the western Canada sedimentary basin has a pronounced affect on this Bouguer field. The values on the Bouguer anomaly map are all negative as is typical for continental regions (Garland, 1965, p. 90).

3.1.3 CORRECTION FOR SEDIMENTARY ROCK

In this study, the focal point is structure of the entire lithosphere, hence it is desirable to remove the effect of the relatively well known western Canada sedimentary basin from the gravity data. This involves a correction for any sediments below sea level as well as an alteration to the Bouguer correction for cover above sea level. Technically, the Bouguer gravity, or more properly,

the Bouguer anomaly, is supposed to be calculated using the average density of the material between sea level and the station elevation in the gravity reductions. However, it is the policy of the Earth Physics Branch to utilize a standard density of 2670 kg/m^3 rather than local density estimates. While 2670 kg/m^3 is an excellent value over the crystalline shield, it is far too high over the plains which are underlain by sedimentary rock.

In an extensive study of over 240,000 metres of density logs in western Canada, Maxant (1975) obtained an average general regression line for the entire sedimentary basin of

$$d = 2266 + 146 h \pm 210 \quad [50]$$

where d is sediment density in kg/m^3 and h is depth below the surface in km. Walcott and Boyd (1971) obtained a near surface density of 2200 plus or minus 50 kg/m^3 at Peace River using a density profile. Their value is reasonably congruent with the first term in Maxant's formula.

Using data from elevation and isopach maps, the average elevation of that portion of western Canada underlain by sediment was calculated to be 0.48 km above sea level. By

substituting into the above formula, the average density of above sea level sediments in the western Canada basin is approximately 2300 kg/m^3 , a value in perfect agreement with the overall average for above sea level sediment given by Maxant (1975) in his study of logs.

The density functions utilized in this study to compute a gravity correction for the sediments are shown in Figure 3.3. For above sea level cover, Maxant's regression equation was used. For sedimentary rock below sea level, Maxant's (1975) average of 2500 kg/m^3 was assumed.

The thickness of sedimentary rock above sea level was obtained by comparing smoothed elevations across the map-area with a smoothed estimate of sedimentary cover thickness (Figure 3.4). This cover thickness map is based mostly on data published in the *GEOLOGICAL ATLAS OF WESTERN CANADA*. The cover thickness map is quite smooth and no doubt misses many local features. For purposes of this study, no sedimentary cover is assumed to exist west of the Rocky Mountain trench mainly due to the scarcity of quantitative information on thickness of sedimentary rocks in the Cordillera. The cover thickness in the western foothills is also generally unknown and here it is assumed that the density of the cover tapers gradually to 2670 kg/m^3 west of the foothills. This is a gross simplification but no other information is available. In the Cordillera, much of the sedimentary rock tends to be metamorphosed, hence the

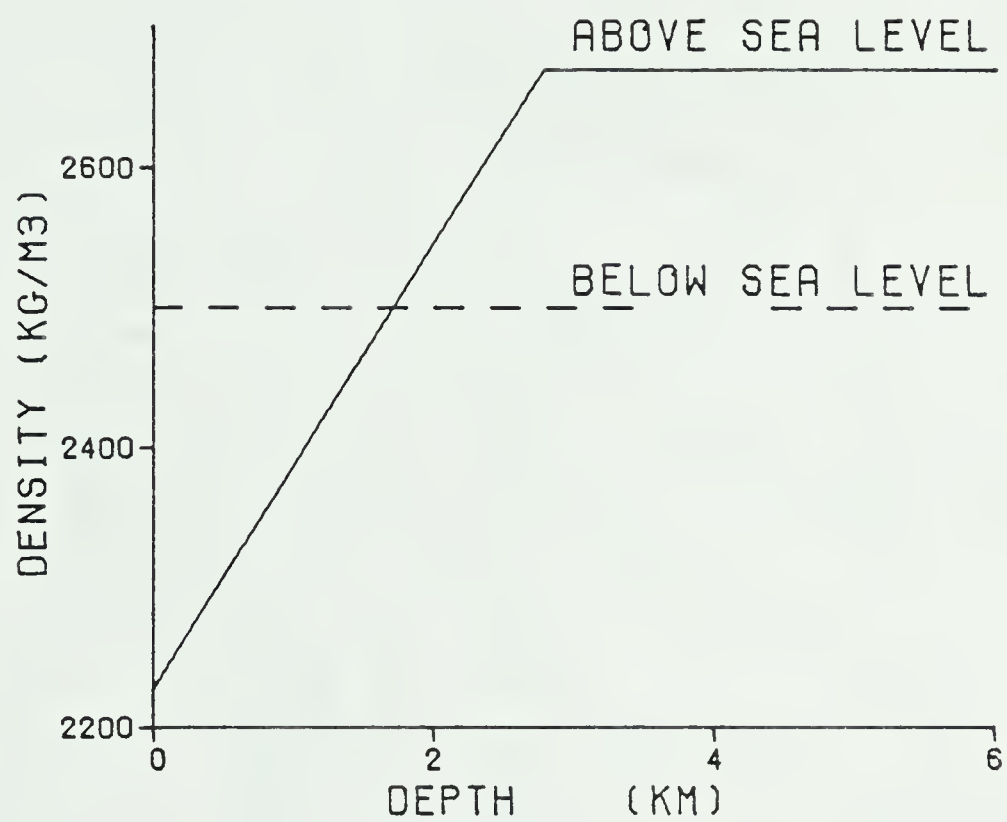


Figure 3.3. The density functions utilized for the sedimentary basin correction.

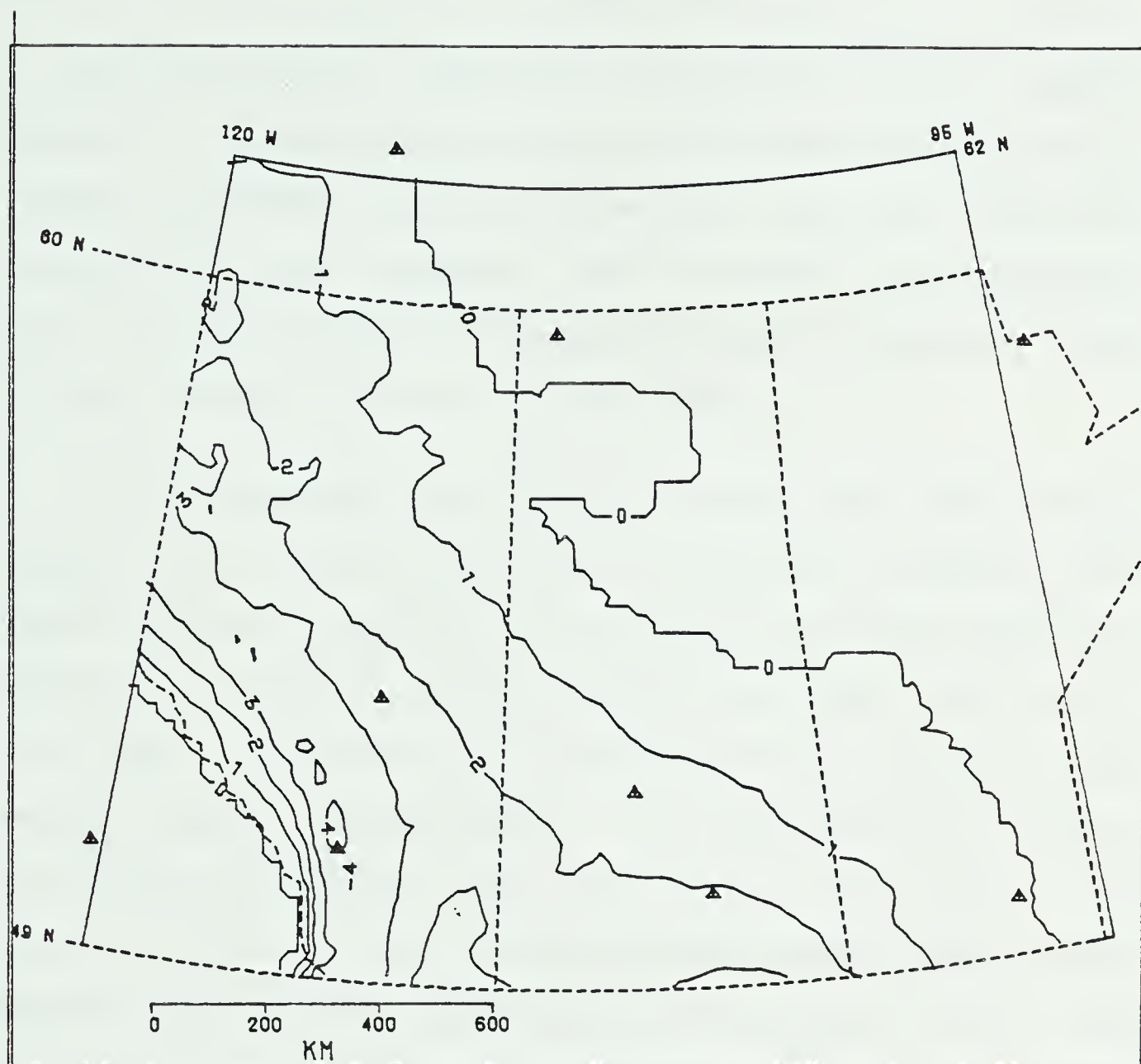


Figure 3.4. A smoothed map of cover thickness in the western Canada basin. The contour interval is 1 km. The small triangles represent major cities within the map-area.

density of 2670 kg/m^3 already incorporated in the gravity data is probably a reasonable estimate.

By utilizing a smoothed topographic map of western Canada for surface elevations and the cover thickness map, a gravity correction for the sedimentary cover was calculated using the simple Bouguer slab formula. The sedimentary basin correction can be quite significant, reaching a value of about 30 mgal over much of the basin.

The correction as computed here does not include compensation for possible local variations in density other than the general increase with sediment thickness toward the mountains. However, Maxant (1975) has noted severe lateral variations in sediment densities based on a study of many density logs. Unfortunately, the distribution of wells available to Maxant was far from random, his spatial maps are badly aliased, and little coherence can be noted between Maxant's density maps and the observed gravity field. Hence no attempt was made to incorporate the local density variations found by Maxant in the sedimentary correction.. However one must keep in mind that many of the anomalies (even those of fairly long wavelength) present on the gravity map of the plains are no doubt due to large lateral density variations within the sedimentary cover.

3.1.4 FINAL CORRECTED GRAVITY MAP

A smoothed gravity anomaly map of the interior of western Canada after correction for the effect of the sedimentary basin is shown in Figures 3.5a and 3.5b. It is worthwhile to compare this map with the original Bouguer map in Figure 3.2. The gravity over the sedimentary basin has been generally raised but the main features of the original map remain.

A highly smoothed version of the corrected gravity over the same map-area is shown in Figures 3.6a and 3.6b. On this map, all features in the gravity field of wavelength shorter than about 60 km have been filtered out. This data set is useful for studies of the deep crust and mantle.

3.1.5 SIMPLE INVERSIONS

To further evaluate the use of the Parker algorithm, the corrected Bouguer anomaly in western Canada was inverted under various different assumptions to yield simple crustal models. Since these models are based only on gravity without reference to other types of data, they are quite hypothetical. However they do tend to illustrate the use of the inverse algorithm as well as to point out some interesting aspects of crustal structure in western Canada. The assumptions used and the crustal models obtained are discussed in Appendix B. Some of the conclusions reached are given below.

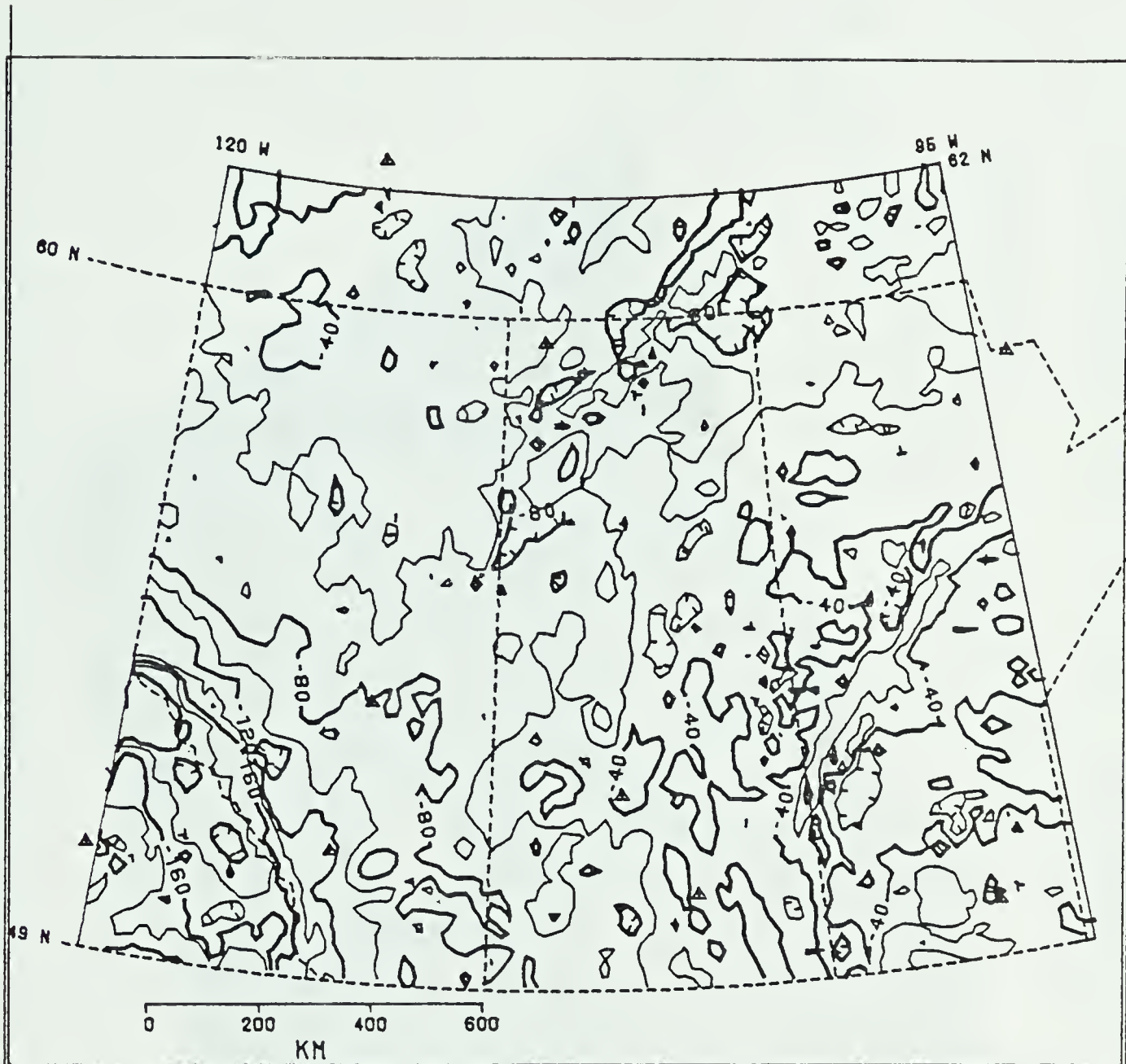


Figure 3.5a. Gravity anomaly map of western Canada after correction for the sedimentary basin. Wavelengths shorter than about 30 km have been removed. The contour interval is 20 milligal.

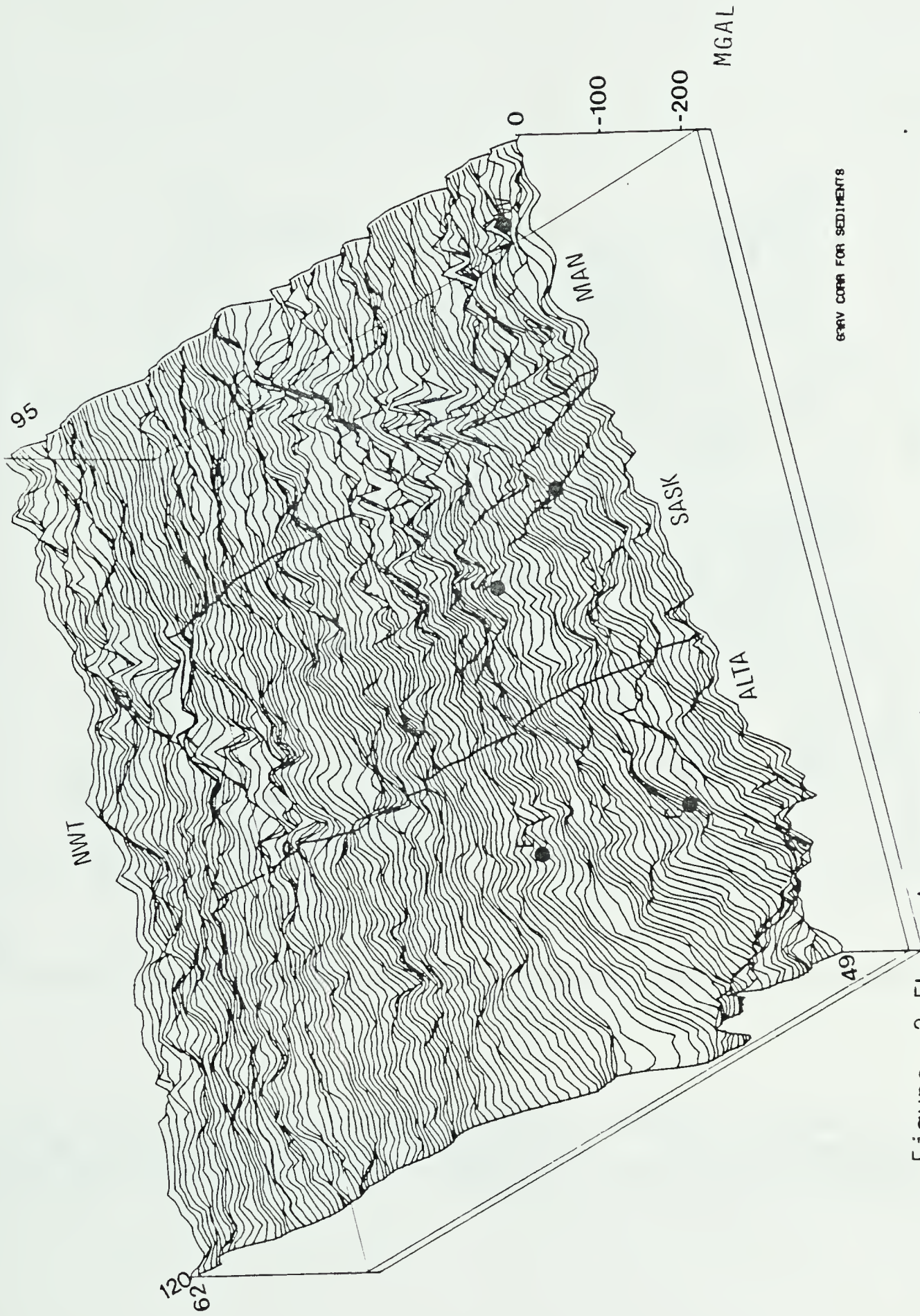


Figure 3.5b. A perspective view of the gravity map of western Canada after correction for the sedimentary basin.

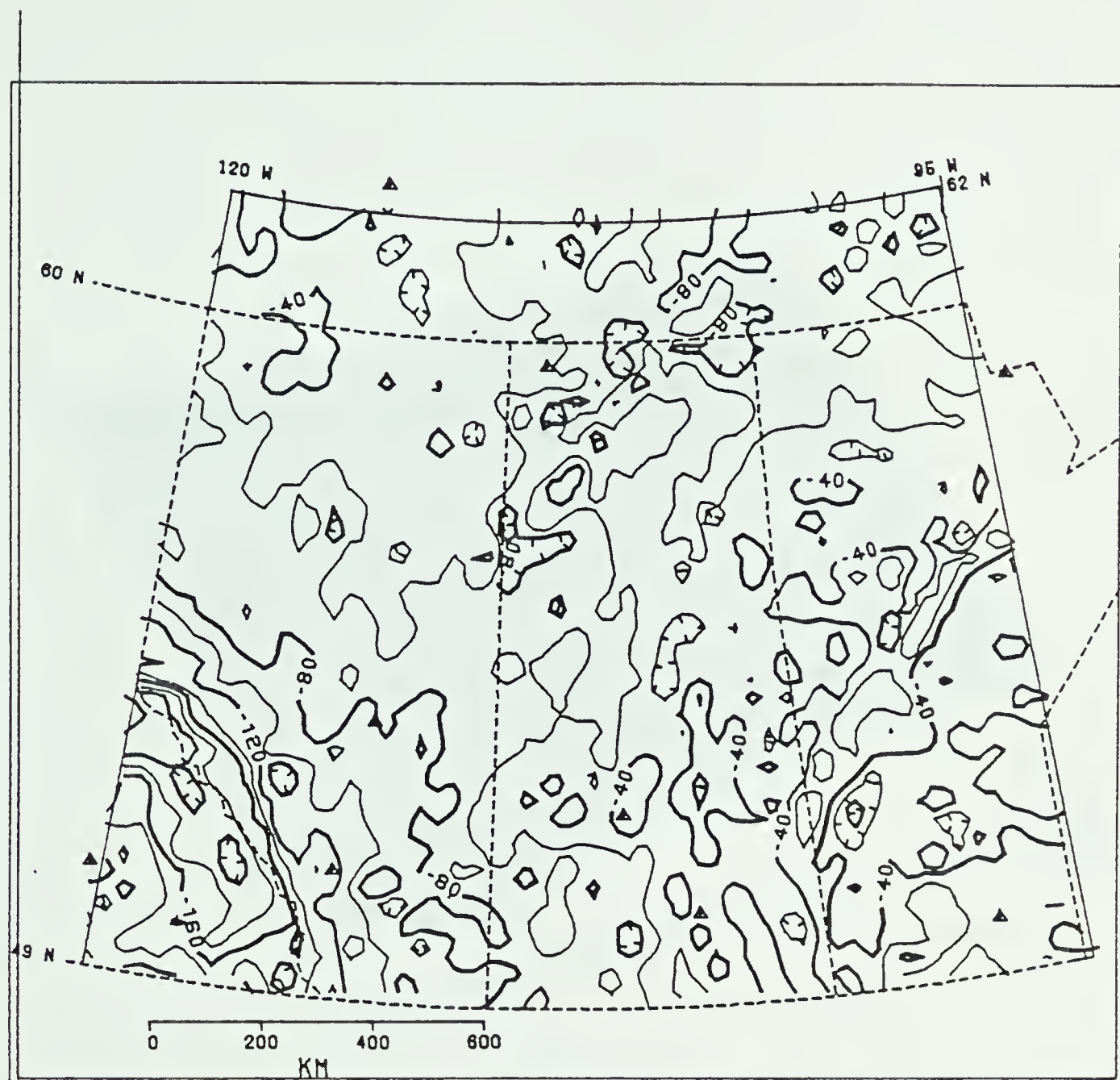


Figure 3.6a. Gravity anomaly map of western Canada after correction for the sedimentary basin. Wavelengths shorter than about 60 km have been removed. The contour interval is 20 mgal.

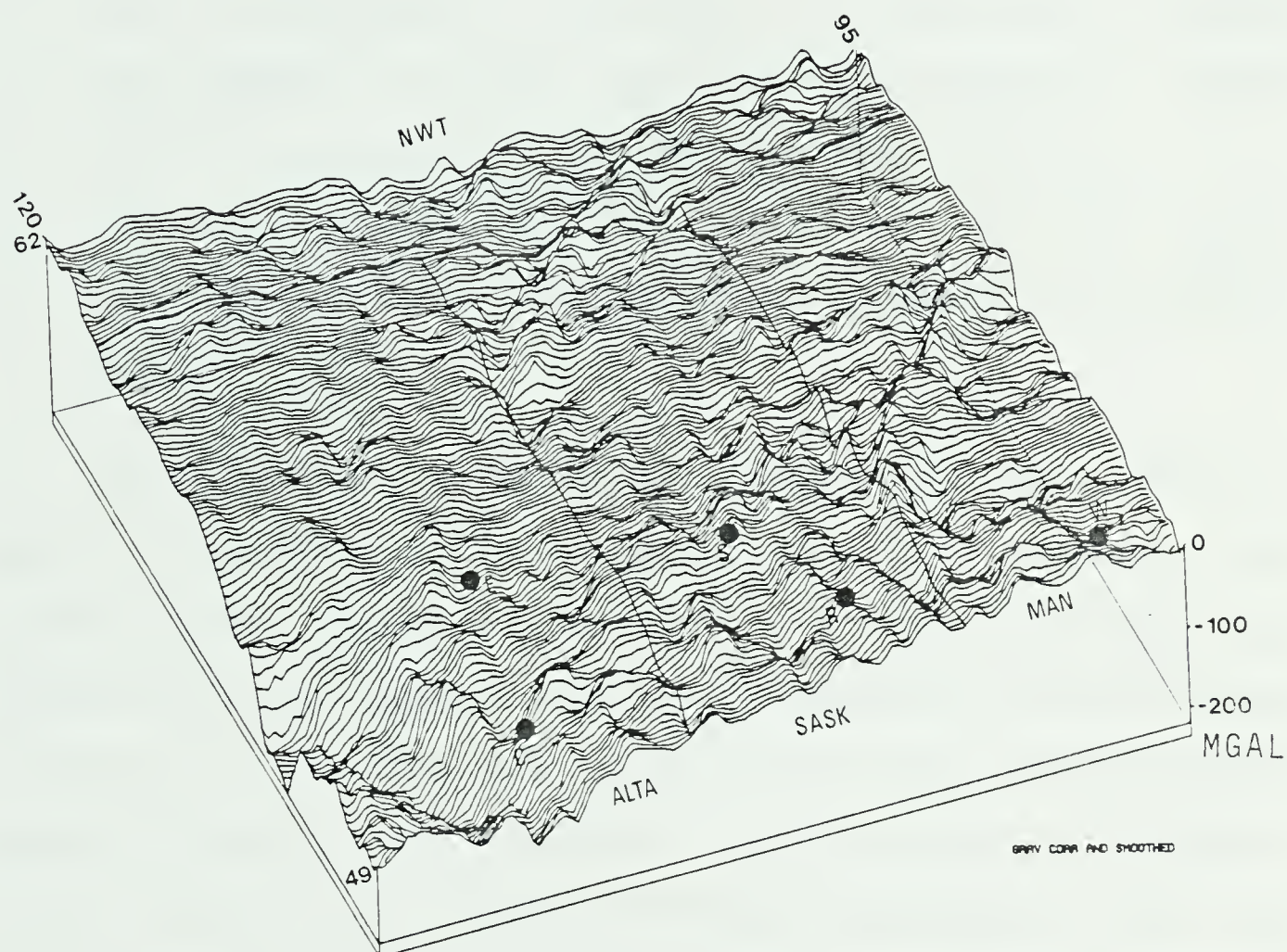


Figure 3.6b. perspective view of the gravity anomaly of western Canada after correction for the sedimentary cover and after further smoothing. Wavelengths shorter than about 60 km have been filtered out. The large dots are major cities within the map-area.

For models consisting of constant thickness lithospheric slabs with laterally varied density, the following points are evident:

1. Overall density variations greater than about 200 kg/m^3 are not expected in the crust from one lateral location to another. In fact, away from the mountains, crustal density variations over 40 kg/m^3 are unlikely.
2. Overall lateral density variations in the mantle portion of the lithosphere are probably less than 120 kg/m^3 .

Most models of the crust consider the Moho surface to more or less mirror the Bouguer anomaly. However, this simple idea can be interpreted in at least five basic ways depending on the geometry of the intermediate crustal layers (Figure B.2, Appendix B). Since these five types of crustal model differ greatly in vertical distribution of density, they produce considerably different topographic amplitudes on the Moho surface upon inversion by the Parker-Oldenburg algorithm (Figure B.3, Appendix B). As more of the anomalous density contrast is shifted up into the crust, less relief is required on the Moho surface to explain the gravity anomaly present.

No attempt has been made to incorporate specific seismic results from across western Canada in the above models. They are based only on the gravity field. As will be shown later, these models generally do not agree with the

known seismic data. Hence the crust must be modelled in a more complicated manner to include lateral variations in crustal densities and layer thicknesses if more realistic results are to be obtained.

3.1.6 RESIDUAL GRAVITY

All the simple crustal models obtained above were used as sources for the forward Parker algorithm and all yielded a similar result. The residual gravity which is the difference between the original gravity anomaly and the gravity anomaly due to the derived structure is thus dependent solely on the choice of the filter which was the same for all the models. However, since the choice of the filter in this study is based on actual examination of the spectra, there is validity in interpreting the residual gravity anomaly in terms of sources somewhere above the reference plane. The residual gravity for these models is shown in Figures 3.7a and 3.7b. The multitudinous anomalies here are all due to some variation in crustal density. Since the original data for this study was presmoothed, the anomalies shown on the residual gravity map are not very useful for further study since much of their character has been filtered out. Some of the anomalies have been previously interpreted. For example, the deep Precambrian rift in southern Alberta as discovered by Kanasewich et. al. (1969) shows up quite well as a long sinuous gravity low.

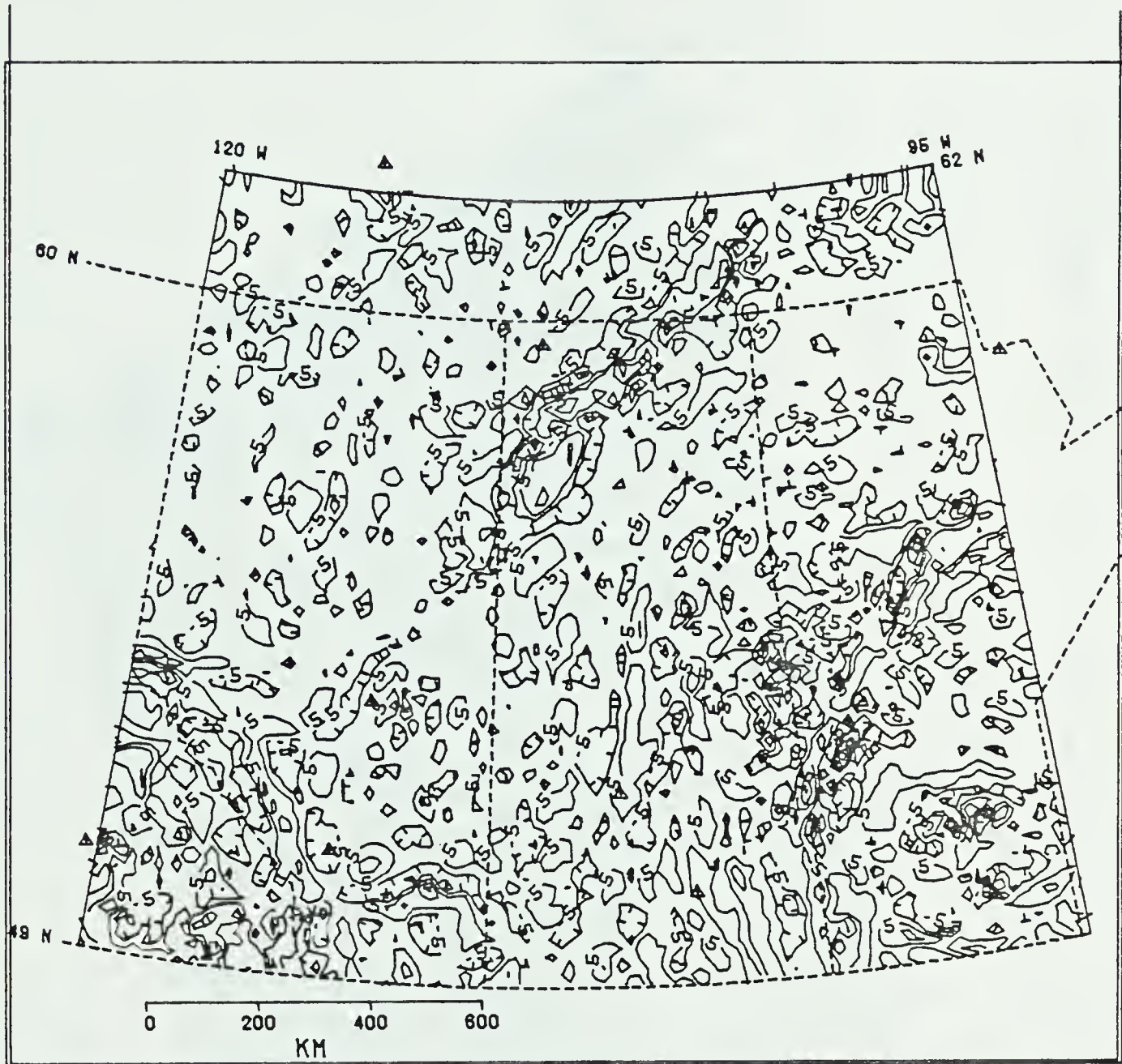


Figure 3.7a. Residual gravity in western Canada. The contour interval is 10 km. These anomalies of wavelength from 30 to 90 km are probably due to lateral density variations within the crust.



Figure 3.7b. A perspective view of the residual gravity in western Canada.

The SW-NE trending central belt anomalies of northern Saskatchewan (Walcott, 1968) are seen to continue southeast to the foothills (and possibly beyond since gravity coverage in the Cordillera is poor) and northeast to at least the edge of the map-area. Short wavelength gravity anomalies associated with the Nelson front dominate the southeast portion of the map-area.

3.2 GRAVITY INVERSION AND ISOSTASY

3.2.1 MASS COMPENSATION

It is apparent that much of the change in Bouguer values across the interior of western Canada is due to the effect of deep seated masses compensating the apparent excess surface mass due to physiographic changes. In order to study other effects on the field, it is necessary to remove the effect of compensation by calculating an isostatic correction. A true isostatic correction is a very laborious task in that it involves the estimation of topographic height in zones extending right to the antipodes of the station. In this study, only data from within the map-area is considered. Hence, the "isostatic correction" determined here should not be considered as valid from a geodetic point of view. However, while distant topography is significant, its effect should tend to be quite smooth over the map-area, and the character of the resulting

anomaly should be little affected.

Two traditional methods were used in this study to obtain the "isostatic" correction. In the first, it is assumed that the excess surface mass is compensated by roots of crustal material as suggested by Airy in 1855. Using 33 km as the depth of the standard crust, a crust-mantle density difference of 500 kg/m^3 , and the elevation data, the Airy correction was calculated by the Parker algorithm and applied to the Bouguer anomaly map. The resulting Airy anomaly map as well as the Airy crustal model are shown in Figures 3.8a and 3.8b.

The second method used was based on the idea of Pratt in 1859 that compensation is due to lateral variations of density in a lithosphere of constant sub-sea level thickness. Using a compensation thickness of 113 km and the elevation data, the Pratt correction was calculated using the variable density slab algorithm discussed in Chapter 2. The resulting Pratt anomaly map is given in Figure 3.9.

The Airy correction tends to be consistently higher than the Pratt correction throughout the map-area. This is probably due to the rather shallow depth of compensation (33 km) utilized for the Airy correction. The difference between the two is only about 4 mgal over the plains. The Cordillera was not included in this analysis due to the lack of sufficient gravity and elevation control.

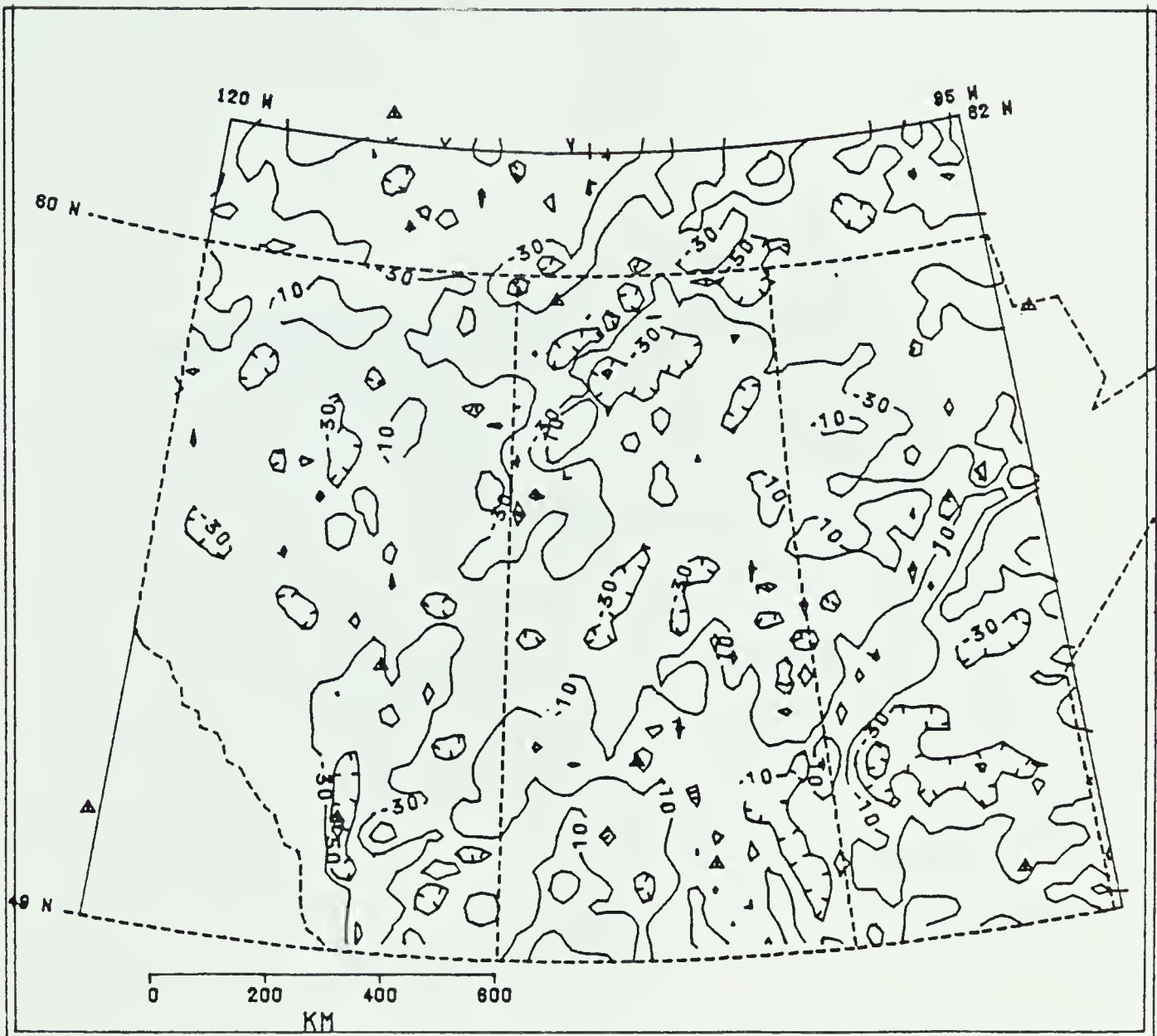


Figure 3.8a.. Airy anomaly map of western Canada for wavelengths greater than 60 km. The contour interval is 20 milligal. There was not sufficient data to include the Cordillera in this analysis.

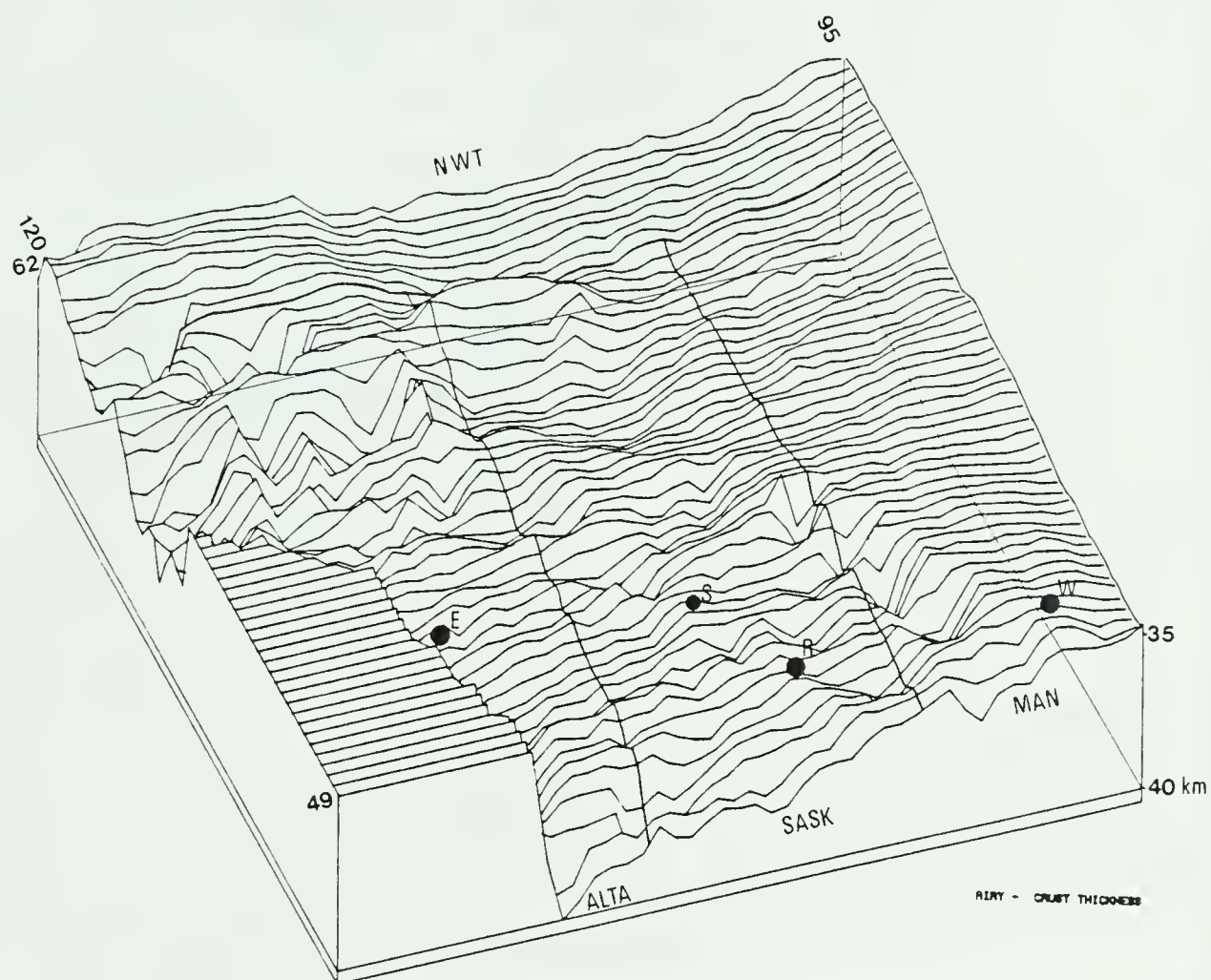


Figure 3.8b. The crustal thickness in western Canada according to the Airy hypothesis in which the mass per unit area above sea level is balanced by an equivalent mass deficiency per unit area at the level of the Mohorovicic discontinuity. A density contrast of 500 kg/m^3 was assumed at the base of the crust.

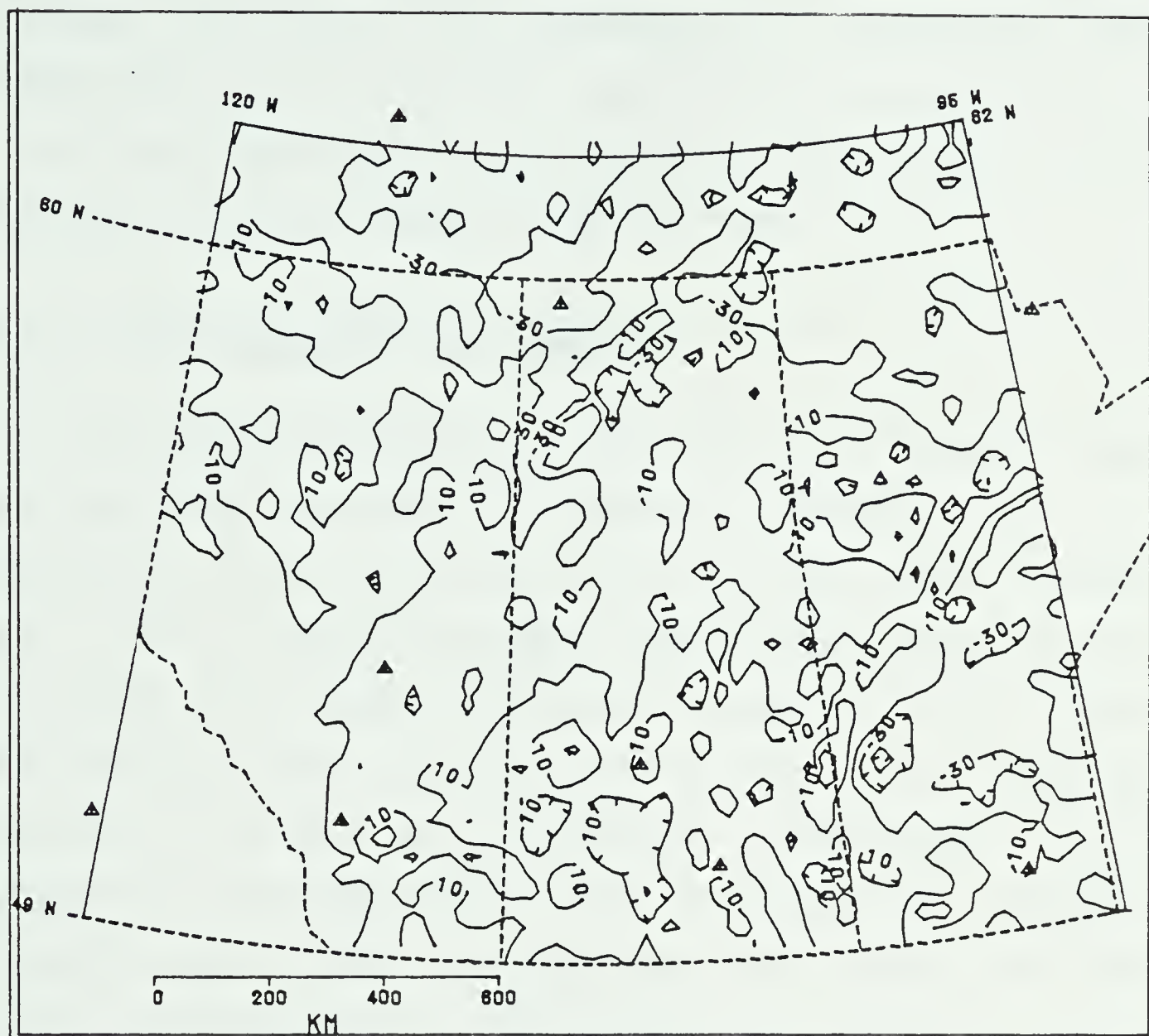


Figure 3.9. The Pratt anomaly map of western Canada for wavelengths greater than 60 km. The contour interval is 20 mg. This anomaly is computed using the density variation in the lithosphere as predicted by the Pratt hypothesis in which the mass per unit area above sea level is balanced by an equivalent mass deficiency per unit area spread evenly within a lithospheric column 113 km thick.

It is apparent from the above maps that large sections of the western Canadian shield and plains are anomalous. Although the nature of the compensation is undoubtedly more complicated than the forms suggested by Airy and Pratt, it is difficult to escape the conclusion that much of the map-area is out of isostatic equilibrium.

3.2.2 LONG WAVELENGTH AIRY ANOMALY

The long wavelength portion of the Airy anomaly over the map-area is shown in Figures 3.10a and 3.10c. All wavelengths shorter than about 1000 km have been filtered out. The filtering process used to obtain this very low wavenumber map produced rather severe edge effects. Hence one should consider only the shape of the surface toward the center of the map as significant. Nonetheless, it is evident that the amplitude of this long wavelength component is quite high in that it ranges from -30 to +9 milligals with a pronounced low in the northeast corner of the map area and a distinct high in the Canadian portion of the Williston Basin.

The trend toward a low "isostatic" anomaly in the northeast corner of the map-area suggests increasing overcompensation in that direction. A very probable explanation of this is incomplete recovery of the lithosphere from the Pleistocene ice loads (Andrews, 1968; Walcott, 1969).

If the long wavelength component of the Airy anomaly is indeed due to the former ice load, then it is possible to estimate the amount of uplift remaining from the gravity. If the lithosphere attained equilibrium under the ice load, then sufficient mantle material had to be displaced to compensate for the glacial load. If the present long wave Airy anomaly is assumed to be a direct measure of the relic glacial roots, then, on the basis of the Airy theory, a mass deficiency per unit area of $h(x,y)d(x,y)$ can be expected where $h(x,y)$ is a depression near the level of the Moho and $d(x,y)$ is the density of the mantle material displaced (Garland, 1965, p. 122). Using the Oldenburg algorithm with the long wavelength Airy anomaly as input, the remaining uplift on the base of the crust was calculated. The result is shown in Figure 3.10b. This amount of depression on the base of the crust across the map-area is somewhat in excess of 200 m in fair agreement with that as calculated by Innes (1960) whose data was based on concentric averages of the isostatic anomaly around Hudson Bay.

Some authors such as Lyustikh (1957) reject the hypothesis of post-glacial emergence, claiming that shields were being elevated long before the glacial period. In fact, Lyustikh (1960, p. 105) defines "shields" as "parts of platforms that show a constant tendency to rise." While a long wavelength negative isostatic anomaly is consistent with the idea of post-glacial uplift, such a gravity effect

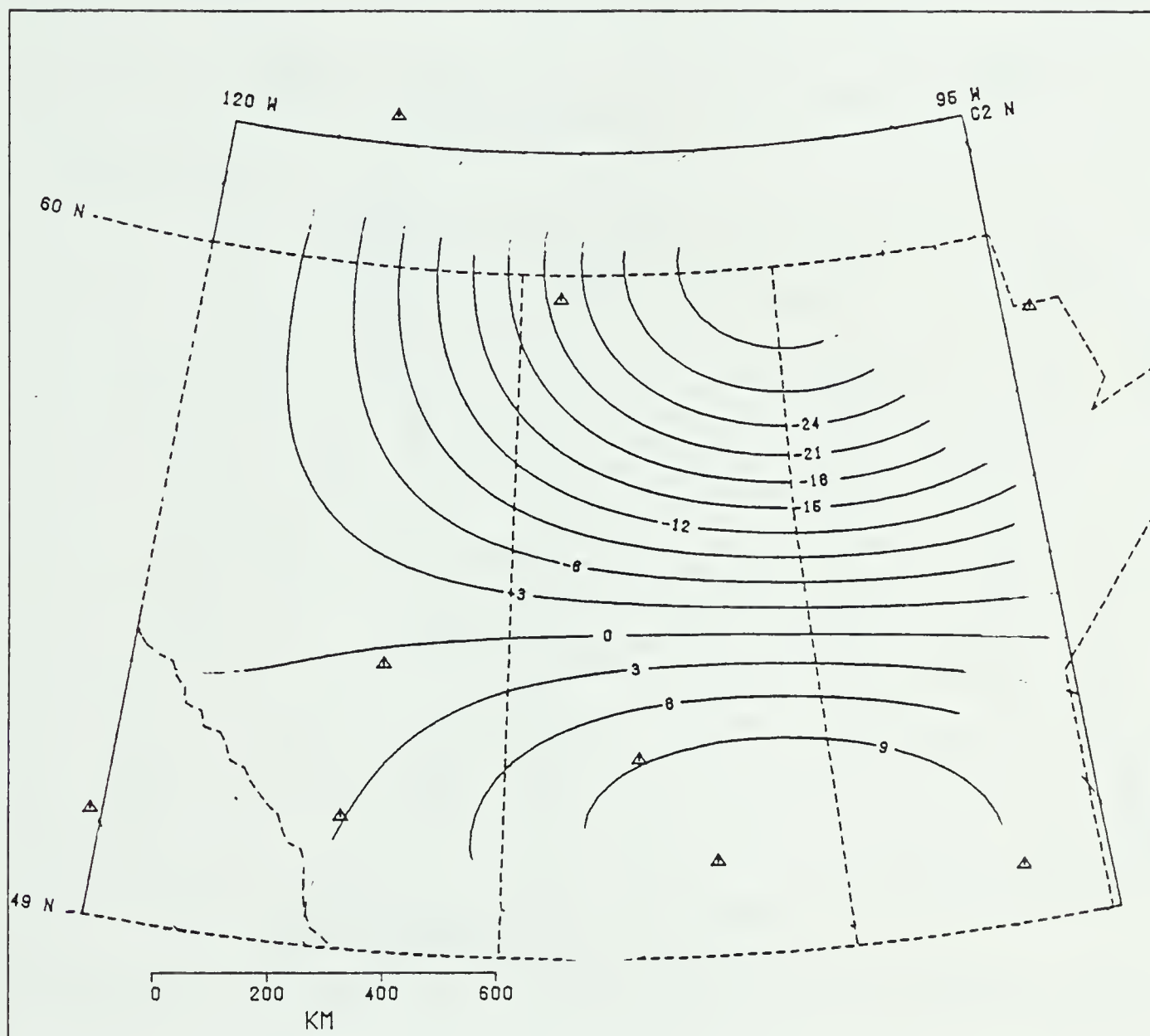


Figure 3.10a. Long wavelength Airy anomaly in western Canada. Only wavelengths greater than about 1000 km are shown. The contour interval is 3 milligal. The small triangles represent major cities within the map-area.

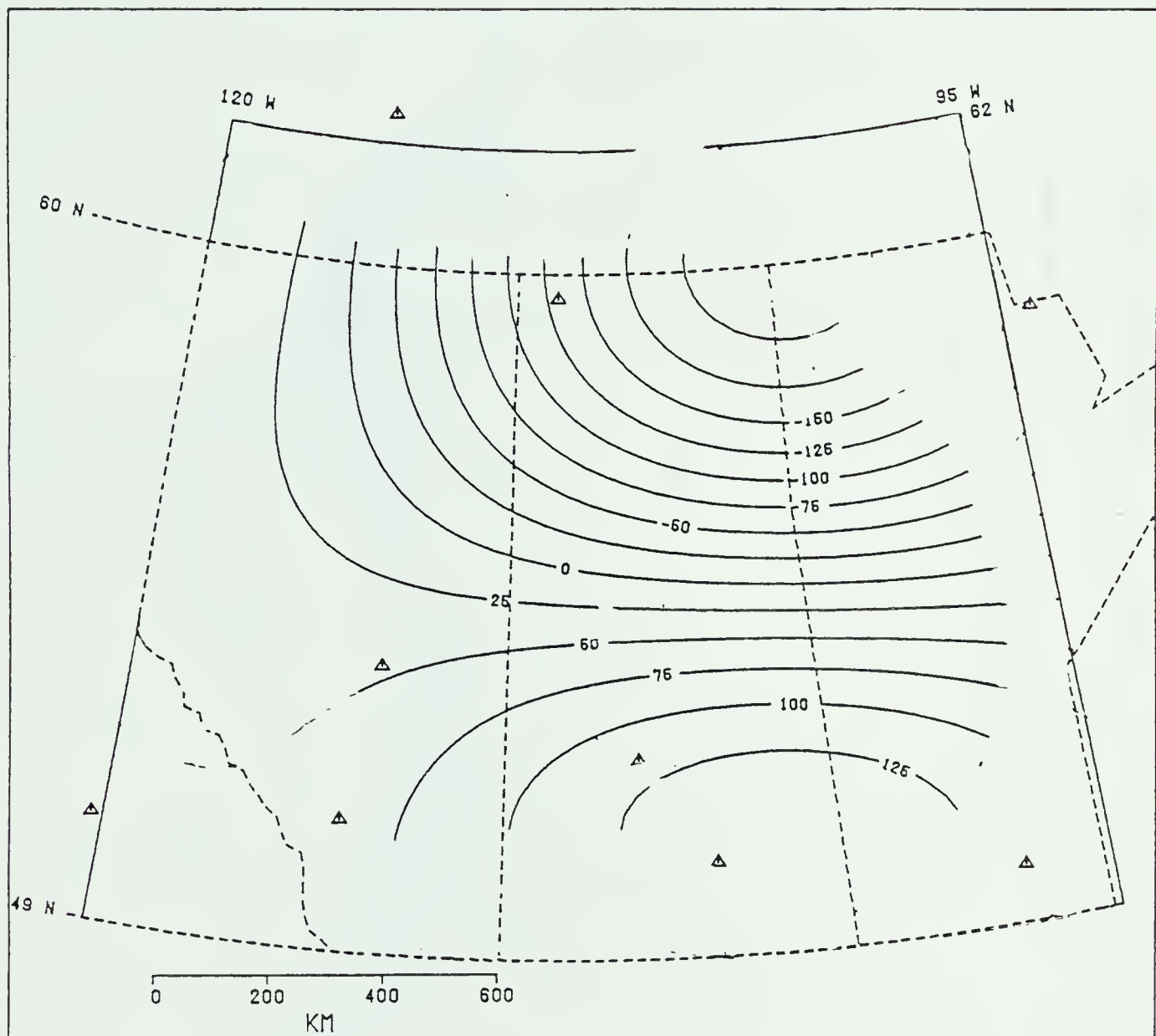


Figure 3.10b. Long wavelength component of structure on the inversion layer. The contour interval is 25m. The depression to the northeast is probably due to Pleistocene glacial loading. Hence, this map may be considered as an indicator of the remaining uplift which may be expected in the future.

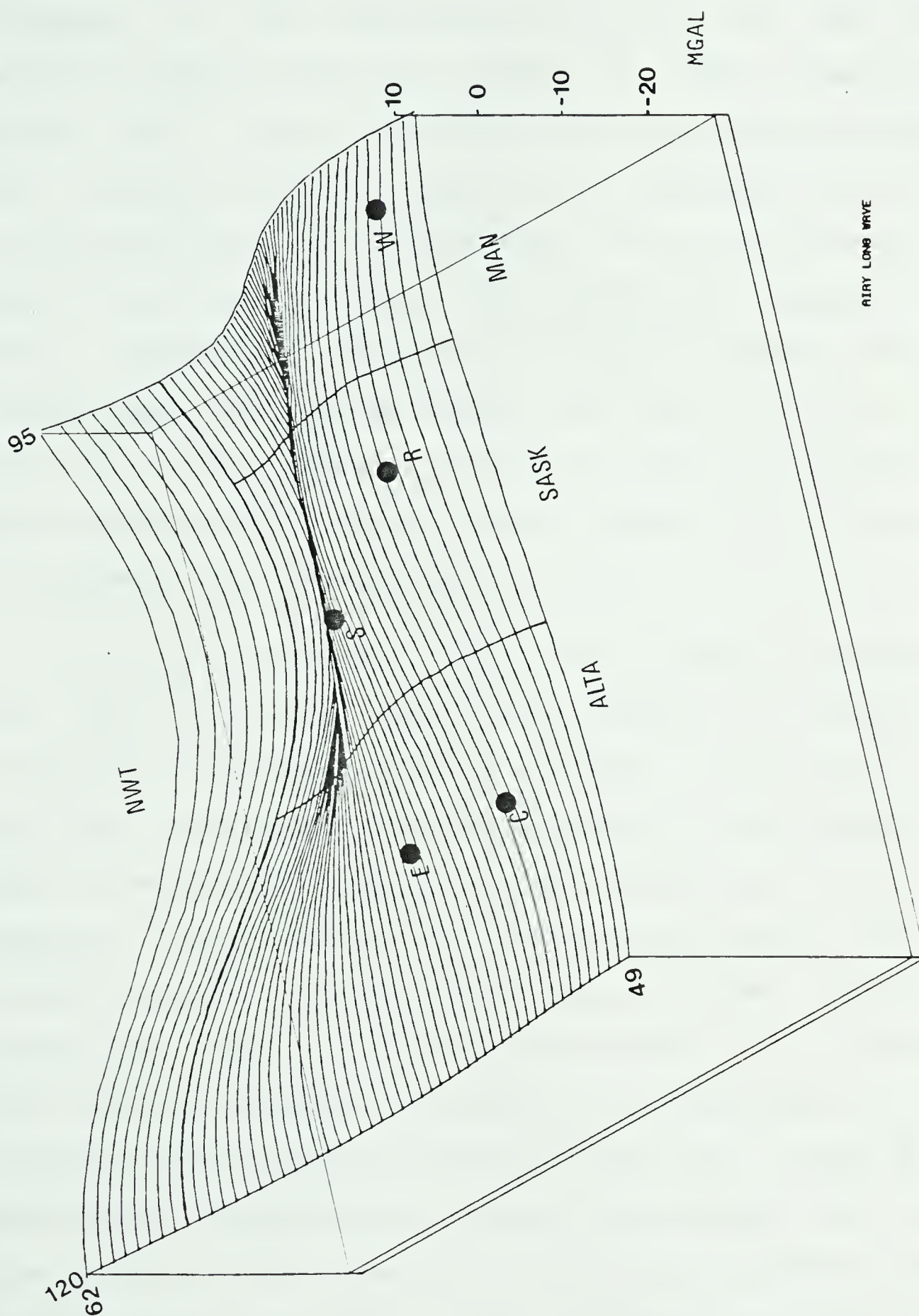


Figure 3.10c. A perspective view of the long wavelength Airy anomaly in western Canada.

can also be interpreted as being due to deep seated tectonic processes. It is interesting to note that the total magnetic intensity chart for Canada in 1975 (Dawson and Newitt, 1977) shows that the maximum very long wavelength total intensity in Canada occurs in the northeast portion of the map-area of this study over 2000 km south of the magnetic north pole. There is no reason to suggest that glacial depression could result in such a magnetic effect. Perhaps, both the long wavelength Airy trend and the long wavelength total magnetic intensity trend are related to a deep seated tectonic regime which controls the elevation variations of the Canadian Shield.

The long wavelength positive Airy anomaly associated with the Williston Basin area cannot of course be interpreted in terms of glacial loading. Nor can it be explained in terms of undercompensation for the sedimentary load in the Basin in which a very thin crust would be expected, since Kanasewich (1966) has pointed out that the thickest crust in North America occurs under geological depressions such as the Williston Basin. It is apparent that the Williston Basin is either still subsiding or that tectonic forces are maintaining the imbalance. These forces could be of a horizontal nature associated with plate interaction or of a vertical nature associated with upper mantle density variations. The Airy anomaly over this area is of a wavelength greater than 1000 km; hence, it does not

seem likely that the negative load of the basin is supported by the crust. The long wavelength also excludes the possibility that the Airy anomaly is due to the dense basement rock of the area (Burwash and Culbert, 1976) being entirely compensated by a deeper root, since in this case, unlike the case for shorter wavelengths to be discussed later, the gravity effect of the dense basement would not be significantly greater than the effect of the deeper root since both have such great lateral extent.

3.2.3 MIDDLE WAVELENGTH REGIONAL AIRY ANOMALIES

A map showing Airy anomalies of wavelengths from 500 to 1000 km is given in Figure 3.11a. Edge effects due to the filtering process for this band of wavenumbers are not so severe as in the low wavenumber map but such effects still occur. However most of the anomalies on the map seem to be significant. Theoretical stress studies suggest that these anomalies are far too great in lateral extent to be explained by masses supported by the lithosphere (Woolard, 1959; Walcott, 1969). It is therefore postulated that these anomalies are possible relics of the earth's attempt to restore isostatic equilibrium. If so, these anomalies represent fundamental divisions of the lithosphere and may indicate the nature of ancient tectonic regimes. As a test of this hypothesis, it is interesting to compare these isostatic anomalies with known geological zones in western

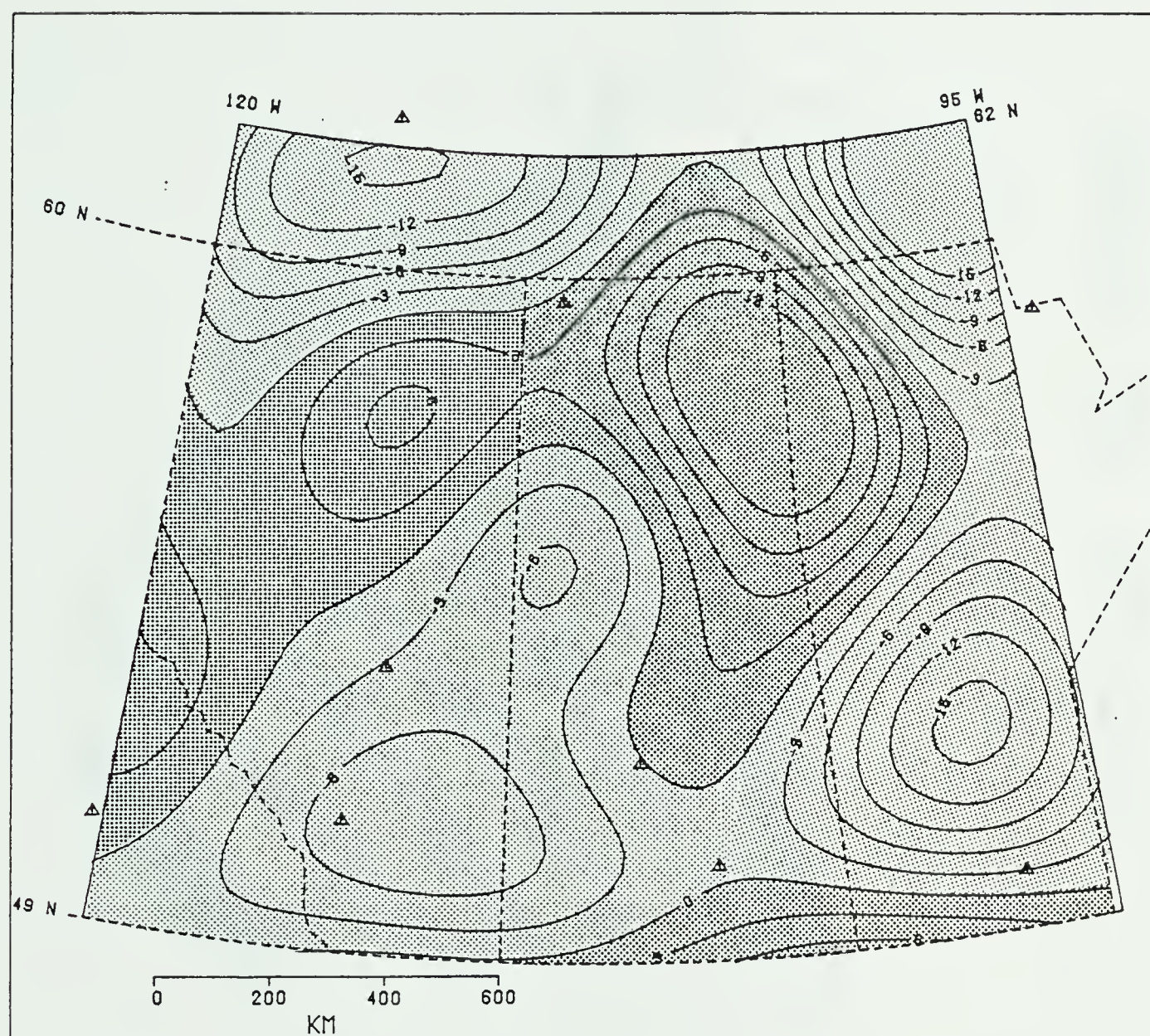


Figure 3.11a. Middle wavelength Airy anomalies in western Canada. Only anomalies with wavelengths from 500 to 1000 km are shown. The contour interval is 3 milligal. The small triangles represent major cities within the map-area.

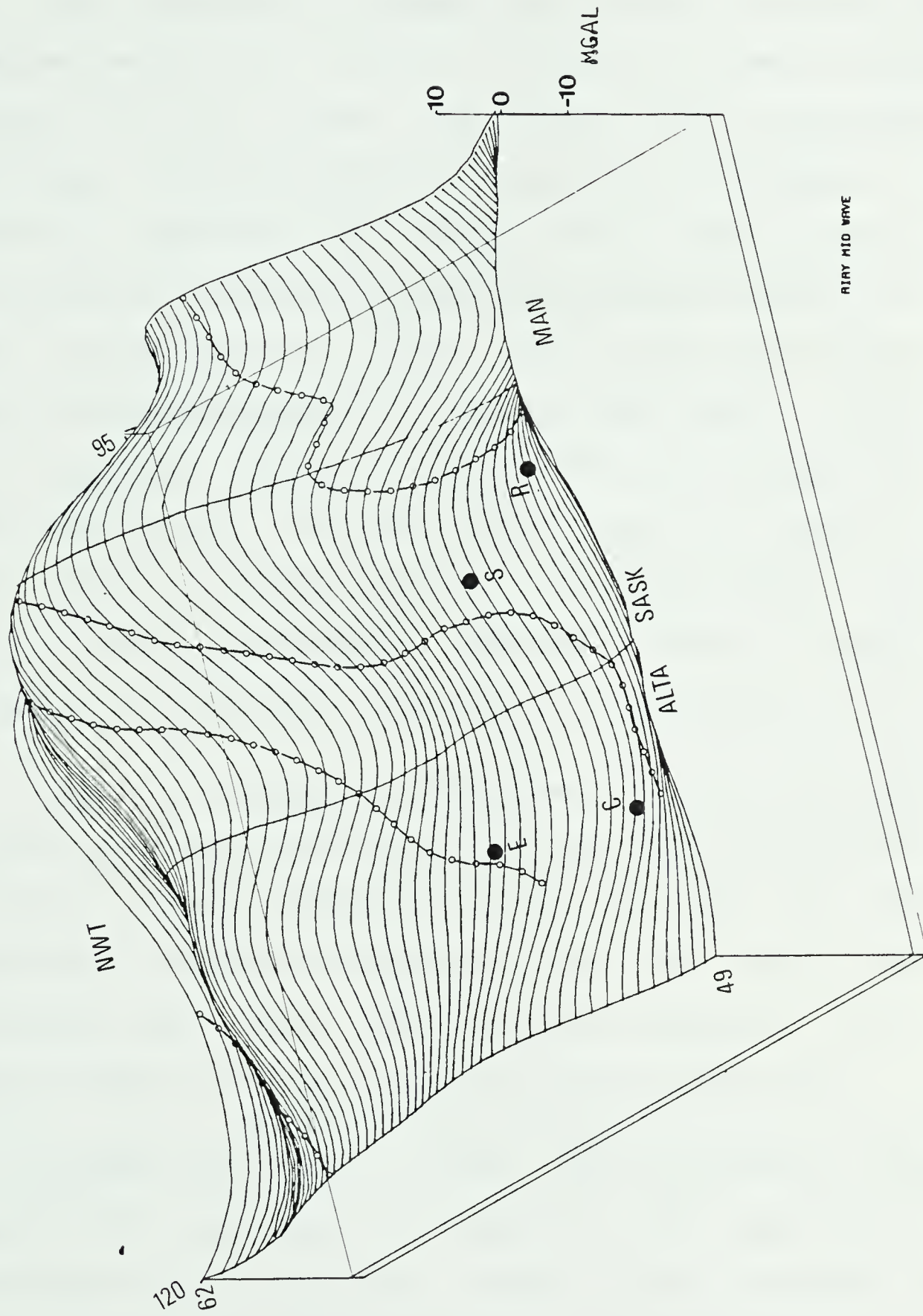


Figure 3.11b. Perspective view of the middle wavelength Airy anomalies in western Canada. Major geological boundaries are also shown.

Canada.

The Precambrian basement and shield in western Canada has been essentially divided into five divisions as shown in Figure 3.12 by Burwash and Culbert (1976) on the bases of petrology, isotope dating and geophysical information. More recently, Camfield and Gough (1977), have suggested the existence of a possible Proterozoic plate boundary in the map area as shown by a dotted line on the same figure. The four division boundaries of Burwash and Culbert (1976) and the suggested boundary of Camfield and Gough (1977) are replotted on the "isostatic" gravity map in Figures 3.11b and 3.13. A NW-SE profile of this map is shown in Figure 3.14. These fundamental lineaments seem to bear some relation to the middle frequency Airy anomalies.

Negative isostasy is indicated for the Liard block, the covered southwest portion of the Cree Lake-Calgary belt, the extreme northeast corner of the map area, and the Superior province. Positive isostatic anomalies occur over the Athabaska mobile belt, the Kiseynew-Sweetgrass belt, and the northeast portion of the Cree lake-Calgary belt.

Burwash and Culbert (1976) have performed extensive statistical analyses of much of the geological data available for the basement rocks of the western Canada basin. By considering together this geological information and the Airy anomalies, some interesting observations can be

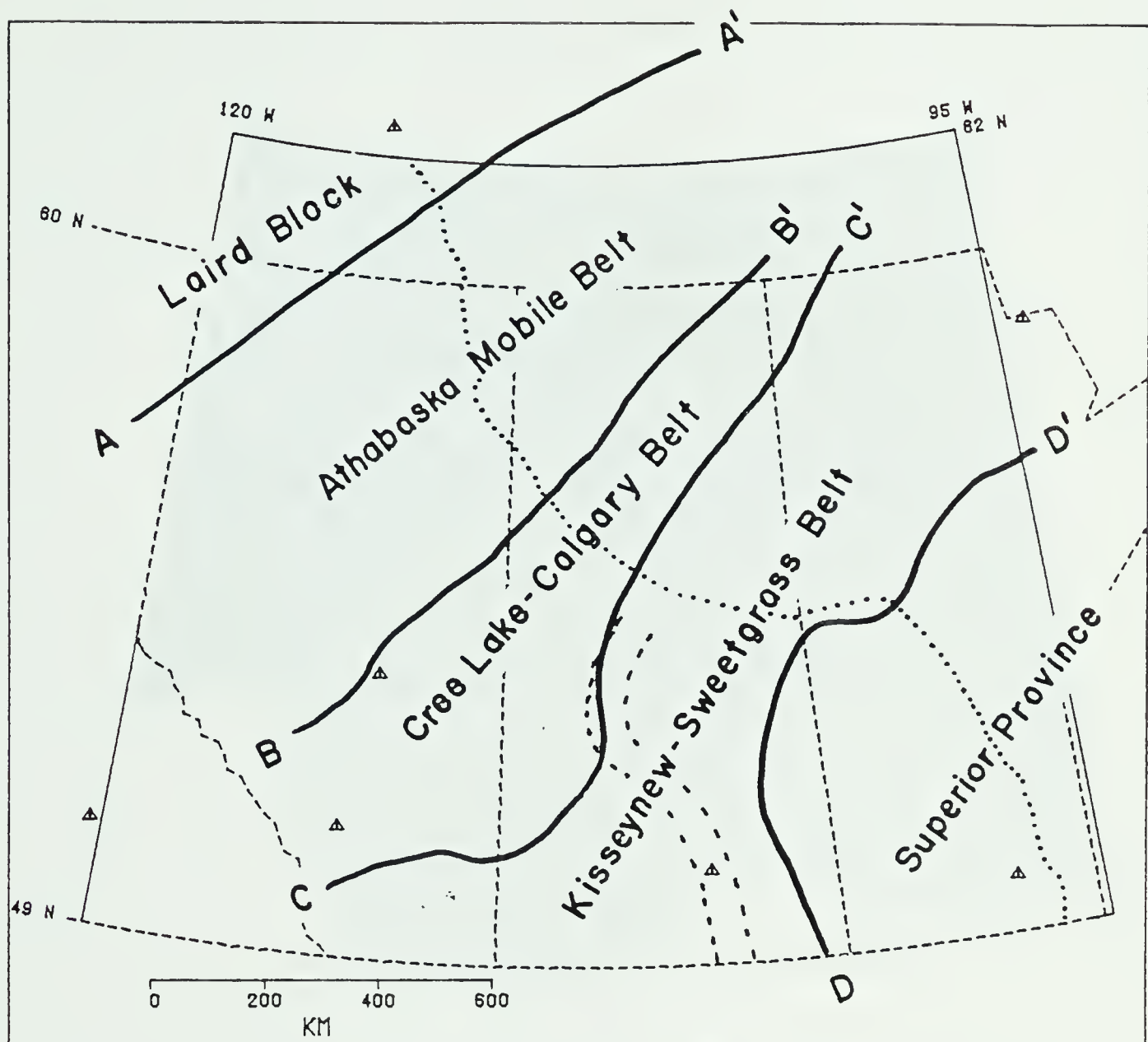


Figure 3.12. Geologic zones and boundaries in western Canada. The small triangles represent major cities within the map-area.

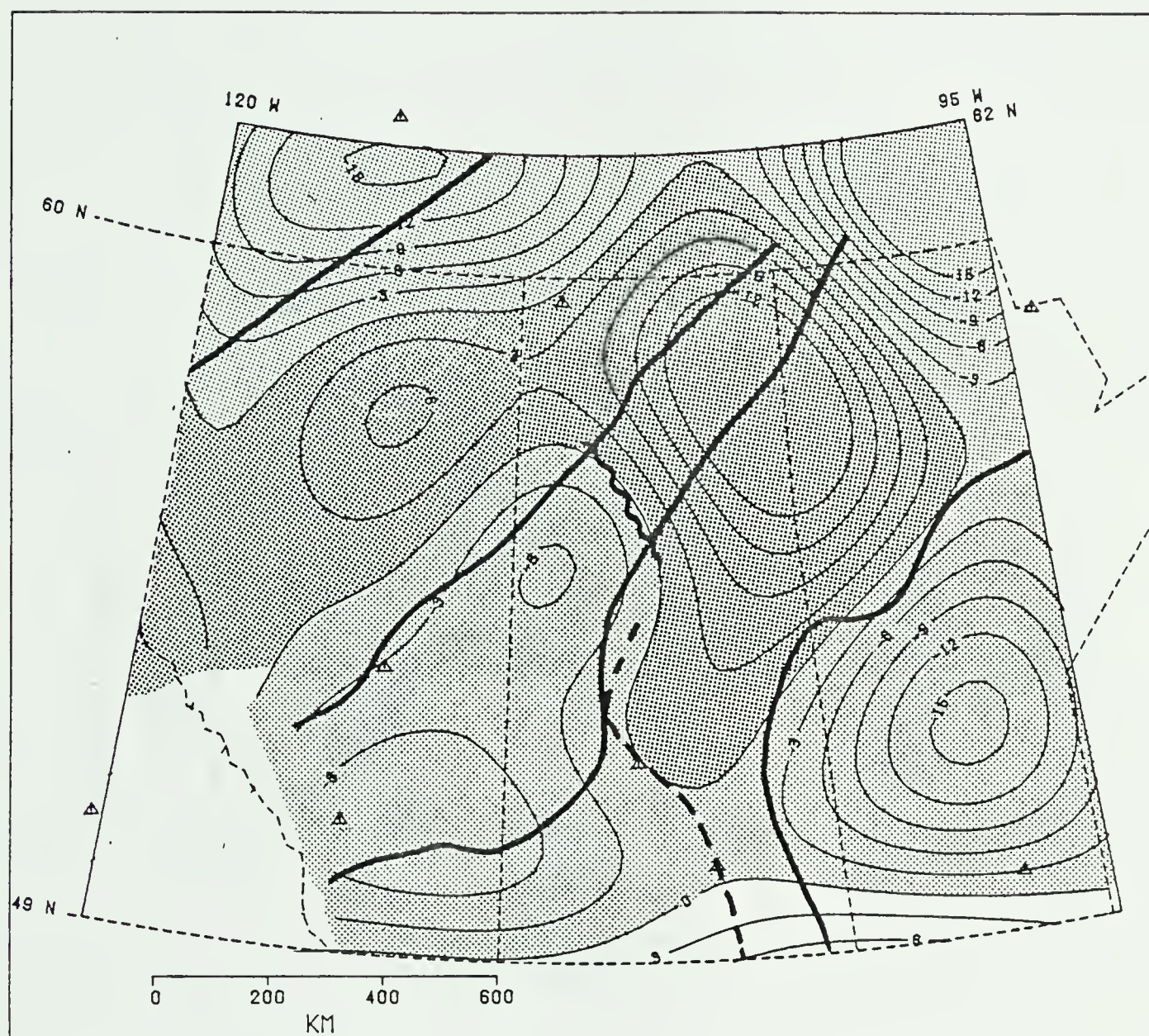


Figure 3.13. Geologic zone boundaries in western Canada plotted on the middle wavelength isostatic map. The contour interval is 3 milligal. The small triangles represent major cities within the map-area.

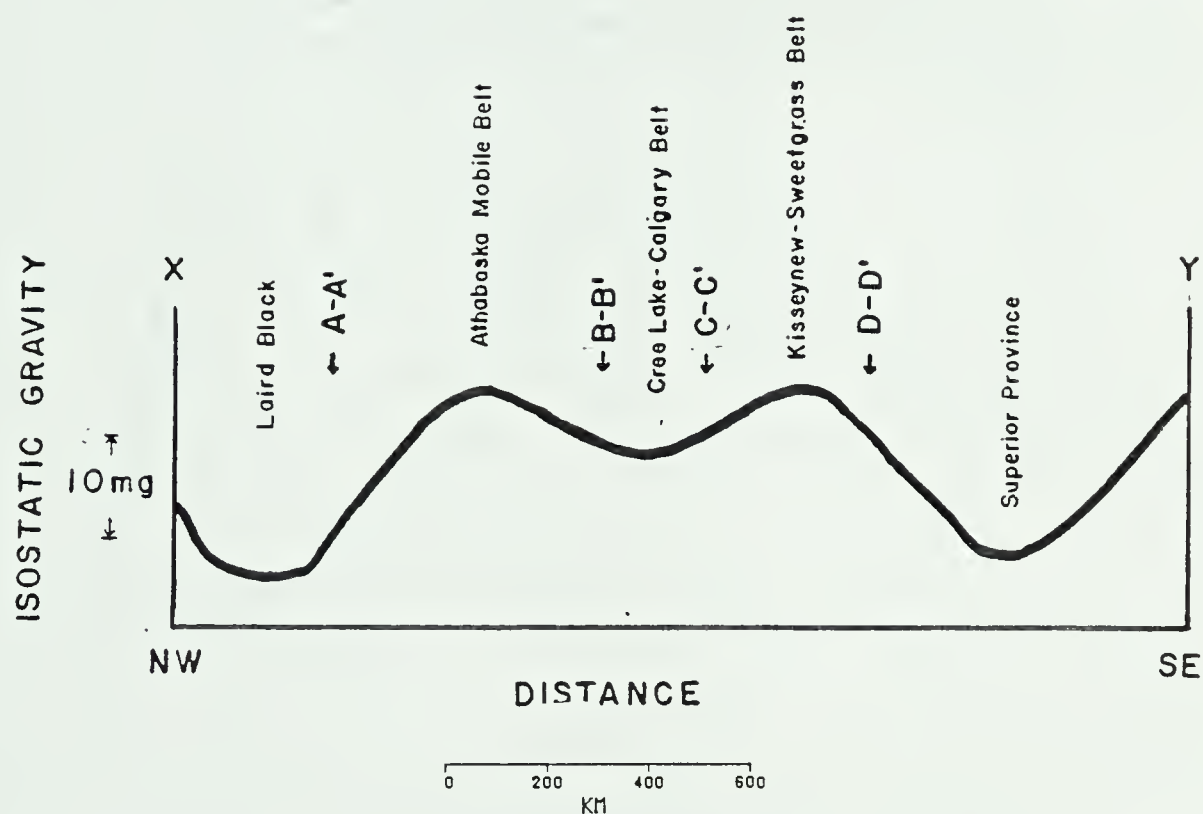


Figure 3.14. A NW-SE profile of the middle wavelength Airy anomaly showing its possible correlation with the known geologic boundaries and zones.

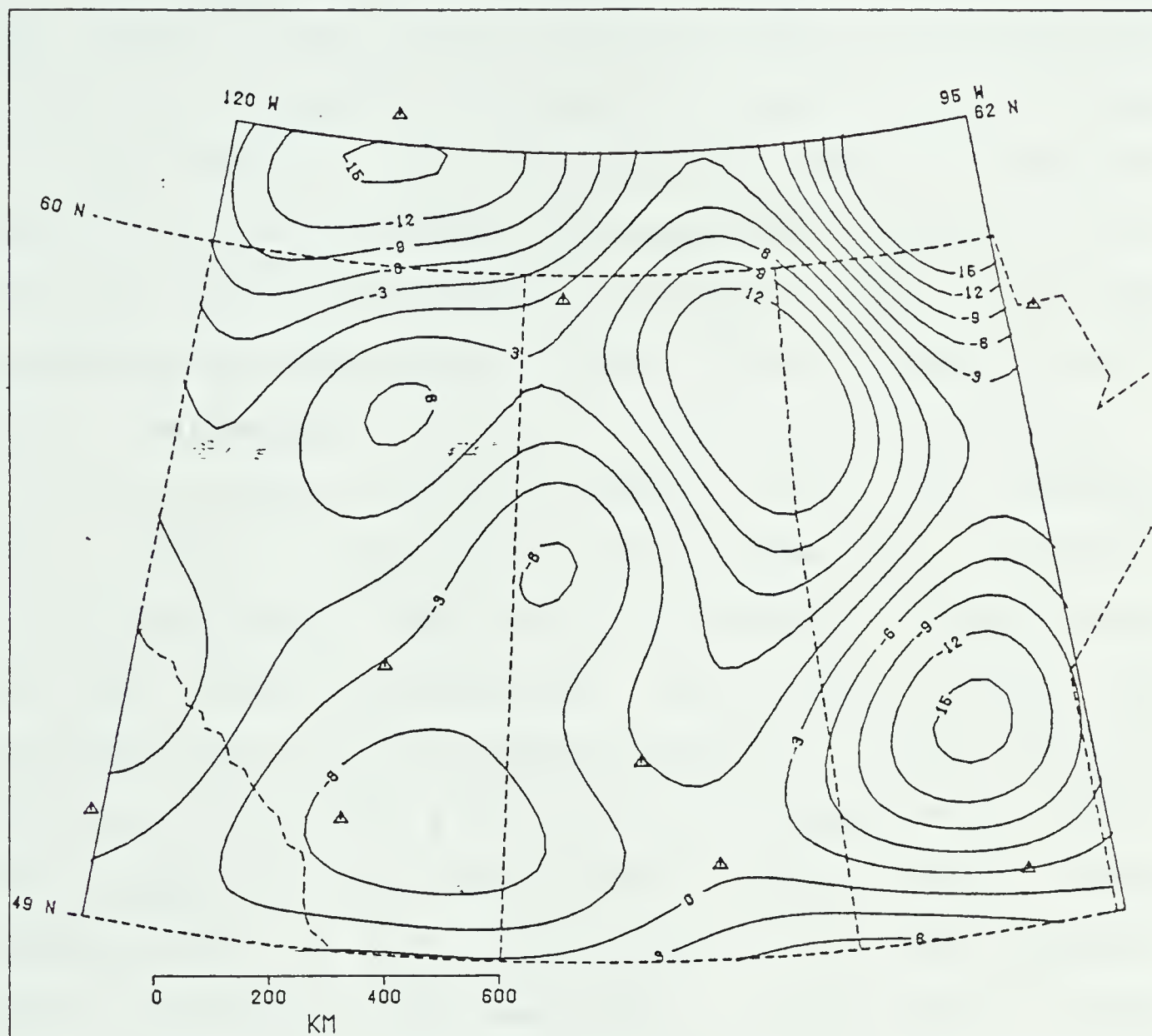


Figure 3.14a. Middle wavelength isostatic anomalies in western Canada. Only anomalies with wavelengths from 500 to 1000 km are shown. The contour interval is 3 milligal.

made about isostasy and its relation to geologic, and in particular, metamorphic history.

The Laird block, for example, has been found by Burwash and Culbert (1976) to be a zone of strong chlorite-epidote alteration, a reaction which possibly results in an increase in rock density. The Athabaska mobile belt, on the other hand, is a zone of intense K-metasomatism, a reaction which proceeds only at the expense of density. Hence, both these zones have had their crustal rocks altered in density during their metamorphic history. The Liard block shows a relatively negative isostatic anomaly while the Athabaska belt shows a positive. Both zones are apparently overcompensated at depth for the density changes which occurred during metamorphism. The strongly recrystallized Athabaska mobile belt has been affected by a large influx of potassium likely from a mantle source (Burwash *et al*, 1973). This suggests a thin crust and a denser mantle during metamorphism. A thin crust would allow easy access of mantle potassium to the upper crust. A dense mantle would naturally follow from the loss of potassium in the mantle and its replacement by heavier minerals. Perhaps a regional high on the Moho or anomalously high mantle densities still exist today beneath the Athabaska mobile belt as a relic of the Hudsonian orogeny. Either would explain the positive isostatic anomaly over the belt. Such an uncompensated feature would have to be supported either by the inherent

strength of the lithosphere or by tectonic forces. In the Athabaska mobile belt, there is some evidence that recurring positive tectonic forces have in fact been active since the Hudsonian orogeny on a continuing basis. Burwash and Krupicka (1970) have concluded using paleogeographic data that the Peace River Arch which lies within the mobile belt has been a long term positive feature during Phanerozoic time. They further postulated that the metasomatic decrease in density of the rocks during the Hudsonian time has resulted in this persistent uplift as a result of the isostatic process. However, the time scale involved for such a process would be many orders of magnitude different. Crittenden (1973) for example, has shown from studies of the unloading of Pleistocene Lake Bonneville that changes in elevation with time due to isostatic imbalance follow exponential curves which decay in a matter of only several thousand years. An alternate explanation of the persistent positive nature of the Peace River area is that recurring vertical tectonic forces have been affecting the Athabaska mobile zone. It is significant in this regard that recent seismicity including at least three events of magnitude greater than 4 have been recorded in this zone (Milne *et al*, 1978).

The Liard block, on the other hand, is quite different in metamorphic history. The low grade regional metamorphism present does not require an influx of mantle material. The

minor density increase due to metamorphism is probably reflected in a relatively thick crust beneath this block.

The southwest portion of the Cree lake-Calgary belt, in contrast to the Athabaska belt, has been found by Burwash and Culbert (1976) to be little affected by K-metasomatism. There is, however, a weak positive development for a "shearing" factor which involves destruction of plagioclase feldspars, biotite, and trace metals with a resultant decrease in rock density. Since the isostatic anomaly over this area is negative, the negative load of the density decrease appears to be supported by the lithosphere.

The exposed northeast portion of the Cree Lake-Calgary belt has, however, a strongly positive isostatic anomaly. This suggests the existence of a possible new fundamental boundary in the lithosphere separating the Cree Lake-Calgary belt into two zones. A long northwest trending fault, known as the Maurice Lake structure, has been observed in this belt in north central Saskatchewan (Byers, 1962). Perhaps this fault as shown in Figure 3.13 marks the location of the subdivision boundary. Alternately, the boundary might lie parallel to this fault but to the southwest such that it is covered by sedimentary rock. It is also interesting to note in this regard that there is a definite change in character in magnetic anomalies from the northeast to the southwest portion of the CreeLake-Calgary belt .

Overall, the Kisseynew-Sweetgrass belt coincides with a net positive Airy anomaly, possibly a result of an anomalously high density mantle in the area, perhaps partly associated with Williston Basin tectonics. In fact, the persistent positive gravity of this belt can be traced considerably southward on the Free Air Gravity Map of the United States (McGinnis *et al*, 1979).

The Superior province which is located to the southeast of D-D' on Figure 3.13 is well delineated on the Airy gravity map. Relative to the zones of the Churchill province discussed above, it shows a negative isostatic anomaly, suggesting possible overcompensation at this time. However, seismic results in the province show evidence of a thin crust in the Superior province relative to the Churchill. Hence, the isostatic imbalance between the two provinces is probably due to the pronounced difference in the nature of metamorphism which has occurred in the two provinces, rather than to gross crustal structure.

If the intense negative anomaly in the extreme northeastern corner of the map-area is not an artifact of the filtering process, it may be due to an Aphebian volcanic mass occurring between Rankin Inlet and Churchill. Perhaps the low isostatic anomaly records the existence of an ancient volcanic regime. Alternately, this isostatic low might represent a local intense depression in the crust due to glacial loading as this area is located at the point of

maximum Pleistocene glacial thickness.

3.2.4 SHORT WAVELENGTH REGIONAL AIRY ANOMALIES

The Canadian Shield, including that portion which underlies the western Canada sedimentary basin has been, with the possible exception of isostatic adjustment and some faulting, stable since the late Proterozoic. The basement geology has therefore remained largely unchanged since the last major orogeny, 1800 million years ago. Yet Airy anomalies of the order of 40 milligals and of wavelength greater than 150 km are present. Walcott (1968) suggested that these anomalies cannot represent departure from isostatic equilibrium since the time constants involved in restoring equilibrium as determined from ice and lake load studies are many orders of magnitude less than the apparent age of the anomalous material. Walcott proposed that the anomalies are due to lateral variations in crustal density compensated at depth by variations in the depth to the Moho (Figure 3.15). Since the proposed crustal mass variations are closer to the observation station than the compensating mass, the former will have the greater effect. Walcott's argument is sound, however, only for a certain band of wavelengths. Wavelengths shorter than about 150 km are probably compensated over a large area by the crust (Woolard, 1959). At longer wavelengths, greater than, say 600 km, the gravity effect of the crustal variation in

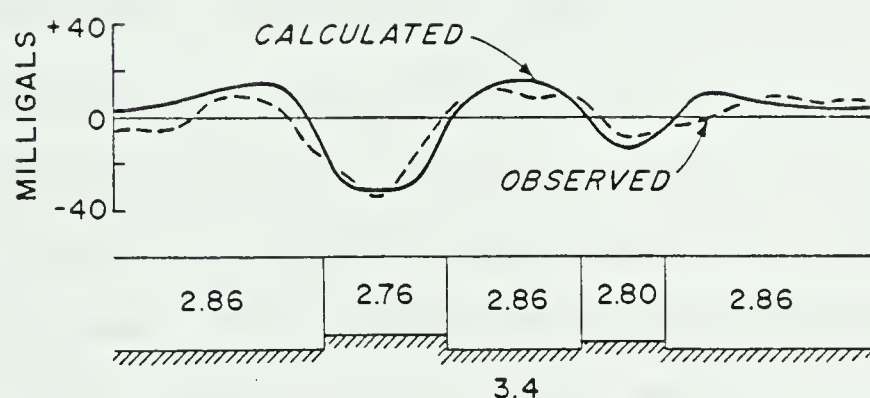


Figure 3.15. Walcott's model for central belt gravity anomalies. This model involves isostatic compensation of lower crustal densities by rises in the base of the crust. Hence, contrary to most gravity modelling schemes, lows in the gravity field correspond to highs on the Mohorovicic discontinuity.

density would cancel the gravity effect of the compensating mass since both would be, in effect, infinite slabs.

Therefore, for the Airy gravity anomalies in western Canada in the band of wavelengths from about 150 km to 600 km, it is reasonable to interpret them in terms of the compensated model discussed above. These short wavelength regional anomalies are shown in Figure 3.16. The Parker-Oldenburg algorithm can easily be modified to do this type of inversion. Only those layers of the crust above the RielM discontinuity (See Table 2) are assumed to possess a lateral density variation, and the RielM discontinuity is assumed to be horizontal. The RielM discontinuity is here taken to represent the presumed geological boundary between the upper and lower crust. The Moho surface is then iteratively adjusted along with the upper crustal lateral density variation until both the gravity data and the condition of isostatic equilibrium are satisfied.

The resulting isostatically balanced density distribution in the upper crust is shown in Figure 3.17, and the relief on the Moho surface is given in Figure 3.18. When the relative isostatic anomaly is negative, the crustal density goes to lower values, and the Moho surface rises accordingly. For positive Airy anomalies, the reverse occurs. It is interesting to compare the gravity due to the crustal density changes with the gravity due to the Moho relief at these wavelengths. The overall effect of the

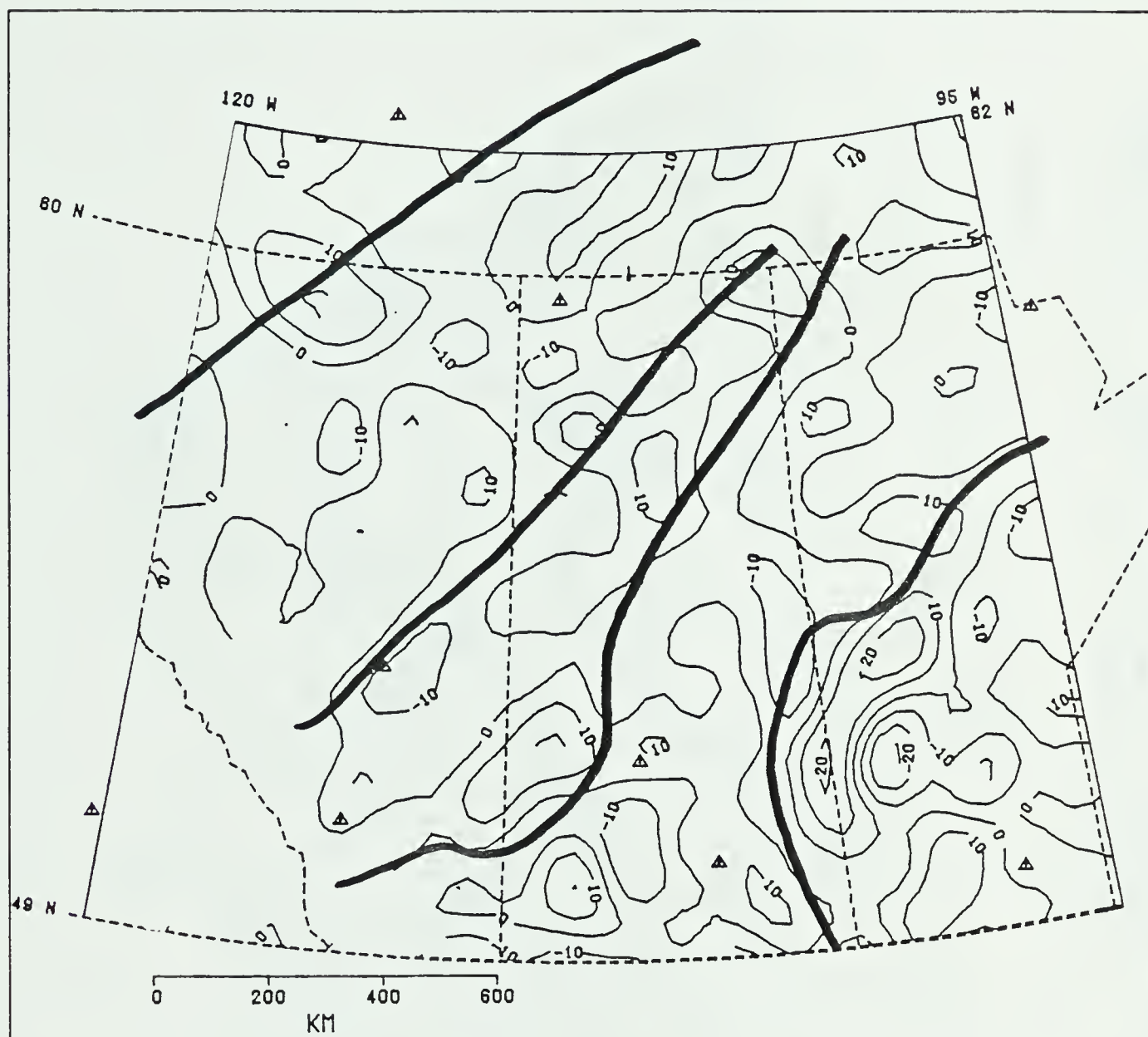


Figure 3.16a. Short wavelength regional Airy anomalies in western Canada. The contour interval is 10 milligal. The small triangles represent major cities within the map-area.

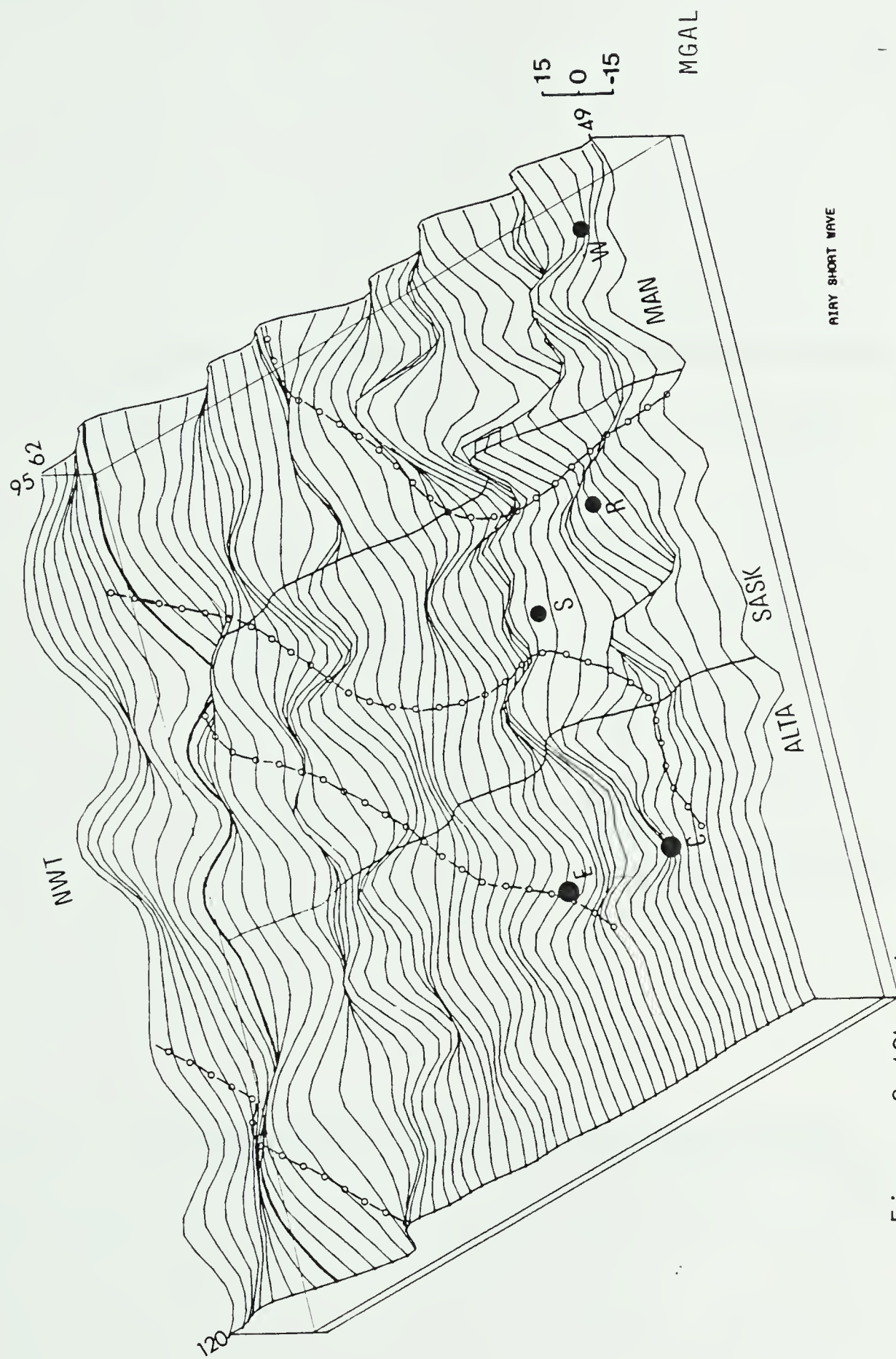


Figure 3.16b. A perspective view of the short wavelength regional Airy anomalies in western Canada. The known geologic zones and boundaries are also shown.

INTERFACE	LAYER	VELOCITY (km/s)	DENSITY (kg/m ³)	THICKNESS (km)
Riel M	Upper Crust	6.1	2800	8
	Middle Crust	6.5	2900	15
Riel A	Lower Crust	7.15	3200	10
Moho	Mantle	8.0	3400	--

Table 2. Standard crust assumed for western Canada.

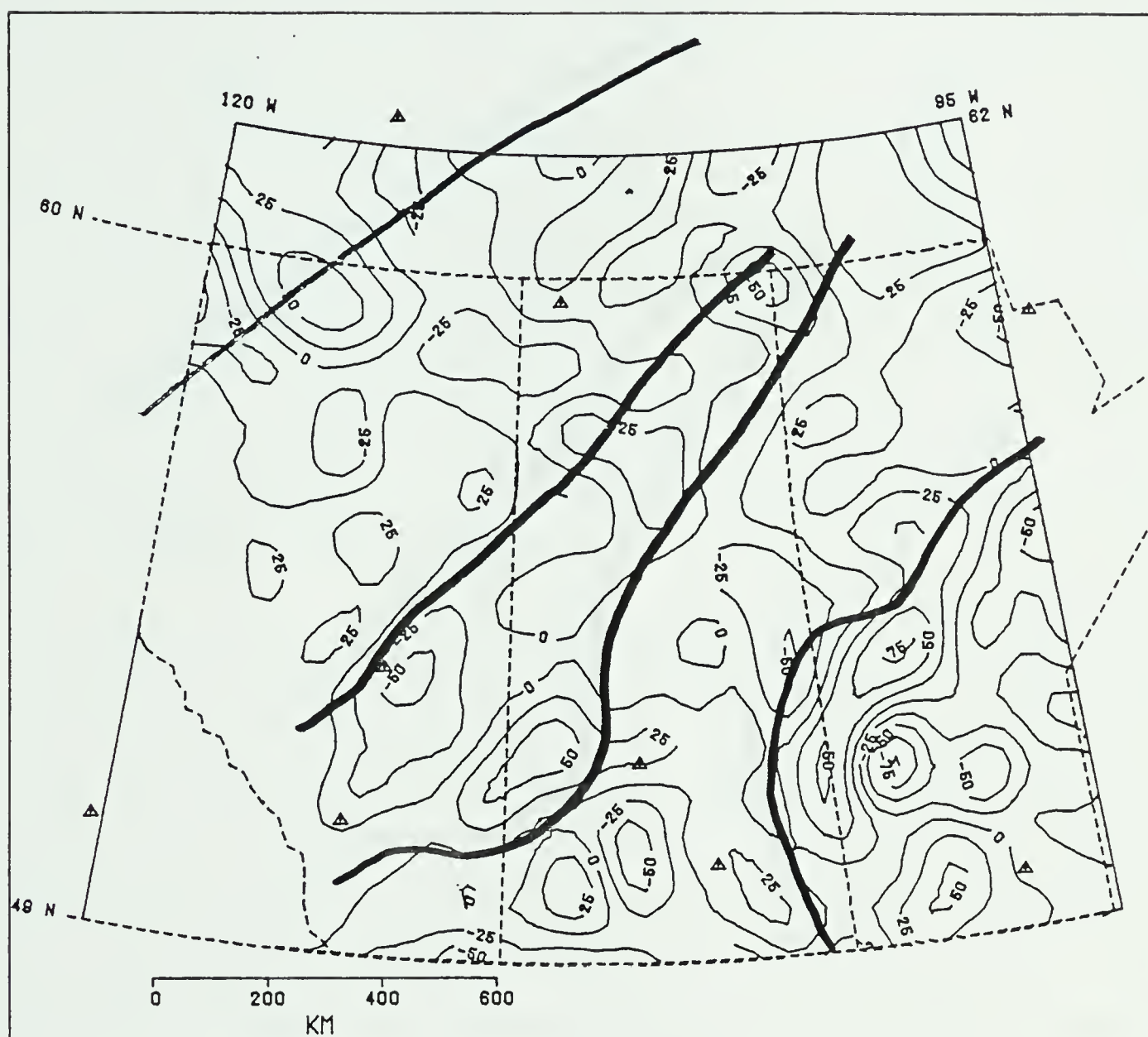


Figure 3.17. Lateral density variations in the upper crust of western Canada as predicted by Walcott's model. The contour interval is 25 kg/m³. The known geologic zones and boundaries are also shown. The small triangles represent major cities within the map-area.

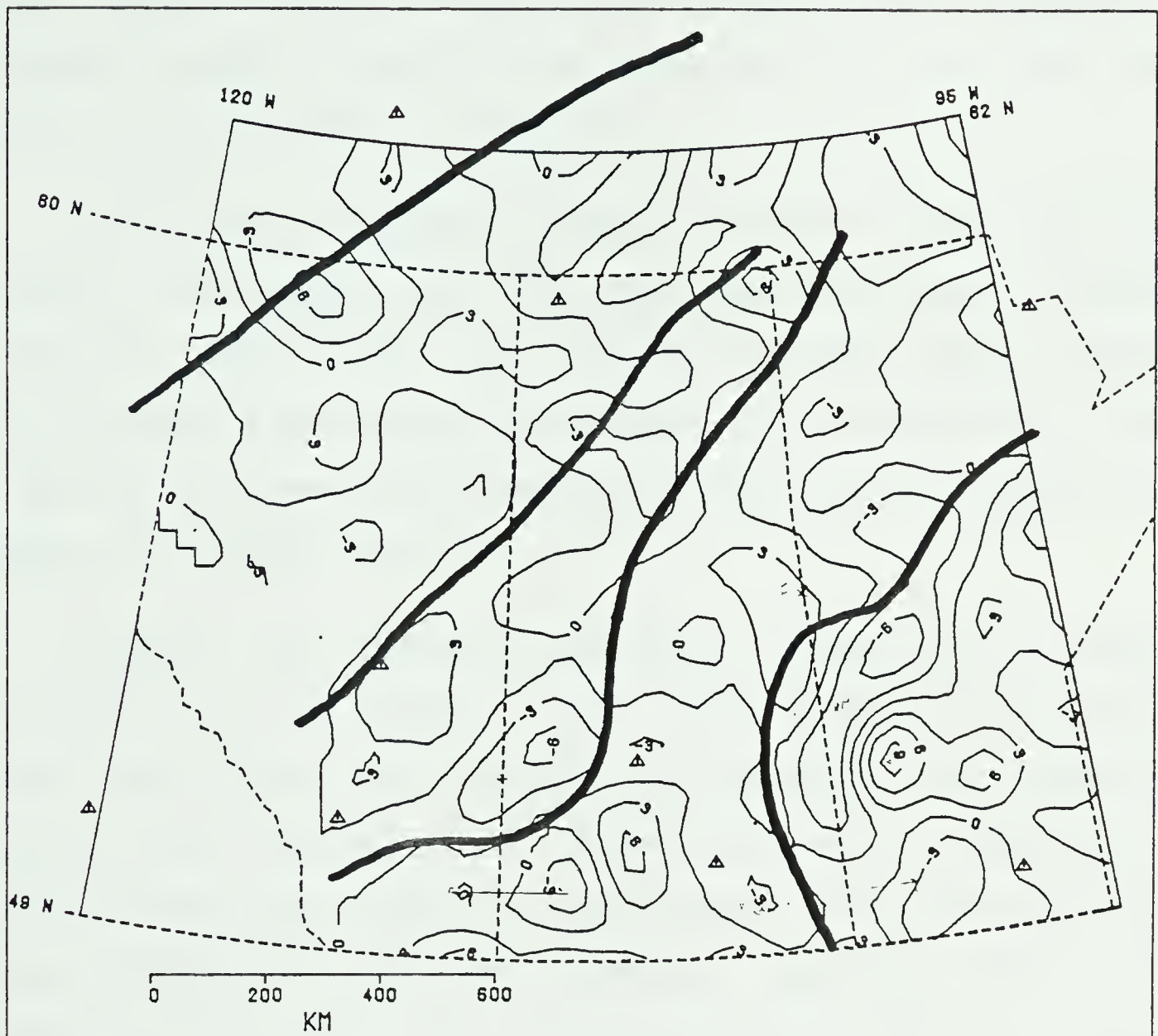


Figure 3.18. Variation in Moho topography as predicted by Walcott's model. The known geologic zones and boundaries are also shown. While there is some correlation between the geologic zones and the derived shape of the Mohorovicic surface, this type of model generally does not agree with seismic results from across the map-area. The contour interval is 3 km. The small triangles represent major cities within the map-area.

crustal density variations is always slightly more important than the effect of the Moho variations provided, of course, that isostatic equilibrium is maintained. The variation of the Moho relief is generally of the order of 8 km on the plains if this model is correct.

While there is some correlation between these derived crustal parameters and the known geologic zones (Figures 3.16b, 3.17 and 3.18)., this type of modelling does little to arrive at a suitable crustal model for the map-area. The high and low areas predicted by the model do not generally agree with seismic results.

However, at certain locations, there may be some validity to this model. Near the University of Alberta Leduc Observatory just south of Edmonton, for example, Ganley and Cumming (1974) have proposed an anomalously shallow Moho depth (35 km). Low crustal densities have also been suggested for this area by Sprenke (1972) and Sommerville and Ellis (1972) from teleseismic studies; and by Darnley (1981) on the basis of uranium distribution. Walcott's type of gravity modelling does in fact predict a thin crust and low crustal densities in the area of the Leduc observatory.

3.3 COMPARISON OF GRAVITY AND SEISMIC RESULTS IN WESTERN CANADA

3.3.1 INTRODUCTION

It is an interesting exercise to compare the Bouguer gravity anomaly with postulated seismic models for the map-area. To do this, seismically determined crustal thicknesses from diverse locations across the map-area will be used as input to the Parker algorithm. The theoretical anomaly so obtained will then be compared and contrasted to the actual Bouguer gravity anomaly.

The approximate locations of the seismic profiles used in this study are shown in Figure 3.19. Table 3 lists the location symbols for the profiles and gives the respective references.

3.3.2 VELOCITY MODEL

The values of P-wave velocity within a crustal layer are plotted against depth to the top of the layer for all the seismic profiles on the map-area in Figure 3.20. In general, at any given depth, the velocities do not seem to vary by more than a few tenths of a km/s; and down to a depth of about 30 km, there seems to be a linear increase in crustal velocity with depth. Below 30 km, however, the velocities tend to remain constant at 7.1 to 7.2 km/s. In a

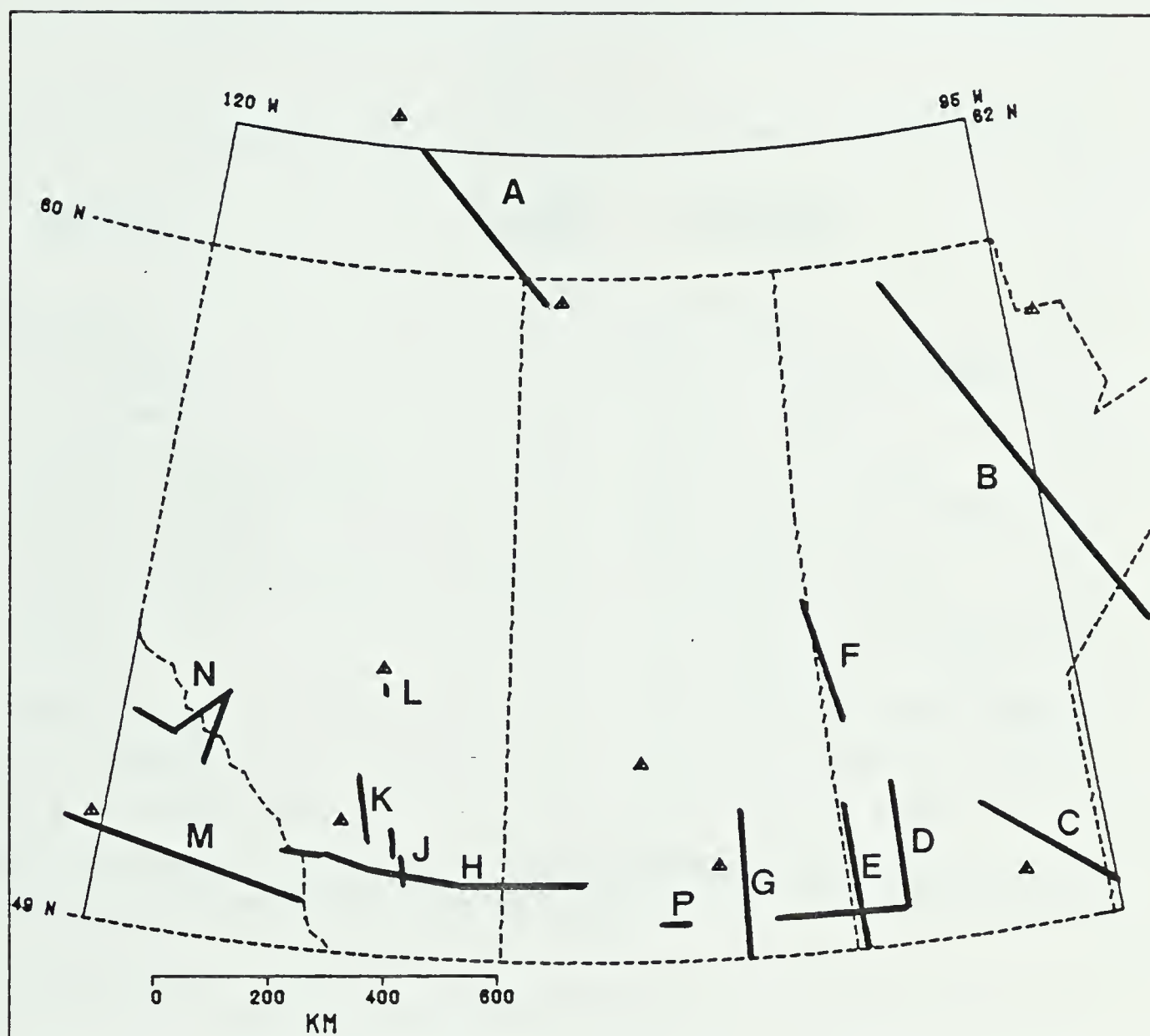


Figure 3.19. Approximate locations of the seismic profiles used as control for the combined gravity and seismic study. The labels are explained in Table 3. The small triangles represent major cities within the map-area.

<u>LOCATION</u>	<u>LABEL</u>	<u>REFERENCE</u>
Yellowknife	A	Barr(1971)
N.E. Manitoba	B	Mereu and Hunter (1969)
S.E. Manitoba	C	Gurbuz (1970)
S. Saskatchewan-Manitoba	D	Green et al (1979)
W. Central Manitoba	F	Hall and Brisbin (1965)
S. Saskatchewan-Manitoba	E G P	Kazmierczak (1980)
S. Alberta	H	Cumming and Kanasewich(1966)
S. Alberta	J	Kanasewich et al (1969)
S. Alberta	K	Richards and Walker (1959)
Central Alberta	L	Ganley and Cumming (1973)
S.E. British Columbia	M	Cumming et al (1979)
Central Rockies	N	Mereu et al (1977)

Table 3. Seismic profiles in the map-area.

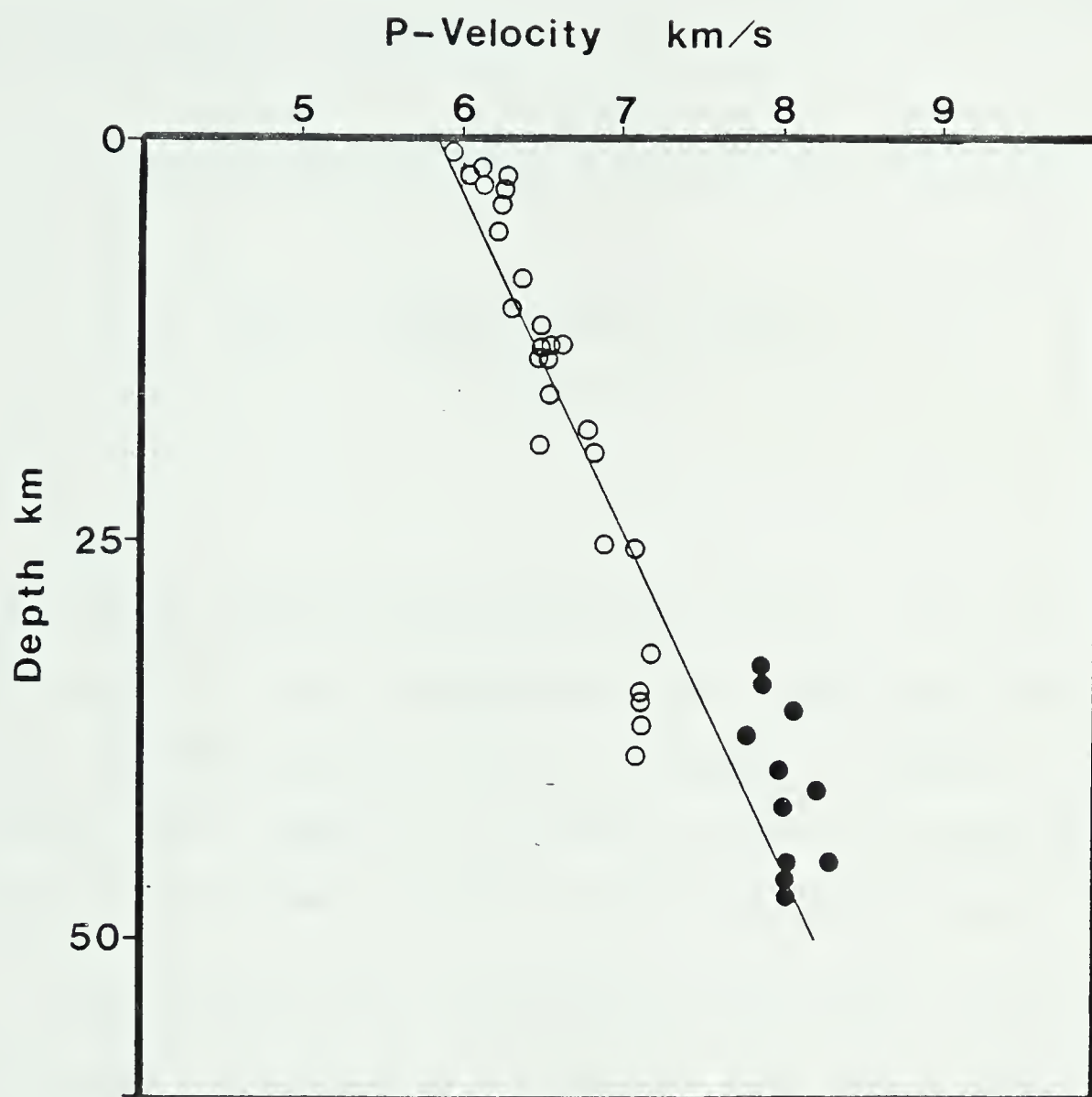


Figure 3.20. The values of P-wave velocity plotted against depth for the seismic profiles in the map-area. The light circles are crustal velocities while the darker points represent mantle velocities. The regression line determined by Goodacre(1972) for data from much of North America is also shown. It is apparent that deep crustal velocities in western Canada fall well below the North American results. It is also apparent that at the base of the crust in western Canada, the velocity jumps from about 7.1 to 8.0 km/s.

similar study, using data from all over North America, Goodacre (1972) obtained the following empirical equation for the velocity function.

$$v(z) = 5.85 + 0.048 z \text{ (km/s)} \quad [51]$$

This line is also plotted on Figure 3.20. It is evident that relative to the whole of North America, the crust in western Canada tends to have a somewhat smaller velocity gradient with depth and a distinct zone of anomalously low velocity in the deep crust in the 30 to 40 km depth range.

The evidence for the deep zone of lower velocity comes from seismic experiments in Alberta and Saskatchewan where an event herein referred to as the RielA discontinuity occurs. The RielA event has not been observed by all the seismic crustal experiments performed on the map-area, but it has been noted in the Cordillera and Churchill Provinces. In the Superior Province, it is sporadically observed but at relatively more shallow depths.

A proposed density function, based on the Nafe-Drake (1957) curve and the velocity results of Figure 3.20, is given in Figure 3.21. The density is seen to increase

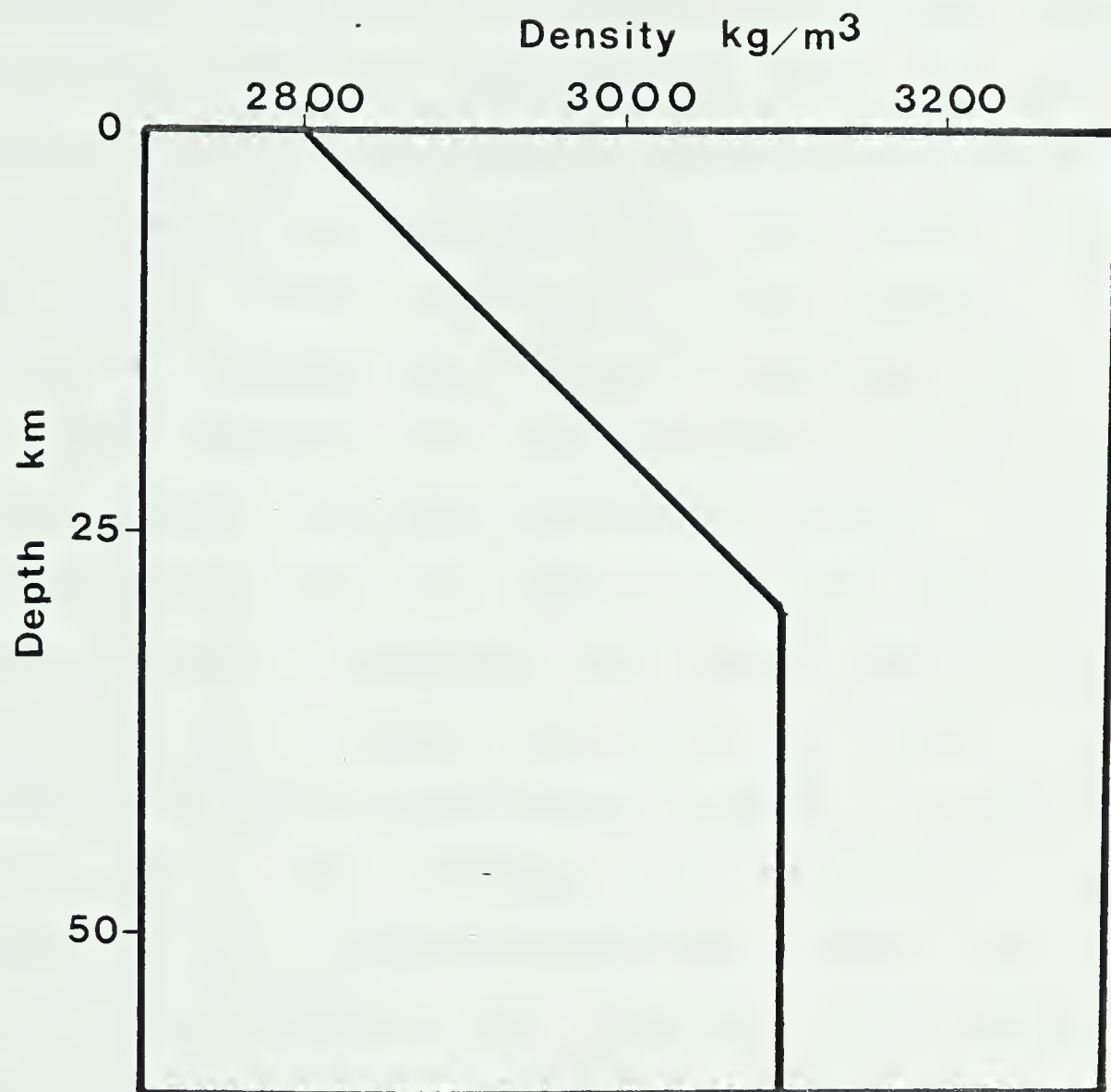


Figure 3.21. A proposed crustal model for western Canada. Variations in thickness of the lower velocity zone at the base of the crust are thought to be the source of the gravity anomaly.

linearly to a depth of about 33 km at which depth the lower velocity zone of constant density 3100 kg/m^3 is encountered. The density contrast at the Moho is then about 300 kg/m^3 . This crustal model is based on the point of view that seismic velocities measured by refraction studies are valid only at the depth measured, not for the entire underlying layer as is often assumed in other studies. It seems reasonable to expect that velocity continues to increase with depth beneath the discontinuities detected by the seismic survey. Of course, the very existence of velocity discontinuities in the crust is evidence that a strictly linear increase in velocity with depth does not occur. However, from a statistical point of view, it is more reasonable to model a continuous increase in velocity with depth than to attempt to incorporate specific discontinuities at specific locations. Since the seismic control is so sparse over this very large map-area, the resulting crustal model would be severely biased. A more deterministic approach however will be attempted in the next chapter of this study for a smaller map-area in which the seismic control is considerably more dense.

The average density contrast assumed at the Moho (300 kg/m^3) is consistent with a value determined by Goodacre (1972) in a statistical analysis of gravity and seismic results across North America.

The occurrence of the zone of lower velocity in the deep crust is also consistent with petrological models of the crust proposed by Mueller (1977) which include a granulite layer at the base of the crust. This granulite layer is thought to be of lower velocity and density than the overlying amphibolite layer which is thought to be the source of the Conrad discontinuity.

3.3.3 PROCEDURE

The gravity anomaly predicted by the seismically determined crustal thicknesses was calculated using the Parker algorithm on interpolated values of the crustal thickness at all grid points. This data set is, of course, rather biased since the control (Figure 3.19) is so sparse. However, this map does form a reasonable approximation of the Moho surfaces for purposes of comparing the predicted and actual values of the gravity field at each control location.

3.3.4 DISCUSSION OF RESULTS

The difference between the observed and expected gravity anomalies across the map-area is shown in Figure 3.22. Statistically, if the seismic control lines were randomly located in the map-area, one would expect the mean difference to be zero. However, the mean station correction (expected anomaly-observed anomaly) was found to be +5.2 mgal suggesting that either the proposed density contrast at the

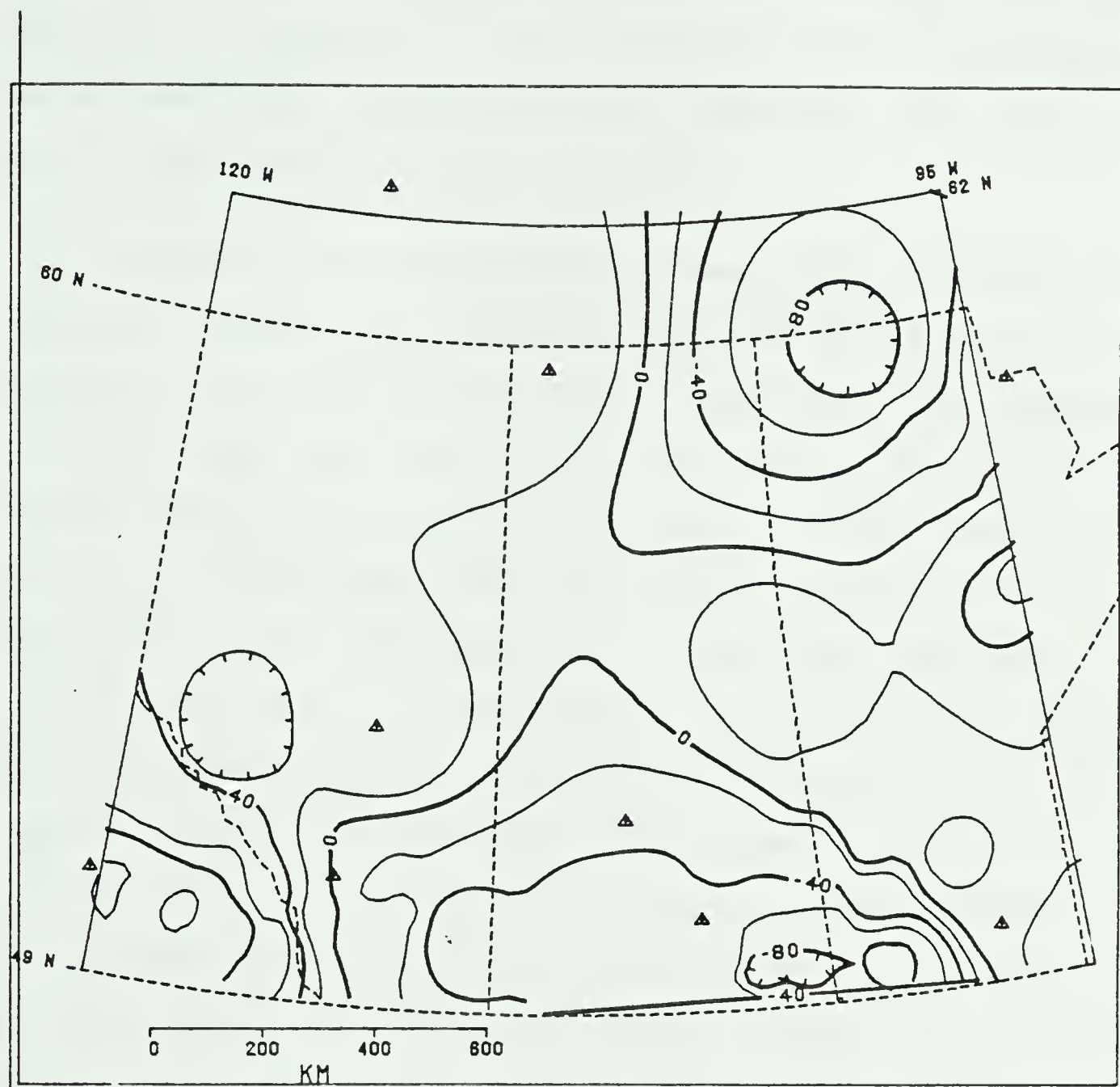


Figure 3.22. The disagreement between the observed and seismically derived gravity anomalies across the map-area. The contour interval is 20 mg. Those areas on this map which are positive require additional mass deficiency in the subsurface to reconcile seismic and gravity results. Hence the Cordillera is thought to possess an anomalously low density upper mantle while the Williston Basin area may possess an anomalously high density upper mantle. The isolated anomaly in the extreme northeastern corner of the map-area may not be significant since the seismic control in that area is very sparse. The small triangles represent major cities within the map-area.

Moho is slightly too small to account for the entire Bouguer field or that an insufficient amount of seismic data was available. However, if one considers that the disparity varies more than 100 mg across the map-area, the mean of only 5.2 mgal does not seem excessive.

In general, the differences between the expected and observed anomaly is strongly positive in the Cordillera, suggesting that the crustal seismic model in this geologic province does not yield sufficient mass deficiency to explain the gravity field. This result is not surprising since most researchers who have studied the Cordillera feel that there is not sufficient root beneath the mountains to satisfy the gravity observations. Generally it is thought that the upper mantle is of anomalously low density in this region. Hence the positive disagreement noted in the present study seems valid if the Bouguer gravity anomaly is to be compatible with what seismic control is available. A strongly negative difference is noted between the seismic models and the gravity field in the extreme northeastern portion of the map-area as well as in the Williston Basin area. In the former area, the seismic control is probably too poor to be of value. In the Williston Basin area, however, an upper mantle density anomaly may plausibly exist, a possibility which will be explored further in the next chapter.

4. MULTILAYERED GRAVITY MODELLING ON THE SOUTHERN PLAINS

4.1 INTRODUCTION

In this chapter, the relationship between regional gravity and seismic data will be analyzed and used to extrapolate multilayered seismic models of the crust to areas for which only gravity control is available.

It is well known that seismic data and gravity data do not always correlate. However, Goodacre (1972) has shown that there is at least 75% agreement between the two in North America as a whole. Weber and Goodacre (1968) and Cumming and Chandra (1972) have also shown that minor adjustments in seismic interpretations can generally yield crustal models which suit both the gravity and seismic data. The base-map for the multilayered gravity modelling study covers the southern plains of western Canada and is shown in Figures 4.1a and 4.1b. This area is of considerable tectonic interest since the boundary zone between the Churchill and Superior provinces extends through this map-area beneath Phanerozoic sediments. The geological and geophysical information about this map-area will be first briefly reviewed. Then the gravity field of the map-area will be inverted using a reformulation of the Parker-Oldenburg algorithm in order to provide further information for a tectonic analysis of this important area.

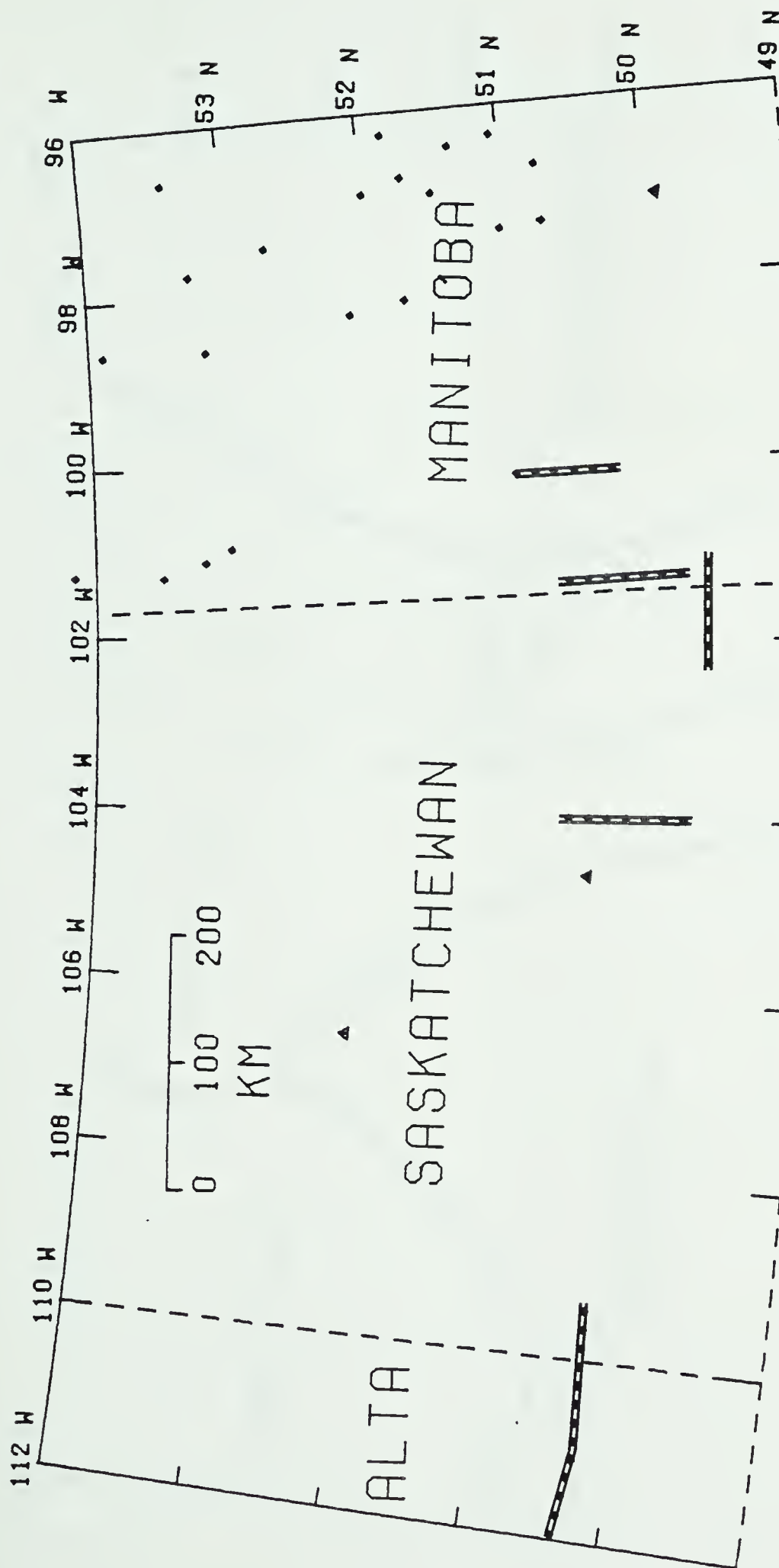


Figure 4.1a. The base-map for the multilayered modelling study showing geographical features and locations of deep crustal seismic experiments. The small triangles represent major cities within the map-area. The bars represent seismic refraction lines shot by the University of Alberta and the COCRUST group. The diamonds represent individual locations shot by the University of Manitoba group where both depths to the RielM and Mohorovicic discontinuities were available.

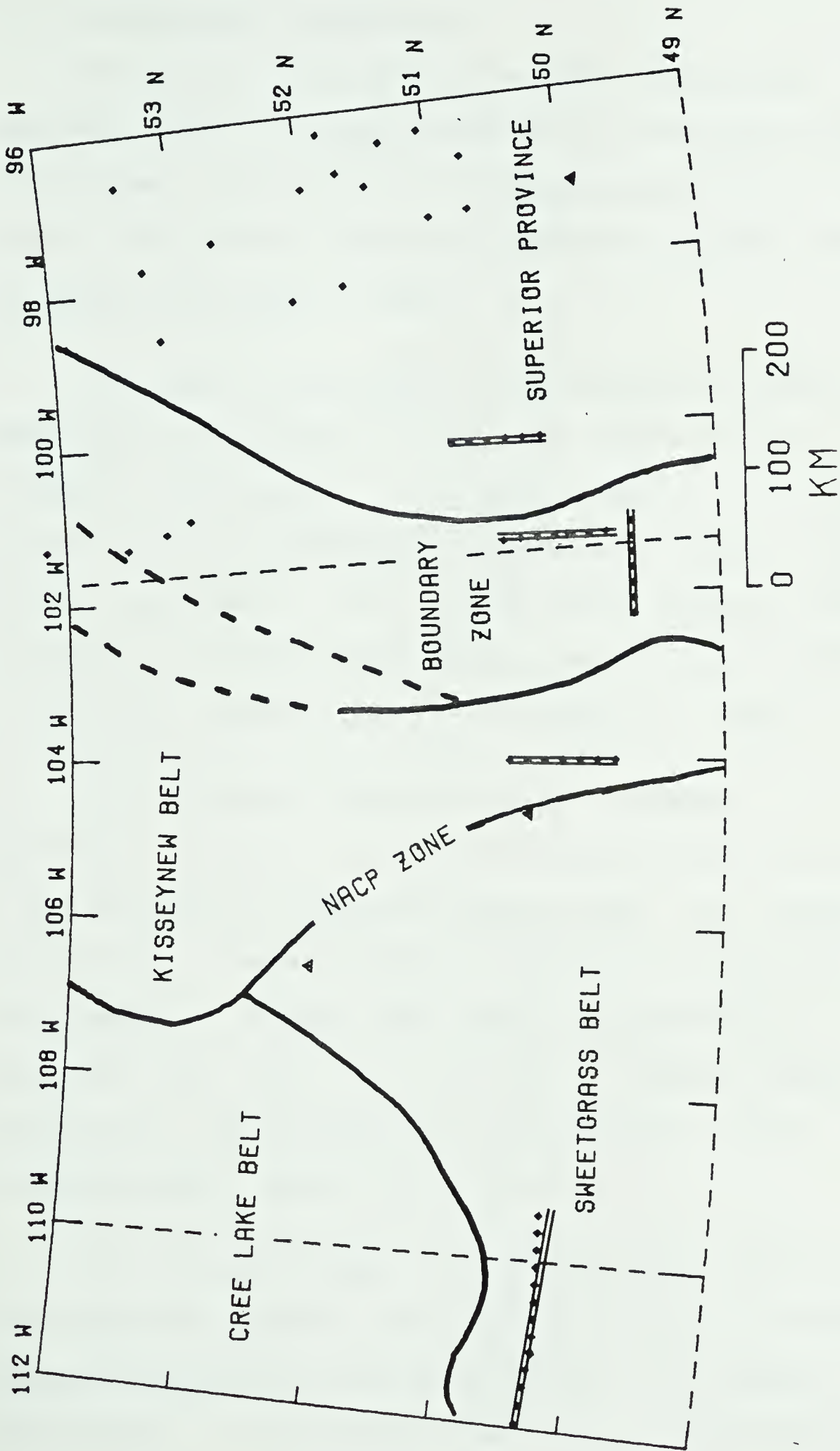


Figure 4.1b. The base-map for the multilayered modelling study showing known tectonic lineaments as well as the location of deep seismic crustal experiments as described in the caption of Figure 4.1a.

4.1.1 GEOLOGICAL BACKGROUND

Geological information on the Precambrian for this map-area which is largely covered by Phanerozoic sedimentary rock comes from studies of the exposed shield to the north (Bell, 1971a, 1971b) and from studies of basement core samples (Burwash and Culbert, 1976).

The Superior province in the exposed shield of northern Manitoba is Kenoran in age and dominated by east-west trending structures. Its rocks consist of greenschist facies volcanic-sedimentary belts and largely amphibolite facies gneisses. In the map-area, basement core samples indicate an absence of cratonic reactivation of the Kenoran crystalline complex during the Hudsonian orogeny.

The Churchill province, as exposed in northern Manitoba, consists mainly of metasediments and migmatites. Its rocks are of Hudsonian age and show no dominant trend direction. Large masses of weakly foliated granitic rocks are common. Among the regional assemblages near the map-area are the Flin Flon belt, largely composed of the Amisk-Missi metasedimentary-metavolcanic units, and the Kisseynew belt, a gneissic terrain.

The transition zone from the Churchill to the Superior provinces is known as the Nelson Front and is divided on the exposed shield into two sub-provinces, the Waboden and the Pikwitonei. The Nelson Front is a geologic feature of

tectonic significance. It extends at least 1600 km from Hudson Bay to near the international border. There is a great deal of controversy in the literature on both the width and location of the boundary zone. Width estimates vary from less than 1 km (Kornik, 1966) to over 200 km (Hajnal and Rose, 1979). The location of the boundary zone seems to have a 400 km uncertainty associated with it (Hajnal and Rose, 1979); and the tectonic evolution of the Nelson Front has been an issue of contention for many years. Most of the proposed hypotheses are based on surface geology of the exposed shield and on qualitative analysis of potential field data. In the present study, a combination of gravity and seismic data will be used to add a third dimension to the problem. Hopefully, the results will provide more insight into the tectonic models for the region.

The Wollaston fold belt on the exposed shield is correlated in this study with a zone of very high electrical conductivity known as the NACP anomaly (Camfield and Gough, 1977). This long, narrow conductivity high is traceable across the map-area as shown in Figure 4.1b. The NACP zone is hypothetically a possible Proterozoic plate boundary in that it can be followed over a distance of 1400 km down to southeastern Wyoming where it has been associated with a postulated ancient subduction zone.

Another lineament of some tectonic significance possibly extends into the map-area from the west. This is a major crustal rift discovered by Kanasewich *et al* (1968) which trends approximately east-west through southern Alberta between latitudes 50°N and 51°N. Its probable extension into the map-area is shown in Figure 4.1b.

The area between the NACP conductor and the rift zone is referred to in this study as the Sweetgrass belt. Only a limited number of widely spaced basement core samples are available for this area, hence the Precambrian geology is not well known. Some relatively unmetamorphosed volcanic-plutonic core samples from near Swift Current (Burwash and Cumming, 1974) suggest that the area was at least partially shielded from the effects of the Hudsonian orogeny.

The region in the north-east corner of the map-area is part of the Cree Lake-Calgary belt which is probably a southwestern extension of the Mudjatic and Virgin River belts of the exposed shield.

4.1.2 MAGNETIC INFORMATION

South of the exposed shield, the Nelson Front is covered by sedimentary rock, and attempts to trace it are based largely on potential field pattern. Recently, Green *et al* (1977), using a newly compiled magnetic map of a

portion of the map-area (Figure 4.12), have postulated that five distinct zones exist as shown on Figures 4.1b. They note that:

1. South-Central Saskatchewan is characterized by low magnetic relief similar to that exhibited by the Kisseynew belt of the Churchill province in the exposed shield.
2. Southeast Saskatchewan contains a zone of high amplitude narrow anomalies striking northeast. This zone is thought to be an extension of the Flin Flon belt of the Churchill province beneath the sedimentary cover.
3. Along the Saskatchewan-Manitoba border, an area of low magnetic relief occurs which is interpreted as the southern extension of the Churchill-Superior boundary zone.
4. In southern Manitoba, the magnetic anomalies show dominant east-west trends, a dominant characteristic of the Superior province.

The boundary between the first two zones discussed above is thought to be a major crustal fault. Although this fault is entirely within the Churchill province, it is of considerable interest in seismic studies of the map-area and is referred to as the 103°W Fault (Kazmierczak, 1980).

In the present study, some issue is taken with point 2 above. There is very little evidence that the zone

immediately east of the 103W fault is an actual extension of the Flin Flon belt. It is just as reasonable and far more intriguing to correlate this zone with a tectonic equivalent of the Waboden subprovince on the exposed shield. From this point of view, the 103W fault becomes a more natural western boundary to the Nelson Front than the boundary postulated by points 2 and 3 above. Placing this boundary at or near the 103W fault is also more in agreement with the studies of Stockwell (1969), Burwash and Culbert (1977), and Lee (1977).

4.1.3 SEISMIC STUDIES IN THE AREA

This map-area, centering on southern Saskatchewan but including parts of both southern Alberta and southern Manitoba, has been the location of a number of deep crustal seismic experiments as shown on Figures 4.1a and 4.1b. The line west of Swift Current is the easternmost coverage of an extensive amount of deep crustal work carried out by the University of Alberta Geophysics group during the 1960's (Cumming and Kanasewich, 1966; Kanasewich *et al* (1969); Chandra and Cumming, 1972). In addition to finding crustal thicknesses in excess of 45 km and upper mantle velocities from 8.1 to 8.3 km/s, their studies indicated the existence of two major discontinuities in the crust. The upper, herein called the RielM, represented a change from about 6.1 km/s to about 6.5 km/s. The deeper one, here called the RielA discontinuity, represented a velocity change from

about 6.5 km/s to around 7.1 km/s.

The two reversed refraction profiles, one north-south and the other east-west, intersecting near Brandon, Manitoba, were shot by the CO-CRUST group in 1977. (Green, 1977; Green and Stephenson, 1978; Green *et al*, 1979). As shown in Figure 4.2, this study indicated that the crust thins from about 48 km in the west to about 41 km or less in the east as one crosses the covered Nelson Front. The east-west profile which crosses the transition zone shows a RielA discontinuity whereas the north-south profile which is entirely within the Superior province, does not.

Two additional north-south reversed refraction profiles were shot by the CO-CRUST group in 1979 as shown in Figure 4.3. The Roblin-Melita line was entirely within the boundary zone. It indicated little variation of crustal parameters along the zone and no RielA discontinuity was evident. The Leross-Ongre line was entirely within the Churchill province. It produced enigmatic results. The depth to the Moho was found to be only 40 km and the upper mantle velocity was found to be very high, 8.26 km/s. No RielA discontinuity was observed. This result led Kazmierczak (1980) to propose the existence of a major crustal division, the "103°W Fault", to explain the drastic changes in crustal models from this profile location to the Brandon east-west profile. A change in crustal thickness of 8 km and a change in upper mantle velocity of 0.2 km/s in a

distance of 110 km is required.

Relating back to the proposed geologic zones of the map-area (Figure 4.1), the covered Kisseynew belt in southern Saskatchewan is therefore thought to have a thinner crust and higher upper mantle velocity than the Nelson Front. The thinner crust in central Saskatchewan is also partly substantiated by the Suffield-Swift Current profile which suggests crustal thinning to the east, away from the very thick crust of southern Alberta.

The scattered seismic locations in Manitoba shown in Figure 4.1 are derived from published seismic reflection and refraction work by the University of Manitoba as compiled by Hall and Hajnal (1973). The points used in this study are those for which depths to both the Rielm and Mohorovicic discontinuities were available. All the scattered results from Manitoba are based on a two layered crustal model with a constant velocity in the upper layer and with a small velocity gradient in the second layer.

4.2 INVERSION PROCEDURE

The inversion procedure followed in the present study makes direct use of two types of geophysical data available for the map-area. The seismic data as illustrated by the location of the points in Figure 4.1 forms a control network for the lithospheric model. The gravity data (Figure 4.4)

is then used as input to the gravity inversion scheme to interpolate crustal structure from one seismic control location to the next.

The lithospheric model used for this study of the southern plains of Canada consists of two crustal layers and the upper mantle. The velocities and thicknesses used are obtained from the deep seismic crustal experiments performed in the map-area. The following crustal parameters are not altered by the modelling procedure, and along with the Bouguer gravity anomaly may be considered as input to the modelling process.

1. The seismic velocity of the upper crust.
2. The thickness and seismic velocity of the lower crust.
3. The seismic velocity of the upper mantle.
4. The depth of compensation for the lithosphere.

Except near the seismic control points, the following crustal features are determined by the inversion process and may be thought of as the output of the process:

1. The depths to the RielM and Mohorovicic discontinuities as calculated by a multilayered reformulation of the Parker-Oldenburg algorithm operating on the longer wavelength portion of the gravity data.
2. The density variation in the upper crust as computed by another reformulation of the same algorithm operating on the shorter wavelength portion of the gravity field.
3. The anomalous density variation in the upper mantle as

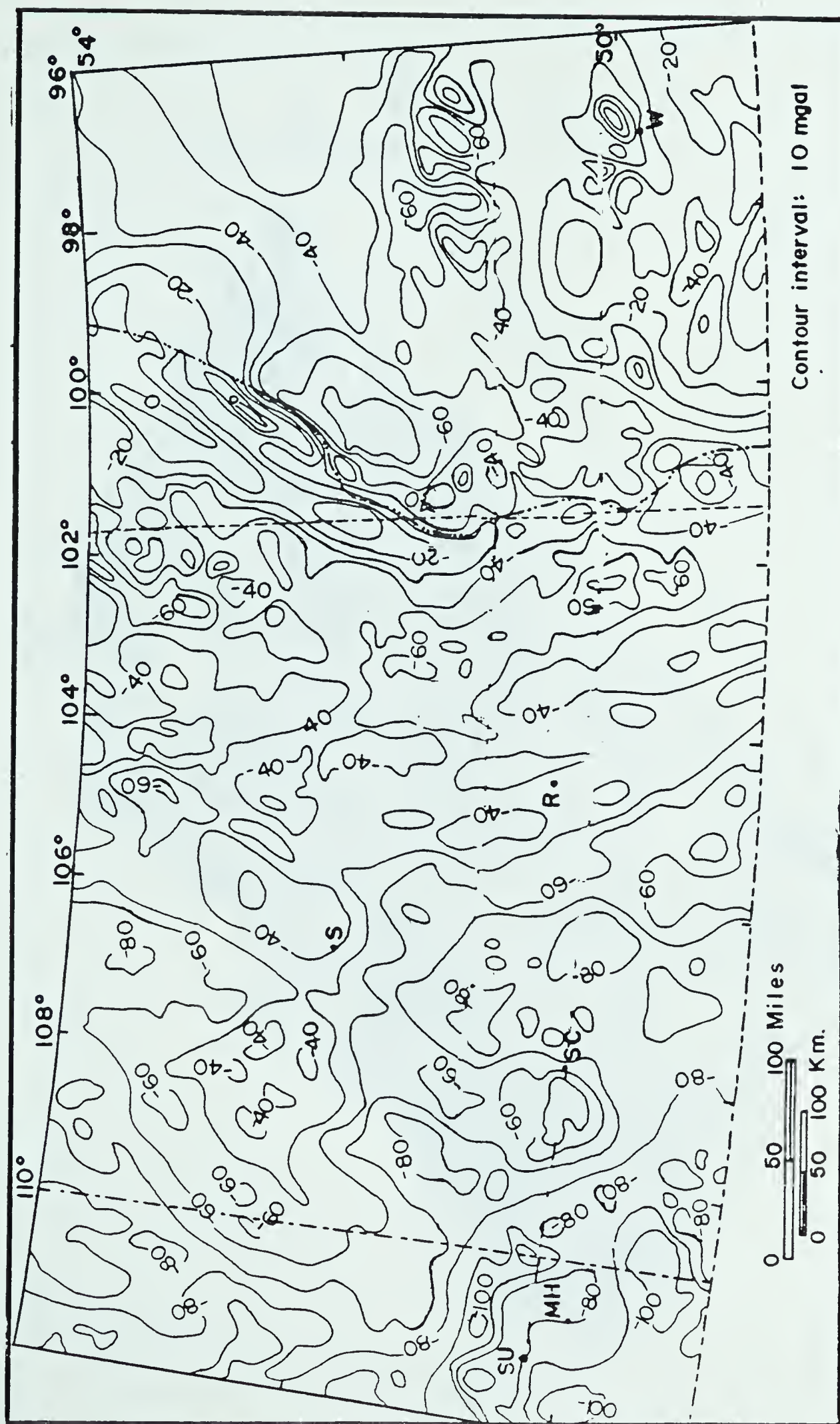


Figure 4.4a. Bouguer gravity anomaly of the southern plains of western Canada. (After Lee, 1977).

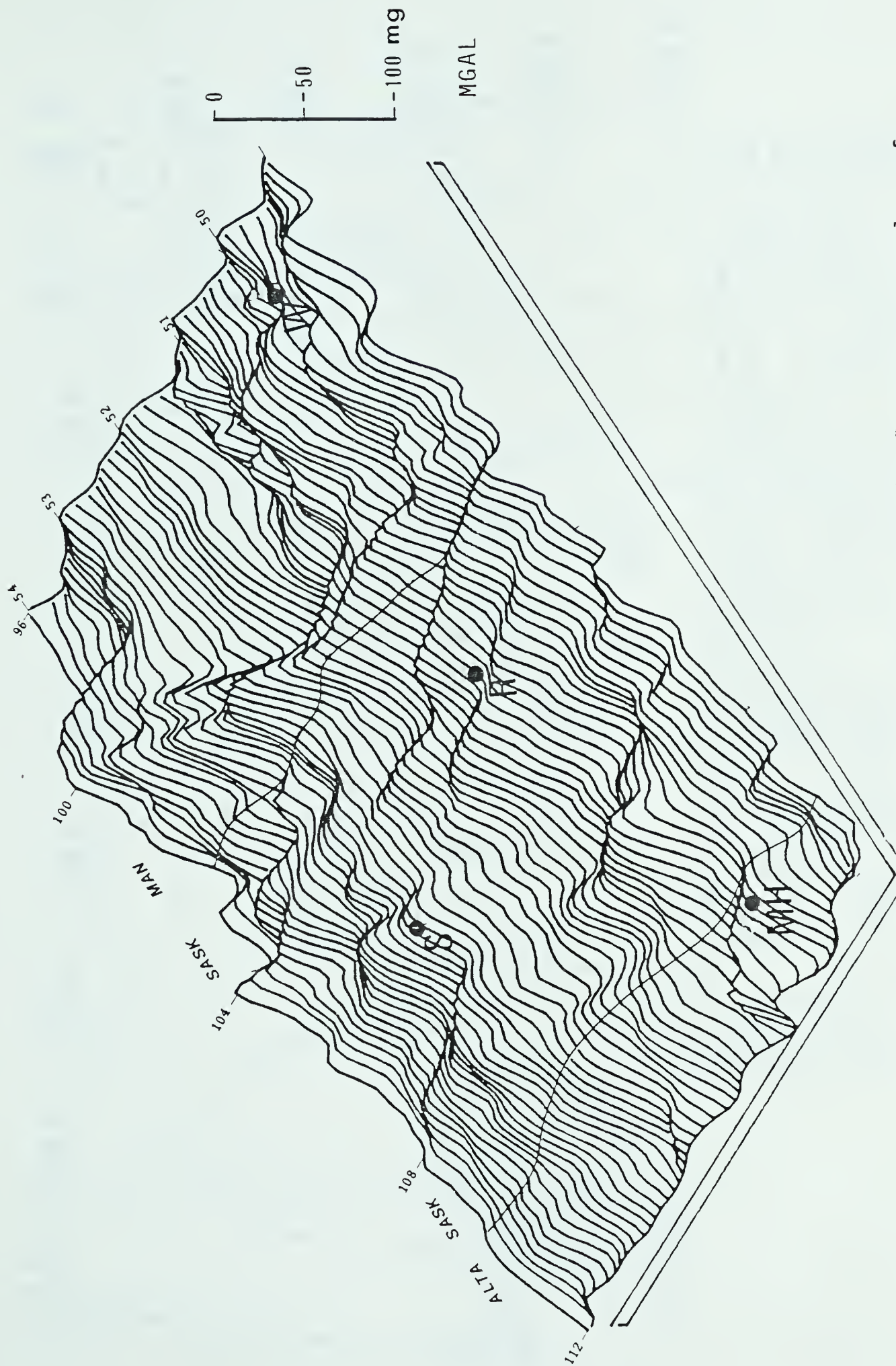


Figure 4.4b. A perspective view of the Bouguer anomaly of the southern plains of western Canada after correction for the sedimentary basin.

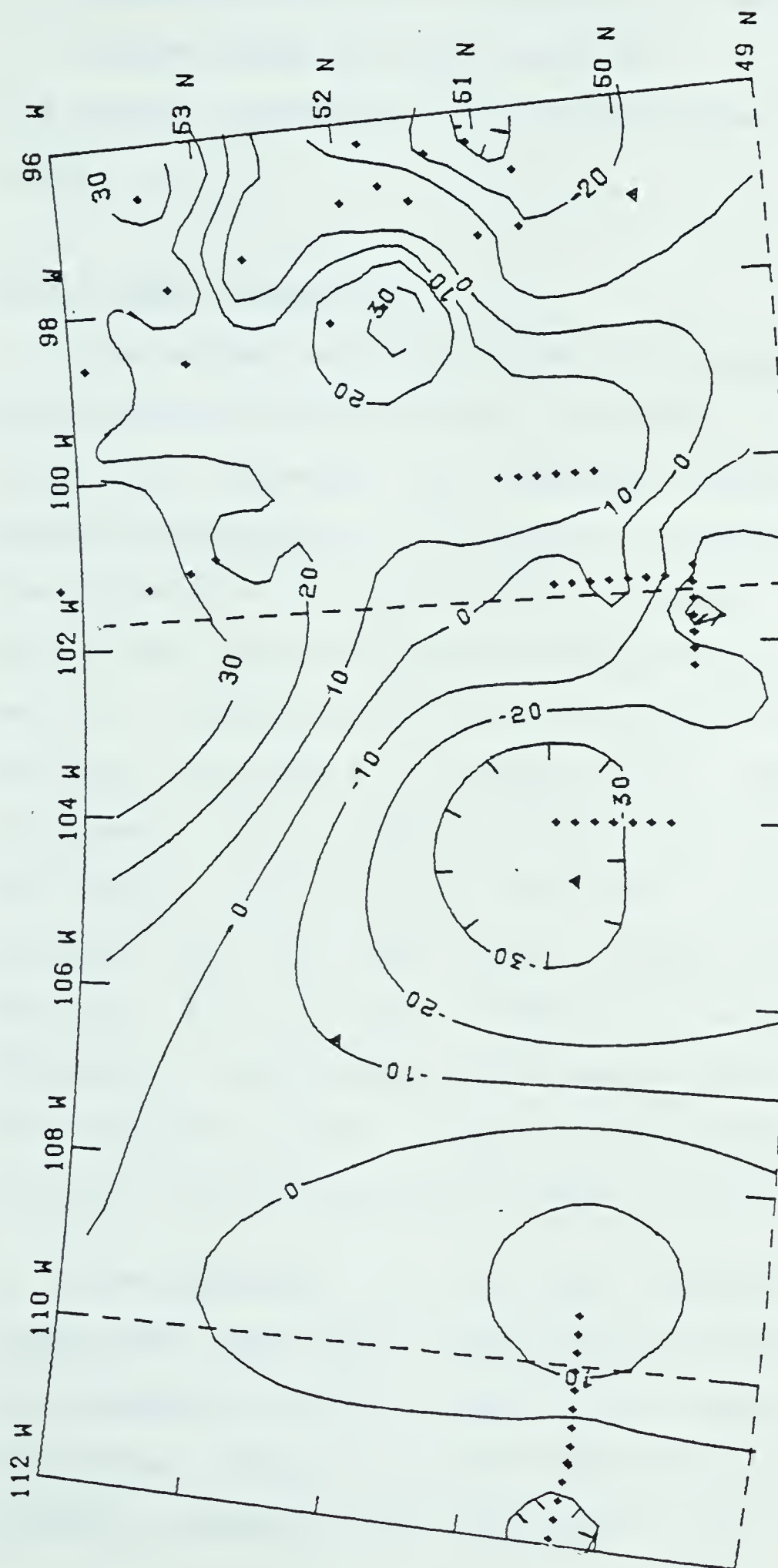


Figure 4.5 The station correction which must be added to the Bouguer gravity in order to achieve agreement between the seismic and gravity data at control locations. A negative station correction implies the existence of mass in the lithosphere in excess of that predicted by the seismically determined crustal model. A positive station correction implies a mass deficiency. The contour interval is 10 milligals. The small triangles represent major cities. The other dots represent the seismic control as described in the caption of Figure 4.1a.

predicted from the disagreement between the gravity and seismic data at control points.

The above parameters will be discussed in further detail below.

4.2.1 MODEL PARAMETERS

The seismic velocity of the upper crust can be expected to be quite variable from one location to another. This layer is bounded by basement above and the RielM discontinuity below. Classically, it might be thought of as the "granitic" or continental crustal layer. In actual fact, this layer is probably composed of a large number of massive intrusions and ancient orogenic belts just as one observes for example in exposed shield areas. Hence, the assignment of a single seismic velocity to this layer is difficult. In this study, the velocities determined by or assumed for the deep seismic crustal experiments in the map-area are utilized. Where the seismic experiments detected interlayering, an average velocity was calculated for the entire layer. A map of the upper layer seismic velocity for the map-area is shown in Figure 4.7.

The thickness of the lower crustal layer is also determined from deep seismic results across the map-area. For purposes of this study, this layer is defined as extending from the RielM discontinuity where seismic velocity becomes about 6.5 km/s to the Mohorovicic

discontinuity where the velocity jumps to about 8 km/s. This lower crustal layer has been referred to as the "intermediate" or oceanic crustal layer in the literature. Like the upper crustal layer, it is probably very complex and likely composed of many rock types. A possible interface within the lower crustal layer, the RielA discontinuity, where velocity jumps to about 7.1 km/s has been detected at several locations in the map-area. The thickness of the lower crustal layer is shown in Figure 4.8. Areas of thick lower crust include the western portion of the map-area and the Williston basin in southeast Saskatchewan. An anomalously thin lower crustal layer occurs in eastern Manitoba.

The RielA discontinuity in the deep crust is problematic in the inversion procedure since it can not be correlated across the map-area. While it occurs in southern Alberta, in the western portion of the Nelson Front, and perhaps in southeast Manitoba; it is not seen on seismic records from other parts of the map-area. The failure of this discontinuity to always appear on seismic records does not preclude the possibility of the existence of material with seismic velocity 7.1 km/s in the deep crust. It does denote that this material does not occur with sufficient abruptness to produce significant refraction or reflection energy on its upper surface. Hall and Hajnal (1973) in attempting to arrive at a velocity model for the Manitoba

deep seismic data had a difficult time choosing among the models illustrated in Figure 4.6. The model on the far left best suited their short range data while the center model which includes a Riela discontinuity best fit the long range results. To reconcile the two types of data, the model on the far right which includes a gradational increase of velocity with depth was chosen as the most reasonable. From the point of view of gravity effect, either of the two models on the right are satisfactory since both produce about the same density contrast at the Mohorovicic discontinuity.

For this study, a two layer crustal model is utilized with the lower crustal layer being assigned an average density determined in one of two ways. For locations where the Riela is known to exist, the lower crustal layer is assigned the average velocity of the two constituent layers. For locations where no Riela is evident on the seismic results, the lower crust velocity is set at the average as determined by the gradational formula. A map of the mean seismic velocity of the lower crust is shown in Figure 4.9. Surprisingly, the velocity of this layer tends to increase gradually from west to east, not at all reflecting any dependence on depth of burial. This suggests that the composition of the lower crust varies considerably in the map-area, perhaps becoming more dense to the east.

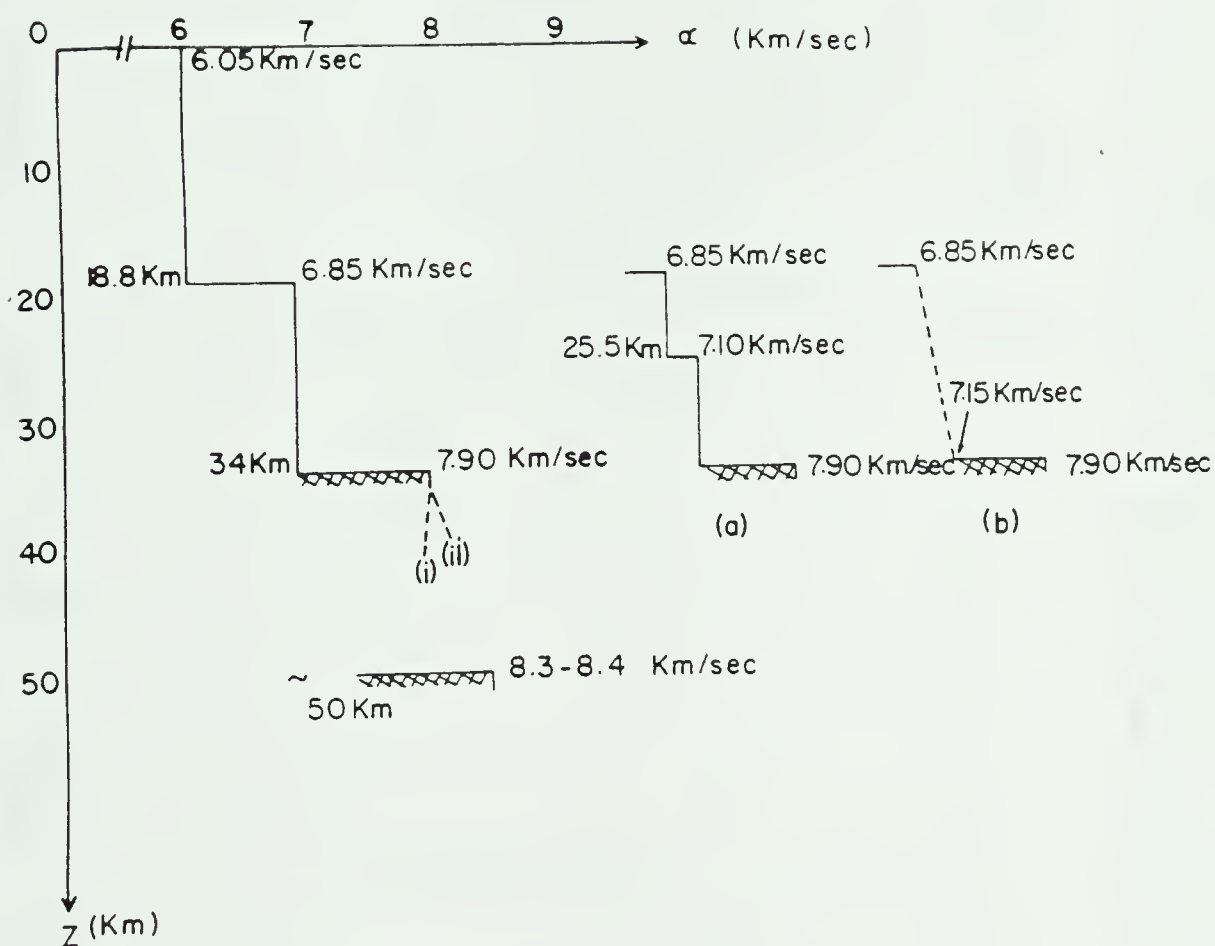


Figure 4.6. Proposed velocity models for Manitoba. (After Hall and Hajnal, 1973). The model furthest left involves only the RielM and Mohorovicic discontinuities. Model (a) utilizes an explicit RielA discontinuity but model (b) involves a gradational lower crust without the RielA discontinuity.

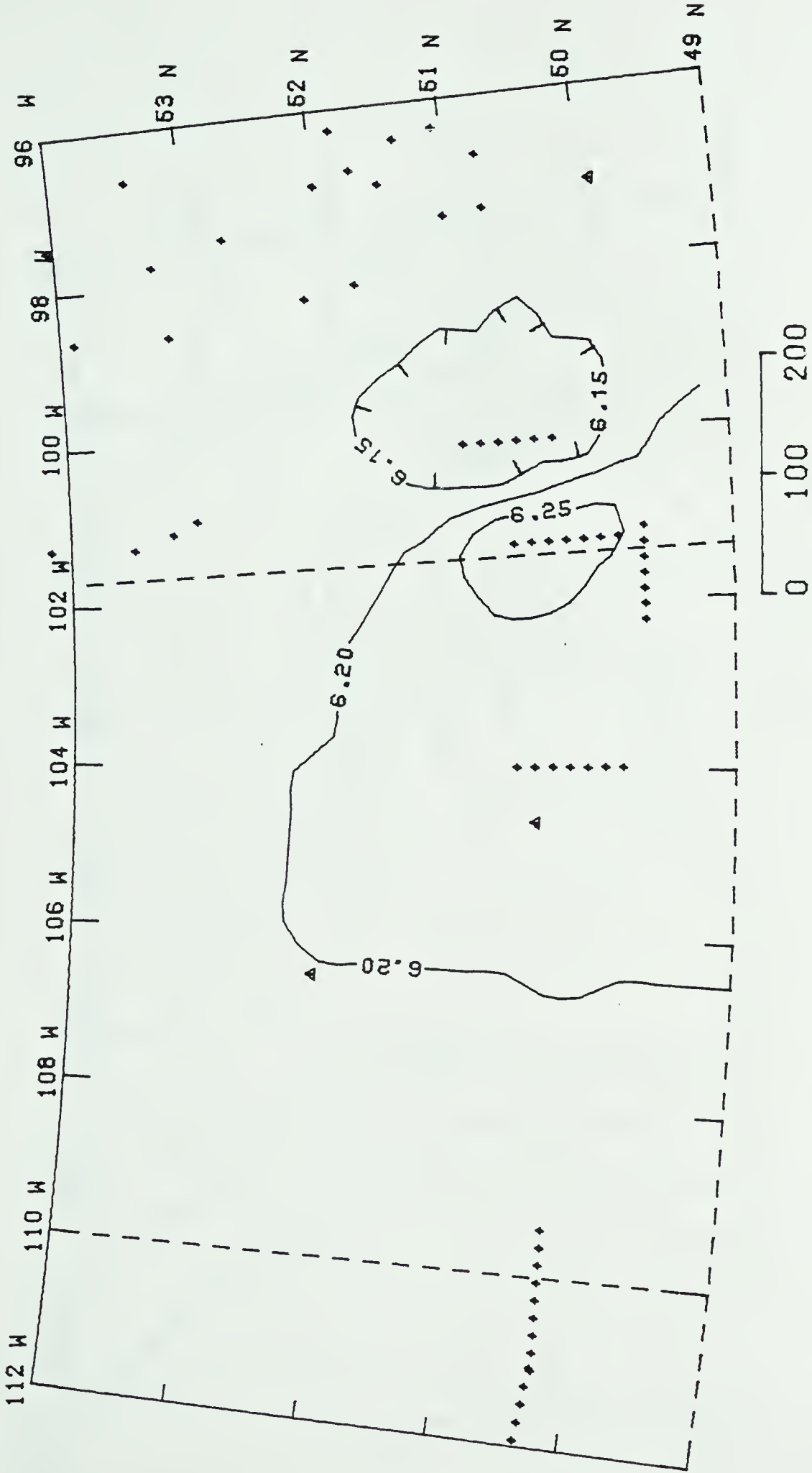


Figure 4.7. The seismic velocity of the upper crust for the southern plains of western Canada. The contour interval is 0.05 km/s. The small triangles represent major cities. The other dots represent the seismic control as described in the caption of Figure 4.1a.

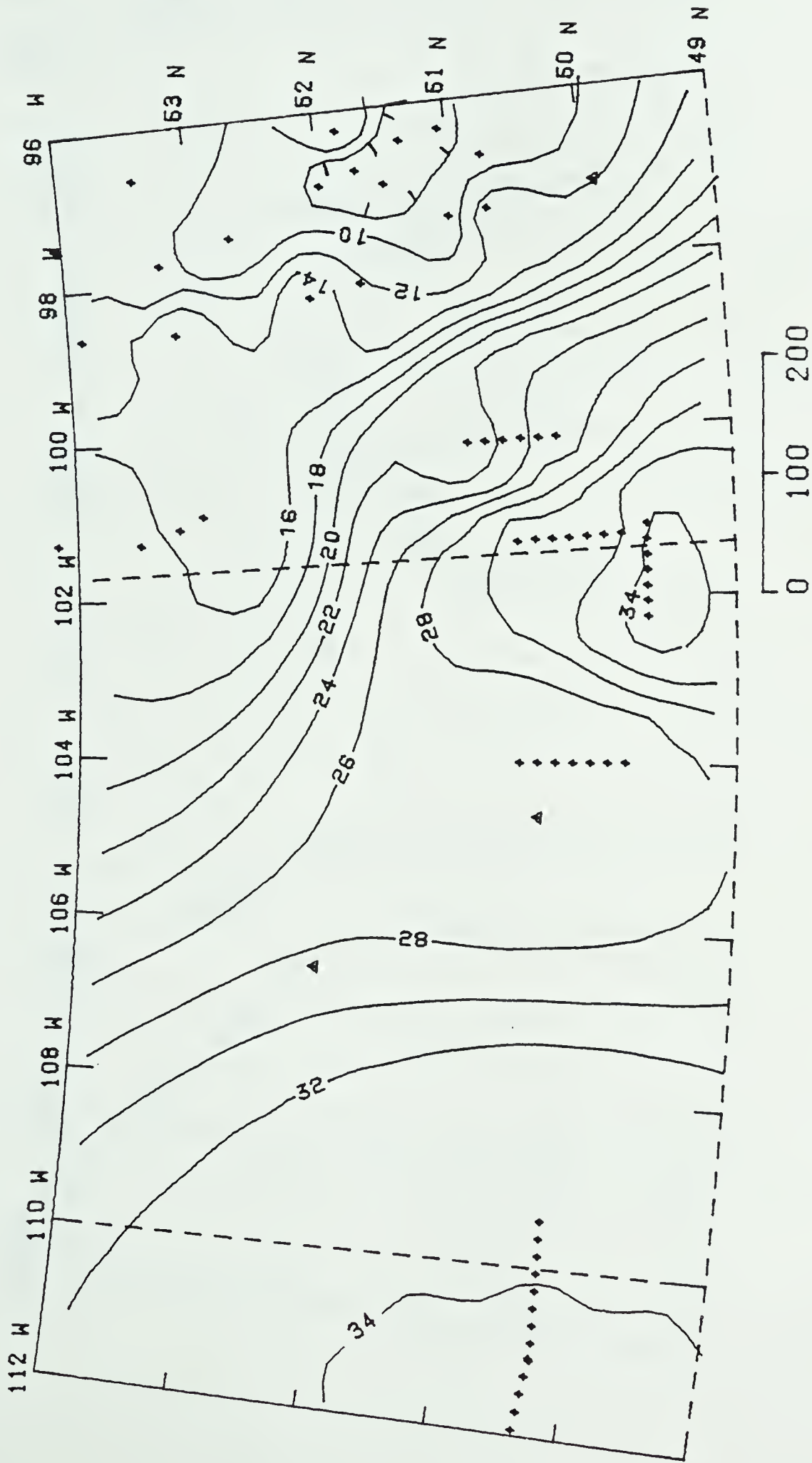


Figure 4.8. The thickness of the lower crust in the map-area. The contour interval is 2 km. This parameter is not altered by the modelling process. The small triangles represent major cities. The other dots represent the seismic control as described in the caption of Figure 4.1a.

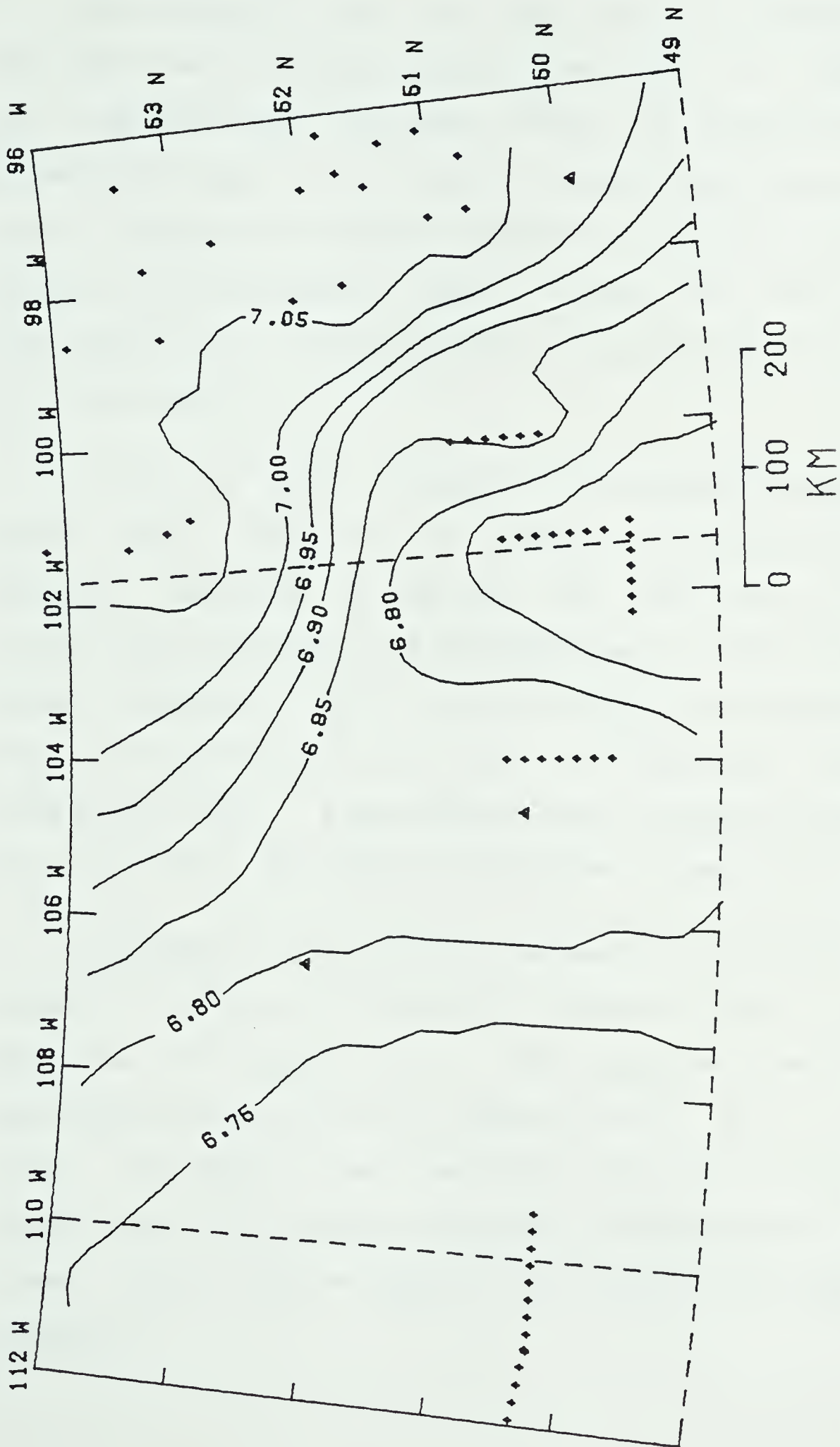


Figure 4.9. The mean velocity of the lower crust for the map-area. The contour interval is 0.05 km/s. The triangles represent major cities. The other dots are the seismic control points.

The velocity of the upper mantle in the map-area is derived from the seismic results and shown in Figure 4.10 for the map-area. The most interesting feature here is the pronounced high in south-central Saskatchewan which suggests that the mantle is denser and perhaps cooler in this region than in the surrounding areas. Perhaps this cool spot in the mantle is related to the development of the Paleozoic Williston basin.

Like the other seismically determined parameters, the upper mantle velocity is subject to uncertainty. For example, azimuthal anisotropy may well exist in the area since such anisotropy has been observed in other continental areas (Bamford, 1973). There is also a strong possibility that the crust-mantle interface is laminated (Clowes and Kanasewich, 1970), a phenomenon creating some uncertainty as to what path a long range seismic head wave actually takes.

A summary of the velocity parameters discussed above is given in the form of velocity cross-sections across the map-area in Figure 4.11. The sections are drawn in an east-west direction at latitudes of 50°N, 51°N, 52°N, and 53°N. The upper line in each box gives the velocity of the upper crust; the middle line gives the mean velocity of the lower crust; and the lowest line indicates the upper mantle velocity.

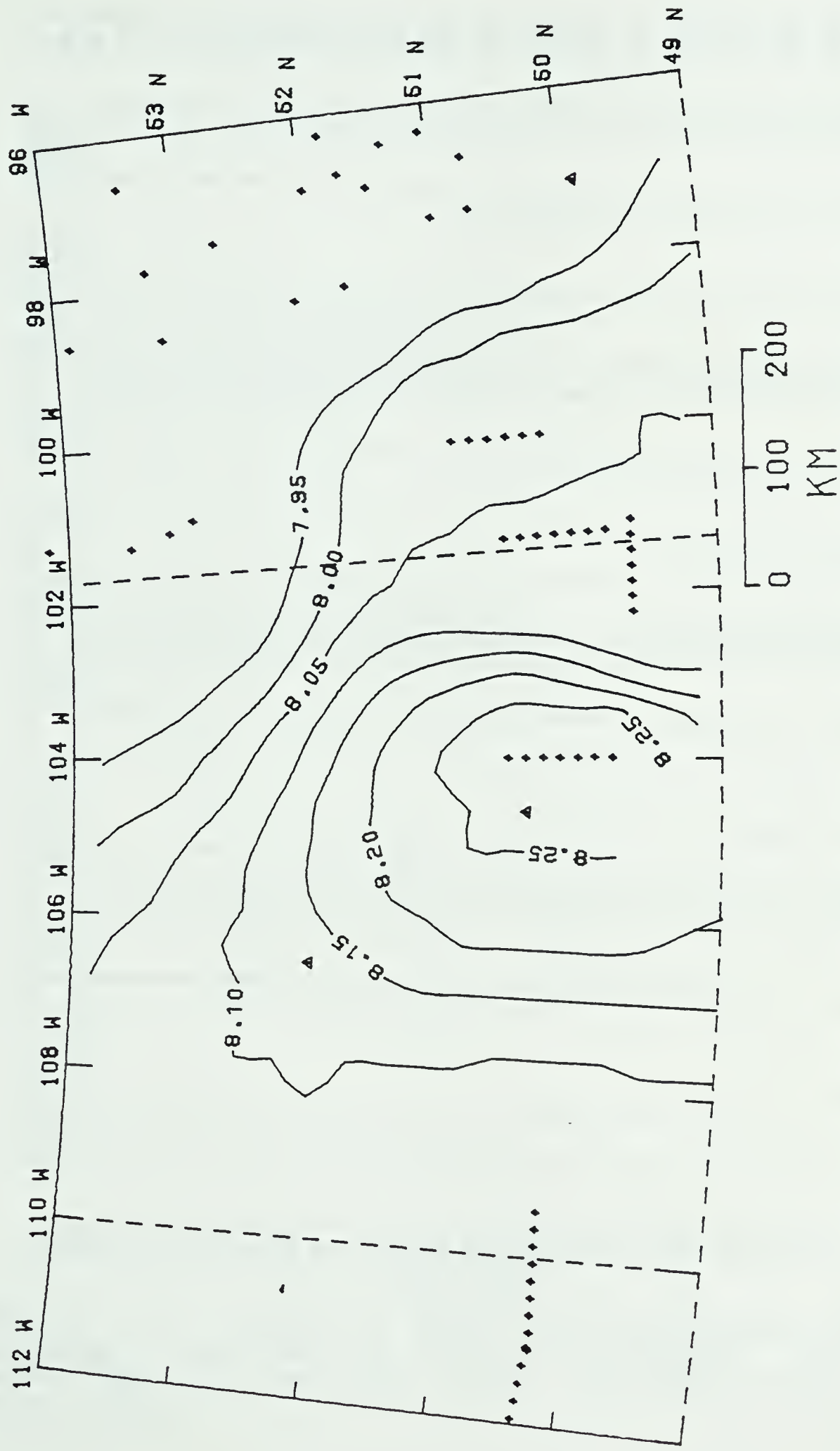


Figure 4.10. The velocity of the upper mantle for the map-area. The contour interval is 0.05 km/s. Known tectonic lineaments are also shown. The triangles represent major cities. The other dots are the seismic control points.

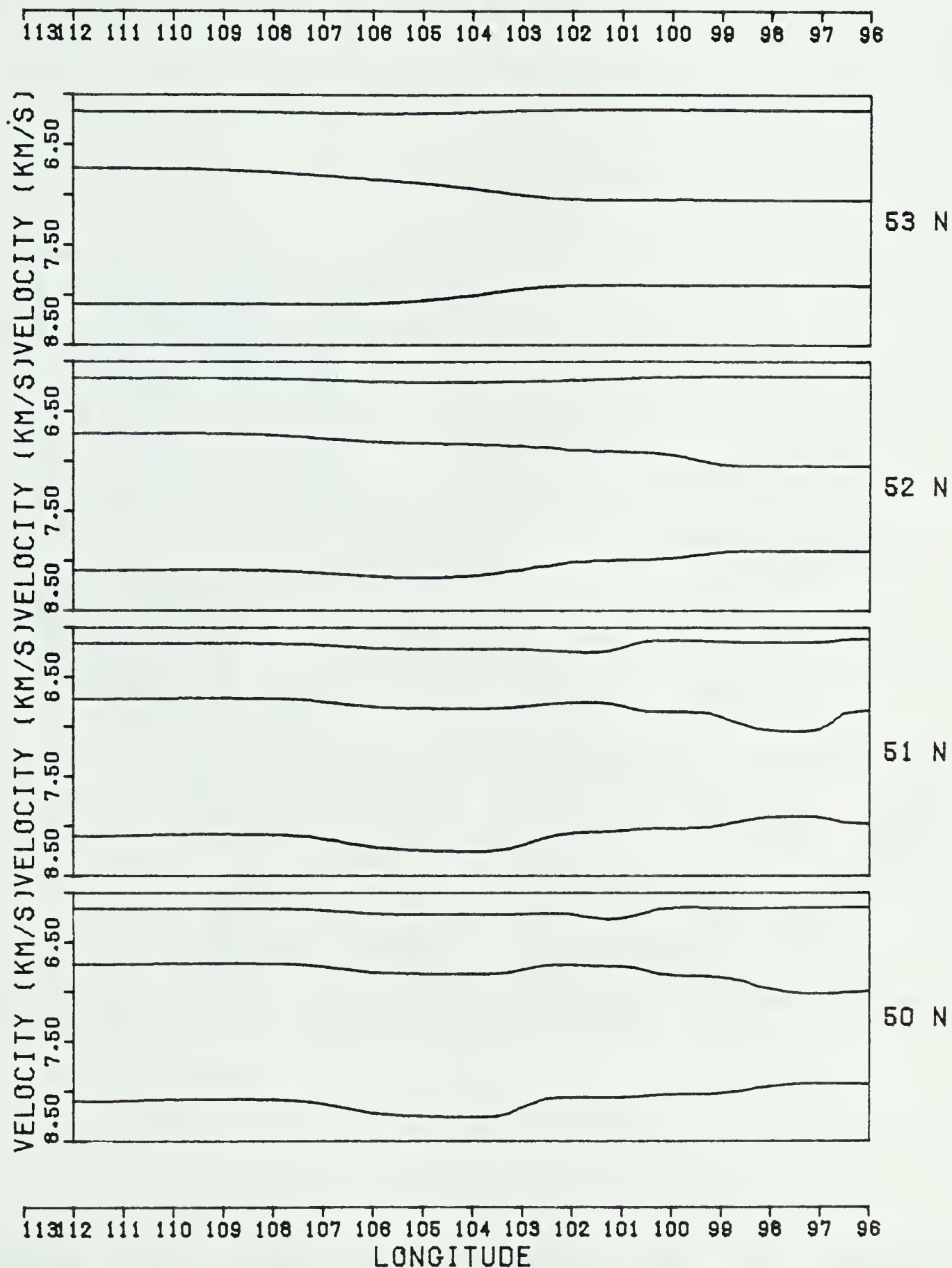


Figure 4.11. East-west velocity profiles drawn across the map-area. The lines in each box represent the seismic velocities of the upper crust, the lower crust, and the upper mantle.

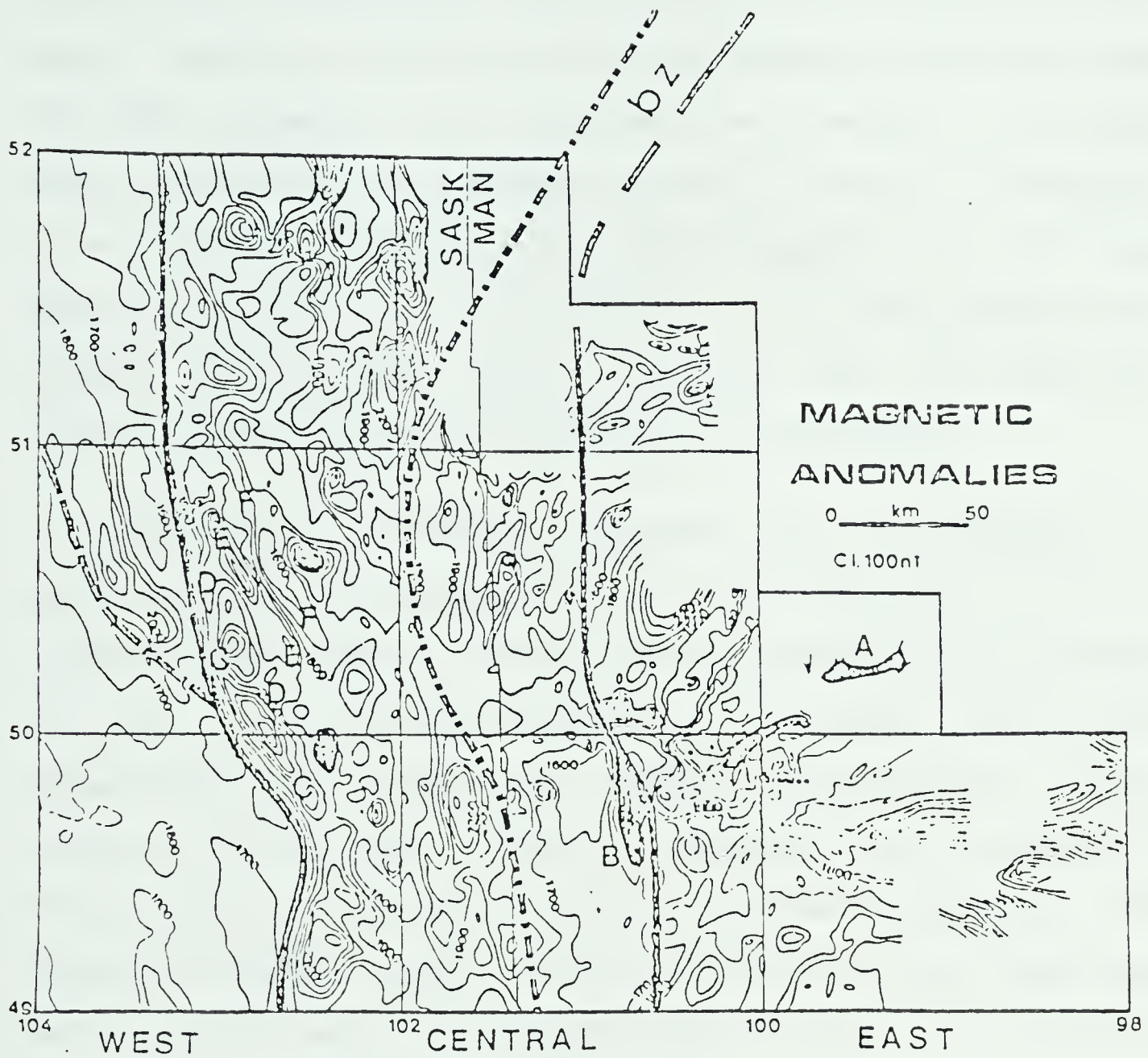


Figure 4.12. Compiled aeromagnetic map of southwest Manitoba and southeast Saskatchewan. (After Green et al, 1977).

For gravitational computations, it is necessary to convert seismic velocities to densities. For the crustal layers, the conventional Nafe-Drake curve was used. For the upper mantle, a curve published by Goodacre (1972) was used with the assumption that the mean atomic weight of the upper mantle material lies midway between 21 and 22. Goodacre's curve yields an average value of 3270 kg/m^3 for the upper mantle material, a value more in line with conventional thought than the 3400 kg/m^3 predicted by the Nafe-Drake curve and used in an earlier part of this thesis.

For gravity inversion purposes, it is necessary to assume a depth of compensation for the lithosphere, that is, a depth below which no lateral density variation is allowed. A value of 50 km was assumed for this study, this being a value found most likely by Cumming and Chandra (1972). Gurbuz (1970) has found evidence for a possible discontinuity well within the mantle beneath Manitoba. This velocity change seems to be detectable only by long range seismic experiments and therefore may be due to a simple velocity gradient rather than an actual discontinuity. Nonetheless, the presence of such inhomogeneity in the upper mantle has serious implications for gravity modelling. However since detailed data on the upper mantle is virtually nonexistent, it is impossible to include such features in this study. Outside the map-area, the crustal parameters discussed above are assumed to gradually approach their mean

values and the Bouguer anomaly is gradually tapered to zero. This procedure is followed to avoid false sharp edges in the data grid. The presence of any such sharp changes generates short wavelength noise fatal to the convergence of the inversion scheme.

The inversion scheme utilizes both the long wavelength and short wavelength portions of the Bouguer anomaly. The long wavelength portion of the field is inverted in terms of deep crustal structure using a multilayered reformulation of the Parker algorithm. The shorter wavelength residual anomalies are inverted in terms of density variation in the upper crustal layer, using still a different formulation of the Parker algorithm. This approach seems quite reasonable in light of studies by Hall and Brisbin (1964), Chandra and Cumming (1972), and Hajnal and Rose (1979) which present evidence that local upper crustal Precambrian masses are a source of disagreement between seismic crustal models and gravity data.

4.2.2 MULTILAYERED MODELLING PROCEDURE

The procedure followed to obtain the depths to the Mohorovicic and Rielm discontinuities was as follows. The original Bouguer gravity readings (Figure 4.4a.) were automatically sampled onto a grid at about 8 km spacings. To remove random noise generated during the sampling process, the gridded set of values was filtered and reduced

to a 16 km grid spacing. A correction for the effect of the sedimentary cover was then made following the procedure outlined in a previous chapter. A perspective view of the Bouguer anomaly after correction for the sedimentary cover is shown in Figure 4.4b. Analysis of the amplitude spectrum of the equivalent stratum at a depth of 33 km indicated that only wavelengths greater than about 100 km were suitable for the multilayered inversion process. The data set was accordingly separated into long and short wavelength components. The short wavelength portion of the data was set aside to be modelled in terms of density variations in the upper crustal layer. The long wavelength component, shown with the total anomaly in Figure 4.13, was used to derive the depths to the Monorovicic and Rielm discontinuities.

In order to obtain a meaningful result, it is necessary that the seismic crustal models and the Bouguer gravity anomalies match at the control points. If they fail to agree, one can only assume that some density variation occurs in that locality which is not detectable by seismic methods. Such a density variation could be due to anything from near surface lithology variations in the upper crust to deep heat flow patterns in the mantle. Since there is no way to avoid this ambiguity, the disagreement is calculated at each control point in milligals, and then simply spread smoothly across the map-area. The net effect of this

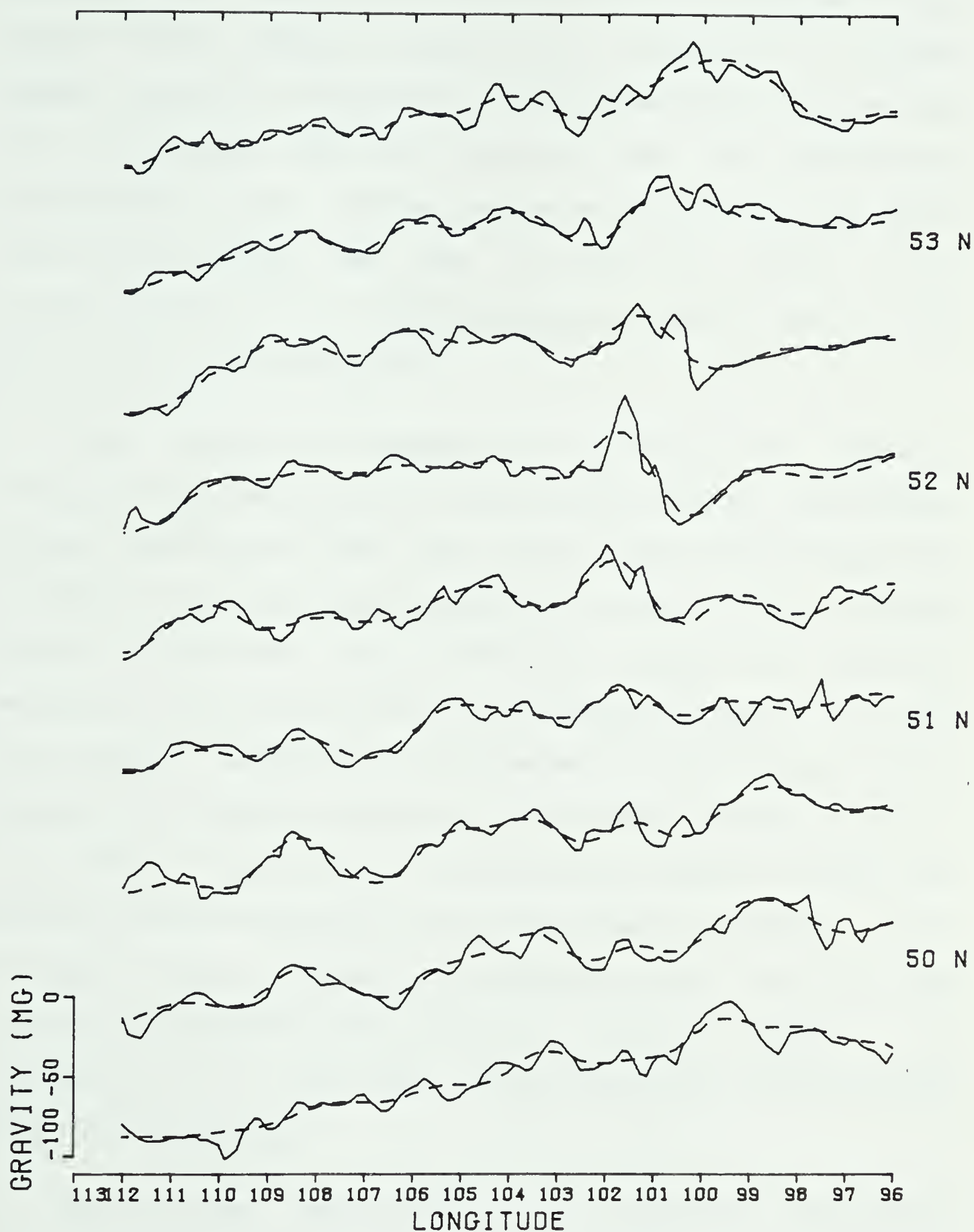


Figure 4.13. Comparison of the Bouguer anomaly with its long wavelength regional component (dashed line) shown in the form of east-west profiles across the map-area.

procedure is that a station correction is applied to the Bouguer anomaly before inversion to account for various unknown density variations in the lithosphere. By applying this correction, one is assuming that the seismically determined crustal models are correct as far as they go at the control points, and that the gravity anomaly is a suitable guide for interpolating the seismic results from one location to another.

The station correction is calculated by smoothly interpolating the seismically determined crustal parameters across the map-area, and then using these interpolated data as input to the multilayered reformulation of the forward Parker algorithm. The difference between the gravity anomaly so obtained and the actual Bouguer anomaly is then the station correction to be added to the anomaly at each control point before inversion. To produce a smooth result, the station correction is interpolated smoothly across the map-area before being applied to the Bouguer anomaly. This procedure tends to spread the uncertainty over the whole map rather than concentrating it at the control points. All interpolation is performed by the weighted squares method described previously.

The station correction is in itself an interesting source of information about the lithosphere. Figure 4.5 shows a map of the interpolated station correction.

A positive station correction indicates that the seismic crustal model is too dense to be consistent with the Bouguer anomaly. A deficiency of mass must therefore exist somewhere in the lithosphere at these locations for compensation.

If the published seismic models are correct, then significant mass deficiency is apparently associated with the region on a line from the the Flin Flon area near 52°N - 102°W toward the south basin of Lake Winnipeg near 51°N - 96°W . Hall and Brisbin (1965) have previously noted the disagreement between the local gravity anomaly and the detailed seismic crustal model near Flin Flon. They attributed the difference to the presence of near surface greenstone belts in the area. However, their explanation does not seem to be satisfactory on a regional basis. Since the greenstone belts are of relatively high density and of only local extent, they can not cause the mass deficiency required to suit the observed regional gravity anomaly.

The disagreement between the regional gravity data and the seismic model near the south basin of Lake Winnipeg is also not easily explained. Hall and Hajnal (1973) have mapped a trough-like thickening of the upper crust over a distance of 350 km from the English River area of Ontario west to the south basin of Lake Winnipeg. Gurbuz (1970) has detected an apparent discontinuity in the upper mantle at the 40 to 50 km depth range in this same area. It is

possible that variations on this sub-crustal discontinuity might provide the mass deficiency along this trend to reconcile the gravity and seismic data.

A negative station correction signifies that an excess of mass undetected by the seismic experiments must exist in the lithosphere at that location. As is evident from Figure 4.5, south central Saskatchewan is dominated by a strong negative station correction possibly associated with the Williston Basin. Burwash and Culbert (1976) have noted that this area shows higher than average specific gravity in basement core samples due to a relative lack of quartz and K-feldspar. Hence the excess mass required to reconcile the gravity and seismic data in this area possibly occurs in the upper crustal layer which may have a higher than average mafic content. Another possible location for the excess mass is the upper mantle, the potential of which will be discussed later in this chapter.

The resulting crustal thickness map is shown in Figure 4.14 and the upper crustal thickness is given in Figure 4.15a. A perspective view of both is given in Figure 4.15b. East-west cross-sections of the derived crustal models are shown in Figure 4.16. Comparison of these results with the seismic data at control points indicates excellent agreement at all locations.

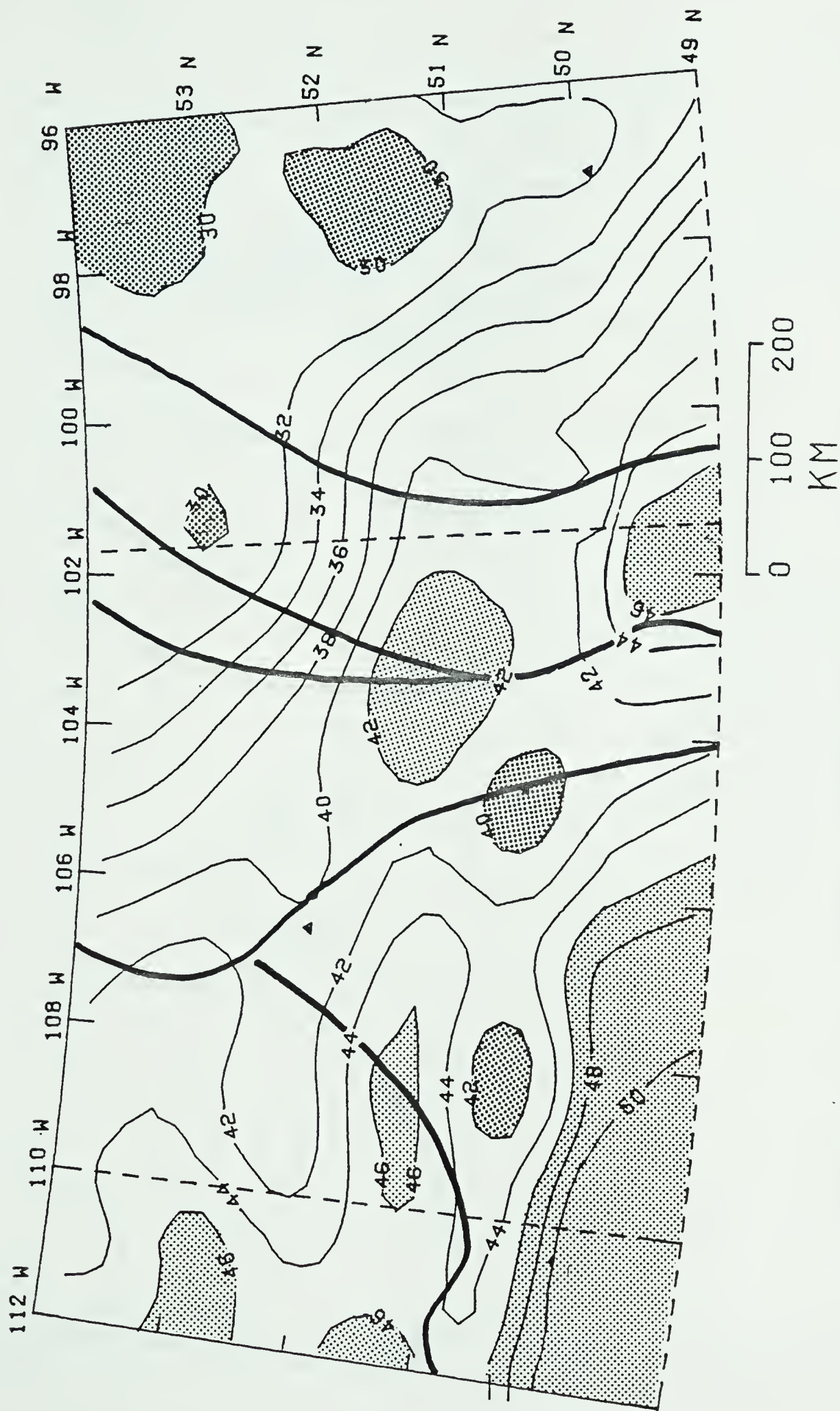


Figure 4.14. Crustal thickness map for the southern plains based on combined analysis of the seismic and gravity data. The contour interval is 2 km. The small triangles represent major cities within the map-area.

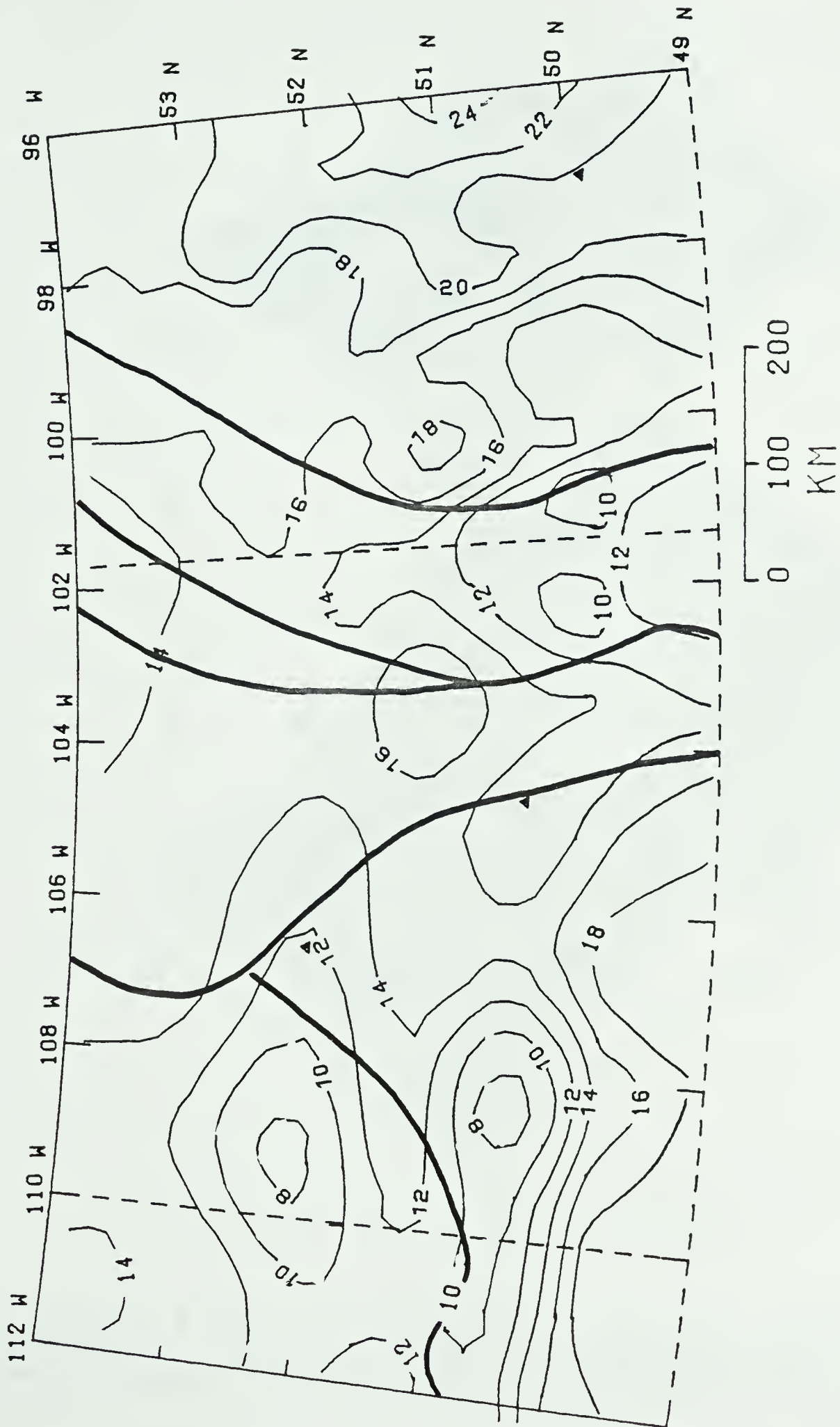


Figure 4.15a. Derived thickness of the upper crust for the southern plains of western Canada. The contour interval is 2 km. Known tectonic lineaments are also shown. The small triangles represent major cities within the map-area.

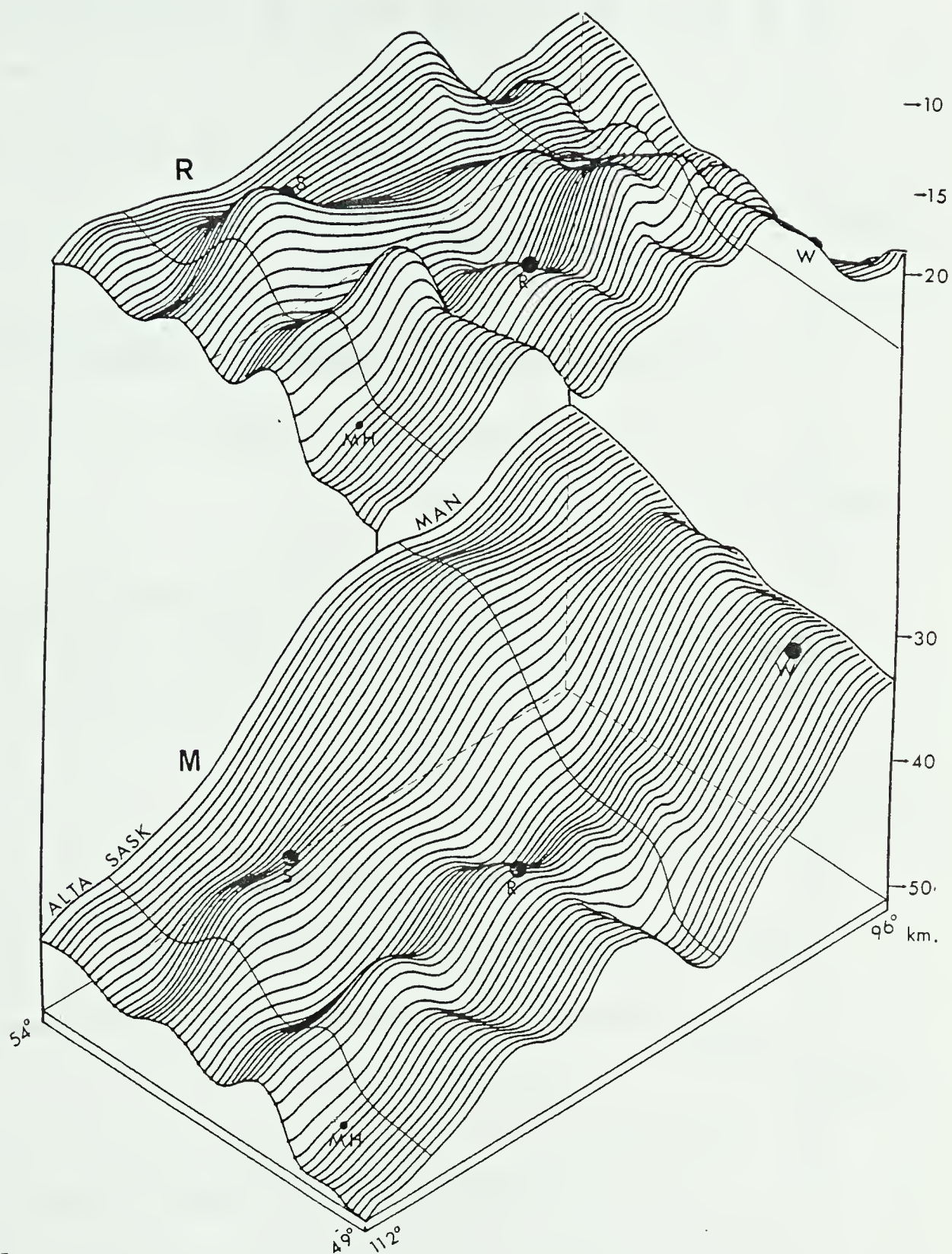


Figure 4.15b. A perspective view of the RielM and Mohorovicic discontinuities in western Canada. The large dots are major cities within the map-area.

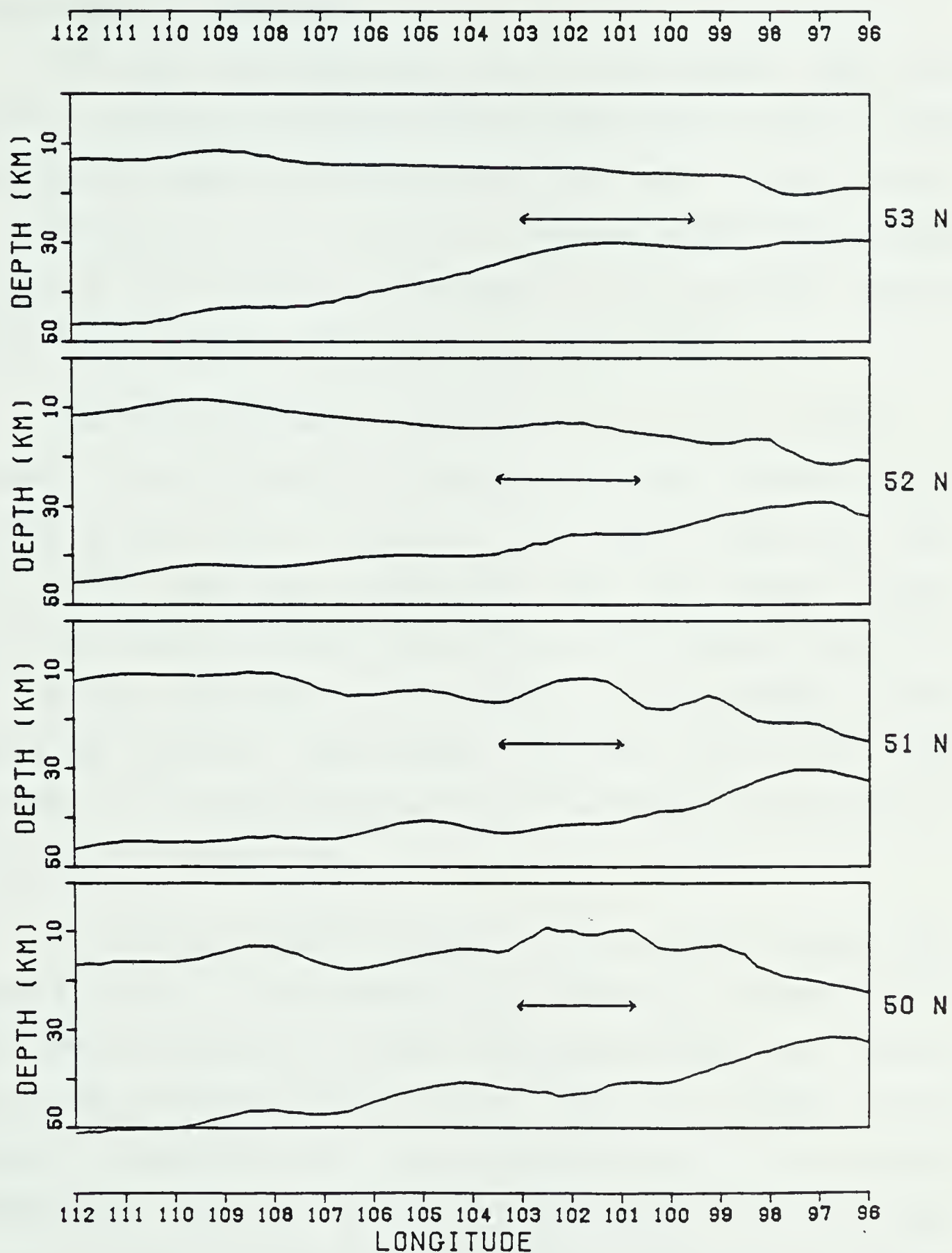


Figure 4.16. East-west crustal cross-sections drawn across the map-area. The upper interface in each box is the RielM discontinuity, and the lower interface is the Mohorovicic discontinuity. The Nelson Front is indicated by arrows.

4.2.3 DENSITY INVERSION

The short wavelength portion of the gravity data not used in the multilayered process above was utilized to find the lateral density distribution in the upper crustal layer. A reformulation of the Parker-Oldenburg algorithm was used in which the thickness of the upper crust was given, and the density variation in the layer was determined.

The short wavelength portion of the gravity anomaly is shown in profile form in Figure 4.17. The largest residual anomalies are on a trend to the north beginning near 101°W - 50°N and are associated with the Nelson Front. Isolated large residuals also occur in the Superior province in eastern Manitoba. In general, the residuals in this map-area, being of wavelengths from 25 to 100 km, are thought to be associated with shallow density variations in the upper crustal layer.

A slab of thickness equal to that of the average upper crustal layer is, for mathematical purposes, assumed to be the only source of the short wavelength anomalies, and the variation of density within this layer is assumed to be solely responsible for the distribution of the residual anomalies. The net density distribution for the upper crustal layer in the map-area is shown in map form in Figure 4.18 and in profile form in Figure 4.19, and as a perspective surface in Figure 4.20b.

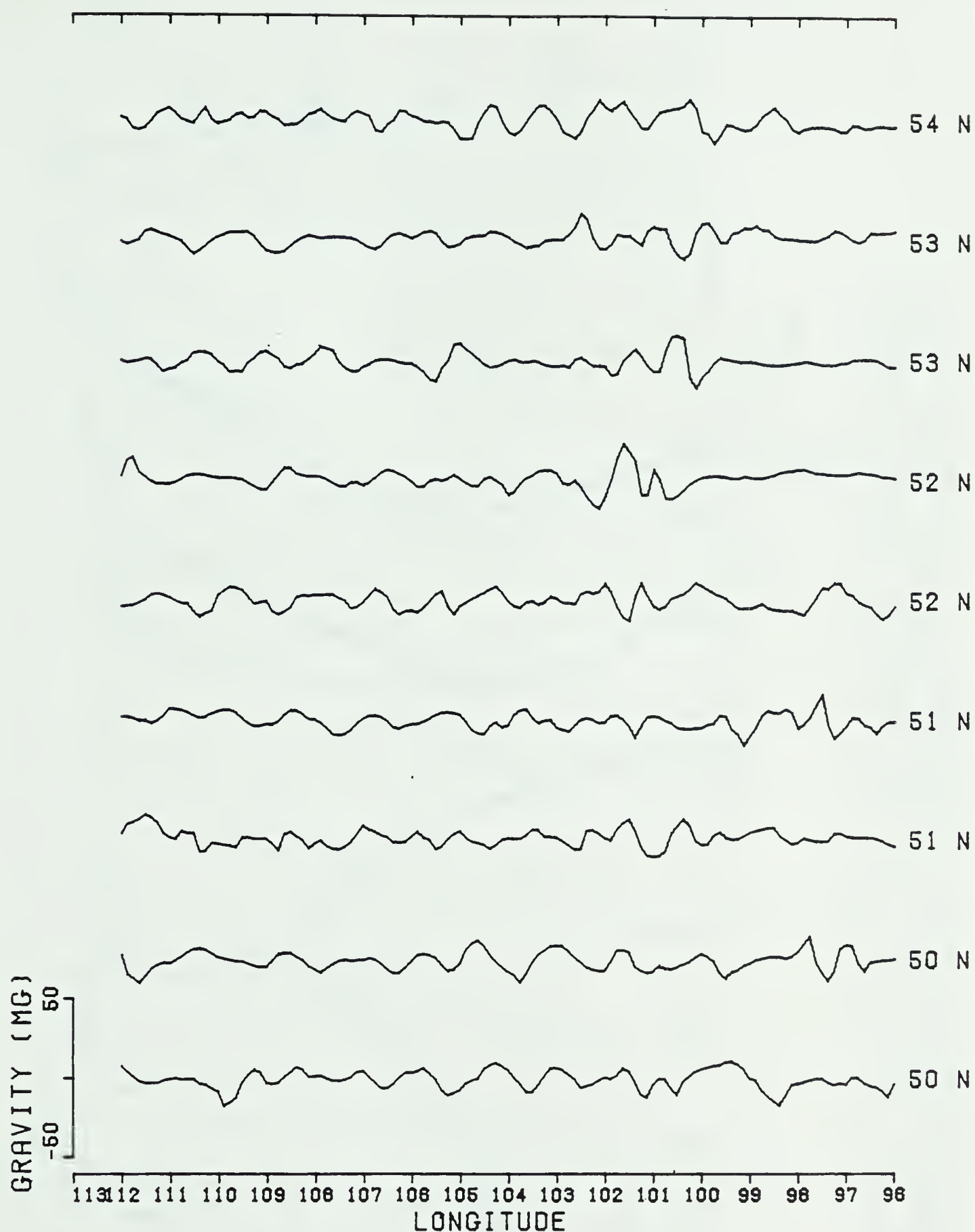


Figure 4.17. A series of parallel east-west profiles of residual gravity across the southern plains of western Canada. These residual anomalies are thought to be due to variations in upper crustal density.

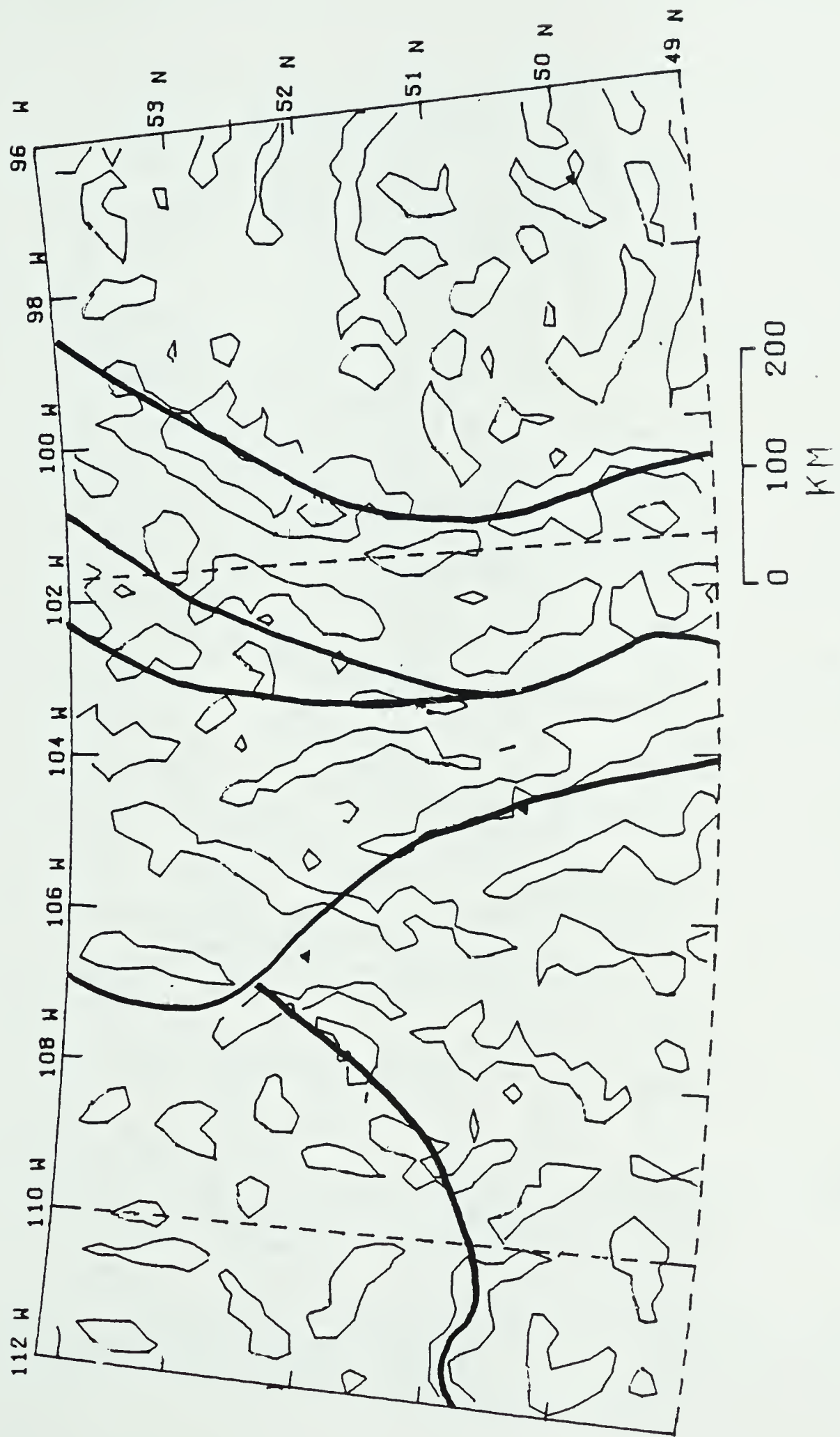


Figure 4.18a. Map showing areas of anomalously low density in the upper crust for the southern plains of western Canada. Known tectonic lineaments are also shown. The small triangles represent major cities within the map-area.

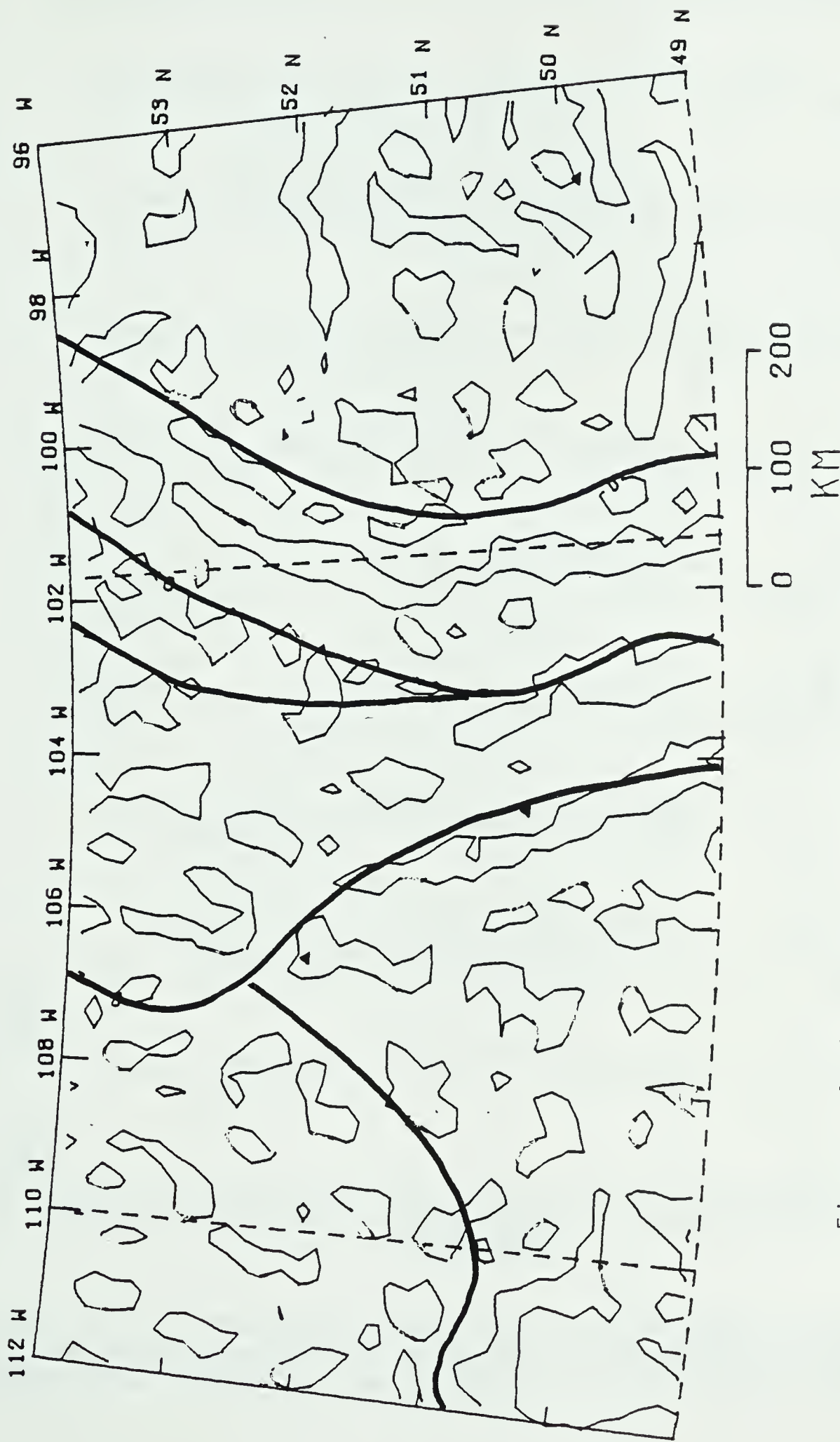


Figure 4.18b. Map showing areas of anomalously high upper crustal density (greater than 20 kg/m^3 above the regional) in the southern plains of western Canada. Known tectonic lineaments are also shown. The small triangles represent major cities within the map-area.

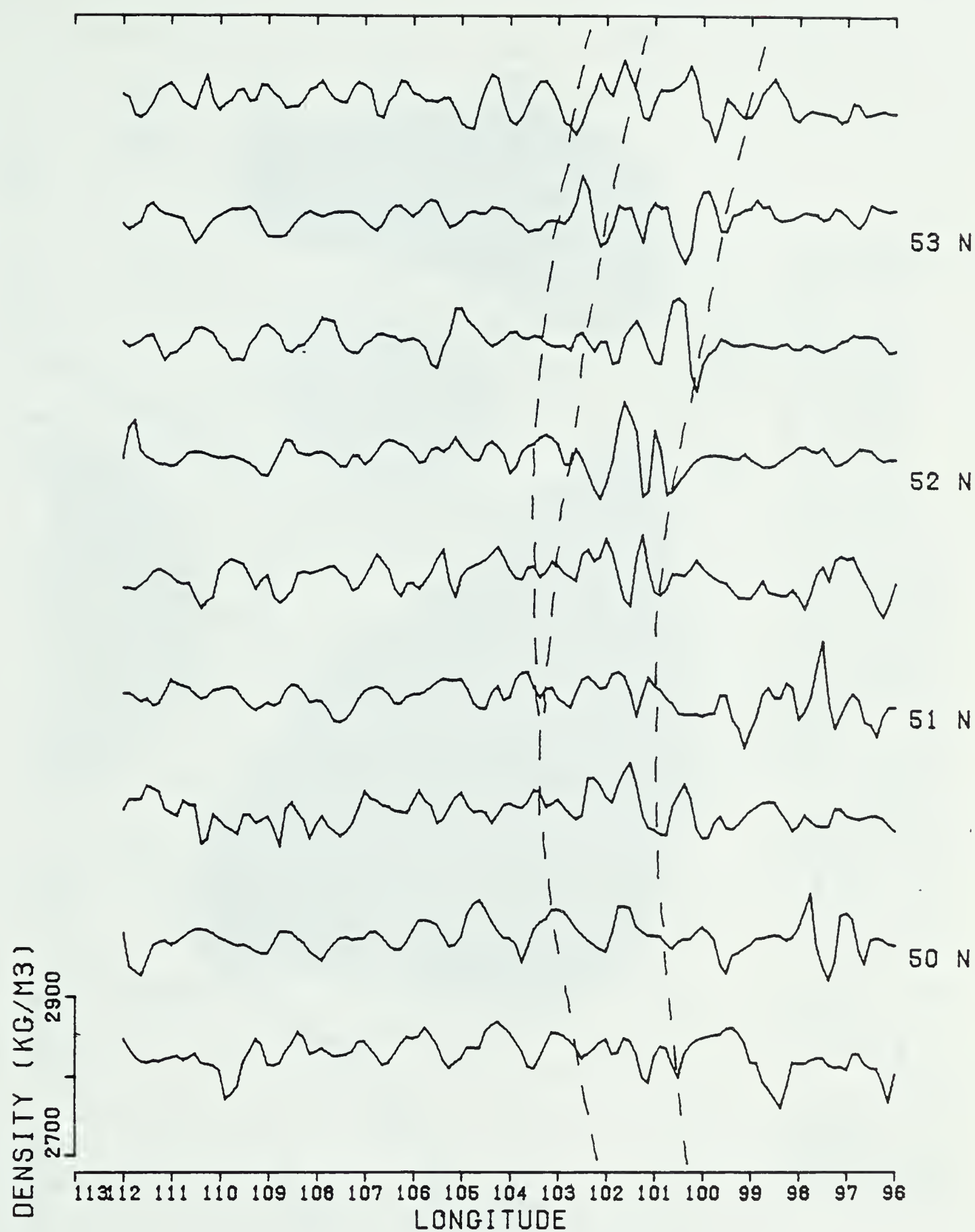


Figure 4.19. The density variation of the upper crust shown in the form of east-west profiles across the map-area. The dashed line indicates the location of the Nelson Front.

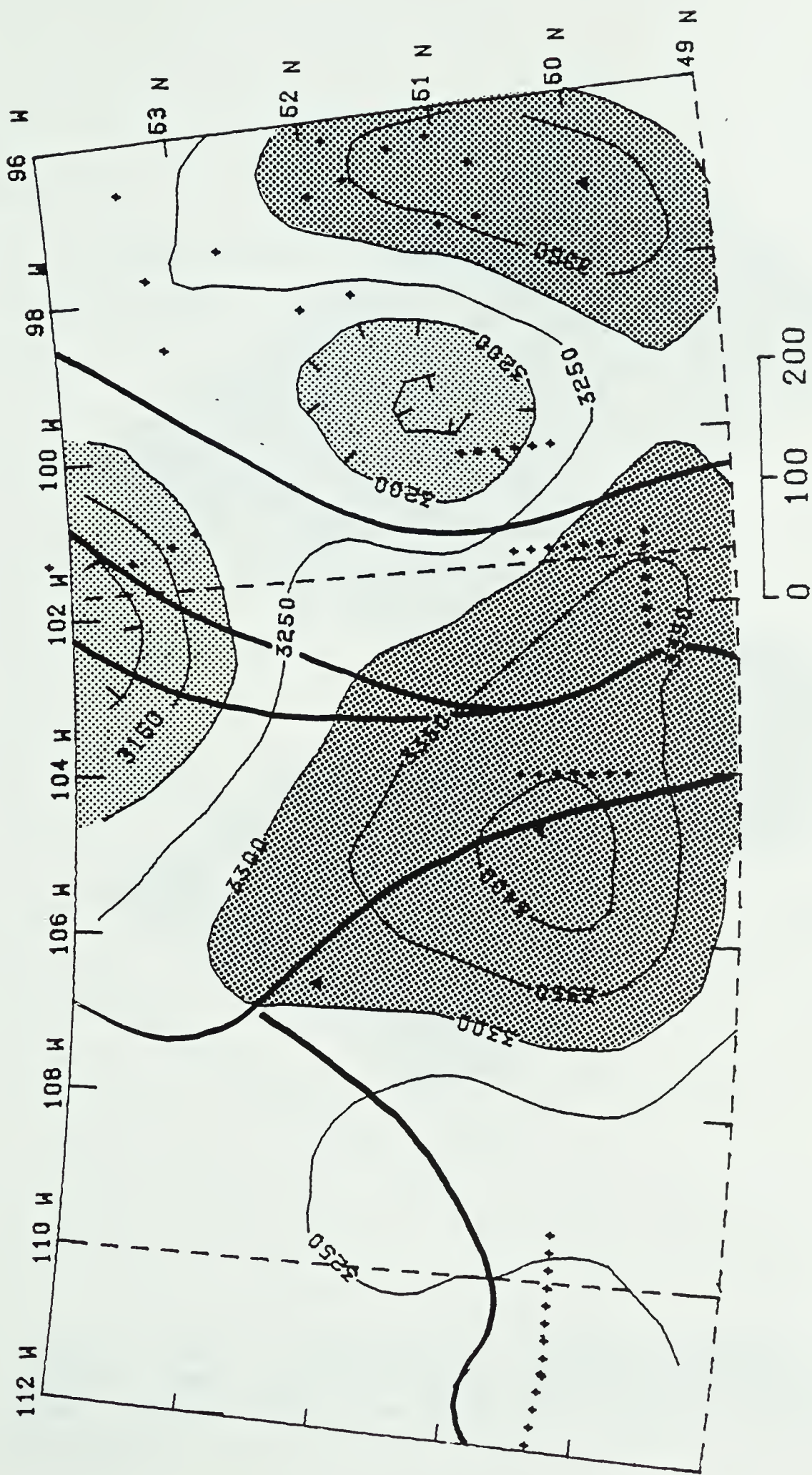


Figure 4.20a. Derived density of the upper mantle in the southern plains of western Canada based on the difference between seismic and gravity results at control points. The contour interval is 50 kg/m³. Known tectonic lineaments are also shown. The triangles represent major cities. The other dots are the seismic control points.

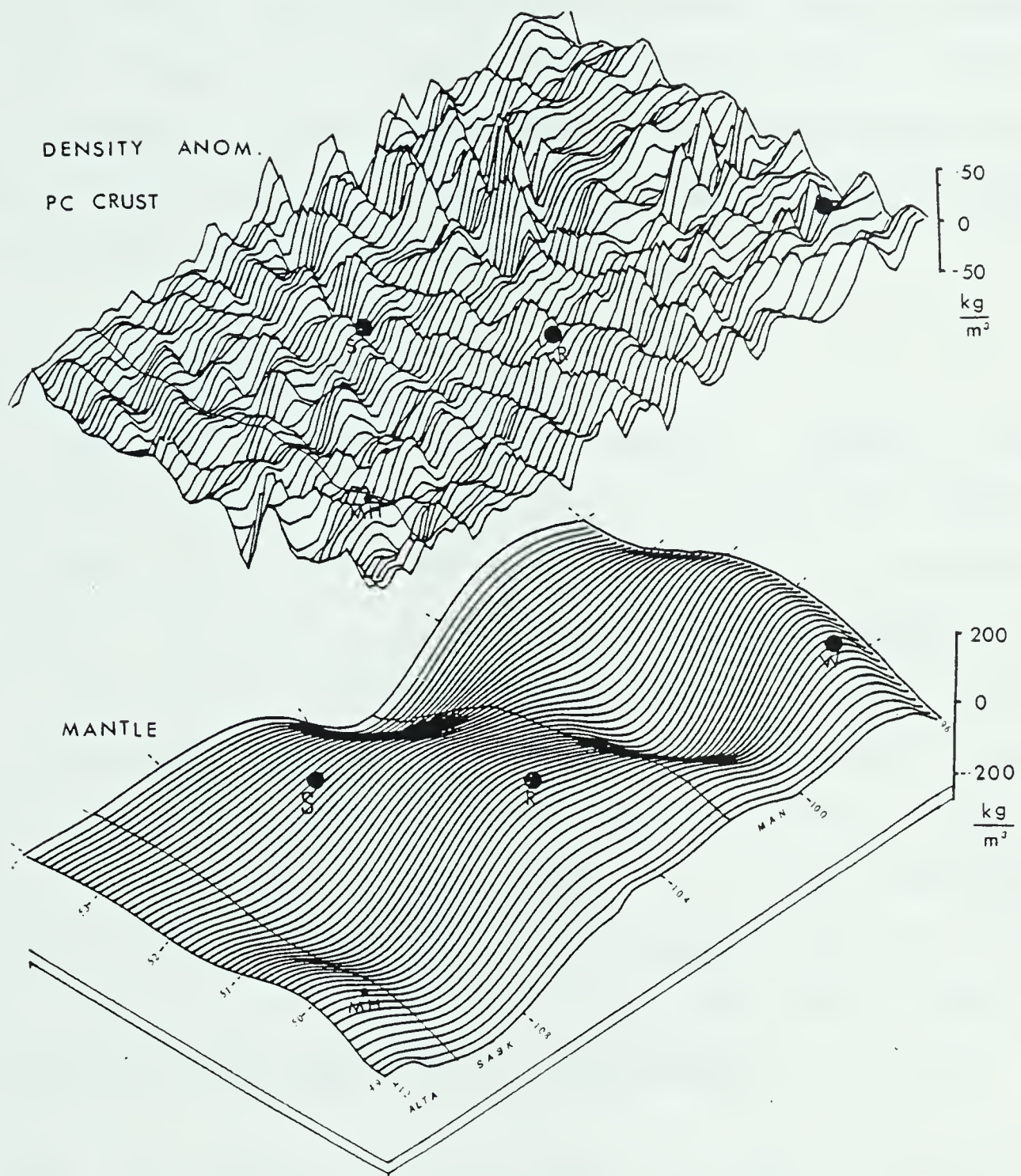


Figure 4.20b. A perspective diagram showing the derived lateral density variations in the upper mantle and in the upper crust. The large dots are major cities within the map-area.

It should be noted that while the derived density distribution is assigned to the upper layer, no attempt was made to alter the distribution of seismic velocity within the layer (Figure 4.7) by means of the Nafe-Drake or similar velocity-density curve. Such alterations would necessitate changes in the seismically determined crustal models which form the basic control for this study

4.2.4 MANTLE DENSITY CONSIDERATIONS

A portion of the original Bouguer anomaly left unmodelled to this point is that portion essentially removed by the application of the station correction, a reduction applied to the gravity data to force agreement between the gravity and seismic results at control points. This rather long wavelength portion of the data is very badly aliased since it has its origin in the very sparse seismic control points in the area. Nonetheless, its long wavelength (generally greater than 200 km) does suggest a source in the mantle, so it is interesting to see what type of density distribution in the upper mantle could explain this data.

For the sake of simplicity, a slab of constant thickness with its top at the average crustal thickness for the map-area (40 km) and its base at the assumed depth of compensation (50 km) is used as an upper mantle model. A simple reformulation of the Parker-Oldenburg algorithm for a slab of constant thickness was then used to determine the

lateral density distribution in the slab. The output was normalized to an average upper mantle density of 3270 kg/m^3 . The result is shown in Figure 4.20a.

4.3 DISCUSSION OF RESULTS

The main results of the overall inversion scheme are given in the form of maps of depth to the Mohorovicic and RielM discontinuities (Figures 4.14 and 4.15), and of maps of density distribution in the upper crustal layer and the upper mantle (Figures 4.18 and 4.20). The geological implications of these maps will be discussed below. To aid in the geological interpretation, the above figures have been plotted with the known tectonic lineaments shown.

4.3.1 THE SUPERIOR PROVINCE

Though the Mohorovicic discontinuity is very flat in the northeast portion of the Superior Province of this map-area, it dips rather sharply in the southwest portion of the province (Figure 4.14). The gradient is to the southwest. In a distance of about 200 km, the crust thickens from about 30 km on the flat plateau to about 40 km at the Nelson Front. Bell (1971b) proposed that the Superior Province was tilted in such a manner as to expose, after erosion, the Pikwitonei rocks along the northern edge of the block. Hajnal and Rose (1979) estimated that about a 4° tilt would be necessary to accomplish this. The gradient

apparent on the southwest edge of the plate is about 3° . Hence the pronounced tilt of the present day Mohorovicic surface may in fact be a remnant of such an ancient tectonic process.

However, the presence of the plateau like area to the northwest does not seem to be consistent with Bell's hypothesis unless there has been accretion of new material from the mantle onto the uptilted base of the crust, thus providing a new flat surface to the Mohorovicic discontinuity. Such accretion of mantle material might be due to cooling and subsequent phase change as the material was uplifted along with the crust. This idea has some support from the seismic velocities encountered in the map-area. In spite of decreased depth of burial, the velocity of the lower crust is higher in eastern Manitoba than in areas to the west (Figure 4.9). An uplift of the plate and subsequent accetion of material from the mantle, would have the effect of increasing the velocity of the lower crustal layer relative to the rest of the map-area.

Several interesting anomalous areas occur within the Superior Province on the RielM depth map (Figure 4.15), which maps the thickness of the upper crust. The English River-Lake Winnipeg downwarp (Hall and Hajnal, 1973) is apparent on the eastern edge of the map-area at 51°N . On the basis of the combined gravity and seismic results, the downwarp appears to have three branches: a minor one to the

southwest toward Winnipeg, a pronounced trough to the west, and the major branch to the northwest.

At approximately 99°W - 50°N , a structural terrace seems to occur on the RielM surface. This feature is associated with a broad gravity high which occurs east of Brandon, Manitoba. Toward the north end of the Brandon N/S refraction line, an isolated low on the RielM surface occurs. This indicates that the gravity data does not support a continuing increase of upper layer thickness to the north as one might extrapolate from the Brandon N/S crustal model (Figure 4.2). The anomalous areas of high and low density in the Superior province of the map-area (Figure 4.18) show a distinctly different pattern from the geological divisions to the west including some of the characteristic east-west trend just as one observes in the magnetic field over the province. A particularly anomalous zone of alternating high and low density occurs about 100 km north of Winnipeg. A long narrow zone of high upper crustal density, perhaps a mafic dyke, strikes ESE beginning just south of Brandon.

The density distribution in the upper mantle as derived from the variance between the gravity and seismic data is quite interesting in the Superior Province portion of the map-area as shown in Figure 4.20. There appears to be a tendency in the Superior Province for the density of the upper mantle to decrease as the Nelson Front is approached.

This result is contradictory to the Pn velocity map of the same area (Figure 4.10) which suggests an increase in velocity (and probably density) toward the Nelson Front. A possible explanation is that the depth of compensation, assumed to be a constant 50 km in the computation of upper mantle density, is actually variable across the Superior Province. The apparent upper mantle discontinuity detected by Gurbuz (1969, 1970) and Hall and Hajnal (1973) in Manitoba at depths from 40 to 50 km could cause the discrepancy between seismic and gravity results. Judging from Figure 4.20, if an upper mantle discontinuity does exist beneath the Superior Province, it probably dips WNW, creating increasing mass deficiency in that direction.

4.3.2 THE NELSON FRONT

The Nelson Front, which forms the transition zone from the Superior to the Churchill Province, is a tectonic boundary of great economic and scholarly interest. To the north of the map-area on the exposed shield, it is associated with the Thompson Nickel Belt, and within the map-area, economic deposits of hydrocarbons occur in the Phanerozoic sedimentary rocks overlying it. Better understanding of the tectonic development of this boundary zone will no doubt result in more successful exploration along its length. Many major advances in earth science in recent years have been the result of studies of tectonic boundaries. It is a matter of considerable interest to

determine whether plate tectonics is as applicable to the ancient shield areas of the earth as it is to modern mobile zones.

Lee (1977) and Hajnal and Rose (1979) have attempted to invert gravity results over the Nelson Front as if the source were two dimensional and invariable along its strike. Inspection of a series of east-west profiles of the gravity field across the map-area (Figure 4.21) indicates that while it is generally possible to trace the Nelson Front, the character of the anomaly changes considerably from north to south. Hajnal and Rose (1979) maintain that the gravitational signature of the front is a strong central low flanked by distinct highs. While one can possibly see such a pattern north of 51°N , there is no such correlation further south. Hence, the three dimensional gravity modelling procedure followed in the present study is both justified and necessary.

The derived crustal thickness map (Figure 4.14) shows a fundamental change in the nature of the Mohorovicic discontinuity as one encounters the Nelson Front from the east. In southwestern Manitoba, where seismic control is close, the 40 km depth contour swings suddenly north, parallel to the front. Further north, the contours bend to the west as the front is encountered. Only in the northern portion of the map-area does the Mohorovicic discontinuity seem to cross the Nelson Front without alteration. As can

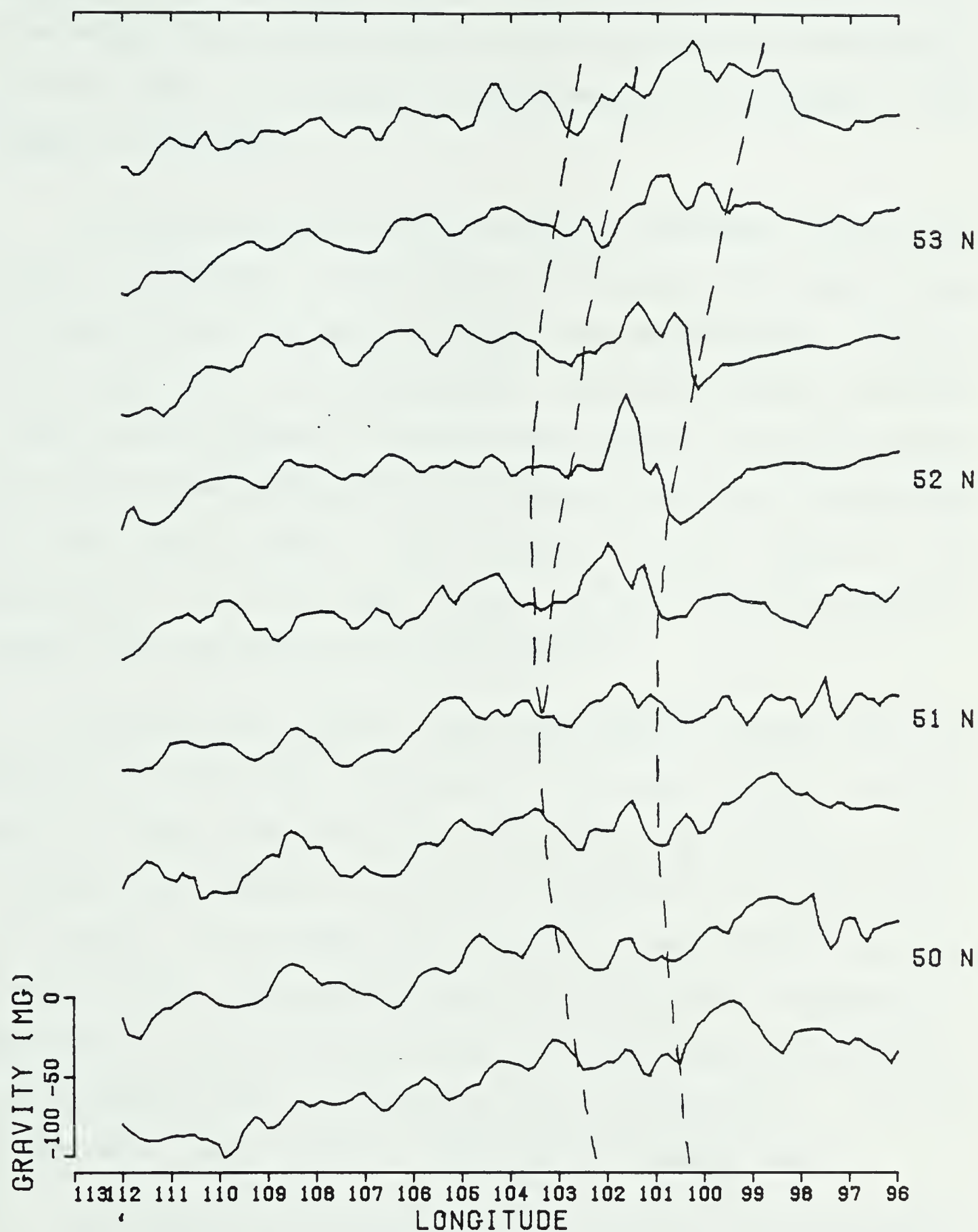


Figure 4.21. Gravity profiles drawn in an east-west direction across the map-area. The inferred location of the Nelson Front is shown by the dashed lines.

be seen in the derived crustal cross-sections (Figure 4.16), the Nelson Front seems to be a zone in which the Mohorovicic surface seems to flatten out relative to its attitude in the Superior Province.

The RielM discontinuity is also affected by the Nelson Front. Relative to the Superior Province, the upper crust is seen to thin out as the front is encountered (Figures 4.15 and 4.16). Hall and Hajnal (1973) and Hajnal and Rose (1979) have proposed a crustal model across the Nelson Front on the exposed shield which includes a pronounced thickening of the upper crust. Such models do not seem to be applicable to the front south of 50°N since the crustal model here indicates quite the opposite.

Though the Nelson Front does seem to affect both the Mohorovicic and RielM surfaces, its main effect on the gravity field does not arise from such deep sources. As is evident from Figures 4.18 and 4.19, density variation within the upper crust seems to be the main characteristic of the Nelson Front. The eastern portion of the front is generally dominated by long sinuous areas of anomalously high density in the upper crust. The western part of the front, on the other hand, tends toward a lower density upper crust.

This model for the Nelson Front beneath the sedimentary cover is quite similar in this respect to the model of McConnell and Gibb (1969) for the Nelson Front on the

exposed shield. There, the gravity highs were correlated with granulite facies mafic rock of mean density 2770 kg/m^3 and the lows with amphibolite facies granodiorites of mean density 2670 kg/m^3 .

In addition to simple changes in rock type or metamorphic facies, other shallow features may be contributing to the intense local gravity anomalies along the Nelson Front in the map-area. Though a general gravity correction was made for the sedimentary cover, no attempt was made to remove the effect of local features within the sedimentary section. For example, McClure (1973) has detected a fault along the Nelson Front which has been active as recent as the Cretaceous. This fault apparently extends into the basement, and has provided a path for salt to be leached out of the sedimentary section, thus contributing to the local high along the Nelson Front in this locality.

The upper mantle density map, Figure 4.20, indicates that the Nelson Front itself does not seem to overlie an anomalous upper mantle. The Nelson Front does, however, separate apparent anomalous areas in the Churchill Province from an anomalous low in the Superior Province.

The Brandon E/W refraction line (Figure 4.2) had its subsurface coverage within the covered western portion of the Nelson Front. The resulting crustal model indicated a

surprisingly thick 46 km crust. Kazmierczak (1980), on the basis of a single seismic travel time measurement, suggested that this thickening of the crust might be contiguous with the 103W fault. The result on the derived crustal thickness map, however, is not a long narrow belt of deep crust striking north, but rather an isolated area of deep crust in southeastern Saskatchewan compensated by a high in the upper mantle cutting through the same area. Perhaps a more reasonable interpretation than that proposed by Kazmierczak (1980) of the thick crust in southeast Saskatchewan is that it represents a northern extension of the Williston Basin. Kanasewich (1966), in a review of deep crustal structure in North America, noted that the thickest crusts are not associated with mountain ranges, but rather with basins. Seismic refraction studies across the Williston Basin do in fact show a crustal thickness in excess of 50 km (Figure 4.22). Hence, the value of 46 km recorded in southeast Saskatchewan does not seem excessive.

Further north along the covered western portion of the front, the Mohorovicic surface is somewhat affected in that it strikes east-west. In the surrounding areas, it strikes northwesterly. The RielM discontinuity tends to be consistently shallow along the front, indicating a thinning of the upper crust over this boundary zone. The rocks of the Nelson Front on the exposed shield are partly of mafic composition. Hence the rise in the RielM surface in

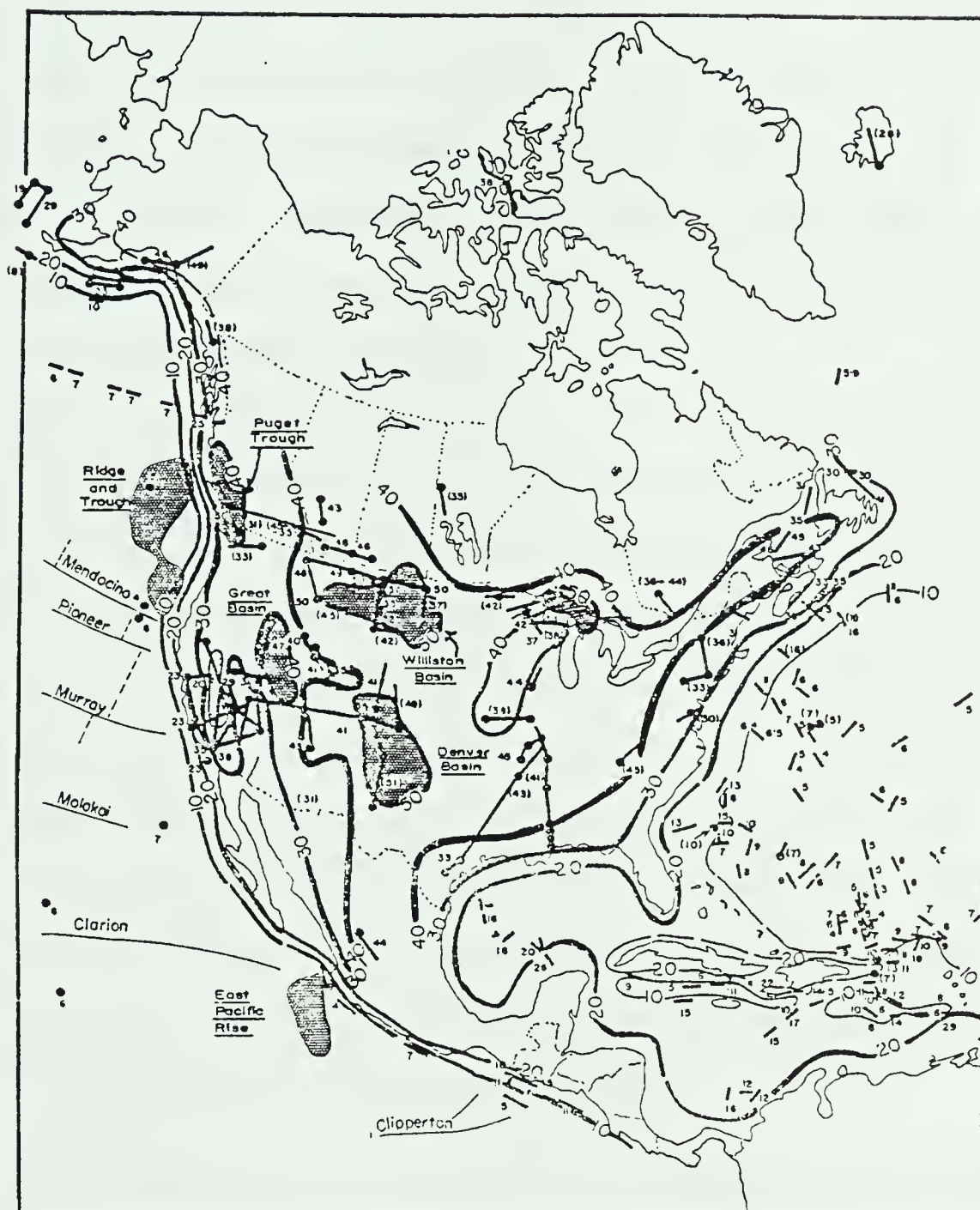


Figure 4.22. Crustal thickness in North America. (After Kanasewich, 1966).

combination with associated faults in the area may have produced an environment satisfactory for such mafic material to rise from the lower crust in these localities. The natural western boundary of the Nelson Front in the map-area is the 103W fault. This fault can be delineated by magnetic data from the international border up to about 52°N where magnetic map coverage ceases (Figure 4.12). On the exposed shield, a similar lineament, the Setting Lake Fault, can be seen separating the Waboden subprovince of the Nelson Front from the Kiseynew gneissic terrain of the Churchill Province. If the 103W fault is the tectonic equivalent of the Setting Lake Fault, then the former is of great economic potential since the latter is associated with one of the world's largest nickel deposits. The possible location of the 103 W fault north of latitude 52° has been estimated using the density maps of the upper crust (Figure 4.18) and has been shown as a solid line on Figure 4.1b and ensuing maps. The more easterly path tends to keep the fault more along the trend of the front, while the more westerly path provides a continuous but serpentine connection via a gravity low with the Setting Lake Fault.

The 103W fault is a feature of great significance to tectonic analysis of the Nelson Front. It affects the entire lithospheric column with greater effects generally in the southern part of the map-area than in the north. As one moves across the fault from east to west, the following

changes occur in lithospheric parameters:

1. Upper mantle Pn velocity increases ((Figure 4.10).
2. Total crustal thickness decreases in the south portion of the map-area.
3. The thickness of the lower crust decreases (Figure 4.8).
4. The thickness of the upper crust increases (Figure 4.15).
5. The density of the upper crust increases (Figure 4.18).

Since the 103W fault is such a significant feature, it is considered in this study to be the boundary between the Nelson Front and the Churchill Province. Clearly, any tectonic analysis of the Nelson Front must take into account this fault and the gross changes in lithospheric parameters which occur near it.

4.3.3 THE COVERED CHURCHILL PROVINCE

The area of the Churchill Province to the west of the 103W fault seems to correlate with the Kiseynew gneissic complex of the exposed shield. This complex is composed of sedimentary and volcanic rocks which have been granitized to varied degrees. Higher gravity anomalies within this terrain tend to be associated with paragneiss and lower gravity anomalies reflect the presence of granite (Gibb and McConnell, 1969). The covered Kiseynew belt within the

map-area tends to be associated with higher upper crustal density (Figure 4.18). Hence, this portion of the covered Churchill Province seems to be largely underlain by paragneissic material.

The NACP conductivity anomaly cuts through this part of the Churchill Province as shown in Figure 4.1b. This conductor has been correlated to graphite occurrences in the Wollaston Domain of the exposed shield. Although the Wollaston Domain, composed of interfingered pelitic schists, paragneisses and granites, can be traced on the basis of gravity character, it does not tend to be associated with any consistent linear gravity anomaly on the shield. However, where it crosses through the map-area, it tends to be associated with long narrow high density trends in the upper crust (Figure 4.18). These linear anomalies are probably due to salt collapse features in the sedimentary cover facilitated by fractures in the basement along the NACP anomalous trend (Camfield and Gough, 1977). An interesting observation about the NACP conductor is that it apparently occurs along a gradational boundary between two different crustal regimes. East of the conductive zone, the crust is of fairly uniform thickness; west of the zone, the crust appears to be broken into a number of distinct east-west trending blocks (Figure 4.14). In particular, a pronounced low on the Mohorovicic discontinuity hemmed in by strong highs strikes east-west through the map-area between

latitudes 50°N and 51°N. This low is contiguous with, and perhaps a continuation of, the known Precambrian rift of southern Alberta (Kanasewich *et al*, 1969). This feature and similar ones in the western part of the map-area are all gradually diminished toward the east as they cross the neighborhood of the NACP conductor. The same phenomenon is apparent on the map of upper crustal thickness (Figure 4.15).

The Sweetgrass belt for this study is defined to be the area south of the southern Alberta rift and west of the NACP conductor. The local density distribution in the upper crust does not show the strong east-west trends apparent in the deep crustal structure of the belt. A few of the local density anomalies have been previously investigated. For example, the arcuate shaped high beginning near 50°30' N on the western edge of the map is associated with a local high on the Precambrian basement composed of rather mafic rock of density 3000 kg/m³ (Chandra and Cumming, 1972).

The Cree Lake-Calgary belt was thought by Burwash and Culbert (1976) to be the extension under the sedimentary cover of the Wollaston fold belt, the Virgin River belt and the Mudjatic Domain of the exposed shield. However, if the Wollaston belt follows the NACP zone southward through Saskatchewan, then the Calgary-Cree Lake belt in the map-area is probably composed only of the Virgin River gneisses and the Mudjatic granites. Though only a small

portion of this belt is within the map-area, what is present seems to possess crustal structure similar in character to that of the Sweetgrass belt. It is apparent that the tectonic relation among the Cree Lake-Calgary belt, the Sweetgrass belt, and the Kisseynew belt requires more study at this time.

4.4 CONCLUSIONS

Combined modelling of the seismic and gravity data of the southern plains of western Canada has resulted in some interesting observations about the tectonic elements in the area. The Superior province in the map-area is characterized by a rather flat and featureless Mohorovicic surface to the northeast, but a strongly tilted surface in the southwest. The Nelson Front in the map-area is coincident with a fundamental change in the nature of the Mohorovicic discontinuity relative to the Superior Province as indicated by changes in the trend of depth contour lines. An area of very thick crust in extreme southeast Saskatchewan may be related to Williston Basin tectonics. Further west, the NACP conductivity zone seems to occupy a gradational boundary between two different crustal regimes. East of the NACP zone, the crust is of fairly uniform thickness; west of the zone, the crust appears to be broken into a number of east-west trending blocks. A pronounced low on the Mohorovicic discontinuity surrounded by strong

highs strikes east-west through the eastern part of the map-area, and is thought to be contiguous with a known Precambrian rift in southern Alberta.

Derived east-west crustal cross-sections across the map-area show a pronounced trend toward crustal thinning to the east accompanied by thinning of the lower crust and thickening of the upper crust. An anomalous thinning of the upper crust occurs in the southern part of the Nelson Front.

The derived upper crustal density distribution for the map-area shows that the Nelson Front is composed of many separate geological units elongate along the trend of the front. It is also apparent that the front is not a two dimensional geological feature since its character changes considerably along strike. Hence, the three dimensional modelling procedure utilized in the present study is both justified and necessary.

Possible upper mantle density variations were also derived from the modelling process. The high density mantle apparent in central Saskatchewan is probably related to Williston Basin tectonics.

The above results have illustrated the usefulness of the Parker-Oldenburg algorithm in gravity field inversion in terms of multilayered models. Extensions of the algorithm have allowed the integration of the gravity data with seismic information in order to arrive at more realistic

crystal models. The computational efficiency of the method makes it very feasible, even for large data sets.

5. A DETAILED STUDY OF POTENTIAL FIELD DATA IN NORTHEASTERN ALBERTA

5.1 INTRODUCTION

In order to further evaluate the application of Parker's algorithm for potential field inversion, the exposed shield area of extreme northeastern Alberta was chosen as a study area. Here it was anticipated that the available ground control on density and susceptibility would greatly aid in the inversion of the magnetic and gravity fields. It was further hoped that the integration of these diverse data would lead not only to increased knowledge of the geology of this map-area, but also to a better understanding of continental crustal structure in general.

5.1.1 NORTHEASTERN ALBERTA MAP-AREA

The map-area which was utilized for this study is in the extreme northeast portion of Alberta. It is roughly bounded on the west by the Slave River, on the north by the Northwest Territories boundary, on the east by the Saskatchewan boundary and on the south by Lake Athabasca (Figure 5.1). For convenience, a somewhat expanded area bounded on the north by the 60th parallel, on the south by latitude $58^{\circ}30'$, on the west by longitude 112°E , and on the east by longitude 110°E , will be considered on the various maps. However, geological ground control on crystalline

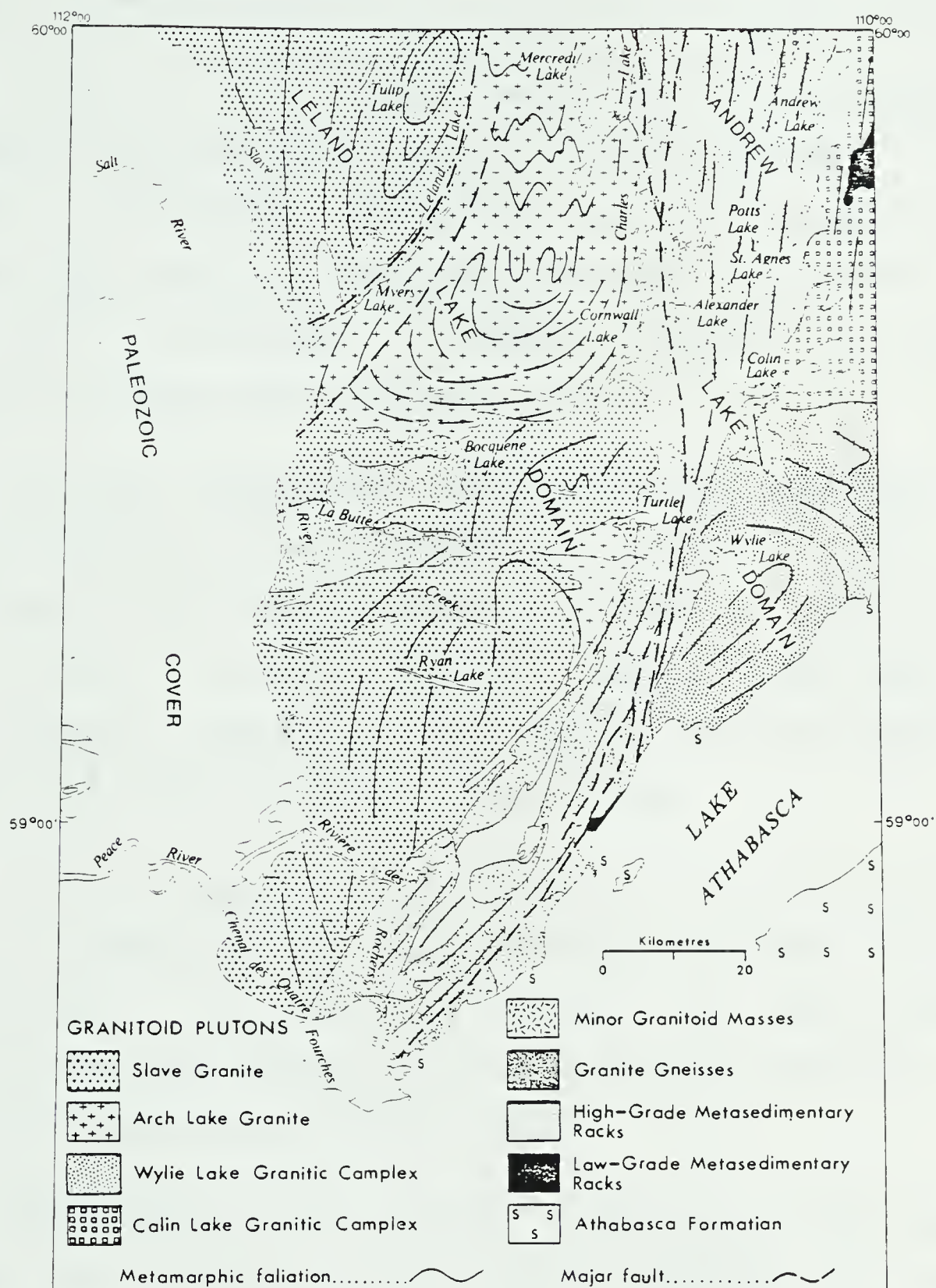


Figure 5.1. Bedrock geology map of the Canadian shield north of Lake Athabasca. After Godfrey and Langenberg (1978).

rocks is available only on the smaller area described above, which is the exposed part of the Canadian Shield in Alberta.

Since J. B. Tyrrell made the initial geological traverse along the north shore of Lake Athabasca in the 1890's, considerable geological work in the map-area has taken place, mainly by the Research Council of Alberta over the past two decades. A summary of much of this work is given by Godfrey and Langenberg (1978).

Regional geophysical work in this map-area began with an aeromagnetic survey in 1958, the results of which are published in the form of "Geophysical Papers," which are, in fact, maps on a scale of 1:63360. Godfrey (1966) noted that the magnetic anomalies in the map-area could be regionally correlated with structures and rock types.

A gravity survey was carried out in the map-area by the Dominion Observatory at a station spacing of about 10-12 km during 1960. The results are plotted in the form of Bouguer gravity contours on Map 19 of the Gravity Map Series of the Dominion Observatory (Walcott, 1968).

Measurements of the physical properties of rock samples from the map-area have been performed by various researchers. Watkins (1961) measured the ratio of remanent to induced magnetization of 23 core samples in the map-area, and found that the effect of remanence was relatively insignificant. Watanabe (1965) did laboratory measurements

of several rock samples in a study of cataclastic rock types. Plouffe (1977) performed laboratory measurements of the magnetic susceptibility and density of over 650 powdered standard samples. Sprenke (1979) made *in situ* measurements of over 130 outcrops in the map-area.

5.1.2 DIGITAL SAMPLING OF POTENTIAL FIELD DATA

The smoothed magnetic field of northeastern Alberta is shown in Figure 5.2. The data for this map were obtained by subdividing the map-area into 5400 smaller areas and sampling the average value in each square. The subdivisions were based on a latitude-longitude type of grid, each small area being 2' of latitude by 3' of longitude in size, which on the average corresponds to 1.84 km by 1.92 km. The average area of each division was about 3.5 km².

The purpose of sampling the average value of the field over these small areas rather than sampling the "exact" value at grid locations was to avoid alias problems. The disadvantages of this procedure are twofold:

- 1) Errors are introduced by incorrect estimations of the average field value in each small area.
- 2) Wavelengths shorter than about 4 km are lost.

Errors due to incorrect estimations of the average field in each area are not that severe if one considers the nature of the data being used. The aeromagnetic survey was

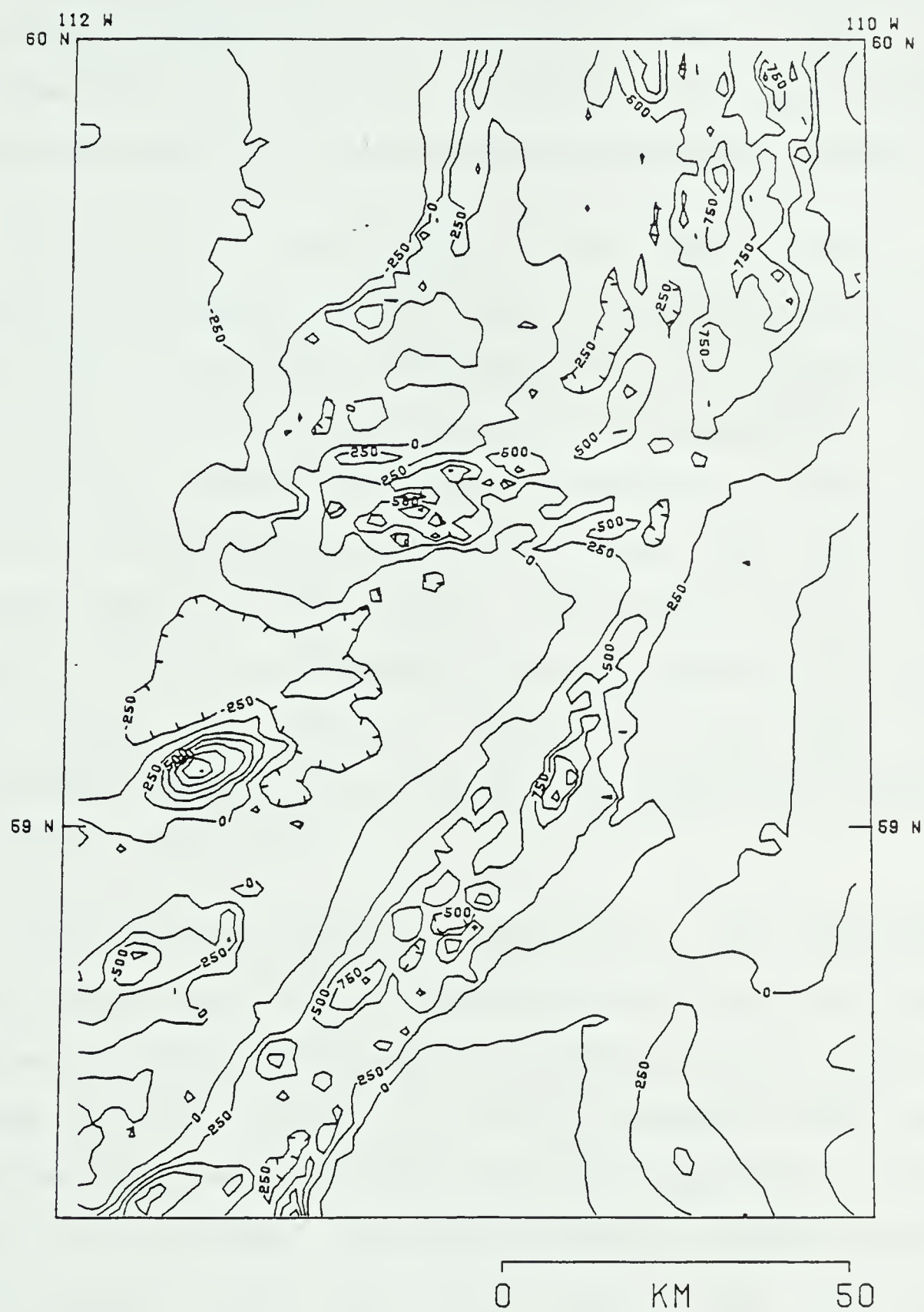


Figure 5.2. Magnetic field over northeastern Alberta. The contour interval is 250 nT.

flown along sub-parallel lines roughly 0.8 km apart. Hence, the field is known exactly only along flight lines. There is therefore no "correct" average value for an area no matter how finely one analyses the contours on the map.

The loss of wavelengths less than 4 km is also compensated somewhat by the flight line spacing which itself effectively eliminates consideration of wavelengths less than about 1.5 km in the direction perpendicular to the flight paths. Hence it is only wavelengths in the band from 1.5 km to 4 km which are being filtered by the sampling process used in this study. This study is of a regional nature in that it encompasses an area of nearly 20,000 km² and, hence, the study of anomalies less than 4 km in wavelength can be left to future more detailed studies of individual localities.

The regional magnetic gradient in the map-area is small, the total field increasing only about 0.5 nT per km from west to east according to the total intensity chart for Canada in 1975. Hence, no regional slope has been removed from the data for this study, although a constant value of 61700 nT has been subtracted from all values to give the field a mean of zero over the map-area. The field values off the edge of the map-area were also gradually tapered to zero to avoid sharp edges in the data.

The gravity data set for the map-area is composed of stations on a grid with roughly 10 km spacings. These Bouguer anomaly values were interpolated using a weighted squares method to the same grid as the magnetic data. No regional trend was removed from the gravity data set, but the mean value of the Bouguer anomaly was subtracted from all the points to give the gravity data a mean value of zero. Off the edges of the map-area, the gravity values were gradually tapered to zero.

5.2 PHYSICAL ROCK PROPERTIES

Ground control on rock density and magnetic susceptibility is vital in the interpretation of the potential field data in northeastern Alberta. This information also aids in the study of variations in rock type and structure in the map-area. The densities and susceptibilities of over 600 standard samples from the exposed shield in northeastern Alberta have been measured by the Research Council of Alberta (Plouffe, 1977). The standard samples were chosen from many thousands of possible samples to be representative of local geology.

The distribution of density for all the standard samples is shown as a histogram in Figure 5.3. The mean is 2695 ± 102 kg/m³ but the distribution is skewed toward the higher densities. The majority of the rocks fall into the

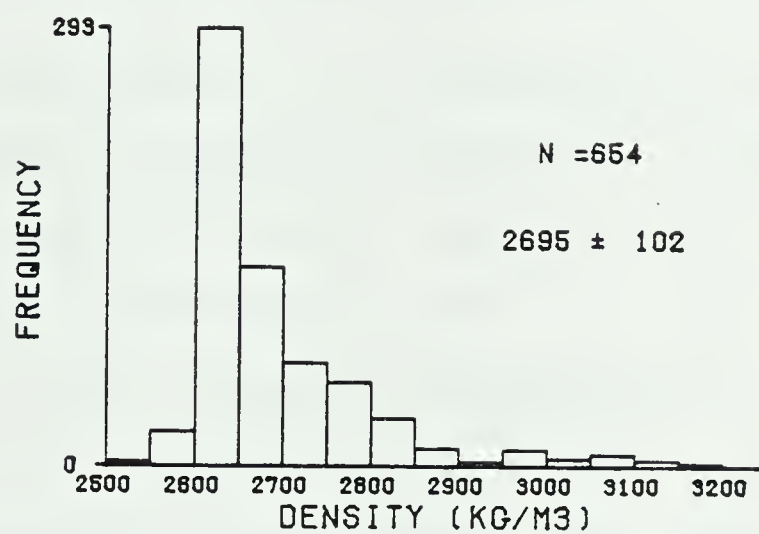


Figure 5.3. Density distribution of the standard samples from northeastern Alberta. The mean and standard deviation are given in kg/m³.

2600 to 2700 range with a mode at 2630 kg/m³, suggesting a low density granitic composition for most of the rock outcropping in the map-area. The average density value is significantly lower than the value of 2740 kg/m³ found by Woolard (1962) as an average density of surface crystalline basement rock in North America. This is an expression of the fact that in northeastern Alberta, the typical rock composition is closer to granite than quartz diorite, the most common basement rock in North America.

The distribution of susceptibilities for all the standard samples is shown in Figure 5.4. Though the c.g.s. unit of susceptibility is used in the present study, it should be noted that the S.I. unit is the microhenry per metre. In order to obtain susceptibility values in S.I., one must multiply the values given in this thesis by 4π . Since susceptibilities range over several orders of magnitude, common logarithms of the susceptibilities have been taken before statistical analysis. This procedure seems reasonable since the histograms would be extremely skewed right otherwise. The mean susceptibilities for all the samples is 461×10^{-6} c.g.s., a value typical for granite gneiss, but low for shield rock in general due to the lack of basic rock in the map-area.

In northeastern Alberta, the Precambrian rocks have been divided into 45 specific types as described on Research Council of Alberta maps. The entire ranges of density and

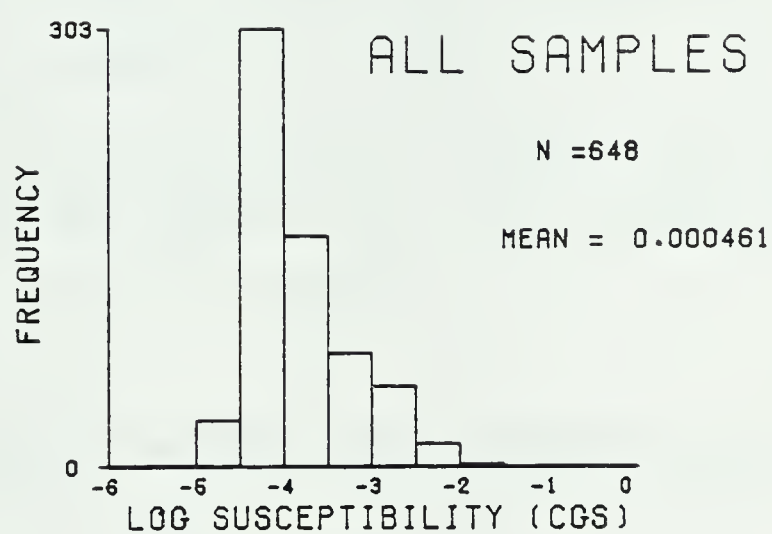


Figure 5.4. Susceptibility distribution of the standard samples from northeastern Alberta. The mean is given in c.g.s. units.

susceptibility for each rock type are given by the lengths of the bars in the lower parts of Figures 5.5 and 5.6. In the upper portion of these figures, the same data are shown but with rock types arranged in order of increasing mean density and susceptibility, the lengths of the bars in this case representing 80% fiducial limits on the mean value.

To help clarify the picture, the rocks have been grouped into broader classes as utilized in the bedrock geology map shown in Figure 5.1. The density and susceptibility distribution of these rocks are shown in Figure 5.7 and Figure 5.8. The lengths of the bars represent 80% fiducial limits.

5.2.1 RELATION OF PHYSICAL ROCK PROPERTIES AND STRUCTURE

Langenberg and Ramsden (1980) have analysed the structural geology of the map-area and their results are generalized in Figure 5.9. The large scale fold structures shown are thought to be immature diapirs. They postdate earlier tighter folding in the map-area (Nielsen *et al*, 1981). Other large structural features of the map-area are major mylonite fault zones.

In order to study the relationship between density and structure in the map-area, the standard samples were sorted into groups based on the structural feature with which they are associated using the structural map (Figure 5.9) as a

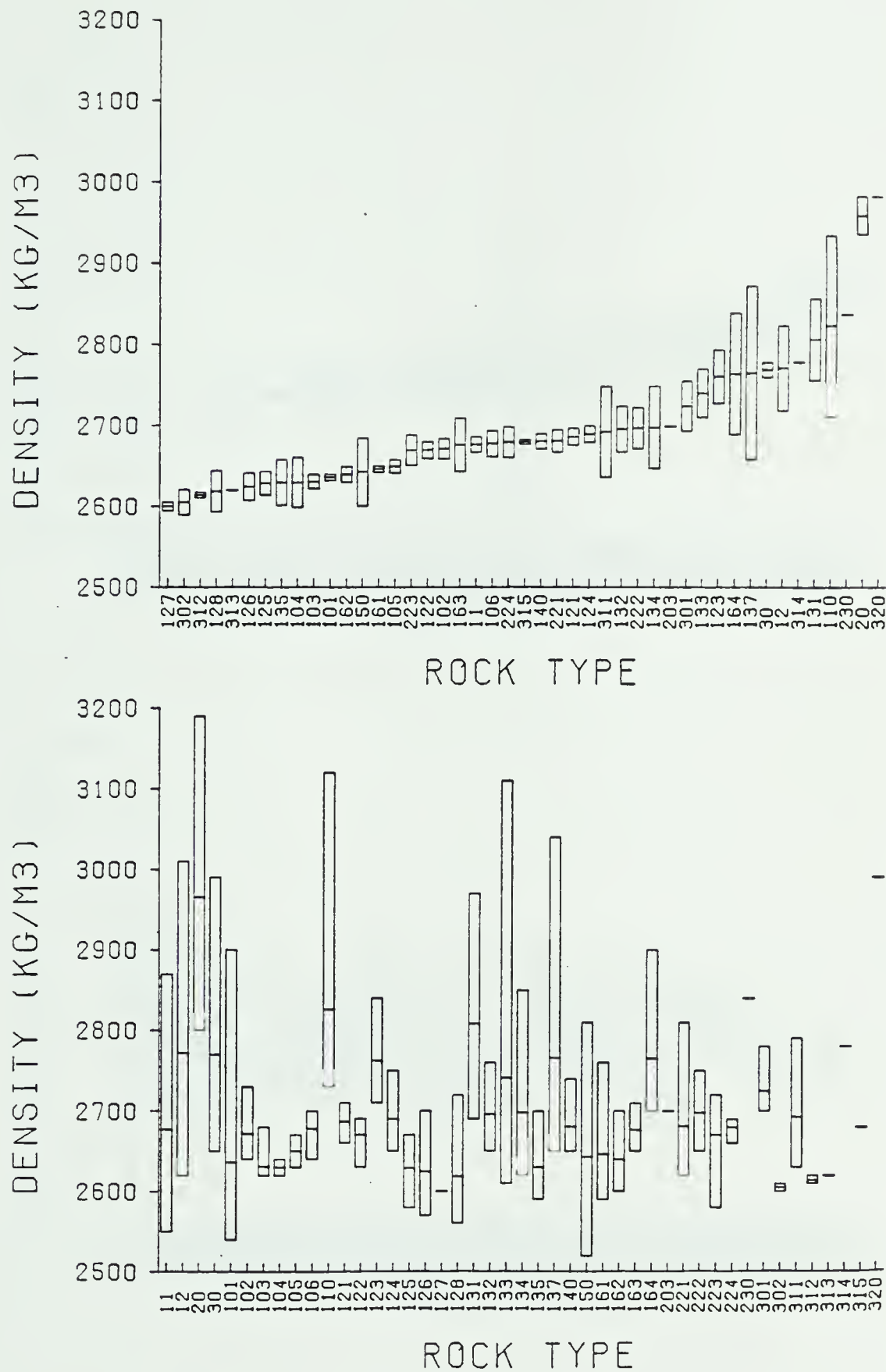


Figure 5.5. Rock densities in northeastern Alberta. In the lower graph, the bars give the entire range for the rock type. In the upper diagram, the bars represent 80% fiducial limits on the mean values.

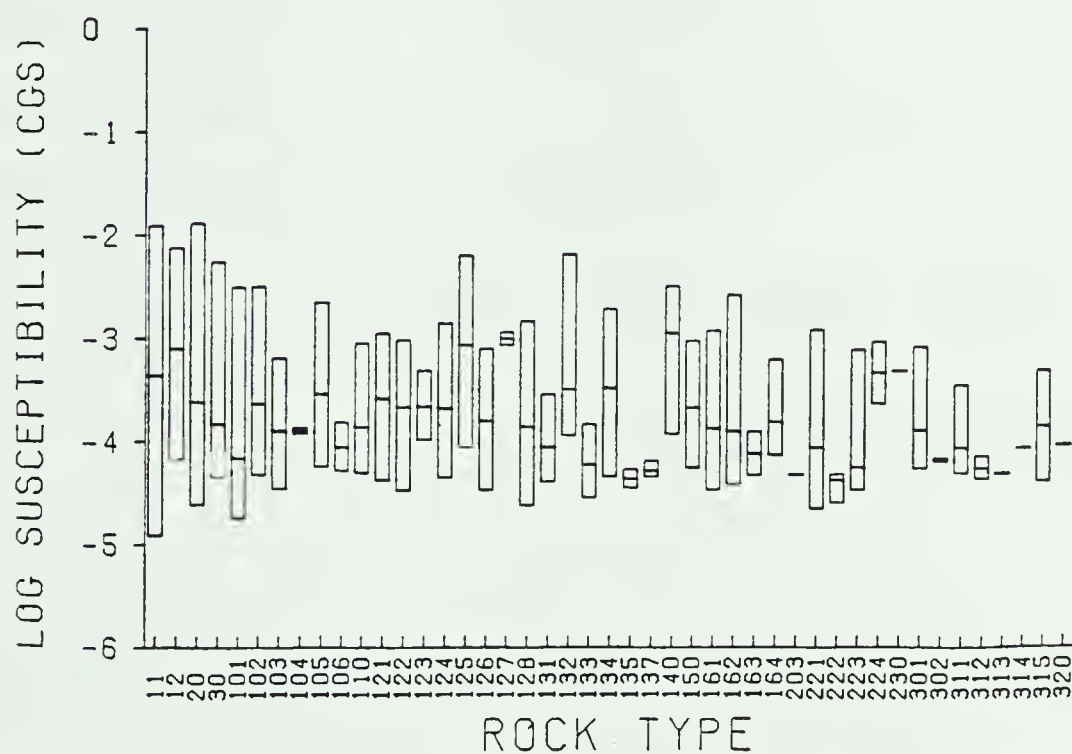
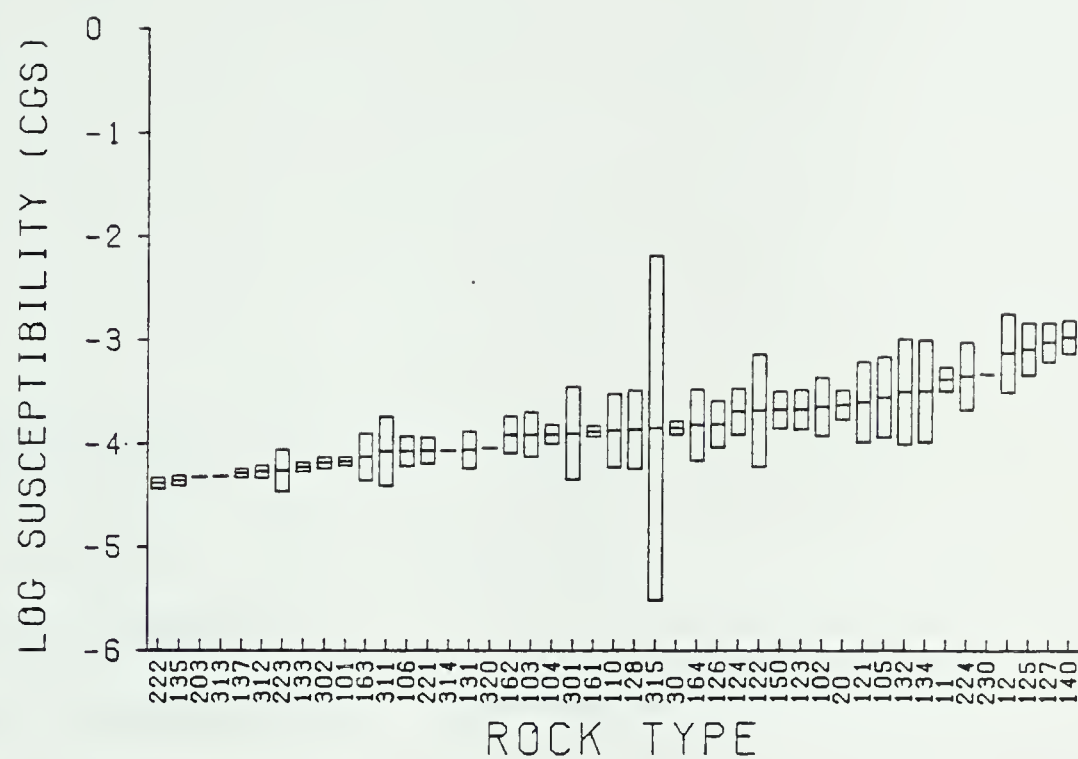


Figure 5.6. Rock susceptibilities in northeastern Alberta. The lower diagram gives the entire range for each rock type, while 80% fiducial limits on the mean are given in the upper graph.

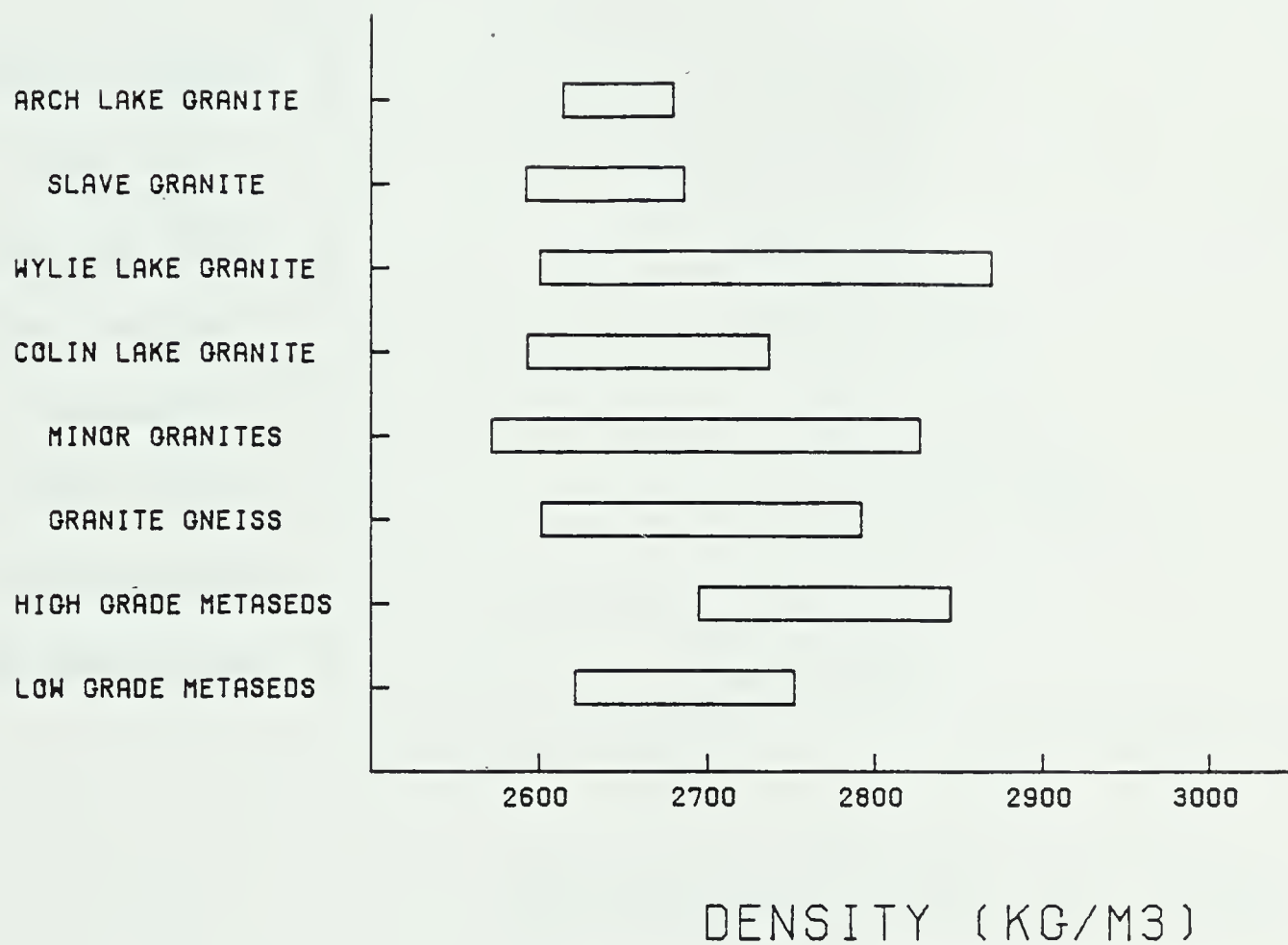


Figure 5.7. Generalized rock densities in northeastern Alberta.



Figure 5.8. Generalized rock type susceptibilities in northeastern Alberta.

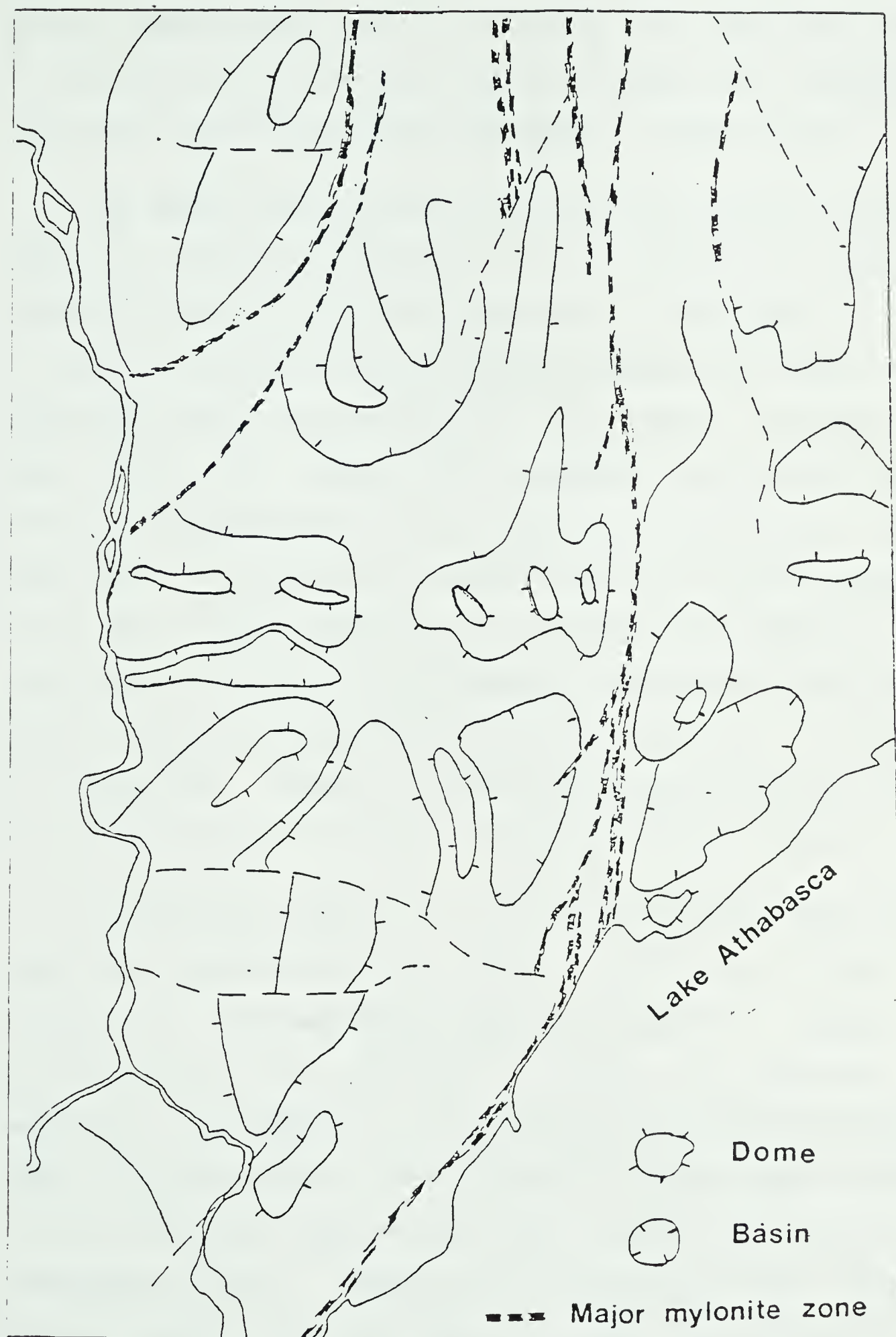


Figure 5.9. Generalized geologic structure map.

guide. Samples not clearly located on the crests or troughs of the folds or in the major mylonite zones were discarded. The resulting distributions are shown in Figure 5.10.

The domal rocks do show lower density than the basinal rocks as would be expected if the structures are indeed of diapiric origin. While the difference in the means is only 25 kg/m^3 , statistically it can be shown that there is 95% confidence that the mean basinal rock density exceeds the mean domal rock density by anywhere from 6 to 44 kg/m^3 . While this might be sufficient density difference to induce diapirism, it would not produce much of a gravity anomaly. For a peak to peak amplitude of folding of the order of 1 km and a density contrast of 25 kg/m^3 , the Bouguer slab formula predicts gravity anomalies only of the order of 1 milligal in amplitude. Hence it is unlikely that the gravity field of the map-area will reflect these structural features.

As shown in Figure 5.11, the mylonite zones also show a lower mean susceptibility ($308 \times 10^{-6} \text{ c.g.s.}$) than the average for the map-area ($461 \times 10^{-6} \text{ c.g.s.}$). Though this difference can be explained in terms of alteration of magnetite to hematite in the cataclastic zones (Watanabe, 1965), the difference is not so great as one might expect; so the mylonite samples have been further subdivided on an aeromagnetic basis. Samples from those zones which show a strong anomaly are referred to as Type 1 and those samples from aeromagnetically quiet zones are classified as Type 2.

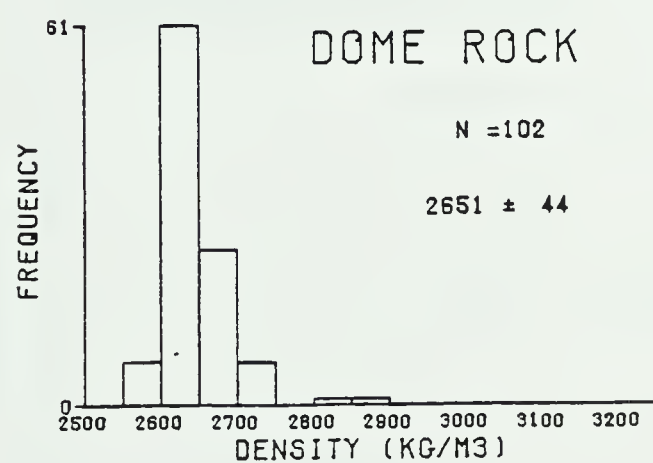
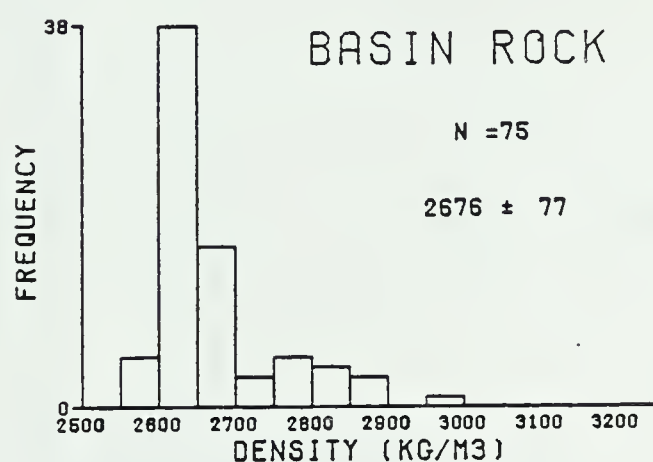
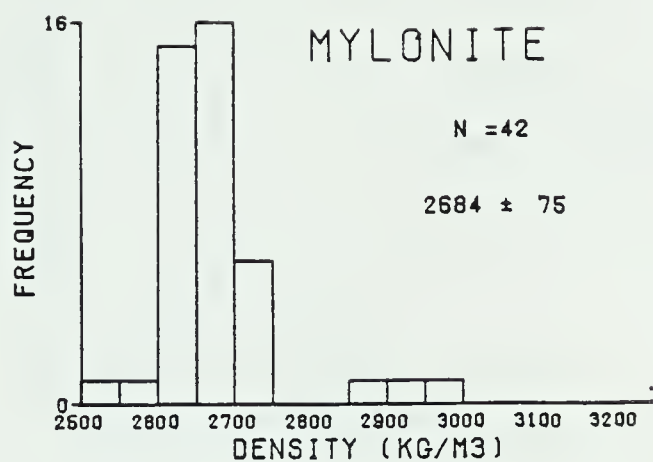


Figure 5.10. Density distributions in northeastern Alberta from standard samples sorted according to associated structural features. The mean and standard deviation are given in kg/m³.

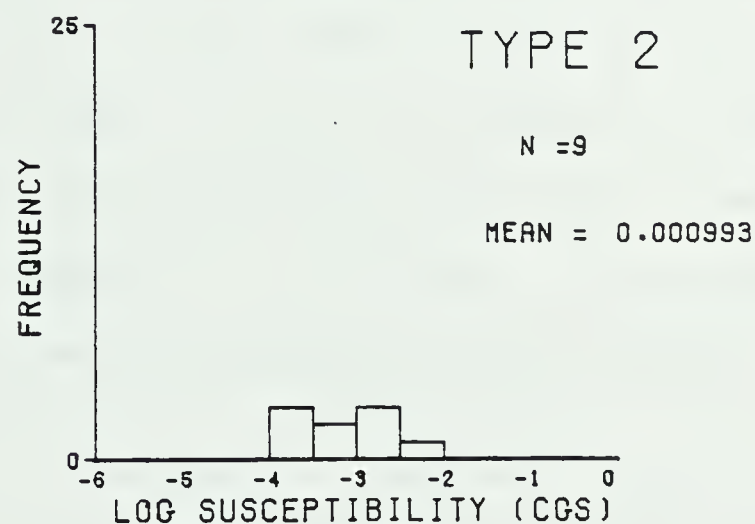
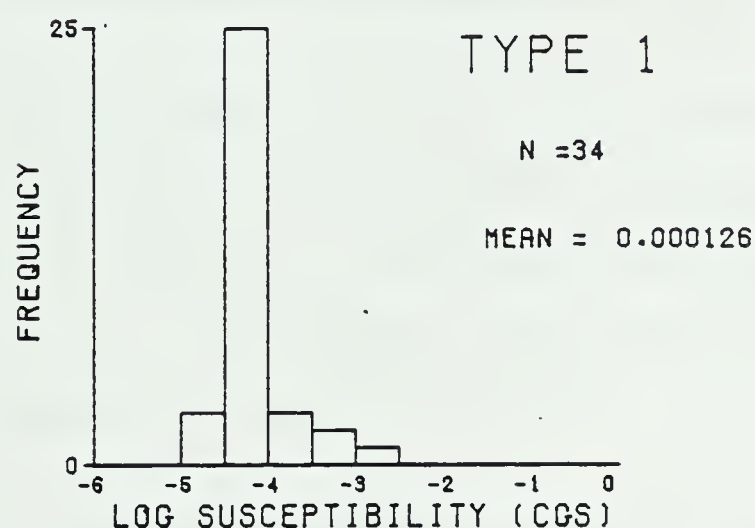
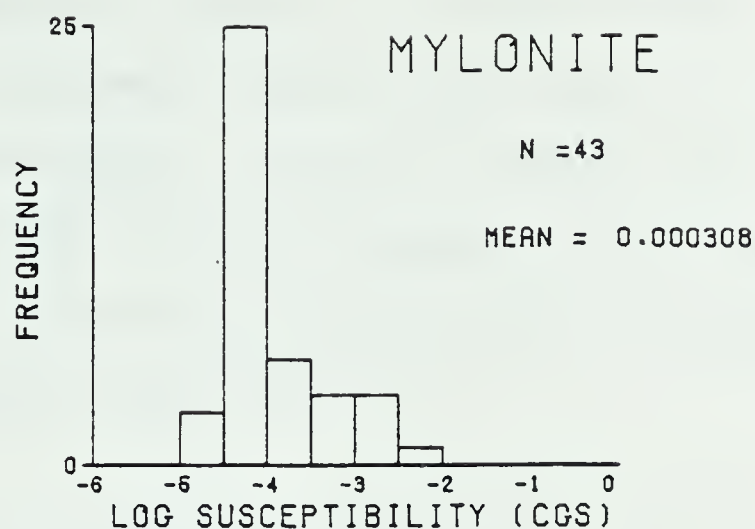


Figure 5.11. The distribution of rock susceptibility in the major mylonite zones of northeastern Alberta. For the upper digram, all mylonite zone standard samples were utilized. In the center histogram, only those samples from aeromagnetically quiet zones were utilized. For the bottom histogram, only those samples from aeromagnetically intense mylonite zones were considered.

The histograms in Figure 5.11 clearly show the fundamental difference between these two types of mylonite zones. Perhaps the magnetic mylonite zones did not attain the necessary temperature and pressure conditions to destroy the magnetite, or perhaps they have been subsequently enriched by new magnetic material.

5.2.2 FIELD MEASUREMENTS OF SUSCEPTIBILITY

This section deals with *in situ* measurements of the magnetic susceptibility of rocks outcropping on the shield of northeastern Alberta. Field stations are shown as dots on Figure 5.12. Fieldwork was carried out by the author during the summer of 1978.

Bedrock has been exposed by glacial scouring over most of the map-area. Very clean, fresh bedrock surfaces border most of the lakes. Such water-washed surfaces were found to be very good for field determination of susceptibility. The ranges of susceptibility on over 130 outcrops from 28 widely spaced areas were determined in this study.

Magnetic susceptibilities were measured on outcrops in the field using a Bison Model 3101 Meter along with a Bison Model 3120 Insitu Sample Coil. The measurements are made in an applied alternating magnetic field with an intensity about the same as the earth's field. The readings are independent of any remanence in the rocks.

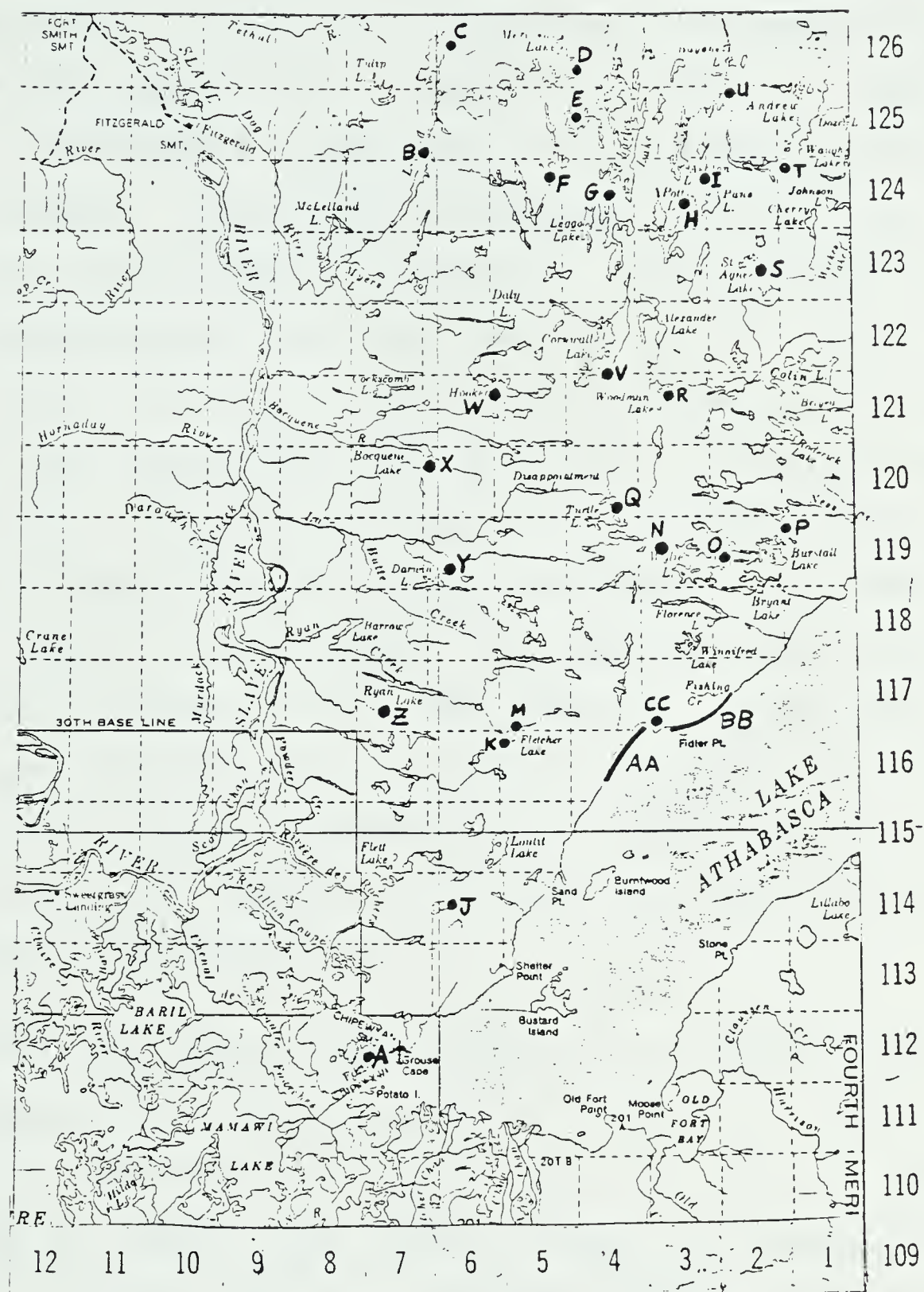


Figure 5.12. Base map of northeastern Alberta showing the locations of the areas visited during the fieldwork.

Perhaps the major problem in determining rock susceptibility *in situ* is in obtaining a reasonable average for the rock type present. Figure 5.13 shows a "contour map" of the magnetic susceptibility of a typical gneiss near Fort Chipewyan. Measurements were made at 15.25 cm (the measuring disk diameter) intervals. The susceptibility of this outcrop varied from less than 1500×10^{-6} c.g.s. to about 6000×10^{-6} c.g.s. This variation does not seem to be related in a simple way to the direction of foliation within the gneiss. Two detailed "traverses" across the outcrop are shown in Figure 5.14, one along the bands, the other at right angles to the bands. For these profiles, readings were taken at about 1" (2.54 cm) spacings. These profiles show more variation than the results of Figure 5.13. While the traverse across the banding shows more variation than that along the banding, the former still has significant variation in susceptibility.

From the above observations, it is evident that many readings must be made on an outcrop in order to obtain any type of representative value. For this study, an attempt was made to obtain the typical range of susceptibility values on each outcrop. Extreme values, such as those associated with a single mineralized band or with a thick vein of quartz were considered as not representative and ignored.

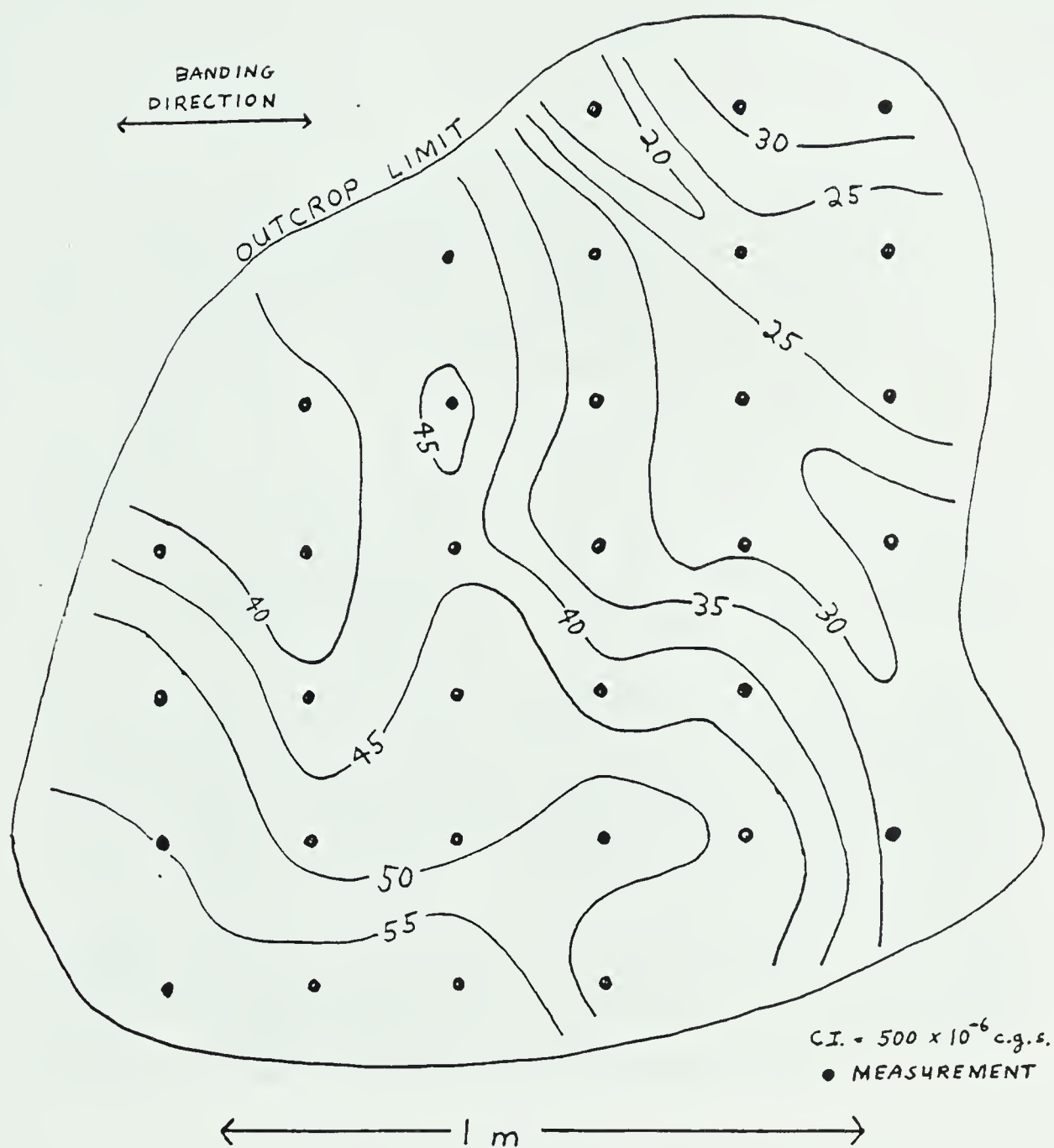


Figure 5.13. A contour map of the susceptibility of a typical outcrop of granite gneiss in northeastern Alberta.

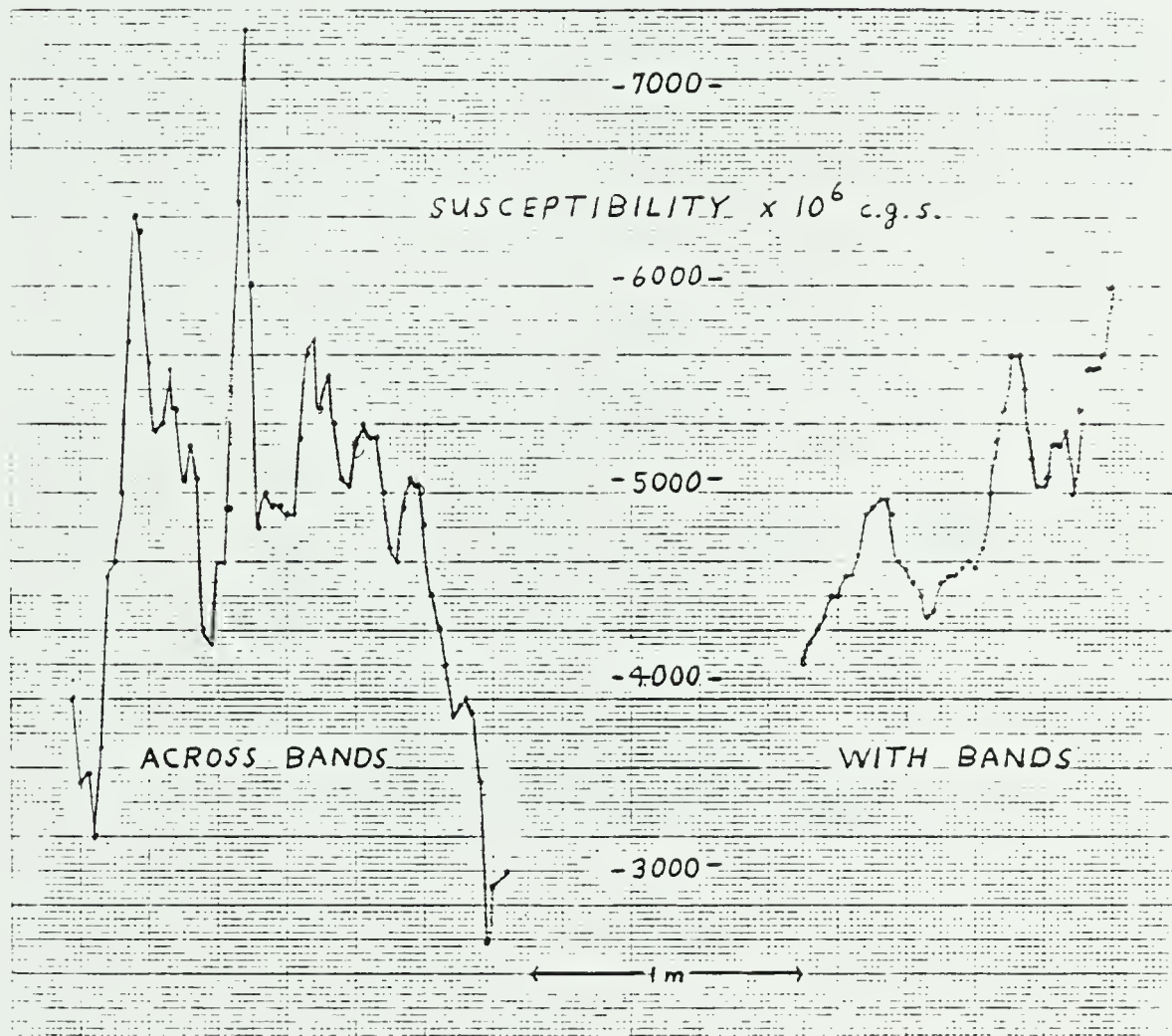


Figure 5.14. Profiles across a typical granite gneiss outcrop in northeastern Alberta.

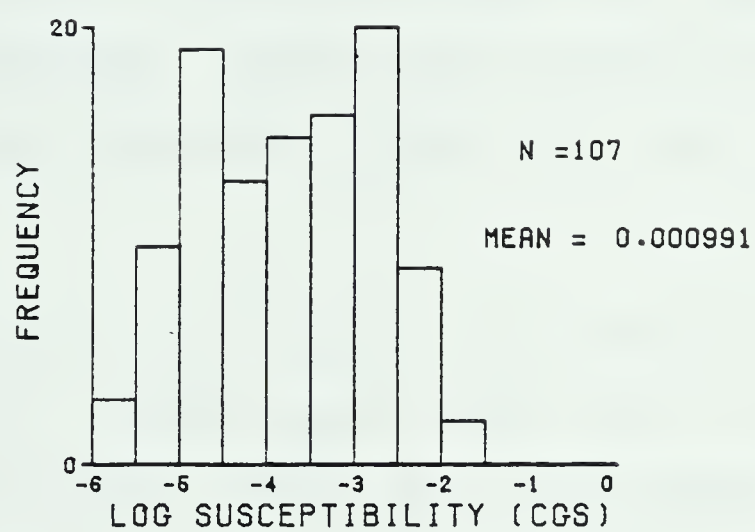


Figure 5.15. The distribution of susceptibilities in northeastern Alberta obtained by *in situ* measurements on outcrops.

The ranges of susceptibility found on the outcrops in this study have serious implications for the validity of a set of susceptibility values based on lab studies of hand specimens collected in the field. A single sample is not representative of the outcrop as a whole. However, it must be noted that the variation of susceptibility of the typical outcrop shown in Figures 5.13 and 5.14 only amounts to a factor of about 3 from lowest to highest reading, while rock susceptibilities as a whole are known to range over six orders of magnitude. Hence, the variability on an outcrop such as the one considered above may not be all that important.

The results of the field work are shown as a histogram in Figure 5.15. The overall mean (991×10^{-6} c.g.s.) is high compared with the average from the standard samples (461×10^{-6} c.g.s.). This is expected since the field locations were not randomly located. There was a strong tendency to make measurements on outcrops in the vicinity of aeromagnetic highs, hence there was a greater chance of sampling the more magnetic outcrops. This bias in the data is also evidenced by the bimodal distribution obtained in the field. The lower peak corresponds to the overall mode obtained from the standard samples, while the higher peak reflects the mode of the magnetic rocks in the map-area.

5.3 THE CURIE ISOTHERM IN NORTHEASTERN ALBERTA

It is possible that the magnetization of crustal rocks terminates at an isothermal surface representing the Curie point of the ferrimagnetic material present. If the Curie isotherm could be mapped in this area, then an estimate of the prevailing geothermal gradient might be made. This information would be useful in analyzing the present state of the crust beneath this shield area.

The actual temperature of the Curie isotherm depends on the mineralogical content of the crustal rocks. The Curie point for iron bearing minerals can range from 580°C for pure magnetite to as low as 100°C if titanium substitutes for some of the iron as typically occurs in volcanic rock. In plutonic rock, however, much of the titanium present tends to crystallize as ilmenite and the Curie point tends to be from 520 to 560°C (Shuey *et al*, 1976). This is the situation one expects in the abundant granitoid rocks of northeastern Alberta.

Previously published methods of determining the depths to the Curie isotherm all suffered from strong initial constraints on the types of models utilized as the source of the anomalies since either individual vertical prisms or, in the case of stochastic methods, equidimensional anomalous bodies, were used. ((Vacquier and Affleck, 1941), (Bhattacharyya and Morley, 1965), (Bhattacharyya and Leu, 1975), (Shuey *et al*, 1976)). The method used in this study,

being based on a Fourier expansion of the source, allows all anomalies in the map-area to be modelled simultaneously without restriction as to source geometry, provided that the magnetized material can be considered to occur in a continuous layer. This method seems particularly well suited to the Curie isotherm problem, since any isotherm can be expected to be a rather smooth and continuous surface.

The map in Figure 5.16 shows the depths to the Curie isotherm in northeastern Alberta as computed by the Parker algorithm for a reference level at a depth of 15 km and a mean crustal susceptibility of 0.01 c.g.s. units. The hatched contours represent areas where the isotherm is relatively shallow. The area of deeper Curie isotherm generally conforms to the outcrop area of the Archean granite gneisses (Figure 5.1), whereas the shallower Curie isotherm seems to be related to younger remobilized granitoid masses.

While the results of this method of deducing the elevation of the isotherm from the magnetic field seem to correlate with the geology, it must be noted that there are many problems with the analysis. Curie isotherm studies are generally undertaken over regions much larger than the map-area considered here. Hence the very long wavelengths most useful in deep crustal studies were not available for this study. Also, the assumed mean crustal susceptibility which had to be used (0.01 c.g.s.) in order to obtain a

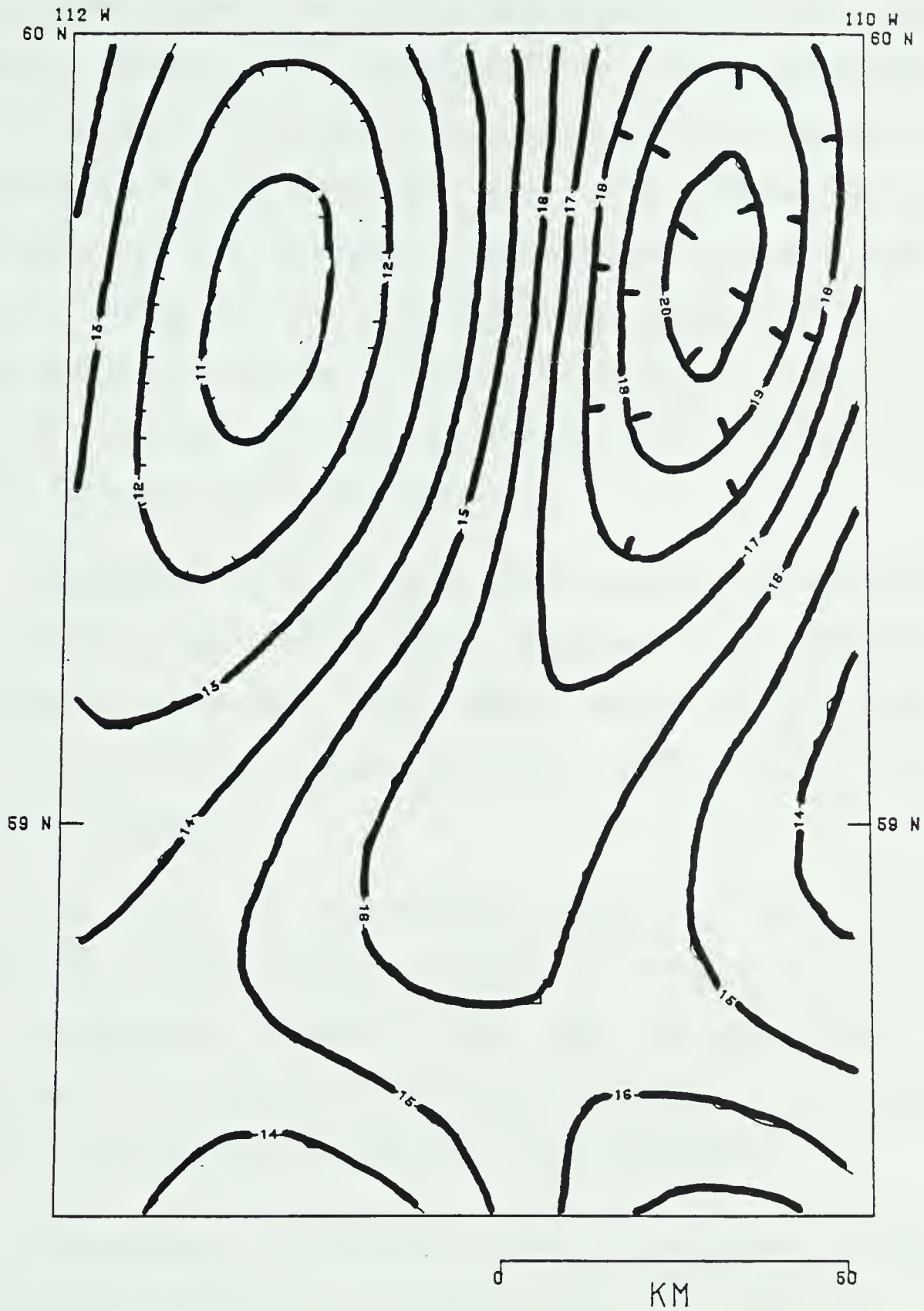


Figure 5.16. The postulated depth to the Curie isotherm in northeastern Alberta. The contour interval is 1 km.

convergent result from the inverse process was an order of magnitude higher than surface measurements would indicate. Hence, unless rock susceptibility increases dramatically with depth in this map-area, the results mapped do not represent an isotherm at all. The magnetization could disappear at a lithospheric discontinuity such as the RielM which likely occurs in the same depth range; or the variations on the map of Figure 5.16 may be due to simple lateral changes in crustal susceptibility with no relation at all to the Curie isotherm.

Nonetheless, this study does demonstrate the utility of the Parker algorithm in Curie isotherm type problems. An interesting further development would be to apply the method to a much larger area, such as the entire basin of western Canada.

In light of the above result, a much different approach, based not on an attempt to invert to the shape of the isotherm but rather to find the average depth to an assumed flat magnetic bottom for the map-area, is suggested. This is a stochastic approach to the problem.

As a model, the magnetic crust is assumed to consist of a slab of constant thickness but with laterally varied magnetization. The thickness of this slab represents the mean depth to the Curie isotherm.

The procedure to determine the thickness of the slab was indirect. The magnetic field was inverted by means of Equation (48) of Chapter 2 to yield the susceptibility variation over the map-area for the assumed slab thicknesses. The distribution of these susceptibilities derived from the magnetic field were then compared with the susceptibility distributions derived from laboratory and field measurements. The magnetic slab thickness which produced the best distribution match with laboratory and field results is thought to be the best estimate for the depth to magnetic bottom.

There are several difficulties with this procedure. The result of the inversion process is not unique. In fact, any constant magnetization can be added to the result (Parker and Huestis, 1974). However, there are some constraints on the range of acceptable magnetizations. "Negative" absolute susceptibilities, such as might actually occur in diamagnetic rocks or apparently occur in permanently magnetized rocks are not expected to exist in this largely granitoid region of the shield. While negative susceptibility contrasts will occur, the lowest absolute susceptibility anticipated is zero. The distributions derived from the magnetic field have been adjusted such that their lowest susceptibility is zero as well. These derived distributions can therefore be shifted to the right toward higher susceptibility but not to the left. Since the

distributions are shown on a logarithmic scale, it should be kept in mind that a shift to higher susceptibility will alter the shape as well as the mean value of the distribution.

Since *in situ* and laboratory measurements were based on field locations distributed in a non-uniform manner across the map-area, it was necessary to interpolate the results of the inversion to these same locations, hence some error due to interpolation can be expected. In addition, the field itself has been fairly well smoothed during preprocessing. Wavelengths shorter than about 4 km are not present. Hence, magnetization anomalies of a very local nature might show up on the *in situ* and laboratory results but not on the inversion results.

Of the standard sample locations on the map-area, about 555 had suitable susceptibility measurements in a laboratory (Plouffe, 1977). While these standard samples were by no means randomly chosen, they probably approach stochastic variability for purposes of magnetic field inversion since they were picked without reference to their geophysical qualities. The *in situ* measurements, on the other hand, were strongly biased in location, many being intentionally placed on local magnetic features. This pattern is apparent in the results discussed below.

Distribution comparisons between the laboratory measurements on standard samples and the derived susceptibilities from the magnetic field are shown in Figure 5.17. The distributions are all normalized to a common maximum for clarity. For a magnetic bottom at 10 km, the distribution of derived values shown as a dashed line, is too high to suit the laboratory values. For a bottom at 15 to 20 km, a reasonable match of at least the mode value is attained. For a depth of 25 km, the derived values appear to be too low.

The 15 to 20 km estimate for the Curie isotherm also suits the lower of the two peaks on the bimodal *in situ* measurement distribution as shown in Figure 5.18 for a 20 km thick slab.

The above results derived from the magnetic field and outcrop susceptibilities, not only yield a Curie isotherm depth of 15 to 20 km in this map-area, but also suggest that a small but persistent susceptibility contrast from 0.000030 to 0.000100 exists to the base of the magnetic crust in northeastern Alberta. Furthermore, if the Curie point is indeed in the range from 520°C to 560°C, then a present day geothermal gradient from 26°C to 37°C per km can be postulated for the map-area.

The higher modal peak on the *in situ* distribution is also interesting. If it does represent overzealousness on

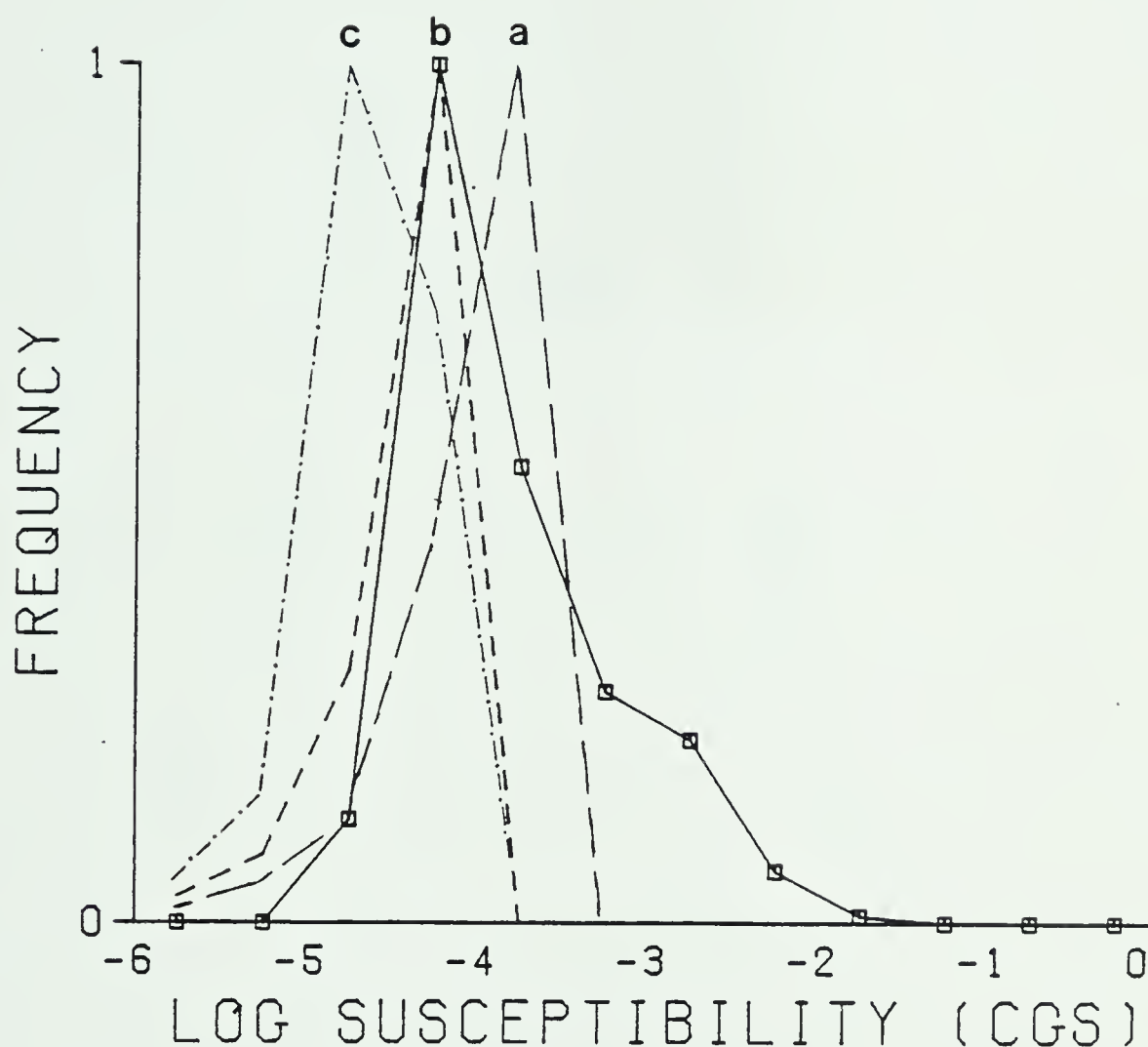


Figure 5.17. Comparison among the susceptibility distributions derived from the magnetic field (dashed lines) and the distribution obtained from laboratory measurements (solid line) in northeastern Alberta for Curie depths of a. 10 km, b. 20 km, and c. 25 km.

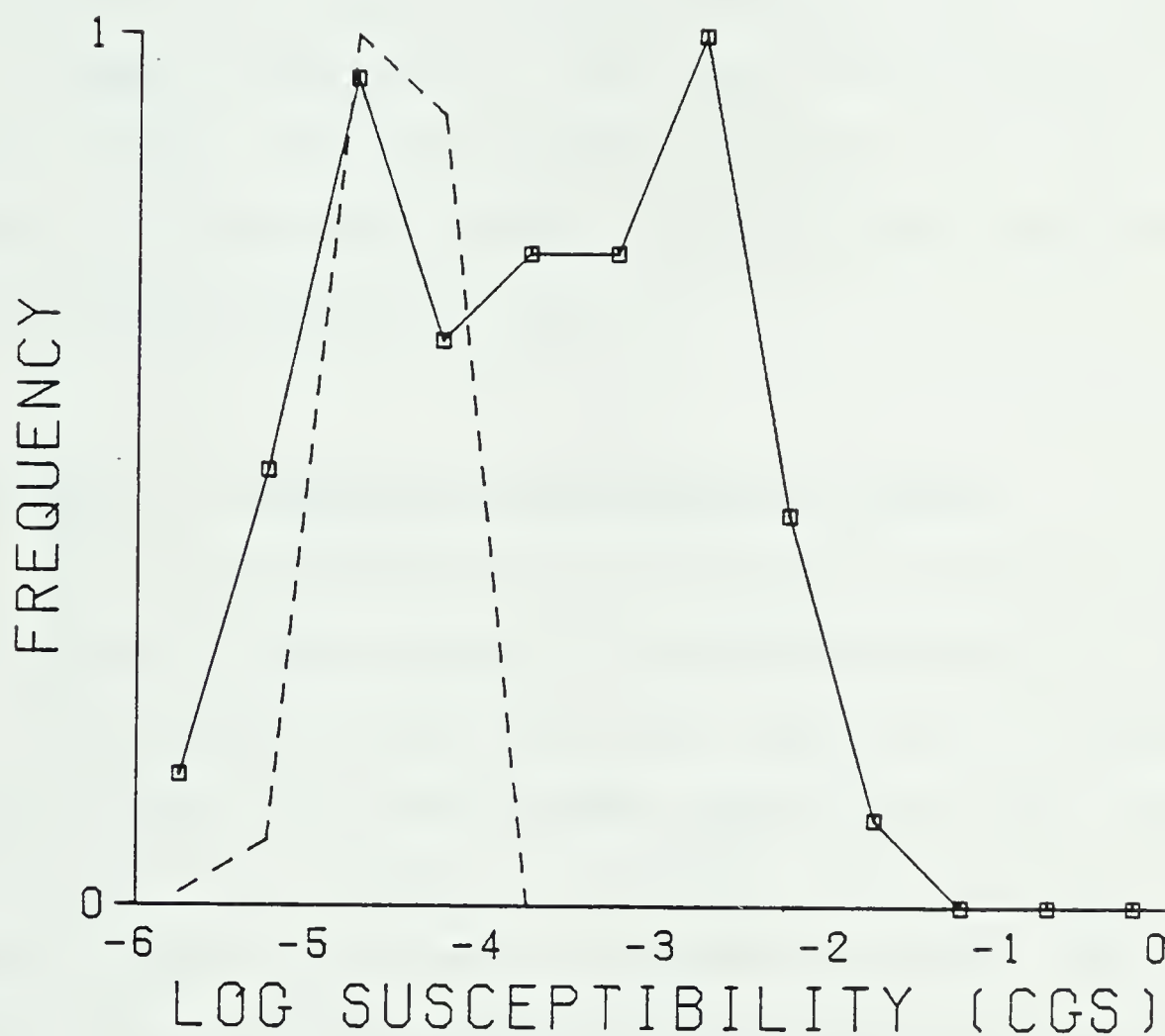


Figure 5.18. Comparison between the susceptibility distribution derived from the magnetic field (dashed line) and the distribution obtained from *insitu* measurements (solid line) in northeastern Alberta for a Curie depth of 20 km.

the part of the observer in locating stations on local and perhaps shallow magnetic features, it might show some correlation with a model consisting of a thin surface slab of magnetized material. Distribution comparisons were calculated for slabs of various thickness and a reasonable fit seems to occur for a 1 km thick slab as shown in Figure 5.19. Hence, the local intense anomalies in the map-area seem to have their sources in near-surface rocks extending to an average depth of 1 km.

5.4 GRAVITY INVERSION IN NORTHEASTERN ALBERTA

The ideal method of utilizing ground control of density in a gravity study would be in the determination of geometry of structures causing individual anomalies in the map-area. Unfortunately, the 630 standard samples available were not sufficient to produce a smoothed and unaliased density function for the map-area. Attempts to invert the gravity data using an interpolated grid based on the standard sample measurements diverged, due to the roughness of the density set relative to the rather smooth gravity variation across the map-area (Figure 5.20). Hence stochastic methods were used to obtain some general conclusions about the relation between gravity and rock density in northeastern Alberta.

The following procedure was used. The crust was modelled as a slab of constant thickness and laterally varied density. The gravity data was then inverted using

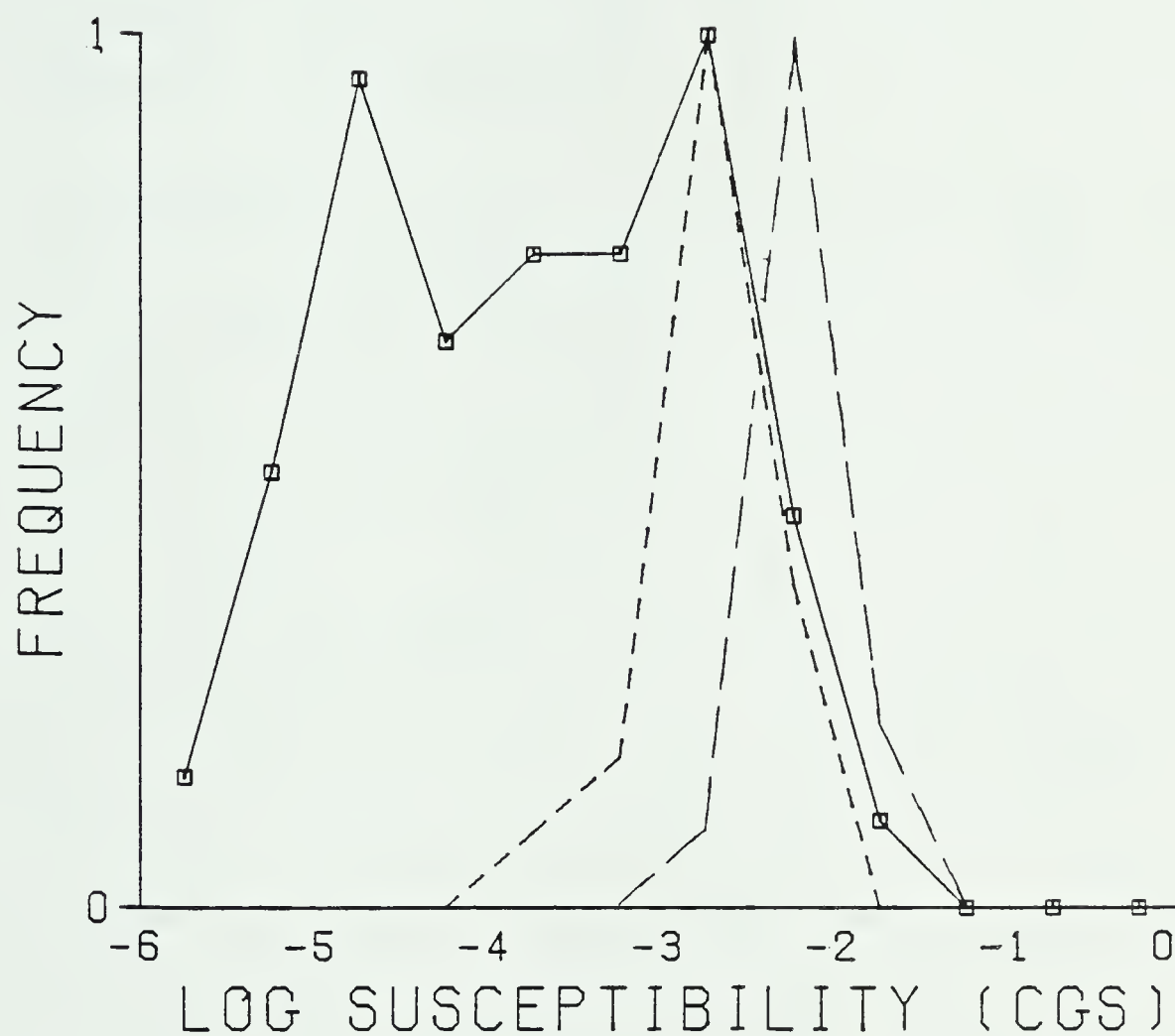


Figure 5.19. A comparison among the susceptibility distributions from *insitu* measurements (solid line) and those obtained from the magnetic field for slab thicknesses of 0.5 km (long dashes) and 1 km (short dashes).

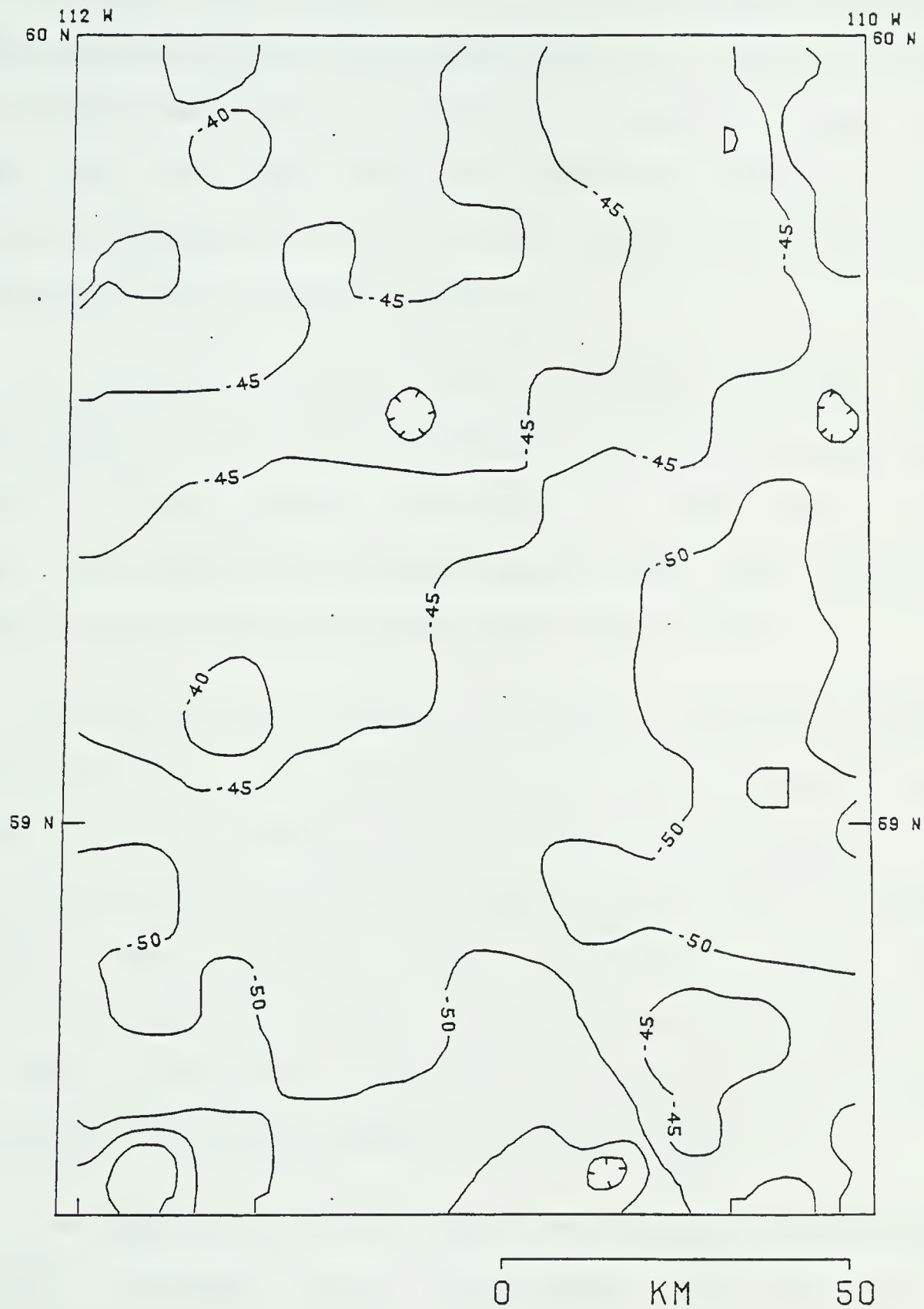


Figure 5.20. Bouguer anomaly map of northeastern Alberta. The contour interval is 5 milligals.

the Parker algorithm for slabs of different thicknesses until the derived density distribution best matched the known distribution from ground control. The slab thickness so obtained was then a reasonable estimate of the average depth to the base of the anomalous material. In this manner, the depth to which the large structures in the map-area extend was estimated.

In order to arrive at a unique derived density distribution for a given thickness, the mean crustal density must be assumed. Here, the value of 2630 kg/m^3 obtained from the laboratory measurements was used so that both distributions would have the same modal value.

The densities derived from the gravity field were interpolated to the locations of the standard samples. Since gravity stations are about 10 km apart in the map-area, local variations in density will not necessarily affect the regional field measured. Hence, density variations of areal extent less than about 100 km^2 will show in the ground data distribution but not on the density distribution derived from the gravity field.

The density distributions from standard samples and the gravity inverse were calculated for various slab thicknesses. Considering the simplicity of this type of modelling, the results are quite interesting. For example, for a slab thickness of 1 km as shown in Figure 5.21, the

standard deviations of the two distributions agree, but the derived distribution from the gravity data is flattened relative to the lab distribution. In fact, since the density distribution of the standard samples seems to be skewed toward higher densities, it is reasonable to expect that these higher density rock occurrences are local in extent and are thus not reflected in the regional gravity field. Hence, disagreement can be expected and, in fact, does occur in skewness and kurtosis of the two distributions.

In view of the above problems, simply comparing the width of the modal peak as a matching criterion is probably as sound a method as any. Using this criterion, it appears that the density distributions best match for a slab thickness of about 20 km, as shown in Figure 5.22. This suggests that the modal density variations occurring on surface outcrops extend deep into the crust of northeastern Alberta. Since the densities can be related to various geologic structures, these structures can be thought of as very fundamental crustal units, perhaps extending to the top of the lower crust.

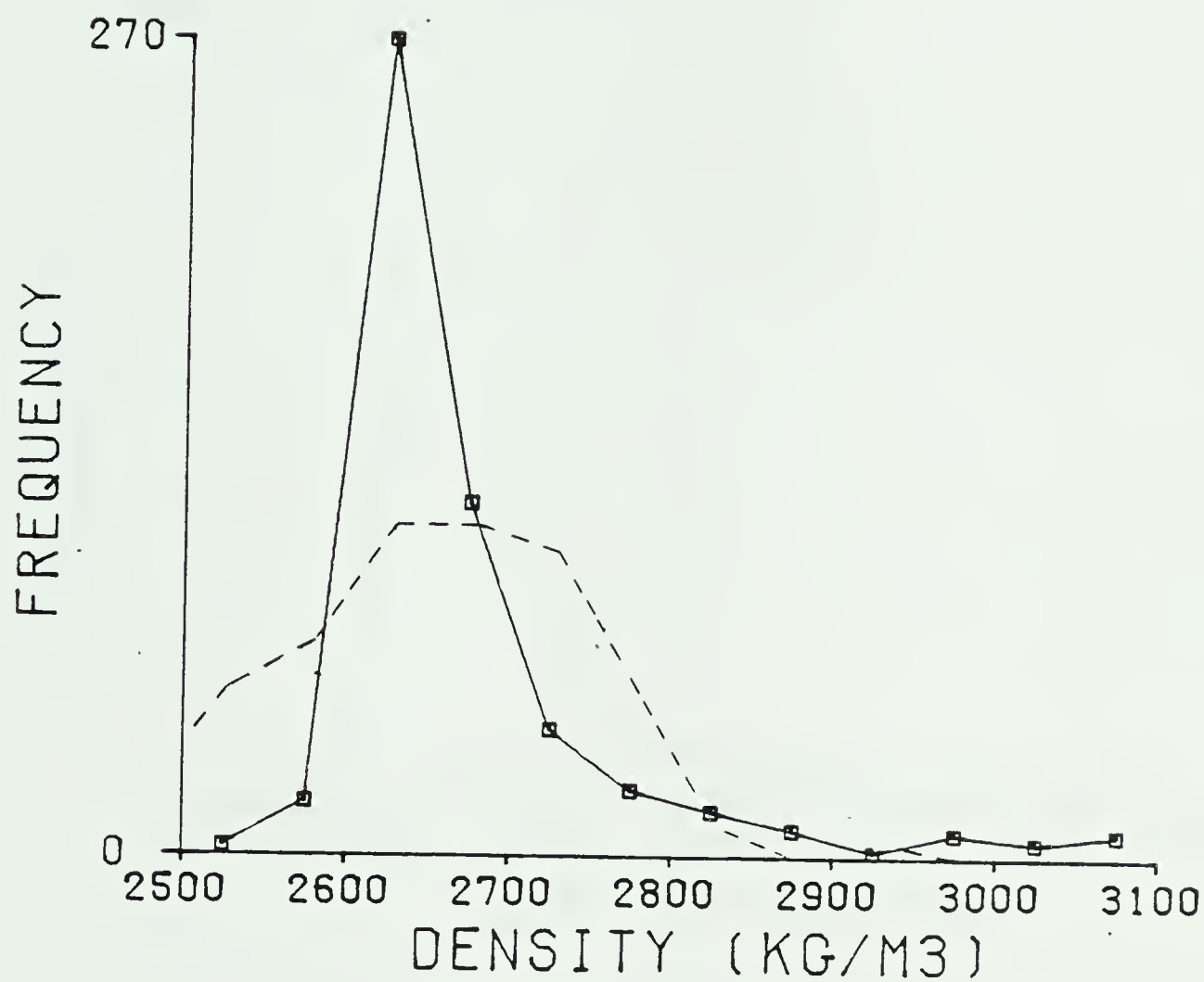


Figure 5.21. Comparison between the density distribution derived from the gravity field for a slab thickness of 1 km (dashed line) with the distribution obtained from laboratory measurements (solid line) in northeastern Alberta.

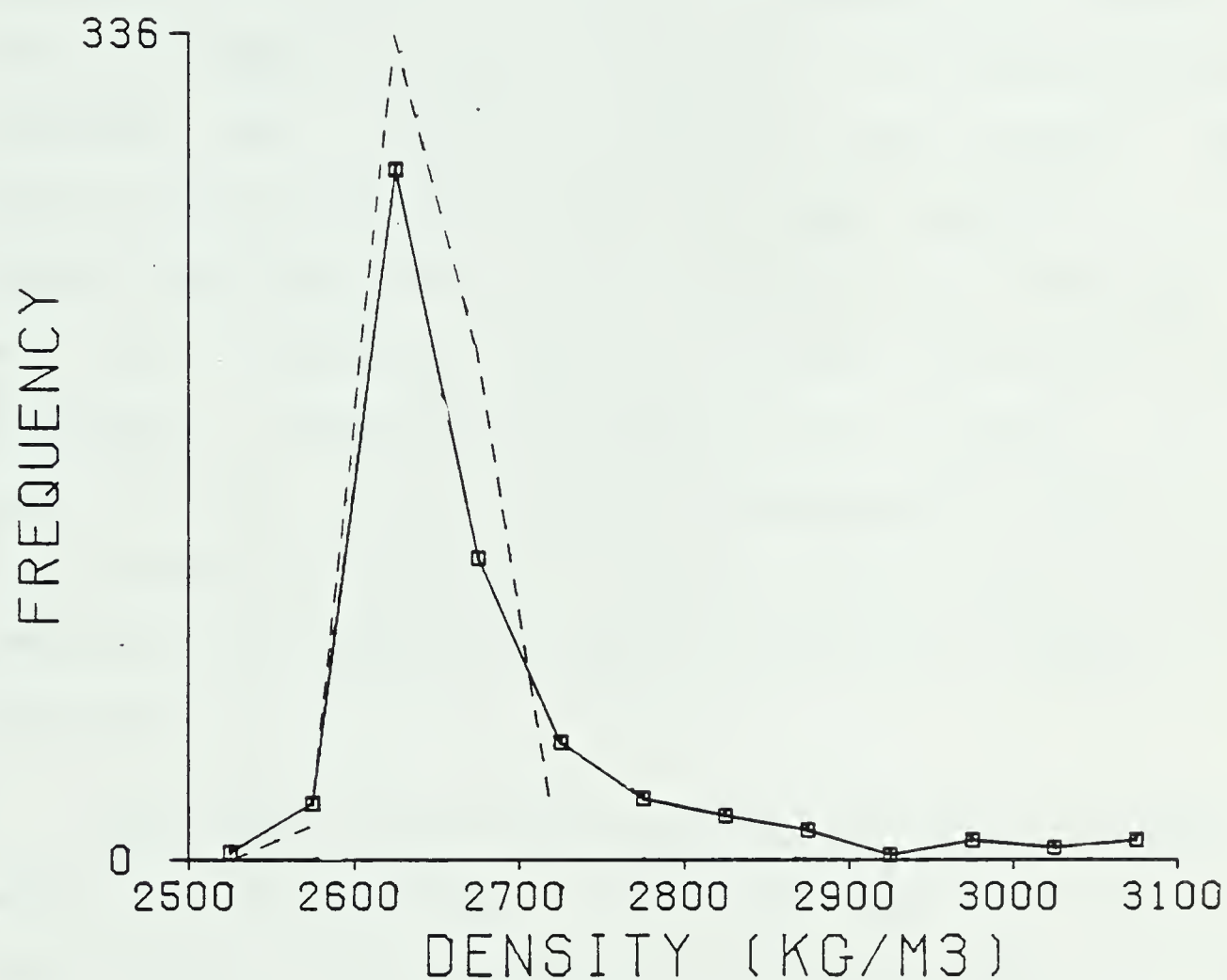


Figure 5.22. Comparison between the density distribution derived from the gravity field for a slab thickness of 20 km with the distribution obtained from laboratory measurements (solid line).

5.5 COMBINED GRAVITY AND MAGNETIC ANALYSIS

If gravity and magnetic field anomalies are due to the same source, then they are related by Poisson's equation. Garland (1951) applied Poisson's equation to obtain the ratio of magnetization to density, J/d , over an area in Arkansas. More recently, Kanasewich and Agarwal (1968) applied two-dimensional time sequence analysis to this problem, and obtained J/d as a function of wavelength as well as a coherency test to validate the results at each wavelength. The method of Kanasewich and Agarwal will be used in this study to obtain representative values of J/d for northeastern Alberta. These derived values will then be compared with measured values from standard samples in the map-area.

The magnetic map was reduced to the pole following the method of Bhattacharyya (1967) although for the 80° inclination of the field in the map-area there is little difference between the total field map and the map reduced to the pole, especially since remanent magnetism is not thought to be important in this map-area. The first vertical derivative of the gravity map was computed in the wave number domain by simply multiplying the Fourier coefficients by their respective wave numbers. The result is a pseudomagnetic map (Figure 5.23) for comparison with the magnetic map reduced to the pole. The coherence between these two maps is a measure of the validity of J/d

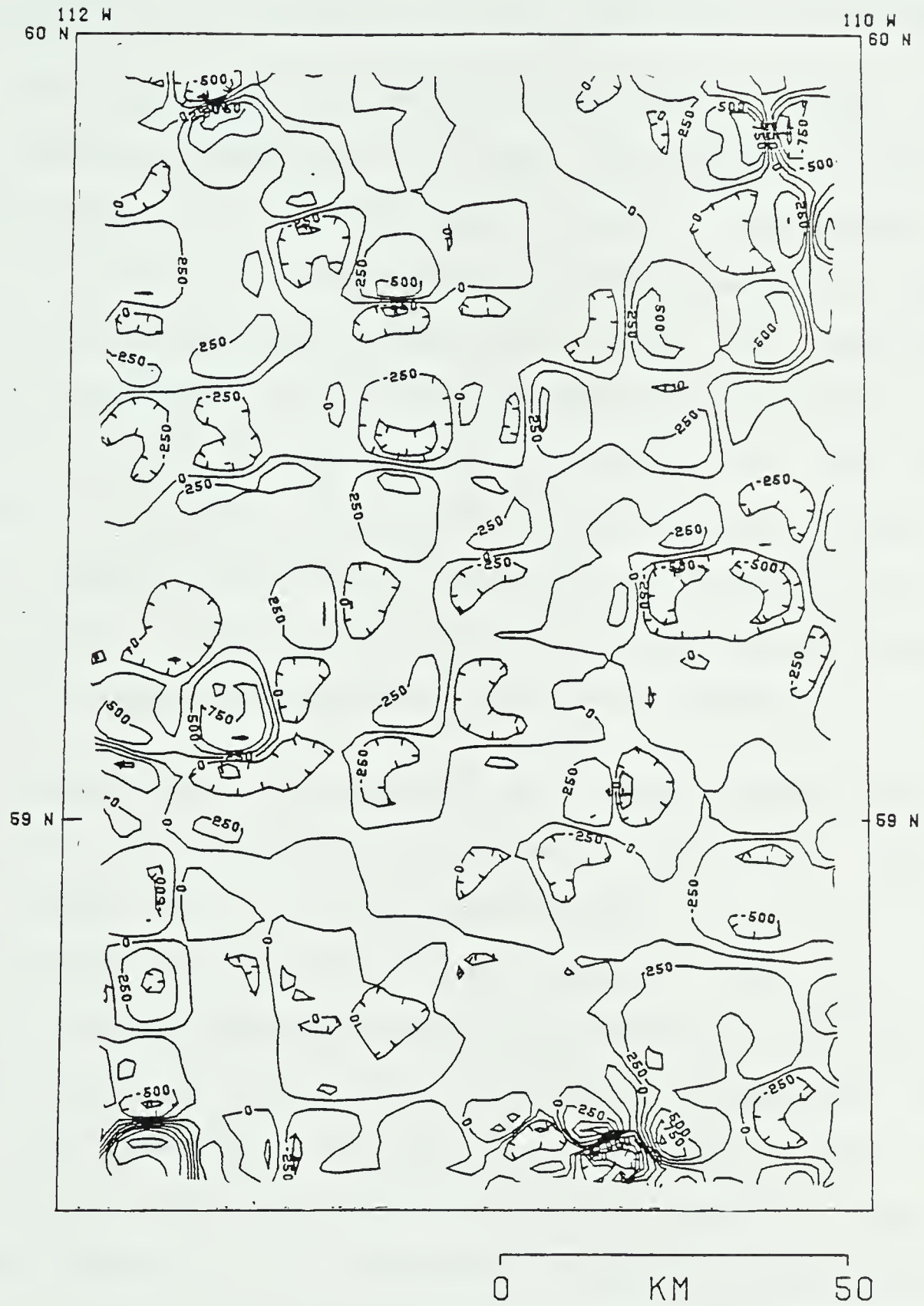


Figure 5.23. Pseudo-magnetic map of northeastern Alberta. The contour interval is 250 nT.

calculations. The Fourier amplitude ratio of the two maps also yielded the values of J/d as a function of wavelength.

The results of this analysis are shown in Figure 5.24. The average coherency for each wavelength is shown as a dashed line. The poor coherence at shorter wavelengths is due to the fact that gravity stations were 10 km apart, hence the pseudomagnetic map is all noise for wavelengths shorter than about 20 km. The valid J/d ratios seem to vary from 0.03 to 0.04 c.g.s. units, except for wavelengths greater than 60 km, where the J/d value rises to about 0.08 c.g.s., possibly reflecting low density contrasts in the deep crust. This would in fact be the situation one would expect in the neighborhood of the Curie isotherm.

Values of J/d measured on standard samples from the map-area are plotted on a histogram in Figure 5.25. Most of the values fall in the interval from 0.03 to 0.10 c.g.s. with a mean at 0.083 c.g.s. and a mode at 0.056 c.g.s. Thus the J/d values determined from the potential field data seem to fall into the lower part of the actually measured range. That the two data sets do not perfectly agree is not surprising. The requirement of Poisson's equation that the source material be homogeneous in magnetic properties and density is not satisfied on the outcrops since the measured values of J/d range over 3 orders of magnitude. The equivalence of the J/d value at very long wavelengths with the overall outcrop mean is interesting since the coherency

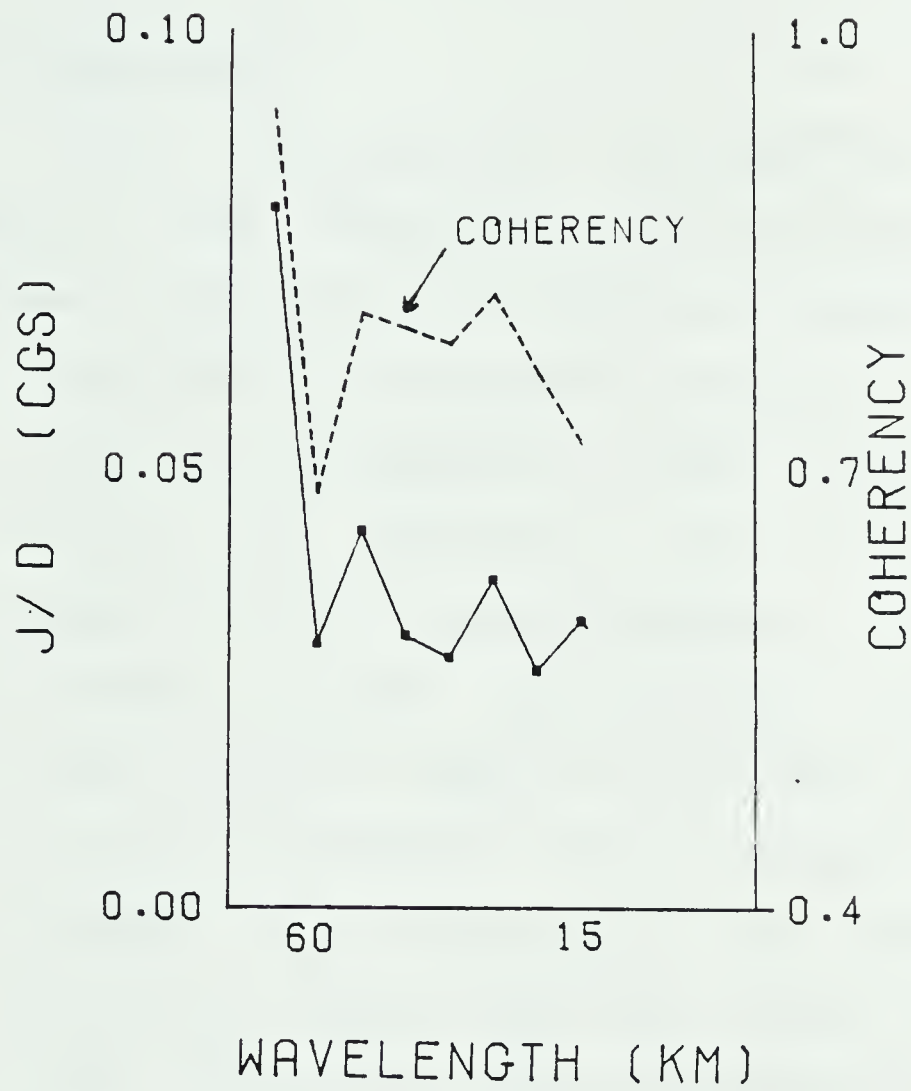


Figure 5.24. Coherency (dashed line) and the ratio of magnetization to density (solid line) as functions of wavelength in northeastern Alberta.

is also very high for this value. If this determination can be taken as representative of the magnetic crust, then a good estimate of J/d for the upper crust in northeastern Alberta is about 0.08 c.g.s.

5.6 CONCLUSIONS

From interpretation of potential field data and physical rock properties in northeastern Alberta, the following conclusions have been postulated.

1. The density and magnetic susceptibility of rocks in the area are low compared to other shield areas, a result which is consistent with the largely granitic composition of the rocks present.
2. The mean basinal rock density in the map-area is significantly higher than the mean domal rock density, a result consistent with a diapiric origin of the larger fold structures. The gravity map of the map-area, however, does not reflect the presence of the fold structures since the measured density difference between the basins and domes is not thought large enough to produce observable gravity anomalies.
3. Two types of major mylonite zones have been identified in the map-area. Those of the first type are associated with magnetically quiet areas and tend to possess low susceptibility. This type of mylonite zone is consistent with the hypothesis of Watanabe(1965)

that the original magnetite in the cataclastic rocks of the area has been altered to hematite. Those mylonite zones of the second type, however, are associated with intense aeromagnetic anomalies and were found to possess high susceptibility. This type of mylonite zone is not consistent with Watanabe's theory. Unless these latter cataclastic rocks have subsequently been enriched by new magnetic material, they apparently did not attain the necessary conditions for magnetite destruction.

4. Under certain assumptions, the Parker algorithm was found to be a useful tool for measuring variations in depth to the Curie isotherm. In this map-area, however, the rock susceptibility required at depth to produce convergence with the inversion scheme was an order of magnitude higher than actual surface measurements. This suggests that the magnetic anomalies in the map-area are due to lateral variations in crustal susceptibility rather than to undulations on the Curie isotherm.
5. Using a stochastic method along with the Parker algorithm to compare lab measured susceptibilities with susceptibilities inverted from the magnetic field, the average depth to the Curie isotherm in northeastern Alberta was found to be in the 15 to 20 km range. This result suggests that the present day geothermal gradient in the map-area is $31^{\circ} \pm 6^{\circ}$ C per km.

6. By comparing *in situ* susceptibility measurements with susceptibilities inverted from the magnetic field, it was concluded that the local intense aeromagnetic anomalies in the map-area have their sources in near-surface rocks extending to a depth of about 1 km.
7. A comparison of laboratory measured densities with densities derived from the gravity field suggested that modal density variations on surface outcrops generally extend to a depth of about 20 km. Since much of the density variation in the map-area is associated with granitoid complexes and major mylonite zones, these geologic features are shown to extend to the top of the lower crust
8. Poisson's relation was used to determine the ratio of magnetization to density as a function of wavelength for the map-area. A coherency test suggested that the results were valid only for large or deep sources. A good estimate for the ratio in the upper crust was found to be 0.08 cgs, a somewhat high value compared to other shield areas, probably a consequence of the small density contrasts likely associated with the predominantly granitoid composition of rocks in northeastern Alberta.

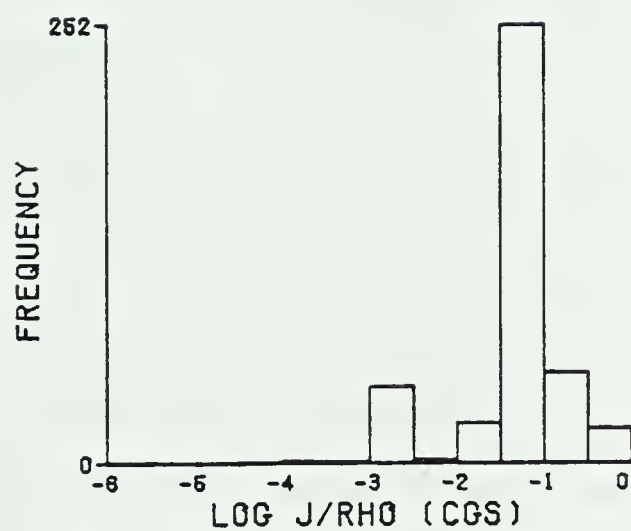


Figure 5.25. Values of the ratio of magnetization to density as obtained from laboratory measurements on standard samples in northeastern Alberta.

6. DISCUSSION

The purpose of this thesis was to investigate the inversion of large potential field data sets and their integration with other geological and geophysical information. The major tool for this study were various extensions of the Parker algorithm all of which involved series expansion of the potential fields in terms of very efficient fast Fourier transforms. Unlike previous studies using the Parker algorithm, the models produced for this thesis were fully three dimensional.

In the theory portion of this thesis, the algorithm was generalized to allow for multilayered models. Algorithms were also derived using Poisson's relation for the forward and inverse magnetic problem. In addition, useful modifications of the algorithms were derived to rapidly calculate lateral variations of physical properties in slabs of constant thickness.

Computer programs were coded for the various algorithms on an AP-190L Array Processor. Listings of many of the programs are given in Appendix D. Various tests were devised for the algorithms, the results of which are described in Appendix A. Generally, calculations with the Parker algorithm were found to be at least an order of magnitude faster than with other published methods. The largest errors encountered when using the Parker algorithm were found to occur along the edges of the grid and were

found to be associated with the cyclic properties of the Fourier transforms. Other smaller errors, due to insufficient sampling occurred near sharp edges on the structural models. Hence the sampling grid used for studies with the Parker algorithm must be fine enough to adequately represent the models, yet large enough to allow for a sufficient number of null values around the area of interest. In regard to prefiltering, it was determined that filter parameters for the inverse procedure were most efficiently chosen by inspection of the amplitude spectrum of the potential field after downward continuation to the reference level.

The first application of the method was to a gravity study of western Canada. The Parker-Oldenburg algorithm was found to be quite useful in the determination of crustal parameters from the gravity field under various assumptions about the intermediate crustal layers. For a crustal model involving a continuous increase of velocity with depth, for example, it was found that a lateral density variation in the upper mantle would have to be invoked in order to satisfy the observed gravity anomaly in western Canada. The Parker algorithm was found to be an efficient means to estimate the relative isostatic anomaly in western Canada. The long wavelength portion of the isostatic anomaly shows a strong trend toward overcompensation to the northeast, probably due to incomplete recovery of the lithosphere from

the Pleistocene ice load. The Parker-Oldenburg algorithm was used to estimate the remaining uplift and a value of over 200 m was calculated, a figure in agreement with other studies. A long wavelength isostatic anomaly also was found to be associated with the Williston Basin area.

Middle wavelength isostatic anomalies (500 to 1000 km) were found to be strongly related to known geologic divisions in western Canada. The Liard block and the Superior province were found to exhibit negative isostasy, while positive isostatic anomalies were found for the Athabaska mobile belt and the Kiseiynew-Sweetgrass belt.

Short wavelength (150-600 km) isostatic anomalies of amplitudes up to 40 milligal were found to occur extensively in the map-area. These anomalies are too large in area to be supported by the crust. They are also associated with rocks far too old to be uncompensated at depth. Hence these anomalies were interpreted as representing crustal mass variations compensated at depth by variations in crustal thickness. The inverse Parker-Oldenburg algorithm was used to model the crustal thickness in western Canada using this interpretation. While the resulting crustal model does not generally agree with the seismic results in western Canada, it does have validity at certain locations, such as in the Edmonton area where the crust seems anomalously thin.

An extension of the algorithm was also found to be useful for gravity inversion in terms of three dimensional multilayered lithospheric models. The gravity and seismic data across the southern plains of western Canada were found to be explicable in terms of such a model. Maps of density variation in the upper crust and upper mantle were derived as well as maps of crustal thickness. This new information should prove valuable for future tectonic analyses of the area.

In order to accomplish the above interpretation, it was necessary to force agreement between the seismic data and the Bouguer anomaly at the seismic control points by adding a correction to the gravity data for various unknown lithospheric density variations. This correction was found to be quite large in the Cordillera, in the Williston Basin, and in the extreme northeast corner of the map-area, suggesting anomalous lithospheric densities in these areas.

The second major application of the method was in a detailed geophysical study of the exposed shield in northeastern Alberta. Here the magnetic inverse algorithm in conjunction with ground control on magnetic susceptibility was found to be a useful means to map the Curie isotherm in the map-area. The average depth to the Curie isotherm was calculated to be in the 15 to 20 km range, suggesting a present day geothermal gradient of $31^{\circ} \pm 6^{\circ}$ C per km. The algorithm combined with *in situ*

susceptibility measurements near magnetic anomalies in the map-area was used in a stochastic process to yield an average vertical extent of 1 km for the local magnetic features. The Parker algorithm was also used in conjunction with ground control on density to invert the gravity field in a statistical manner. From this it was concluded that modal near surface density variations extend to an average depth of 20 km in the map-area. From this observation, the large granitoidal masses in the map-area might be considered as rather fundamental crustal units in that they extend to the top of the lower crust

In summary, an algorithm based on a series expansion of Fourier transforms was found to have diverse applications in potential field problems. It was found to be a very efficient tool for both forward and inverse applications. The algorithm was found to be sufficiently flexible to allow for a large range of model parameters and to allow for integration of other types of data. Finally, the algorithm was shown to have utility not only in deterministic problems but in stochastic ones as well.

With the advent of larger and cheaper computer storage, the inverse of very large potential field data sets will no doubt become a very routine process. This algorithm for two-dimensional Fourier transform inversion of potential fields will unquestionably be an essential part of the software in these applications. This thesis has only

pointed out a few of the many possible uses of the algorithm in geophysical inverse problems.

BIBLIOGRAPHY

- Bell, C. K., 1971a, History of the Superior-Churchill Boundary in Manitoba: Geological Association of Canada, Special Paper, v. 9, pp. 5-10.
- Bell, C. K., 1971b, Boundary geology, Upper Nelson River Area, Manitoba and Northwestern Ontario: Geological Association of Canada, Special Paper, v. 9, pp. 11-39.
- Andrews, J. T., 1968, Pattern and cause of variability of post-glacial uplift and rate of uplift in Arctic Canada: Journal of Geology, 76, pp. 404.
- Bamford, D., 1973, Refraction data in western Germany- A time term approach: Zeitschrift fur Geophysik, 39, pp. 907-927.
- Bhattacharyya, B. K. and Morley, L. W., 1965, The delineation of deep crustal magnetic bodies from total field aeromagnetic anomalies: Journal of Geomagnetism and Geoelectricity, v. 17, pp. 237-252.
- Bhattacharyya, B. K. and Clay, D. N., 1966, Machine methods as aids in the preparation of geophysical maps: Geological Survey of Canada, Paper 66-9, 18 pp.
- Bhattacharyya, B. K., 1967, Some general properties of potential fields in space and frequency domains-A review: Geoexploration, v. 5, pp. 127-143.
- Bhattacharyya, B. K. and Leu, L. K., 1975, Analysis of magnetic anomalies over Yellowstone National Park: mapping of Curie point isothermal surface for geothermal reconnaissance: Journal of Geophysical Research, v. 80, pp. 4461-4465.
- Bhattacharyya, B. K., 1978, Computer modelling in gravity and magnetic interpretation: Geophysics, v. 43, pp. 912-929.
- Burwash, R. A. and Cumming, G. L., 1974. Helium source

rock in southwestern Saskatchewan: Bulletin of Canadian Petroleum Geology, v. 22.

Burwash, R. A. and Krupicka, J., 1970, Cratonic reactivation in the precambrian basement of western Canada: Canadian Journal of Earth Sciences, v. 7, pp. 1275.

Burwash, R. A., Krupicka, J., and Culbert, R. R., 1973, Cratonic reactivation in the Precambrian basement of western Canada III. Crustal evolution: Canadian Journal of Earth Sciences, v. 10, pp. 283-291.

Burwash, R. A. and Culbert, R. R., 1976, Multivariate geochemical and mineral patterns in the precambrian basement of western Canada: Canadian Journal of Earth Sciences, v. 13, pp. 1-18.

Byers, A. R., 1962, Major faults in western part of the Canadian shield with special reference to Saskatchewan: The Royal Society of Canada, Special Publication No. 4., pp. 40-59.

Camfield, P. A. and Gough, D. I., 1977, A possible plate boundary in North America: Canadian Journal of Earth Sciences, v. 14, pp. 1229-1238.

Chandra, N. N. and Cumming, G. L., 1972, Seismic refraction studies in western Canada: Canadian Journal of Earth Sciences, v. 9, p 1099.

Clee, T. E., Barr, K. G., and Berry, M. J., 1974, Fine structure of the crust near Yellowknife: Canadian Journal of Earth Sciences, v. 11, pp. 1534-1549.

Cochran, J. R. and Talwani, M., 1977, Free-air gravity anomalies in the world's oceans and their relationship to residual elevation, v. 50, pp. 495-552.

Cook, K. L., 1962, The problem of the mantle-crust mix: Advances in Geophysics, v. 9, pp. 296-360.

Crain, I. K. and Bhattacharyya, B. K., 1967, Treatment of non-equispaced two-dimensional data with a digital

computer: Geoexploration, v. 5, pp. 173-194.

Crittenden, M. D., 1963, Effective viscosity of the earth derived from isostatic loading of Pleistocene Lake Bonneville: Journal of Geophysical Research, v. 68, pp. 5517-5530.

Cumming, G. L. and Kanasewich, E. R., 1966, Crustal structure in western Canada: Final report. Contract AF19(628)2835, AFCRL, Bedford, Mass.

Cumming, W. B., Clowes, R. M., and Ellis, R. M., 1978, Crustal structure from a seismic refraction profile across southern British Columbia: Canadian Journal of Earth Sciences, v. 16, pp. 1024-1040.

Darnley, A. G., The relationship between uranium distribution and some major crustal features in Canada: Minerological Magazine, v. 44, pp. 425-436.

Dawson, E. and Newitt, L. R., 1977, An analytic representation of the geomagnetic field in Canada for 1975. Part II: The main field: Canadian Journal of Earth Sciences, v. 14, pp. 477-487.

Fuller, B. D., 1967, Two-dimensional frequency analysis and design of grid operators: in Mining Geophysics, v. 2, pp. 658.

Garland, G. D., 1965, The earth's shape and gravity: Pergamon Press, Ltd, 183 pp.

Ganley, D. C. and Cumming, G. L., 1974, A seismic reflection model of the crust near Edmonton, Alberta: Canadian Journal of Earth Sciences, v. 11, pp. 101-109.

Garland, G. D., 1951, Combined analysis of gravity and magnetic anomalies: Geophysics, v. 16, pp. 51-62.

Gibb, R. A. and McConnell, R. K., 1968, Gravity anomaly field in northern Manitoba and northeastern Saskatchewan: Gravity map series of the Dominion Observatory, No. 68-76.

- Godfrey, J. D., 1966, Geology of the Bayonet, Ashton, Potts and Charles Lake District, Alberta: Research Council of Alberta, Preliminary Report 65-6, 45 pp.
- Godfrey, J. D. and Langenberg, C. W., 1978, Metamorphism in the Canadian shield of northeastern Alberta: Geological Survey of Canada Paper 78-10, pp. 129-138.
- Goodacre, A. K., 1972, Generalized structure and composition of the deep crust and upper mantle in Canada: Journal of Geophysical Research, v. 77, pp. 3146-3161.
- Grant, F. S. and West, G. F., 1965, Interpretation theory in applied geophysics: McGraw, Hill, Inc., 583 pp.
- Green, A. G., 1977, A cooperative near vertical incident reflection and refraction/wide angle reflection seismic survey across the Churchill-Superior boundary zone in southern Canada, Part 1, A technical report.
- Green, A. G., Stephenson, O. G., Mann, G. D., Kanasewich, E. R., Cumming, G. L., Hajnal, Z., Mair, J. A., West, G. F., 1979, Cooperative seismic survey across the Superior-Churchill boundary zone in southern Canada, A final report.
- Gurbuz, B. M., 1970, A study of the earth's crust and upper mantle using travel times and spectrum characteristics of body waves: Bulletin of the Seismological Society of America, v. 60, pp. 1921-1935.
- Hall, D. H., 1968, Regional magnetic anomalies, magnetic units, and crustal structure in the Kenora District, Ontario: Canadian Journal of Earth Sciences, v. 5, pp. 1277.
- Hall, D. H. and Brisbin, W. C., 1965, Crustal structure from converted head waves in central western Manitoba: Geophysics, v. 30, pp. 1035-1067.
- Hall, D. H. and Hajnal, Z., 1973, Deep seismic crustal studies in Manitoba: Bulletin of the Seismological Society of America, v. 63, pp. 885-910.

- Hajnal, Z. and Rose, T. C., 1979, A quantitative correlation of seismic, gravity and tectonic models along the Nelson Front: In press.
- Innes, M. J., 1960, Gravity and Isostasy in northern Ontario and Manitoba: Dominion Observatory, v. 21, No. 6.
- Kanasewich, E. R., 1966, Deep crustal structure under the plains and Rockies Mountains: Canadian Journal of Earth Sciences, v. 3, pp. 937-945.
- Kanasewich, E. R. and Agarwal, R. G., 1968, Analysis of combined gravity and magnetic fields in wave number domain: Journal of Geophysical Research, v. 75, pp. 5702-5712.
- Kanasewich, E. R., Clowes, R. M. and McCloughan, C. H., 1969, A buried Precambrian rift in western Canada: Tectonophysics, v. 8, pp. 513-527.
- Kornik, L. J. and MacLaren, A. S., 1966, Aeromagnetic study of the Churchill-Superior boundary in northern Manitoba: Canadian Journal of Earth Sciences, v. 3, pp. 547-557.
- Kazmierczak, Z., 1980, Seismic crustal studies in Saskatchewan: M. Sc. Thesis, The University of Alberta.
- Langenberg, C. W. and Ramsden, J., 1980, The geometry of folds in granitoid rocks of northeastern Alberta: Tectonophysics, v. 66, pp. 269-285.
- Lee, S. K. J., 1977, Multilayer gravity inversion using Fourier transforms: M. Sc. Thesis, The University of Alberta, 141 pp.
- Lefehr, T. R., 1980, Gravity method: Geophysics, v. 45, pp. 1634-1639.
- Lyustikh, E. N., 1957, Isostasy and isostatic hypotheses: American Geophysical Union, Washington, D. C., 119 pp.

- Maxant, J., 1975, Distribution and regional variation of density in the western Canada basin: *Geophysics*, v. 40, pp. 56-78.
- McClure, J. E., 1973, Seismic investigation in the Yorkton Area of Saskatchewan: M. Sc. Thesis, University of Saskatchewan.
- McDougal, E. B., 1976, Computer programming for spatial problems: John Wiley and Sons, New York, 159 pp.
- McGinnis, L. D., Wolf, M. G., Kohsmann, J. J., and Ervin, C. P., 1979, Regional free air gravity anomalies and tectonic observations in the United States: *Journal of Geophysical Research*, v. 84, pp. 591-601.
- Mereu, R. F. and Hunter, J. A., 1969, Crustal and upper mantle structure under the Canadian shield from m Project Early Rise data: *Bulletin of the Seismological Society of America*, v. 59, pp. 147-165.
- Milne, W. G., Rogers, G.C., Riddihough, R. P., McMechan, G. A., and Hyndman, R. D., 1978, Seismicity of western Canada: *Canadian Journal of Earth Sciences*, v. 15, pp. 1170-1193.
- Mueller, S., 1977, A new model of the continental crust: in *The Earth's Crust*, Geophysical Monograph Series, American Geophysical Union, pp. 289-317.
- Nafe, J. E. and Drake, C. L., 1957, Society of Exploration Geophysicists Annual Meeting. Unpublished paper.
- Nielsen, P. A., Langenberg, C. W., Baadsgard, H., and Godfrey, J. D., 1981, Precambrian metamorphic conditions and crustal evolution, Northeastern Alberta: In press.
- Oldenburg, D. W., 1974, The inversion and interpretation of gravity anomalies: *Geophysics*, v. 39, pp. 526-536.
- Parker, R. L., 1973, The rapid calculation of potential anomalies: *Geophysics*, v. 39, pp. 447-455.

- Parker, R. L., 1974, A new method for modelling marine gravity and magnetic anomalies: *Journal of Geophysical Research*, v. 79, pp. 2014-2016.
- Parker, R. L. and Huestis, S., 1974, Inversion of magnetic anomalies in the presence of topography: *Journal of Geophysical Research*, v. 79, pp. 1587-1593. Plouffe, R., 1977, A technical report on bulk susceptibility measurements of the Precambrian shield of Alberta: unpublished Research Council of Alberta Report, 8 pp.
- Press, F., 1960, Crustal structure in the California-Nevada region: *Journal of Geophysical Research*, v. 65, pp. 1039.
- Reford, M. S., 1980, Magnetic method: *Geophysics*, v. 45, pp. 1640-1658.
- Shuey, R. T., Schellinger, D. K., Tripp, A. C., and Alley, L. B., 1977, Curie depth determination from aeromagnetic spectra: *Journal of Geophysical Research*, v. 50, pp. 75-101.
- Smellie, D. W., 1967, Elementary approximations in aeromagnetic interpretation: *Mining Geophysics*, v. 2, pp. 474-410.
- Sprenke, K. F., 1972, An application of the P-coda spectral ratio method to crustal structure in central Alberta: M. Sc. Thesis, The University of Alberta.
- Sommerville, P. G. and Ellis, R. M., 1972, P-coda evidence for a layer of anomalous velocity in the crust beneath Leduc, Alberta: *Canadian Journal of Earth Sciences*, v. 9, pp. 845-856.
- Sprenke, K. F., 1979, Field measurements of the magnetic susceptibility of outcrops on the Precambrian shield of Alberta: unpublished report, Research Council of Alberta, 10 pp.
- Stockwell, C. H., 1969, Tectonic map of Canada: Geological Survey of Canada, Map 1251A.

- Talwani, M. and Ewing, M., 1960, Rapid calculation of gravitational attraction of three dimensional bodies of arbitrary shape: *Geophysics*, v. 25, pp. 203-225.
- Vacquier, V. and Affleck, J., 1941, A computation of the average depth to the bottom of the earth's magnetic crust, based on a statistical study of local magnetic anomalies: *Transactions of the American Geophysical Union*, 22nd Meeting, pp. 446-450.
- Wagner, C. A., Lerch, F. J., Browne, J. E., and Richardson, J. A., Improvement in the geopotential derived from satellite and surface data: *Journal of Geophysical Research*, v. 82, pp. 901-914.
- Walcott, R. I., 1968, The gravity field of Saskatchewan and northeastern Alberta: Gravity map series of the Dominion Observatory, maps 16-20.
- Walcott, R. I., 1969, Isostatic response to loading of the crust in Canada: *Canadian Journal of Earth Sciences*, v. 7, pp. 716-727.
- Walcott, R. I. and Boyd, J. B., 1971, The gravity field of northern Alberta: Gravity map series of the Earth Physics Branch, maps 103-111.
- Watanabe, R. Y., 1965, Petrology of cataclastic rocks of northeastern Alberta: unpublished Ph. D. thesis, University of Alberta, 235 pp.
- Watkins, N. D., The relative contributions of remanent and induced magnetization in northeastern Alberta: *Geophysical Prospecting*, v. IX, pp. 421-426.
- Weber, J. R. and Goodacre, A. K., 1968, An analysis of the crust-mantle boundary in Hudson Bay from gravity and seismic observations: *Canadian Journal of Earth Sciences*, v. 5, pp. 1297-1303.
- Woolard, G. P., Crustal structure from gravity and seismic measurements: *Journal of Geophysical Research*, v. 64, 1975, pp. 1521-1544.

APPENDIX A: TESTS OF THE ALGORITHM

PYRAMID MODEL

The gravity anomaly for the three dimensional pyramid-like body mapped in Figure A.1 and profiled in Figure A.2 was calculated. This irregular body has both base and top in the shape of horizontal four sided polygons of areas 525 km^2 and 18 km^2 , respectively. The height of the body is 0.8 km and the assumed density contrast is 1000 kg/m^3 . The gravitational attraction of this body has been calculated over a square area of 4096 km^2 on a 64 by 64 grid with 1 km spacings between points by two different methods.

The first method used was the numerical integration method of Talwani and Ewing (1960). The three dimensional body is divided into a series of horizontal lamina 0.1 km thick. By means of Green's Theorem, the surface integral of each lamina is transformed into a line integral about these "contours" and expressed in digital form. The attraction of the complete three dimensional body is obtained by numerical integration over all the lamina. In practice, this method was found to be cumbersome particularly since the entire procedure had to be repeated for each observation point.

The second method used for this model utilized Parker's algorithm. The result after only four iterations is shown in Figure A.3. This result required less than one tenth the

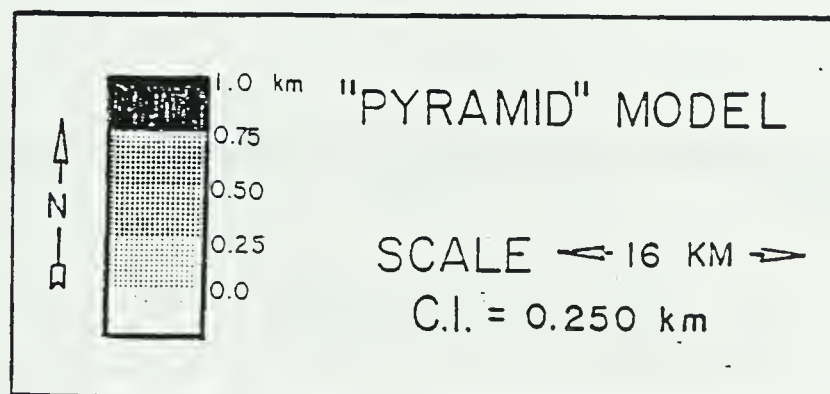
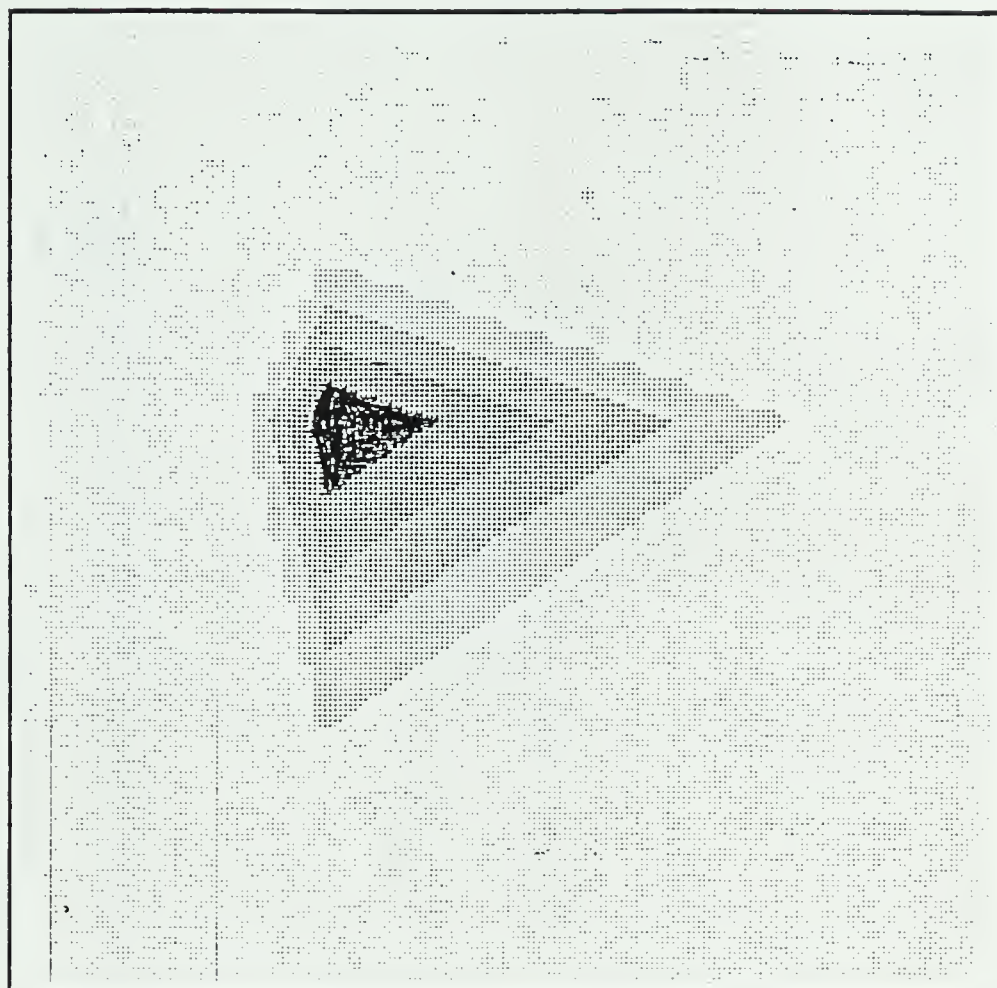


Figure A.1. Contour map of the asymmetrical "pyramid" structure used to test the forward and reverse algorithms. The structure is flat on top with a maximum height of 0.8 km.

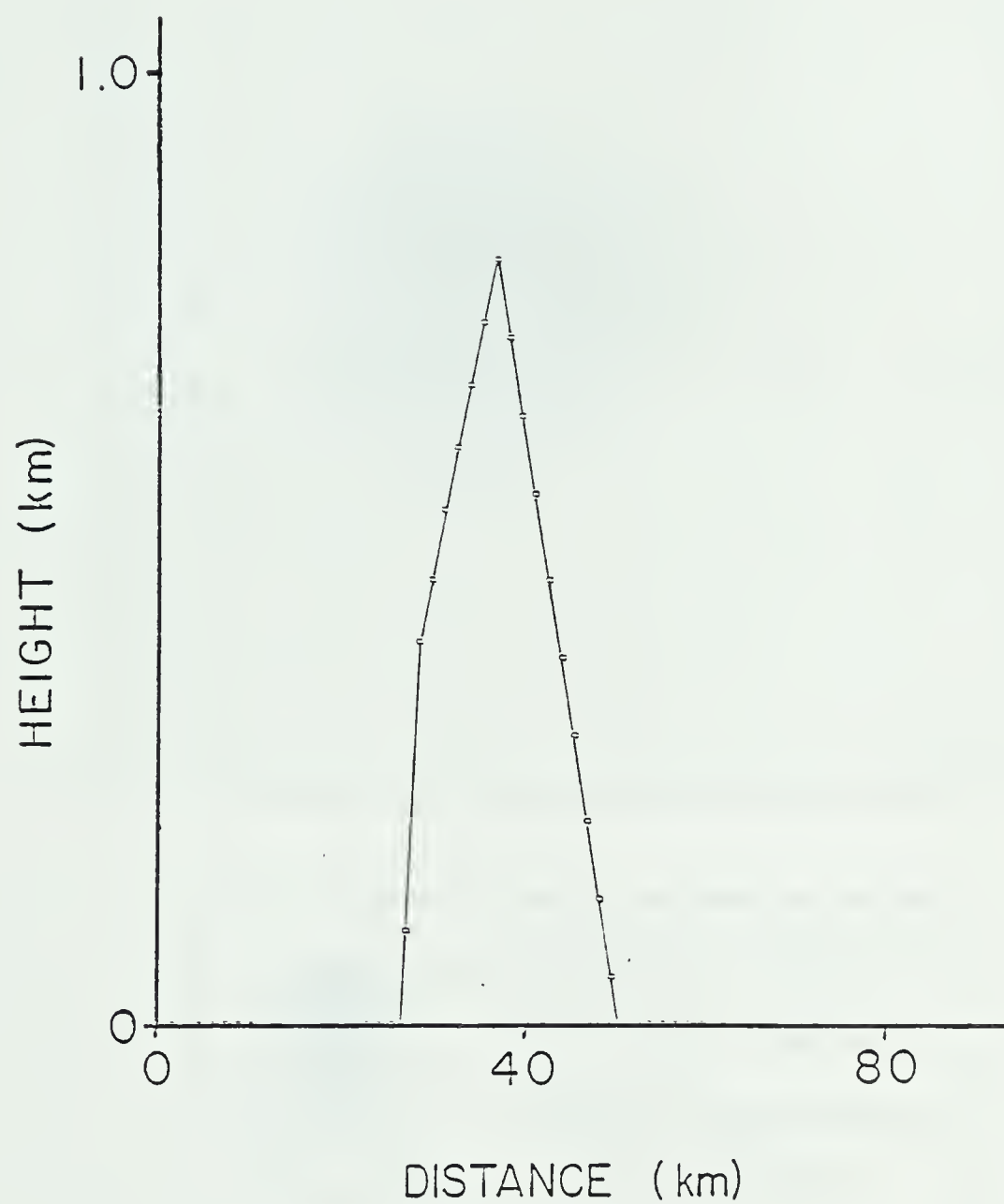


Figure A.2. A NW-SE profile of the "pyramid" model.

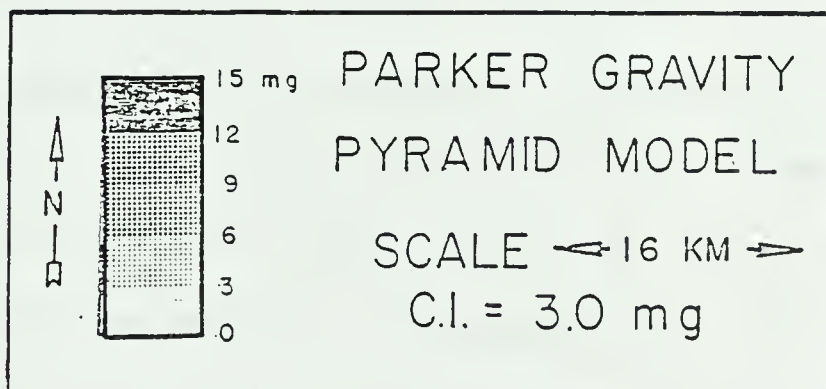
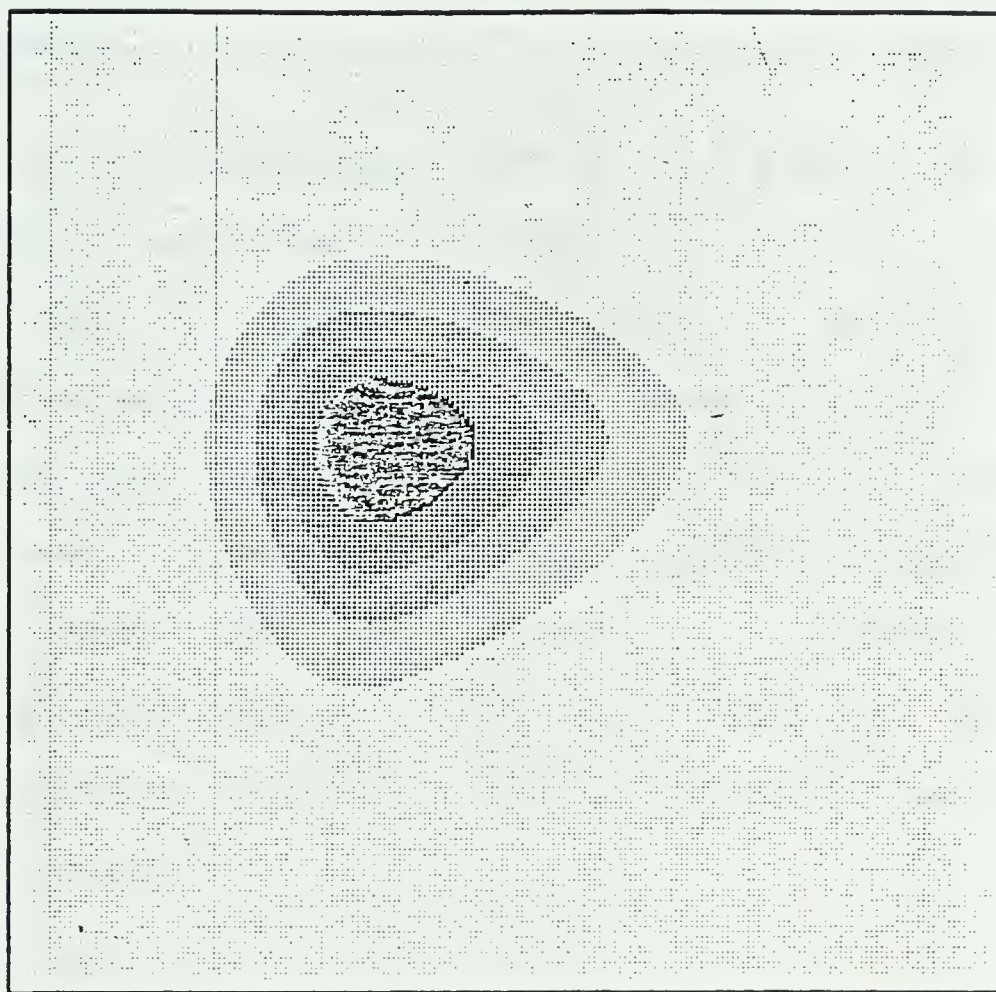


Figure A.3. The gravity anomaly due to the pyramid model as calculated using the Parker algorithm.

computing time than the result from the Talwani and Ewing (1960) method.

Profiles from the upper left to the lower right corners of both results are shown in Figure A.4. It is clear that the two agree to within a fraction of a milligal. A map showing the absolute value of the error between the two results was also studied. The average error in the area of the model seems to be about 0.3 mg. Slightly higher errors about the edges are due to the cyclic properties of the Fourier Transforms used in the Parker algorithm and these could have been eliminated by adding additional zeros around the model structure.

SPHERICAL MODEL

Perhaps the simplest model structure for which to theoretically calculate a gravity anomaly is a spherical distribution of constant density since the external effect of such a distribution is equivalent to that of a particle of equal mass at the center. The spherical structure used as a test model here was assigned the following parameters: radius 4 km, density 1000 kg/m³, and depth to center 5 km. The gravity anomaly for this model was calculated over a square area of 1024 km² on a 64 by 64 grid with 0.5 km spacings.

The gravity anomaly over the sphere was calculated exactly and by the Parker algorithm. A diagonal profile of

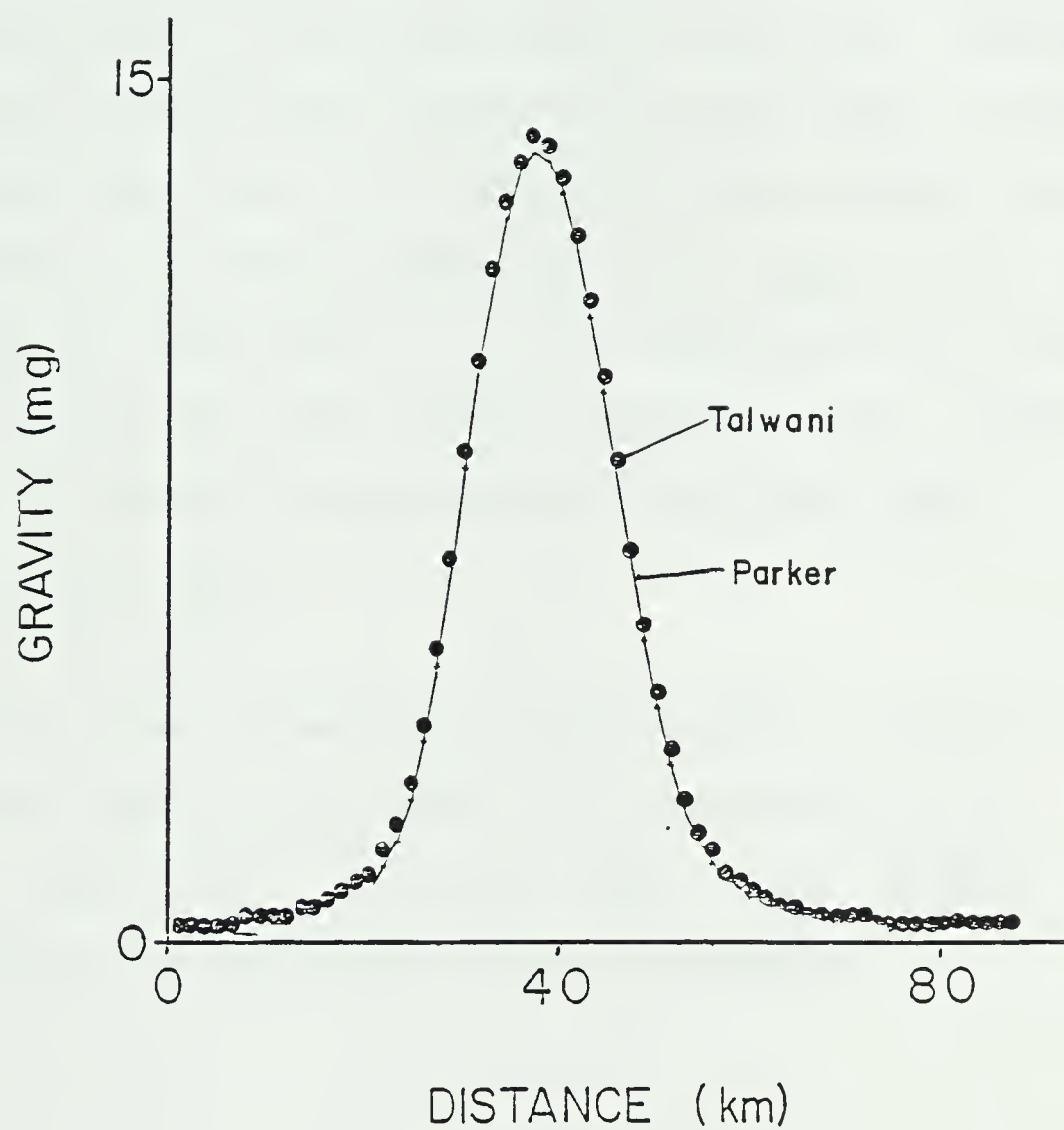


Figure A.4. A comparison of NW-SE profiles of the gravity anomaly due to the pyramid model as computed by the Talwani and Parker algorithms.

each result is shown in Figure A.5. While there is some difference between the two results, it is only over the edges of the sphere that the error becomes rather high. The explanation for the error once again lies in the Fourier transformations within the Parker algorithm. The spherical structure utilized here shows very sharp edges relative to the sampling interval. While the exact formulation is not affected by the coarse sampling at the edges of the sphere, the Parker algorithm is. It is imperative that structural models used with the Parker algorithm be satisfactorily sampled in order to avoid errors near sharp edges

THE OVAL MODEL

The three dimensional model which was used to further test the algorithms is essentially a cosine function 1 km in height and "oval" in plan view. Its height, $h(x,y)$, relative to the reference plane is given by:

$$h(x,y) = 0.5 + 0.25 \cos(\pi x/10) + 0.25 \cos(\pi y/20) \quad [52]$$

$$\text{for } -10 < x < 10 \text{ and } -20 < y < 20, \text{ and by } h(x,y) = 0 \quad [53]$$

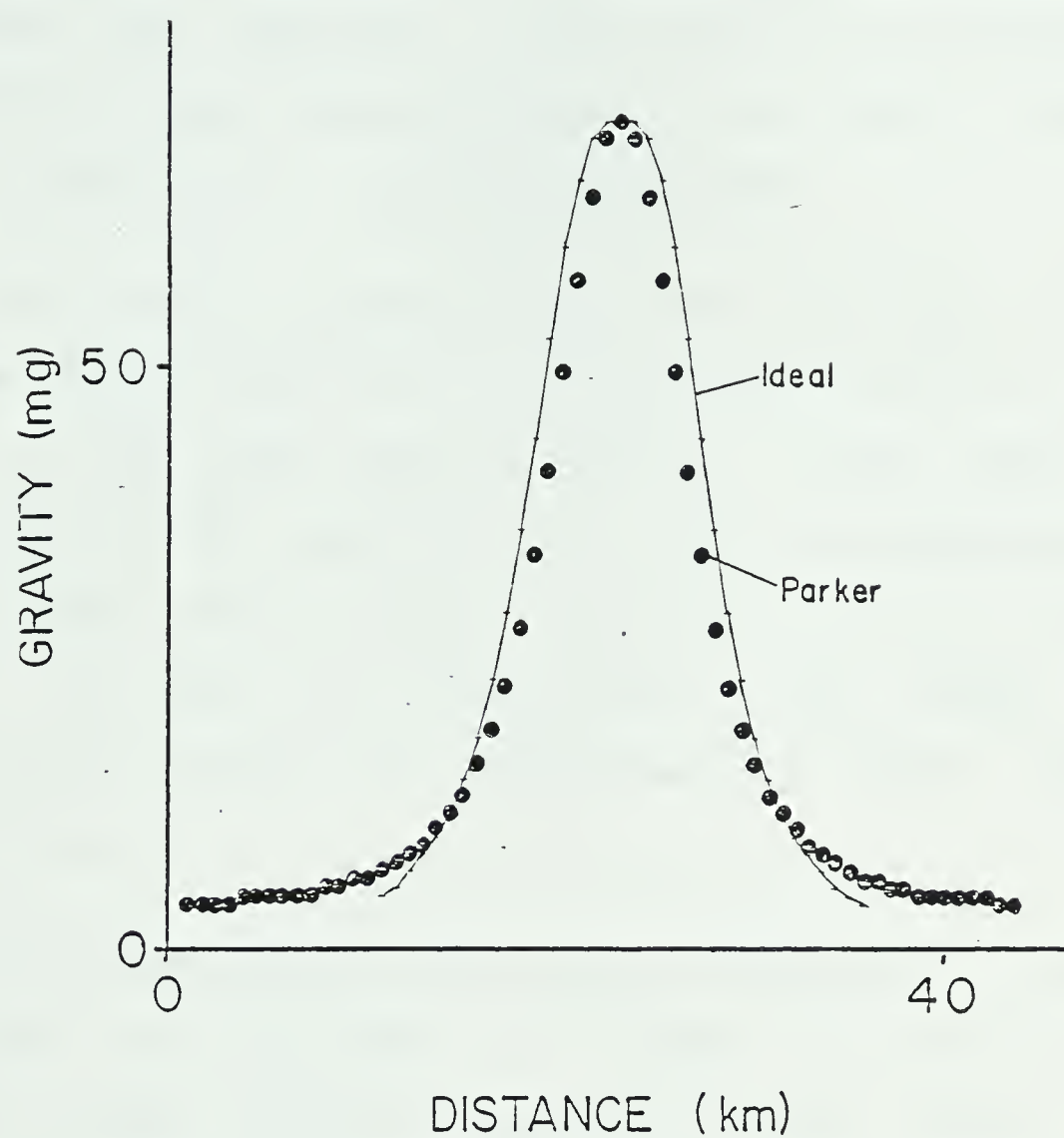


Figure A.5. A comparison of NW-SE profiles of the gravity anomaly due to a buried sphere as calculated by the exact formula and by the Parker algorithm.

for all other values of x and y .

A map of this test function referred to as the oval model is shown in Figure A.6. The gravity anomaly for this structure was computed at 4096 points on a 64 by 64 grid. The depth to the reference plane, Z_0 , was set at 1 km and a density contrast of 1 kg/m^3 was assumed.

This gravity anomaly was then inverted using the inverse Parker algorithm for the assumed value of reference level (1 km) and density contrast (1000 kg/m^3). As Oldenburg (1974) pointed out, this algorithm contains a downward continuation type of operator. In actual fact, the result of the first iteration in his method is the "equivalent stratum" as discussed by Grant and West (1965,p.214).

The success of the inversion procedure for the oval structure test is shown in Figure A.7 which is a NW-SE section through the oval structure (solid line) and the structure found by the inversion procedure (data points); and also in Figure A.8 which is a map of the absolute value of the difference between the original model structure and the structure from inversion. The poorest agreement, which is still less than 10 m on a 1 km thick structure, occurs along the sharp N-S ridge of the oval structure which can be seen in Figure A.6. This error is no doubt largely due to the effect of the low pass filter which probably removed the

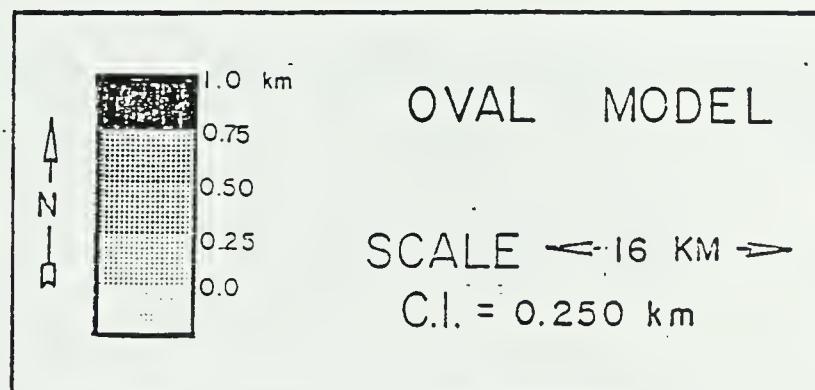
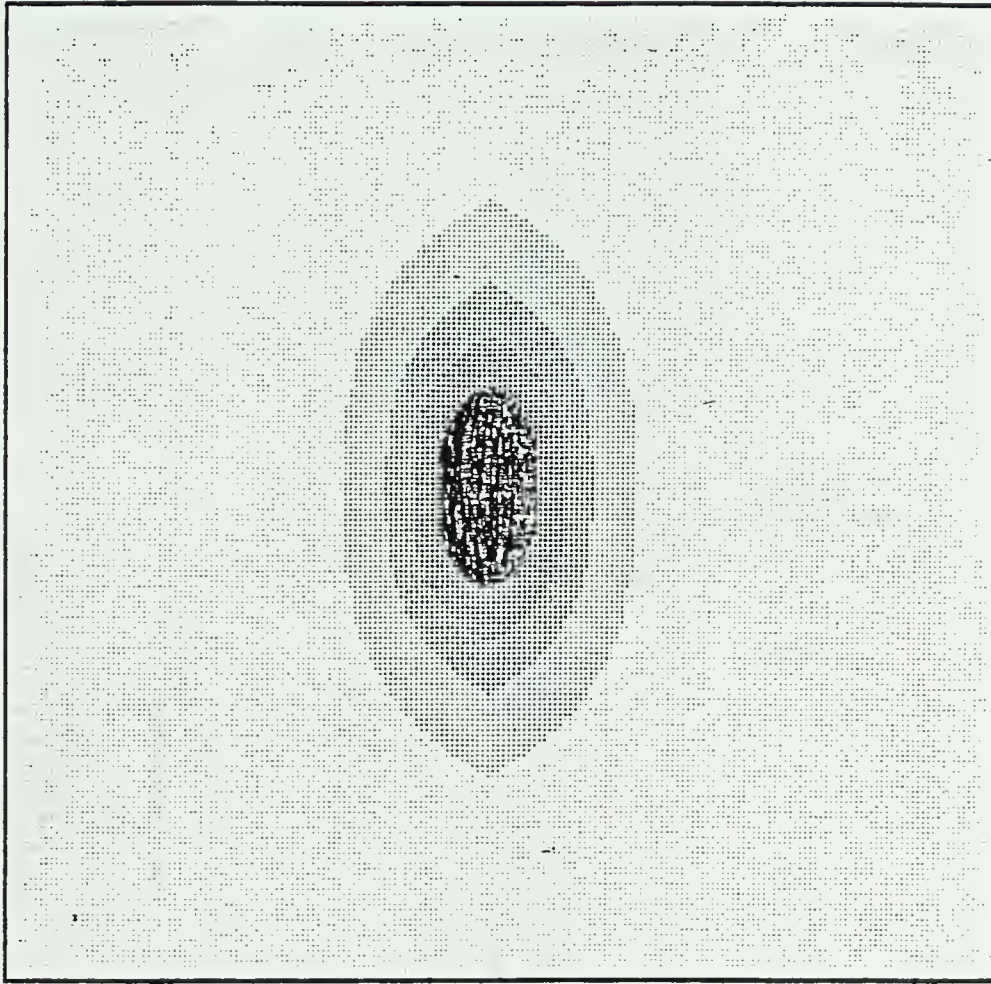


Figure A.6. Contour map of the oval model used to test the inverse Parker algorithm.

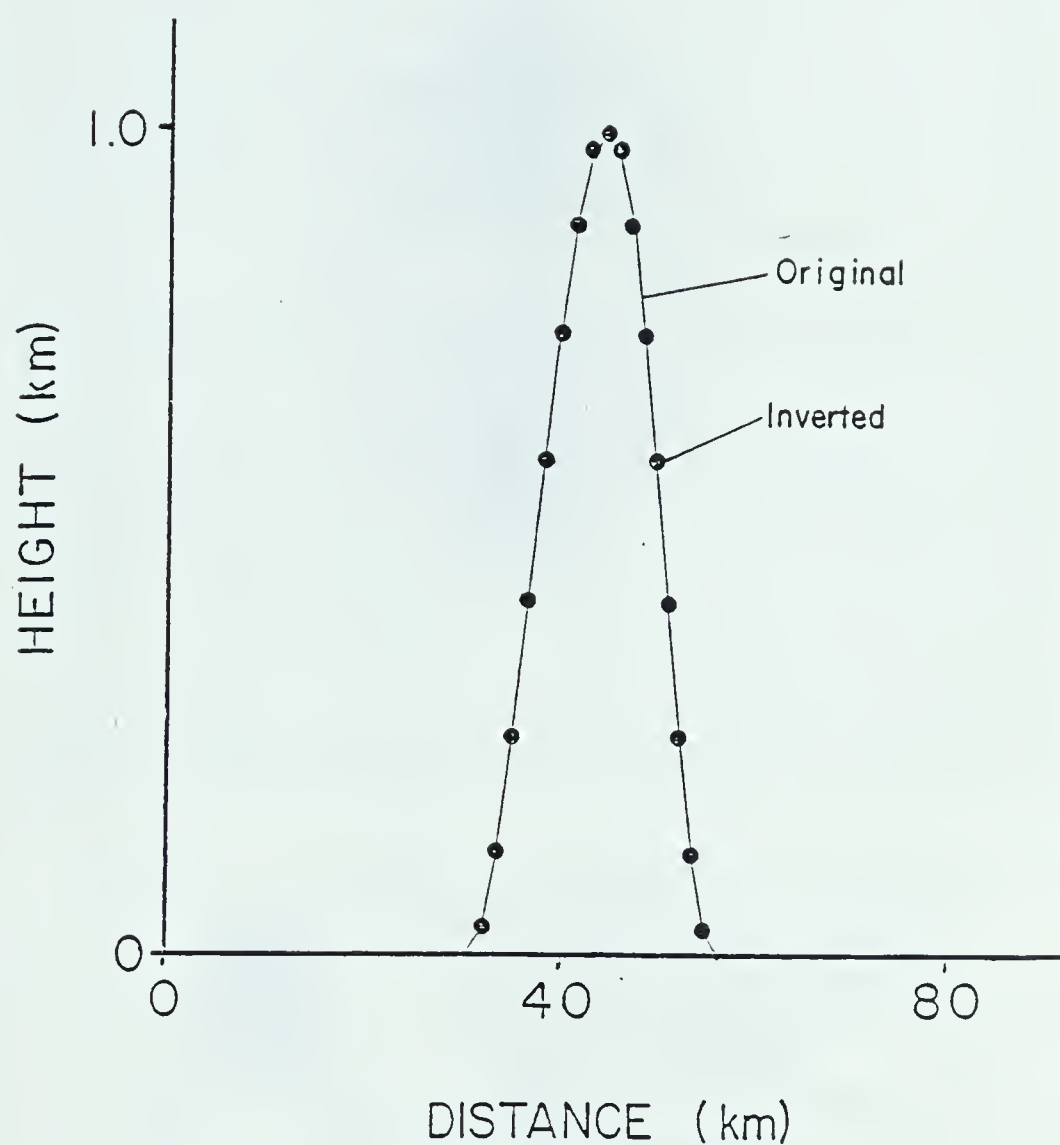


Figure A.7. A comparison of the NW-SE profiles of the original oval structure and the structure as obtained by inversion utilizing the inverse Parker algorithm.

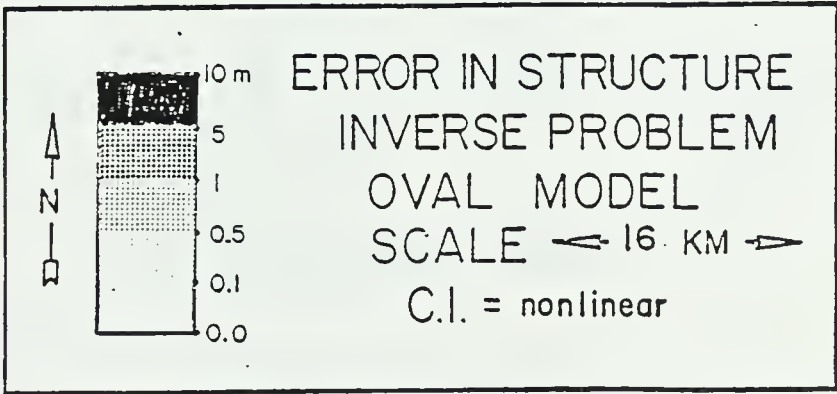


Figure A.8. Absolute value of the difference between the original oval model and the structure obtained by the inversion process.

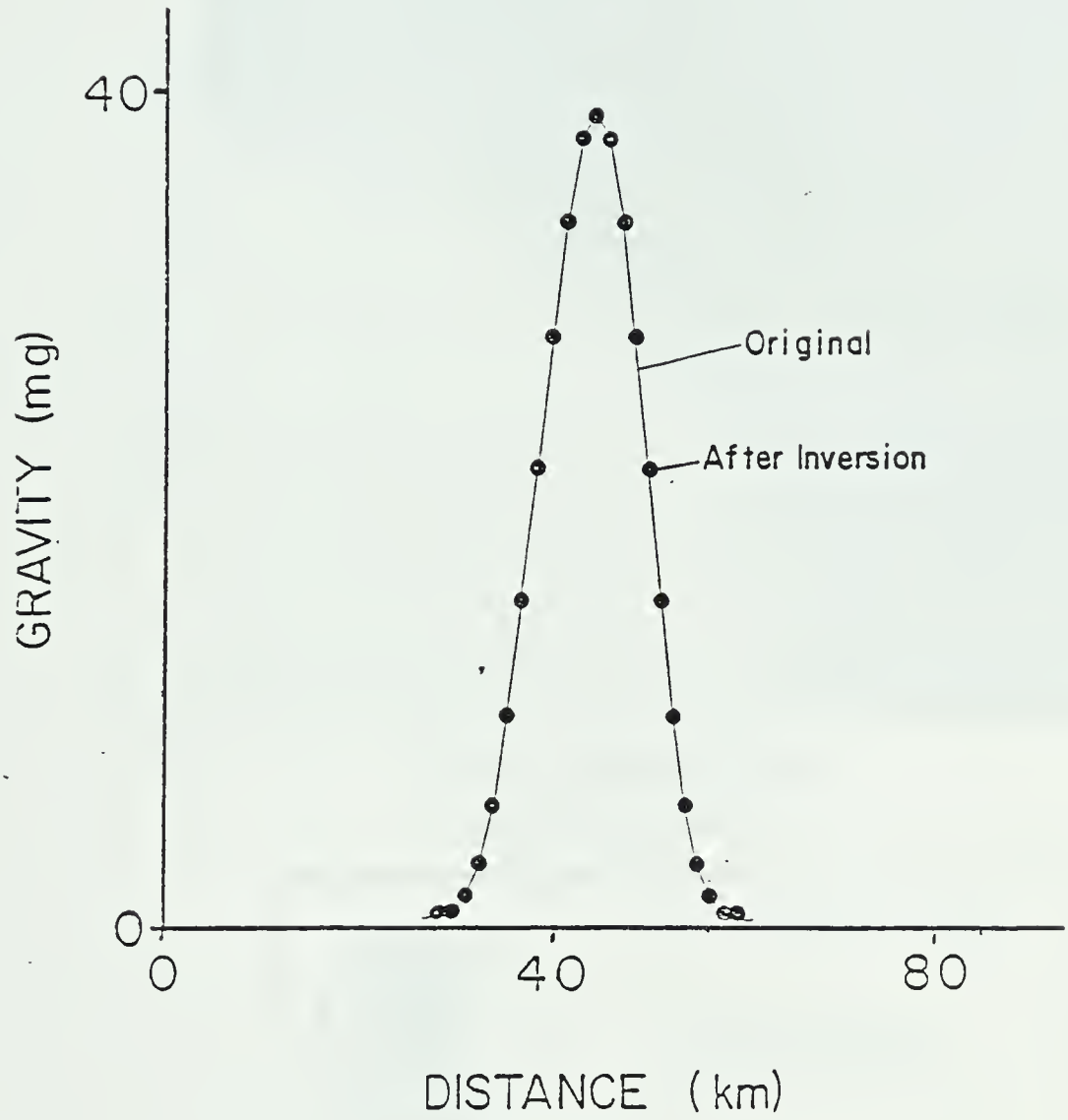


Figure A.9. A comparison of NW-SE profiles of the gravity anomaly due to the original oval model and the gravity anomaly due to the inverted structure.

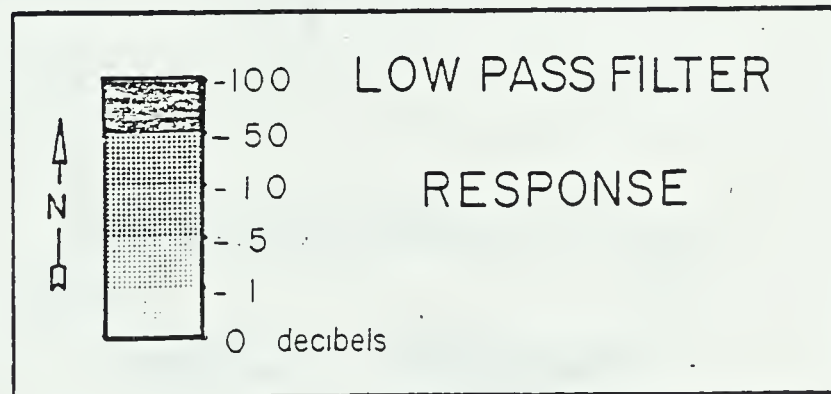
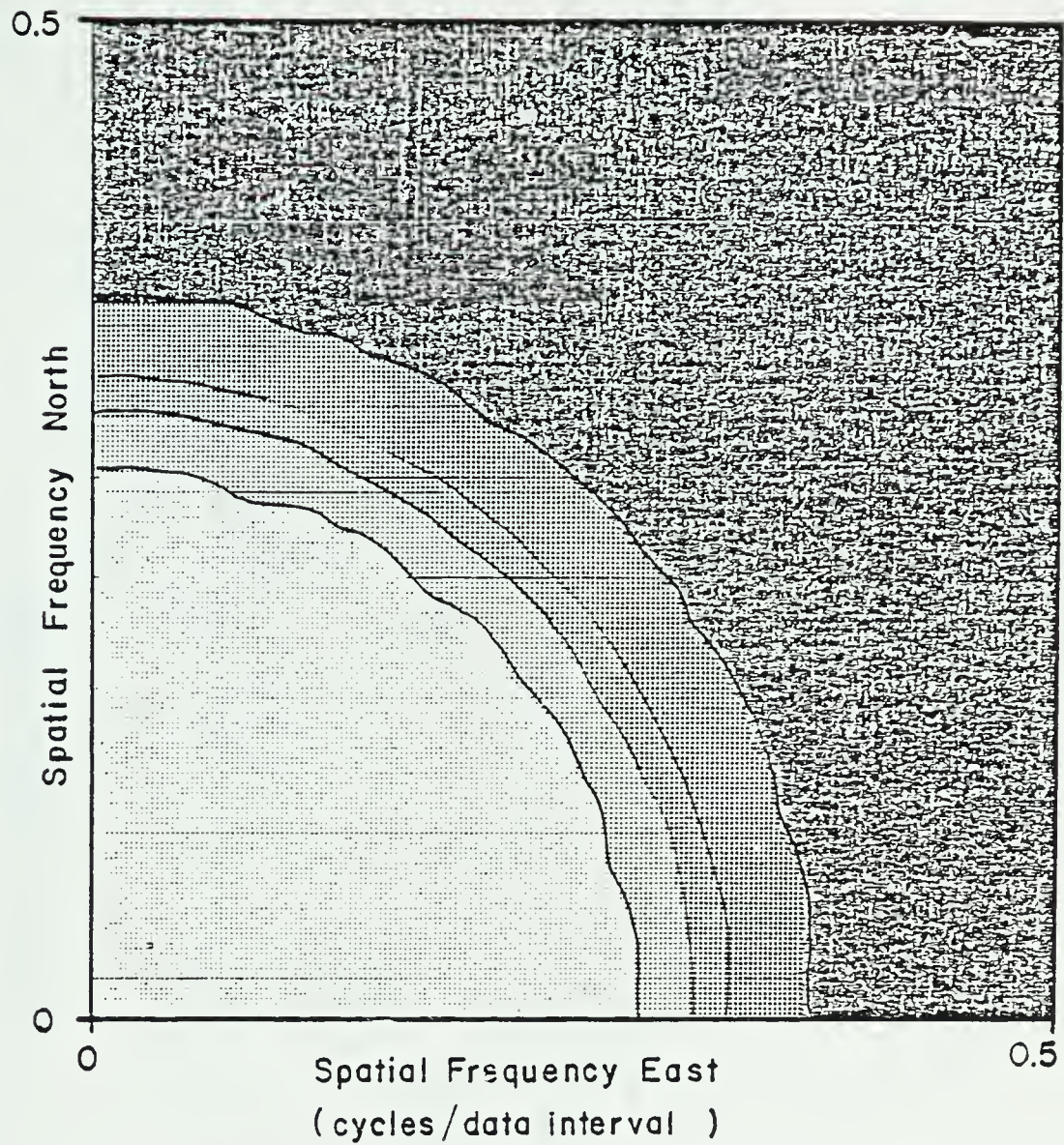


Figure A.10. Frequency response of a low pass filter of the type utilized in this study.

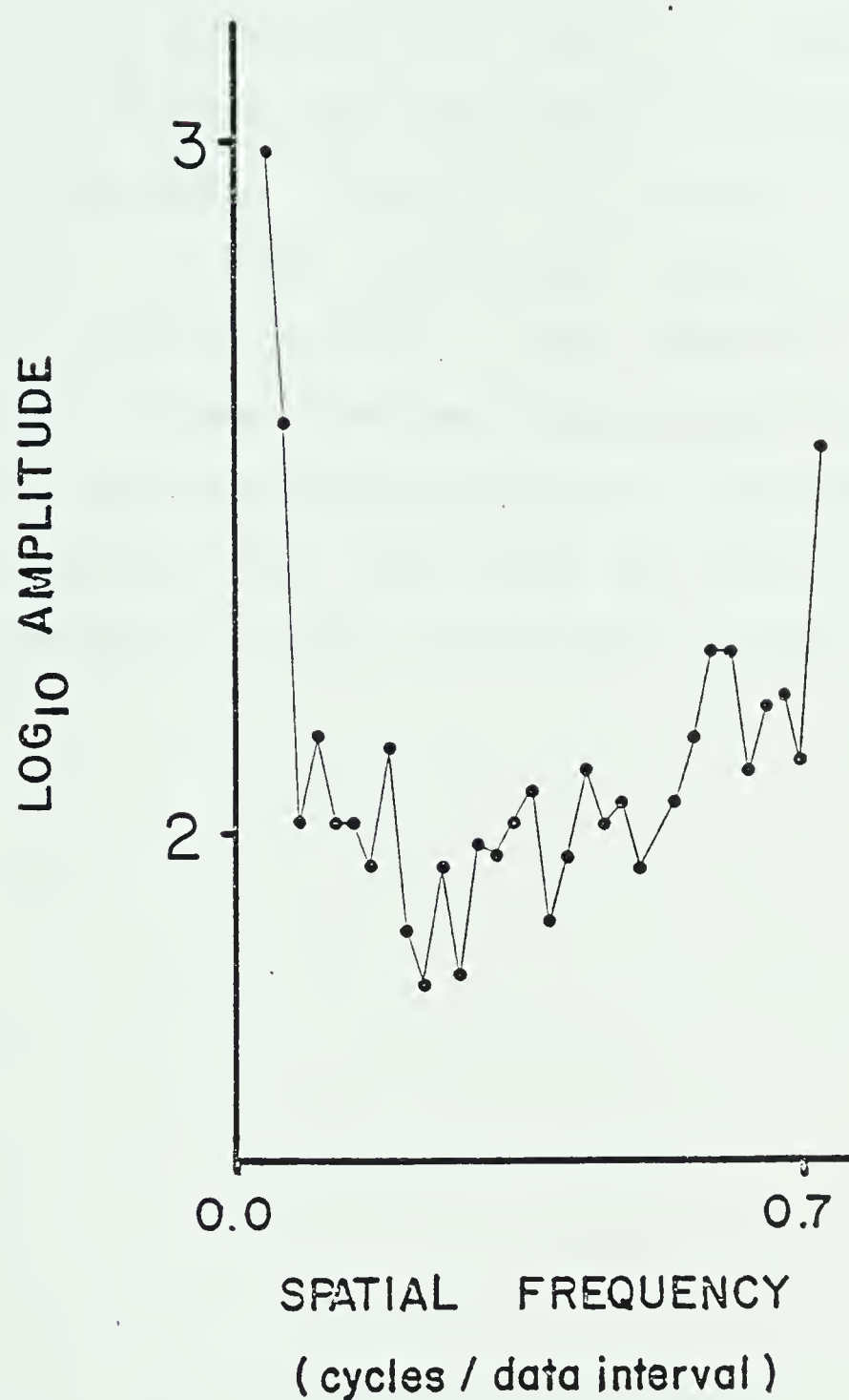


Figure A.11. Radial spectral amplitude of the equivalent stratum for the oval model. The reference level is quite shallow, 1 km, hence the spectrum is well behaved except for spatial frequencies greater than 0.5 cycles per data interval.

high frequencies required to generate the sharp ridge.

This new structure was then used as a source for the forward Parker algorithm in order to compute a gravity anomaly to compare with the anomaly calculated for over the original structure. The profile in Figure A.9 shows this result as the data points superimposed on the solid line original gravity profile. The absolute value of the difference between the two results was also mapped and the largest error was found once again on the sharp ridge of the oval structure, but the error was only 0.2 milligal in a gravity anomaly of about 40 milligal in amplitude.

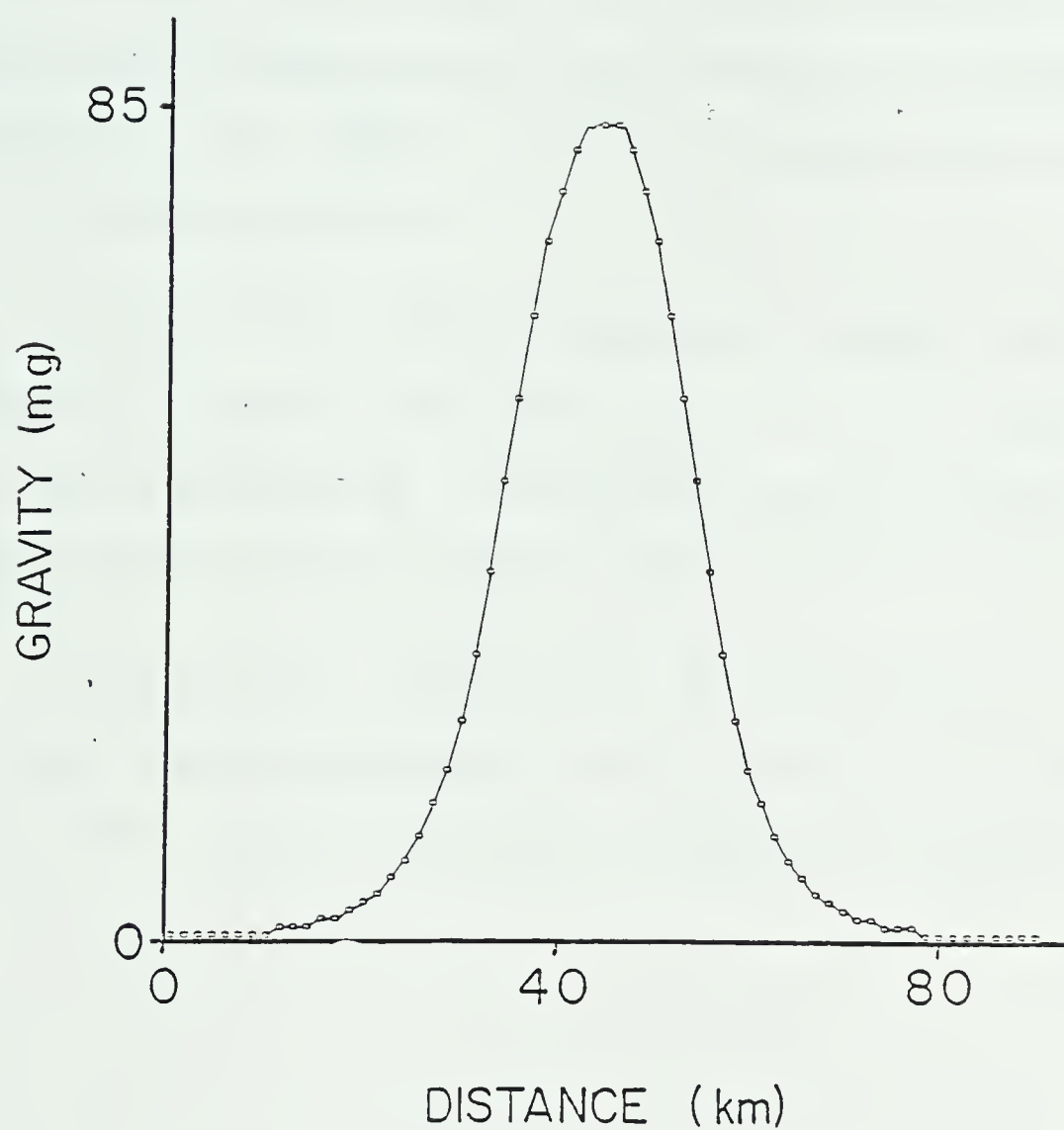


Figure A.12. Gravity anomaly due to a cylindrical shaped distribution of anomalous density as calculated by the Parker algorithm.

LATERAL DENSITY VARIATION TEST

An offshoot of the Parker algorithm is a method of determining that lateral variation in density of a slab of constant thickness which could produce an observed gravity anomaly. The theory for this procedure has been discussed in a previous section.

As a test, a cylindrically shaped distribution of density of height 5 km and radius 10 km with depth to top of 10 km is considered. The density varies abruptly from 1000 kg/m³ within the cylinder to zero outside the structure.

The gravity anomaly for this cylindrical distribution of mass was calculated on a 64 by 64 grid with spacings of 1 km. The result is shown in profile in Figure A.12. This

anomaly was then used as input to the inverse problem. As with all such inverses, some prefiltering was required as is evident from the average radial spectral amplitude of the first approximation of the density distribution (Figure A.13). The strong positive slope on the semi-log plot is indicative of random noise being continued downward. Hence a high cut frequency of 0.25 cycles per data interval was chosen to eliminate this noise. The inverted density distribution is shown in profile in Figure A.14 along with the original cylindrically shaped distribution. The agreement is quite satisfactory considering the inherent problems involved in utilizing Fourier transforms of functions with such sharp edges.

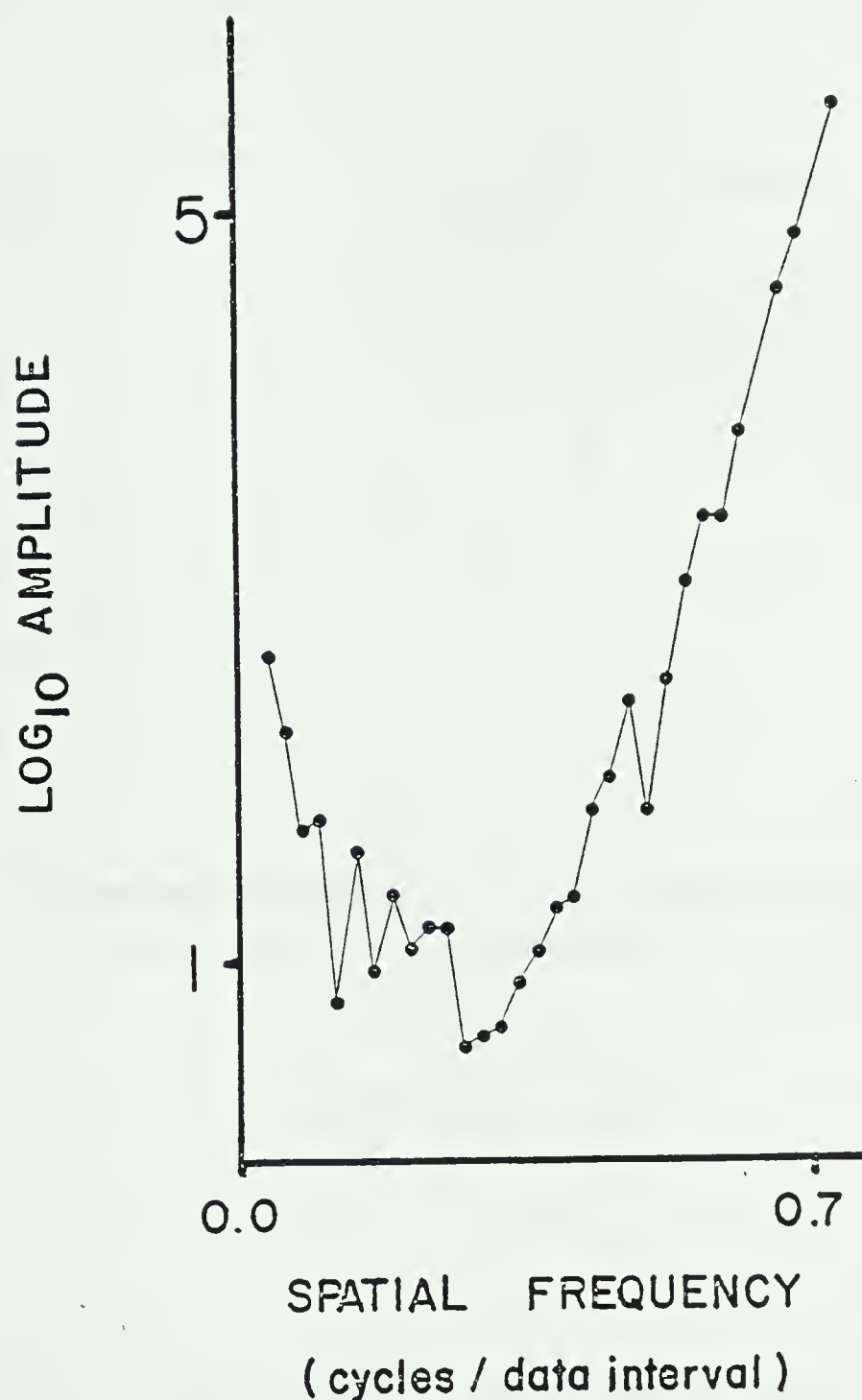


Figure A.13. Radial spectral amplitude of the equivalent stratum for the cylinder model. The reference level is fairly deep (15 km), hence a strong upward slope indicating undesirable amplification of white noise occurs for frequencies greater than about 0.25 cycles per data interval.

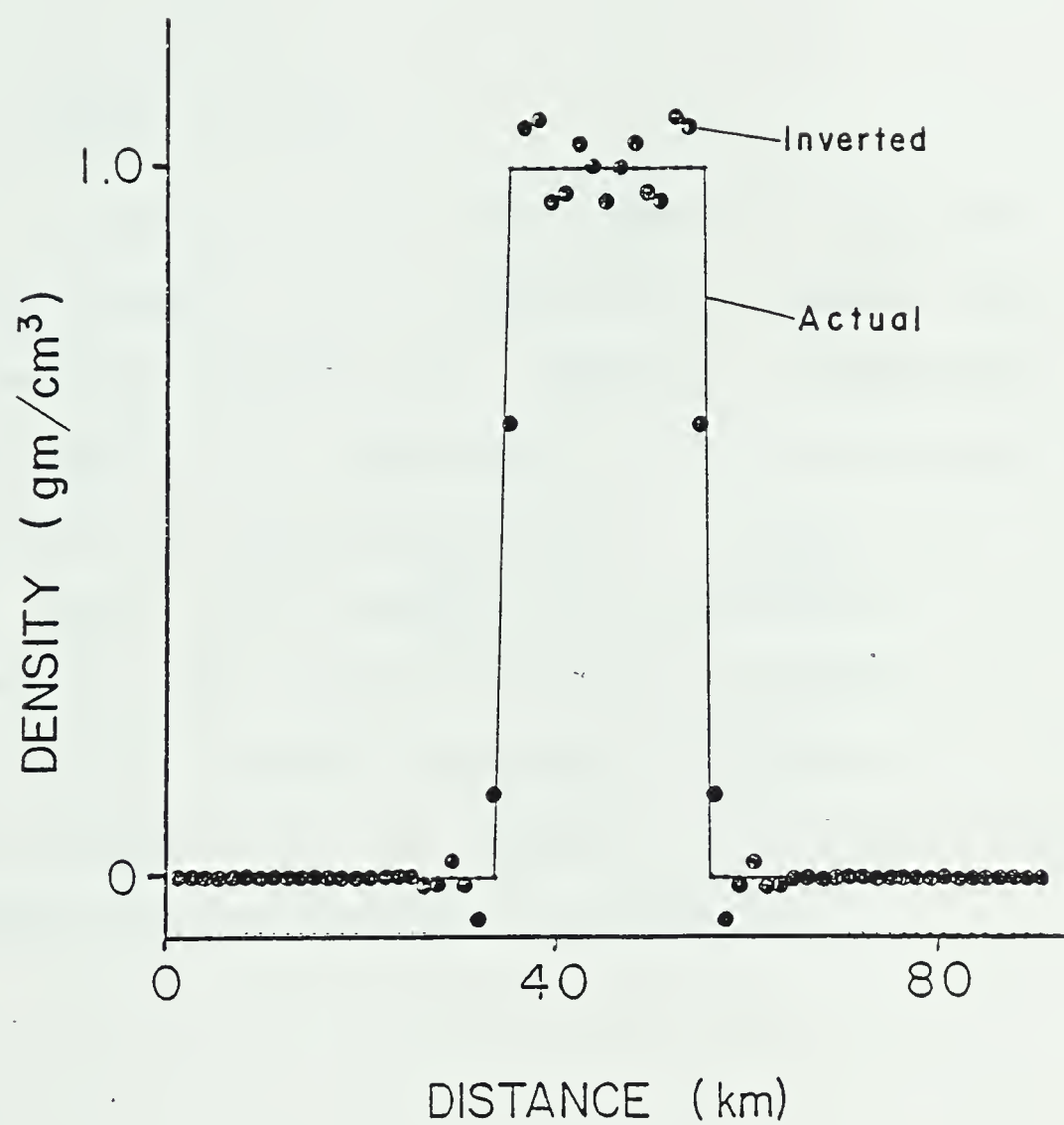


Figure A.14. Comparison of a profile of the actual disc shaped density distribution with a profile of the density distribution obtained by the inversion process.

MAGNETIC TESTS

In order to test the magnetic algorithm, the total field anomaly of a spherically shaped distribution of magnetized matter was studied. Physically, such a distribution is equivalent to a dipole magnetized in the direction of the ambient field. A comparison of profiles of the total field anomaly as calculated by the exact formula (Smellie, 1967) and by the Parker algorithm for inclinations of 0° , 45° , and 90° are shown in Figure A.16. The profiles are aligned along the magnetic meridian. The agreement between the two results is satisfactory.

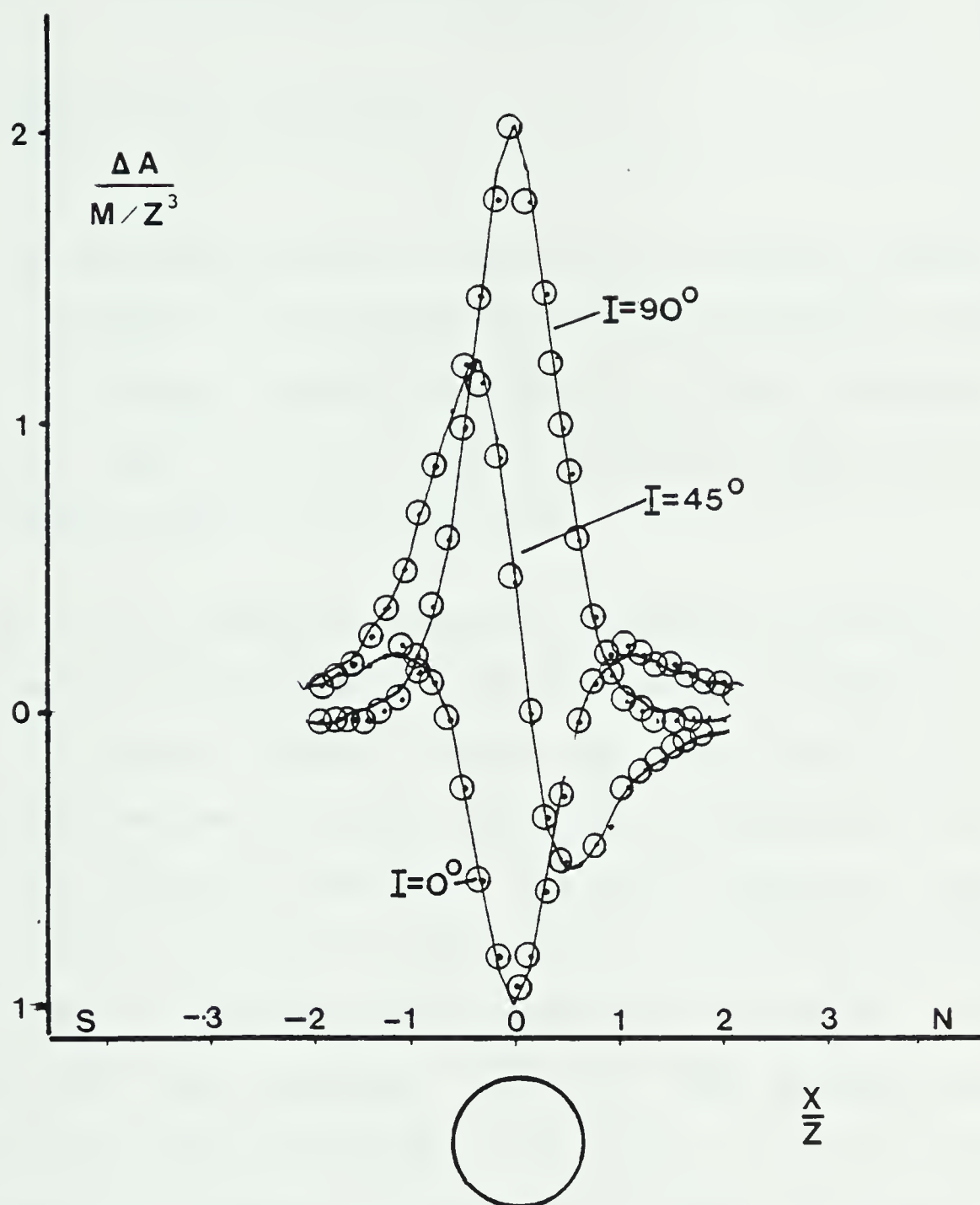


Figure A.15. A comparison of profiles of the total field anomaly due to a sphere as calculated by the exact formula and by the Parker algorithm for various inclinations.

APPENDIX B: SIMPLE GRAVITY INVERSIONS

SIMPLE SLAB INVERSIONS

The easiest method of inverting the gravity data from western Canada is in terms of a slab of constant thickness but with a lateral density variation. If the thickness is assumed, then the Parker algorithm can be used to calculate the required density distribution.

As a first model, a slab of thickness 37 km with top at sea level is utilized as a reasonable approximation of the crust in western Canada. Here, the entire gravity field is assumed to be due to lateral density variations within a crust of constant thickness. The radial spectral amplitude of the resulting density distribution was examined and found to be well behaved and in need of no filtering. This is because the slab extends right to the surface and no downward continuation operator is active. The final density distribution is shown in Figure B.1. Since no filtering of the data was required, this map is quite detailed and is "exact" in the sense that if this slab were used as a source for the forward problem, the resultant gravity and the original gravity would agree; there would be no residual gravity.

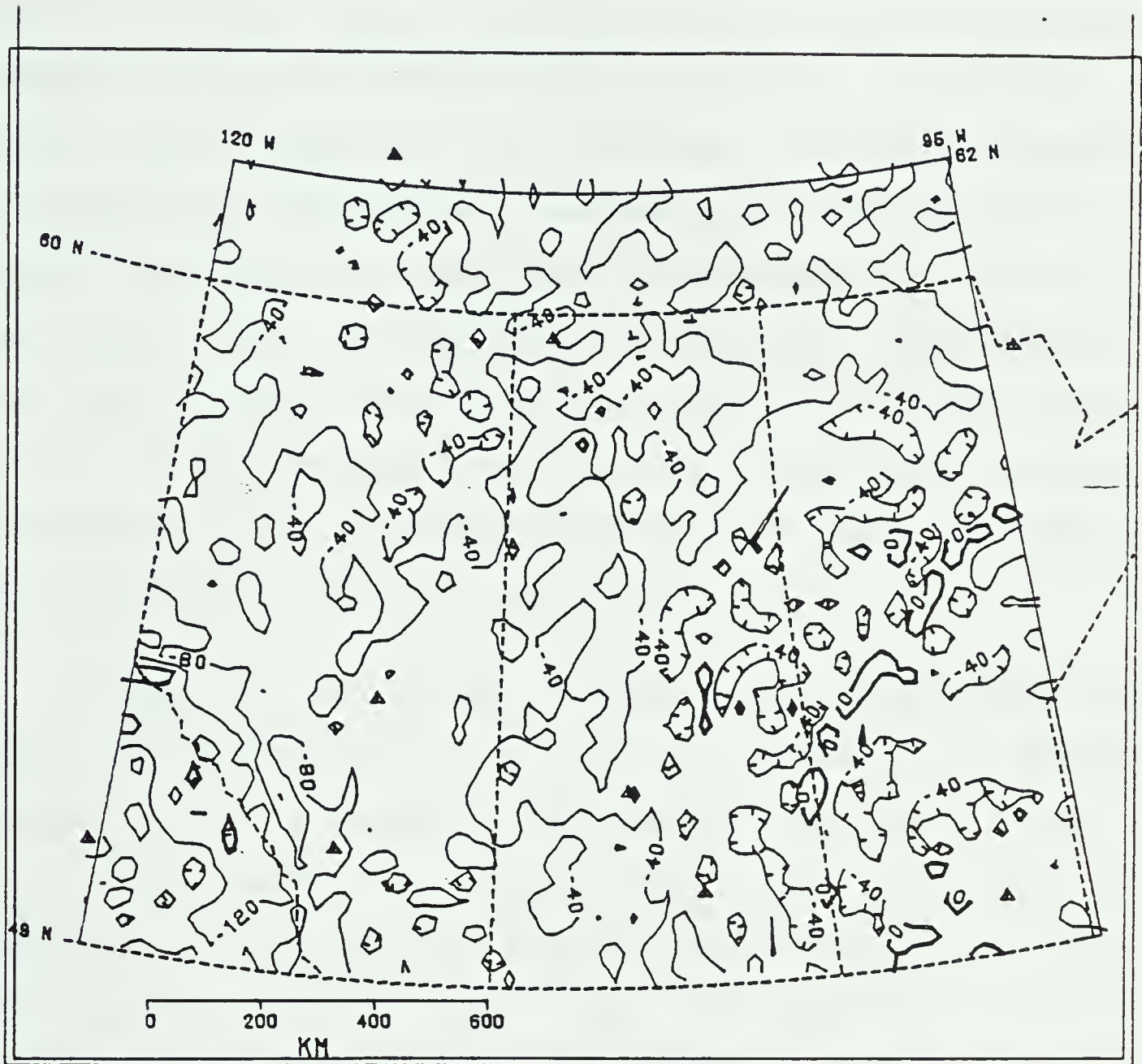


Figure B.1. The density variation in a crustal slab of constant thickness which would satisfy the gravity anomaly in western Canada. The contour interval is 40 kg/m^3 .

The other slab type of model to be considered is of lithospheric dimensions, 100 km thick with its top at a depth of 35 km. Now it is assumed that the entire gravity anomaly in western Canada is due to lateral variations in upper mantle density. As this model involves a downward continuation of over 30 km, considerable amplification of noise occurs as is evident from the average radial spectral amplitude of the resulting density variation. Accordingly a low pass filter with a high cut spatial frequency of 0.22 cycles per data interval was applied effectively removing wavelengths less than about 140 km. The resulting density distribution is shown in Figure B.2.

Either of the above distributions could produce at least the smooth part of the gravity anomaly in western Canada. On the basis of the crustal slab result, density variations greater than about 200 kg/m^3 would not be expected in the crust as a whole from one lateral location to another. In fact, away from the mountains, overall crustal variations over 40 kg/m^3 would be unlikely. Similarly, using the thick mantle slab result, overall density variations in the mantle portion of the lithosphere are probably less than about 120 kg/m^3 .

SIMPLE INVERSES IN TERMS OF MOHO STRUCTURE

The Parker-Oldenburg algorithm is well suited for determining the structure on the Moho surface which would

satisfy the gravity observations. The assumptions required are the depth to the reference level and the density contrast at the Moho. In this study, the depth to the reference level is chosen to have a very real geological meaning. It is the depth below sea level to the Moho when both the gravity anomaly and the surface elevation approach zero. In other words, the depth to the reference level is the thickness of the "standard" continental crust. By choosing this reference depth, the topography on the Moho measured relative to the reference surface will approach zero at the edges of the sampled grid where the gravity anomaly and surface elevations are both gradually tapered to zero. Thus, a criteria for the convergence of the Parker algorithm, that $h(x,y)$ vanishes outside a finite domain, is satisfied. The standard continental crust for purposes of this study is defined to be 33 km thick and to have an average density of 2900 kg/m³. This density value was estimated from regionally averaged seismic velocities by means of the Nafe-Drake velocity-density curve.

The five general types of crustal models considered are shown in Figure B.10. The mean overall crustal density was kept as close as possible to the standard value of 2.9 while the mantle density was set at 3400 kg/m³.

The average radial spectral amplitude for the equivalent stratum at 33 km was analysed (Figure B.4) and a high cut frequency of 0.22 cycles per data interval was

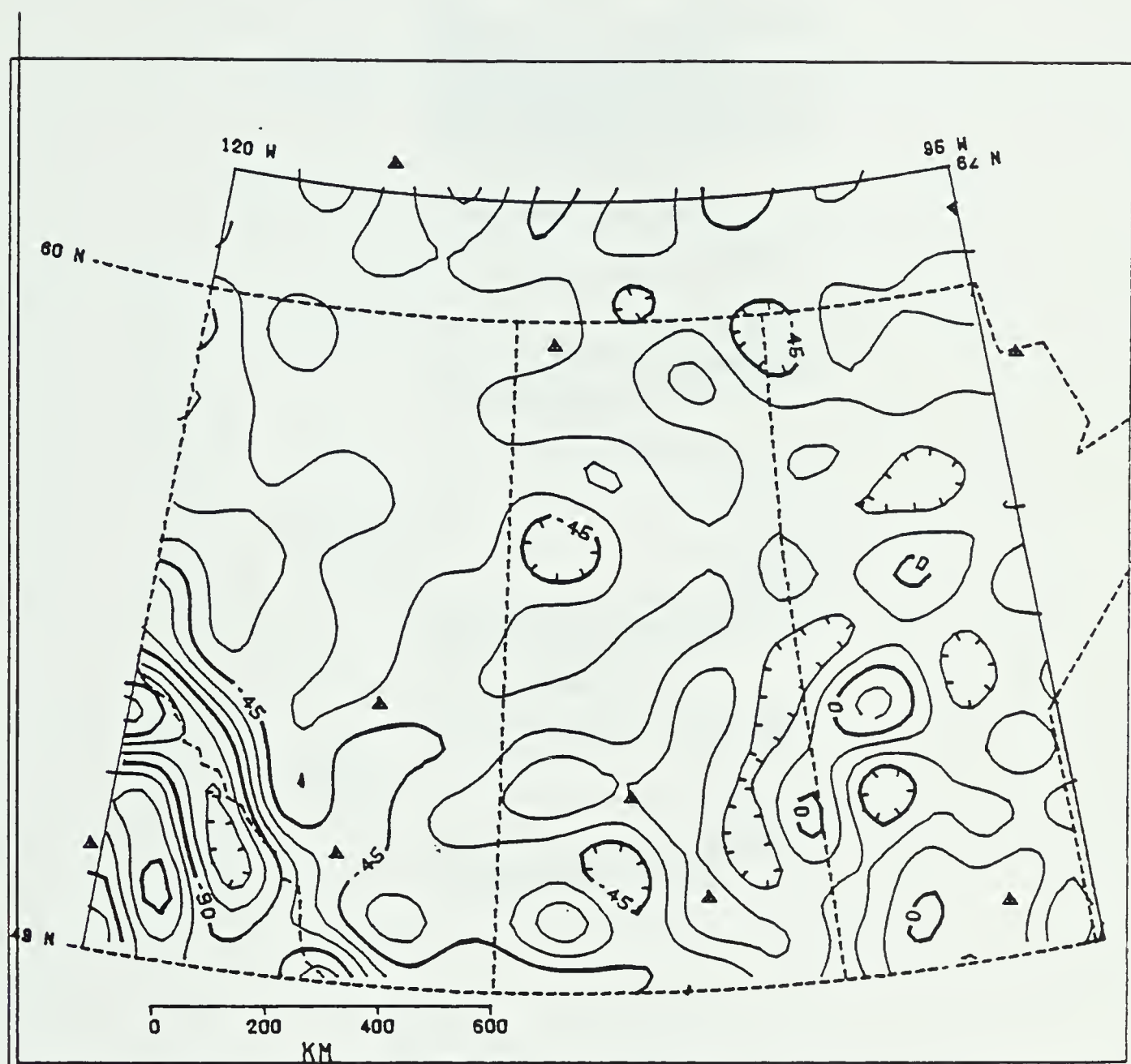


Figure B.2. The density variation in a mantle slab which would satisfy the gravity anomaly in western Canada. The contour interval is 15 kg/m^3 .

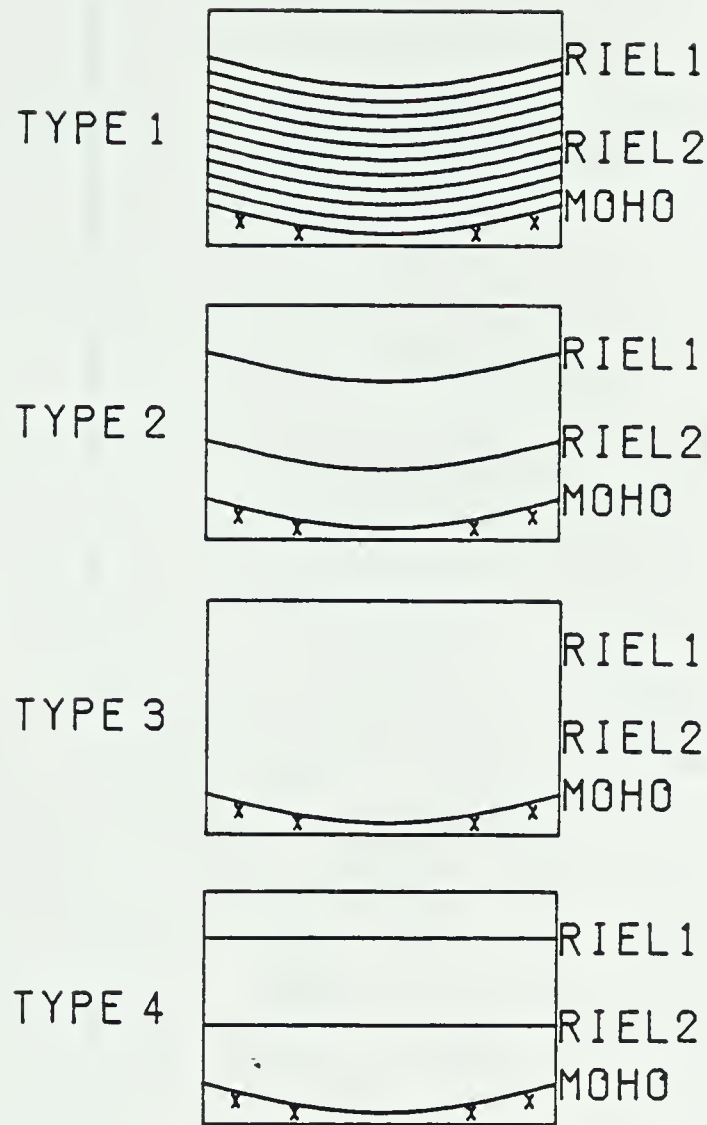


Figure B.3. The five simple types of crustal models considered. They are shown in order of decreasing mass deficiency for a given Moho topography. The five types are:

1. Crust composed of many lamini which increase in density with depth and which are parallel to the Moho.
2. Crust with intermediate boundaries, each of which is parallel to the Moho.
3. Homogeneous crust.
4. Crust with several intermediate horizontal layers.

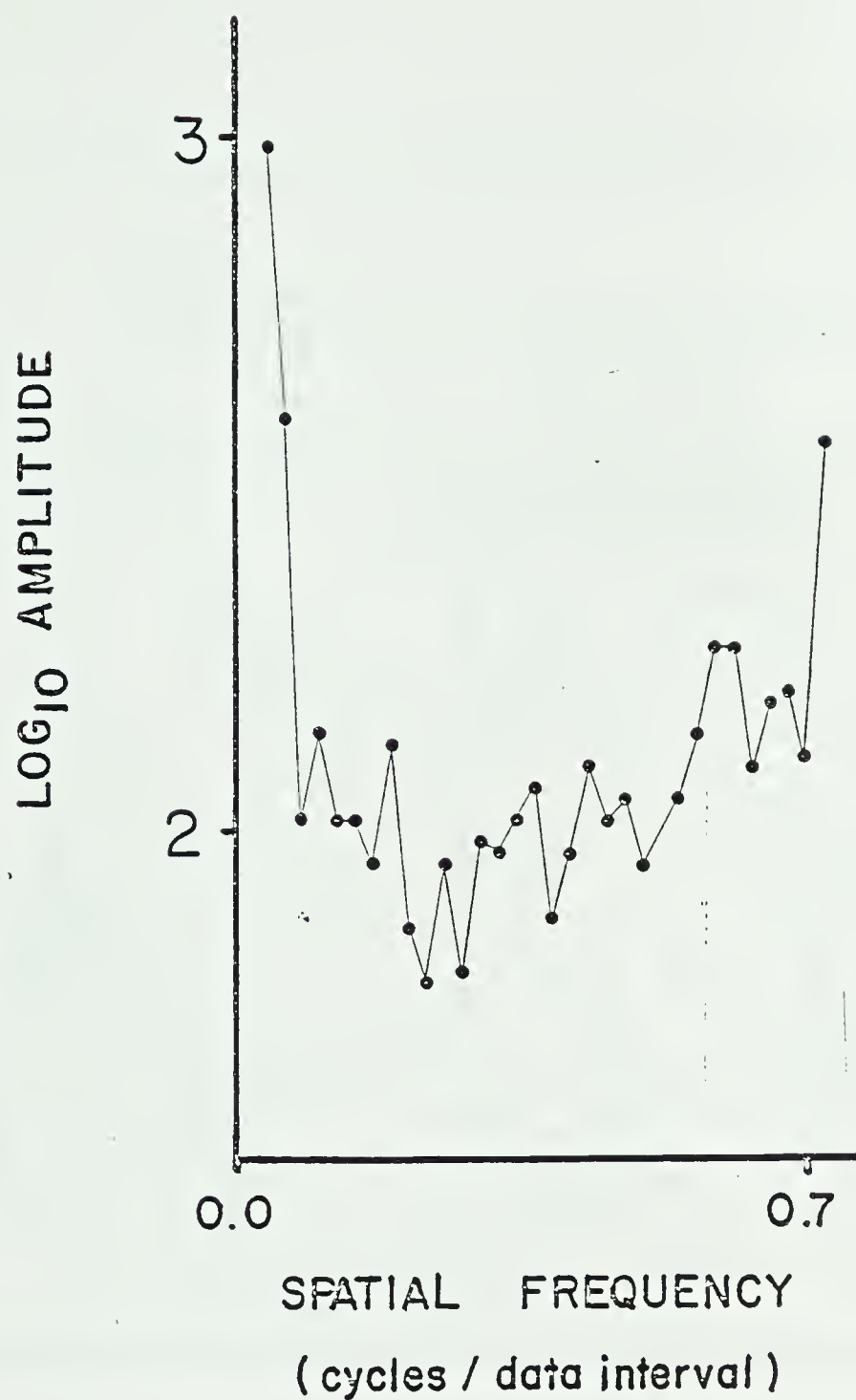


Figure B.4. Radial spectral amplitude for the gravity field in western Canada for a reference level at a depth of 33 km. The positive slope due to the continuation operator is apparent for frequencies greater than about 0.25 cycles per data interval.

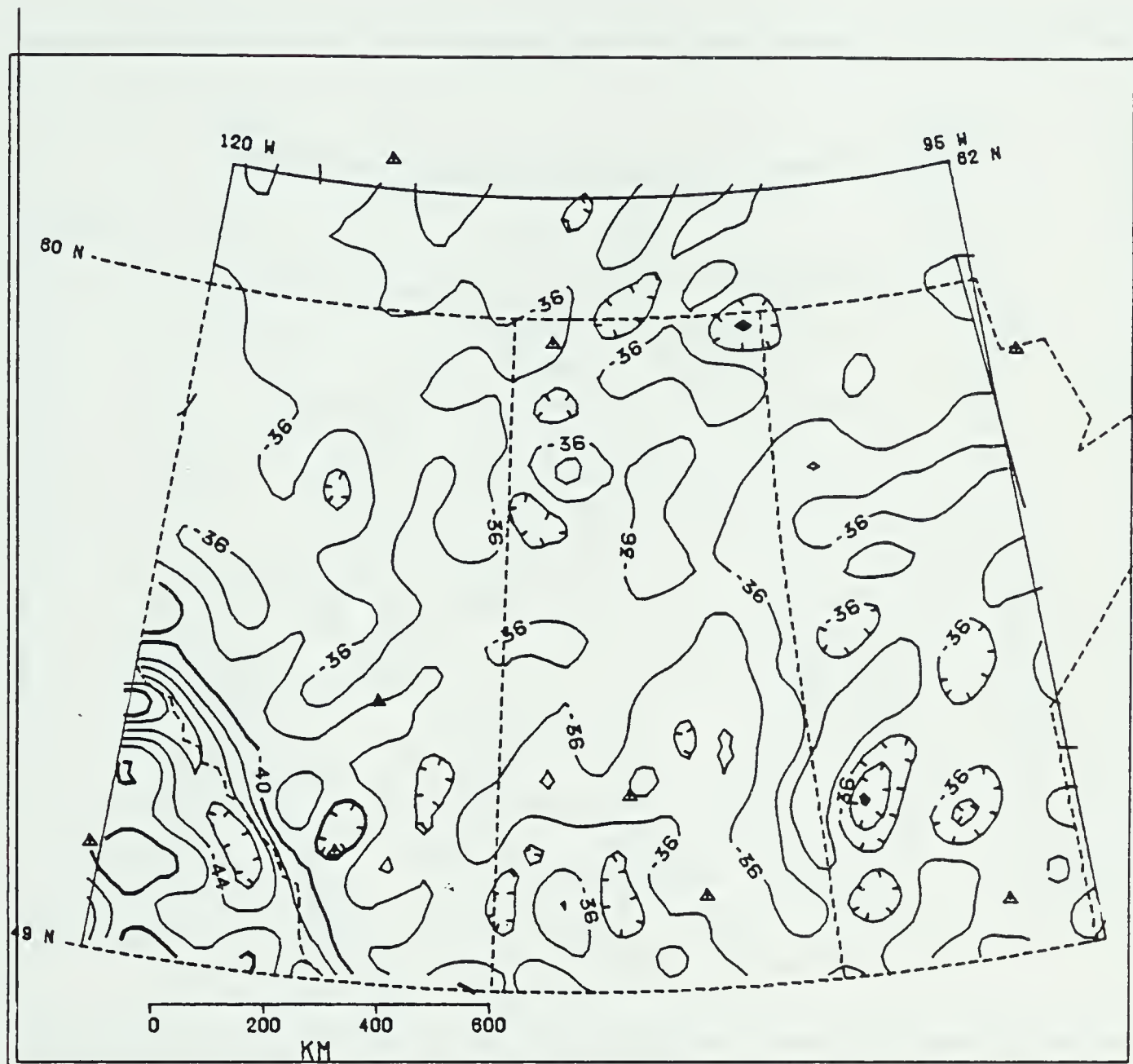


Figure B.5. Moho structure in western Canada for a Type 3 crustal model. The contour interval is 2 km.

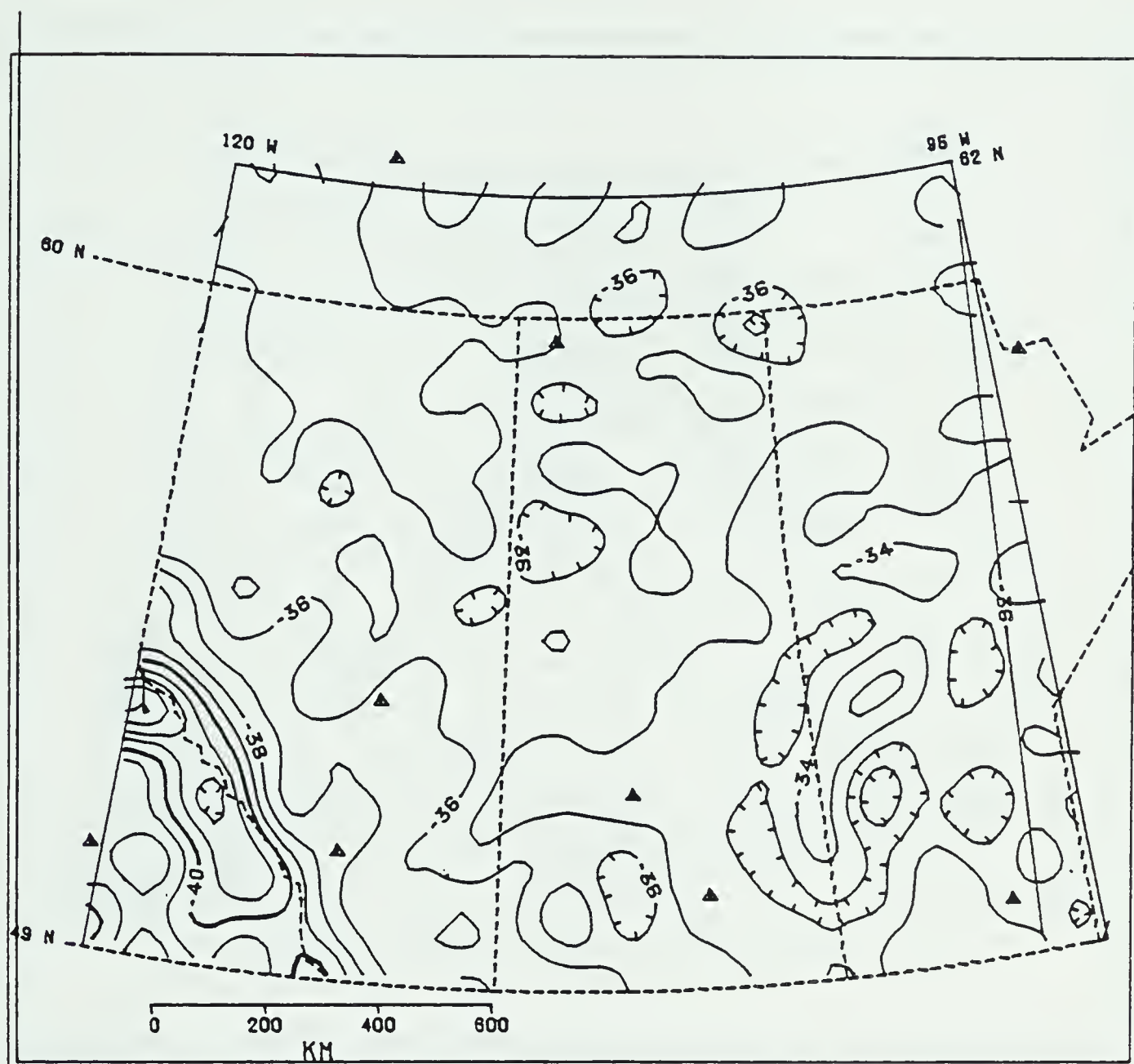


Figure B.6. Moho structure in western Canada for a Type 2 crustal model. The contour interval is 1 km.

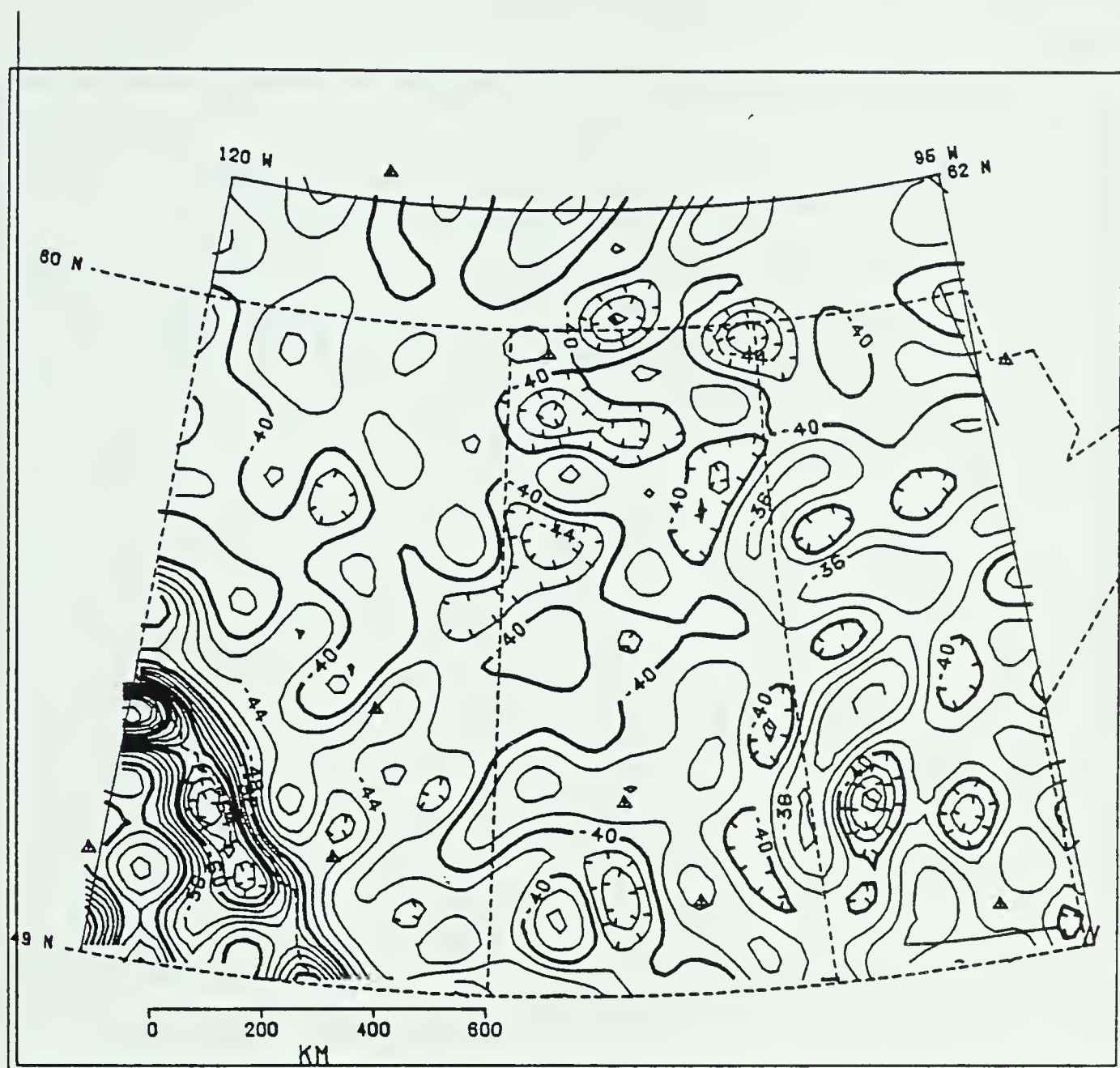


Figure B.7. The Moho structure in western Canada for a Type 4 crustal model. The contour interval is 2 km.

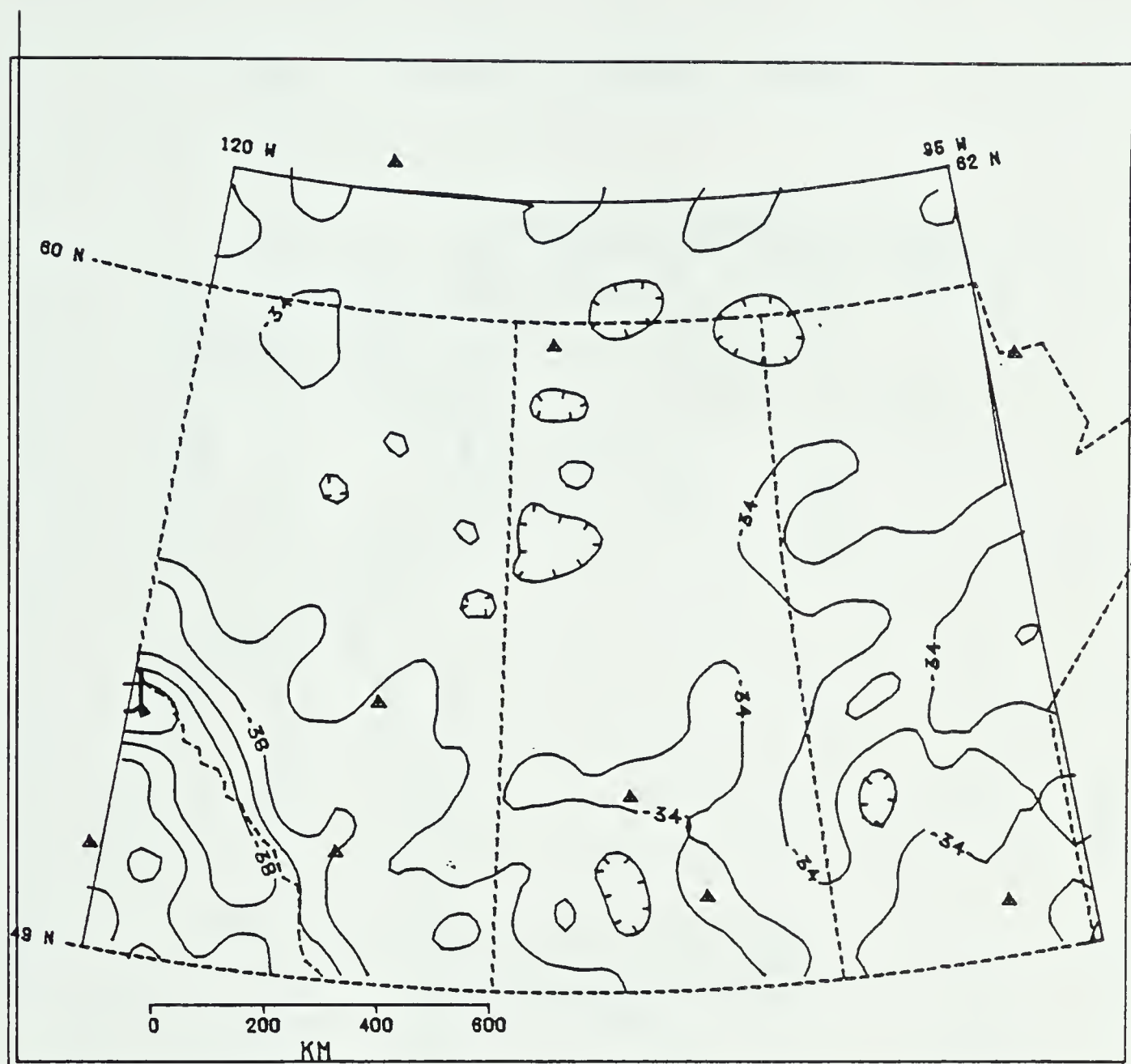


Figure B.8. Moho structure in western Canada for a Type 1 crustal model. The contour interval is 1 km.

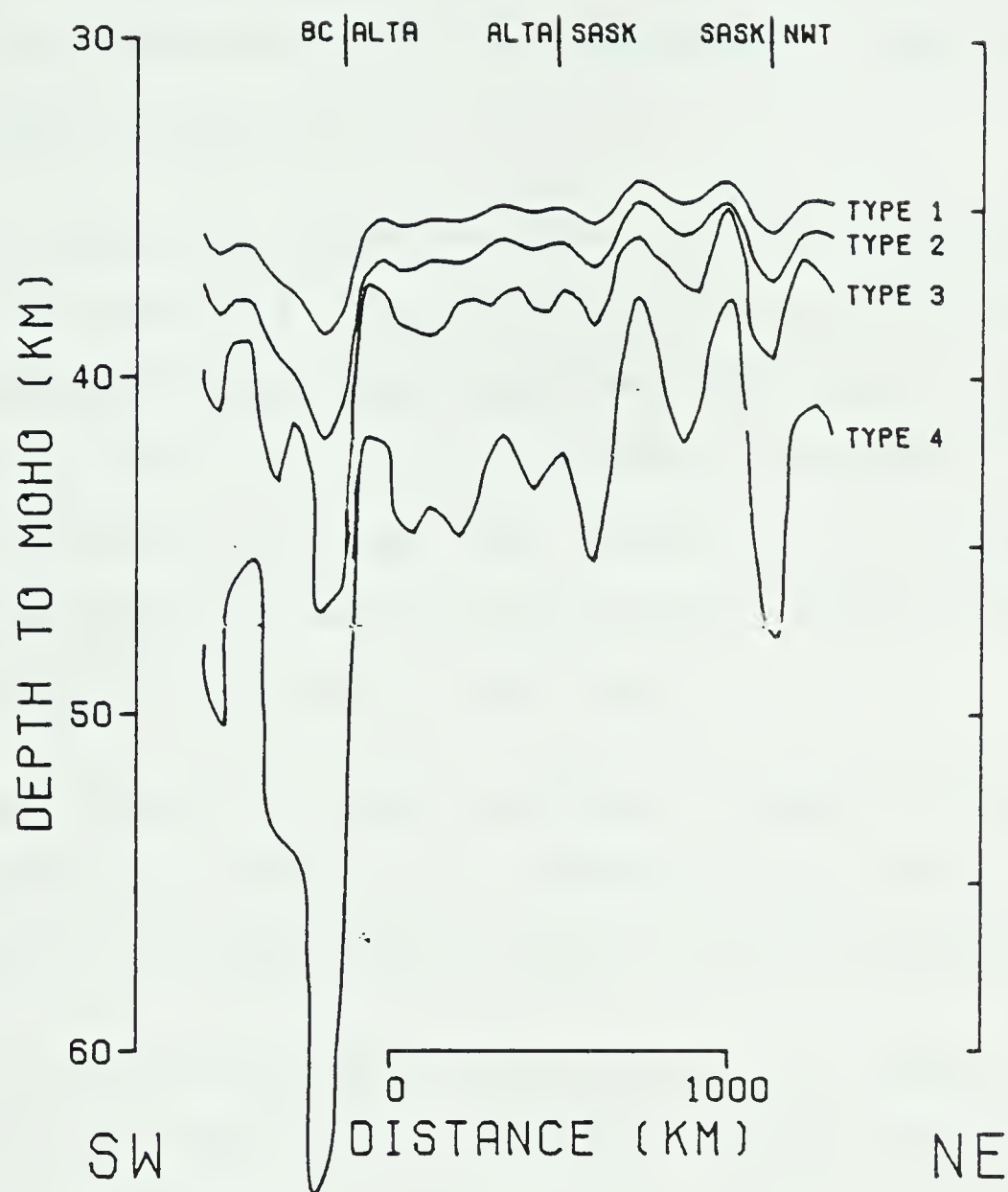


Figure B.9. SW-NE profiles of Moho structure in western Canada for the four types of crustal models.

chosen to eliminate the strong positive slope due to high spatial frequency noise. The high pass was set at 0.17 cycles per data interval. Hence wavelengths less than about 150 km were filtered out.

The simplest inverse for Moho structure considered was Type 1 in Figure B.4. The crust was taken to be homogeneous with constant density 2900 kg/m^3 and the upper mantle is assumed to be of constant density 3400 kg/m^3 . Thus the density contrast is about 500 kg/m^3 at the Moho. The reference depth was set at 33 km, which is the thickness of the standard crust used in this study.

The resulting Moho structure is shown in Figure B.5. The depth below sea level of the Moho varies from 33 km at the edges of the map-area to about 47 km in the mountains.

A more reliable model for the crust in western Canada is that of Type 2 in Figure B.3 which involves several intermediate layers. A "standard" crust of this nature based on seismic surveys on the plains is given in Table 2. The net average density of this model is 2900 kg/m^3 , the same as that of the previous model. If the assumption of Lee (1977) is used, that the relief on all the interfaces is the same, then it is possible to use the Parker algorithm for this model. For this simple example, the crustal layers are assumed to be of constant vertical thickness and of constant density throughout the map-area. The fraction of

the gravity which is due to the Moho itself is first calculated according to the theory presented in a previous section, and then the Parker-Oldenburg algorithm is applied to this fraction only.

The resulting Moho structure is shown in Figure B.6. The relief on the Moho is considerably less than for the case of no crustal layers. The maximum depth on the Moho is only 44 km beneath the mountains. The decrease in Moho structure is due to the fact that much of the gravity anomaly now has its source in parallel structure on the two Riel discontinuities.

Alternately, a crustal model of Type 4 in Figure B.3 could be used. Here, the intermediate crustal layer interfaces are essentially horizontal, hence, producing no effect on the resultant gravity field. In this case, the field is due entirely to the density contrast between the lowest layer and the mantle material, which from Table 2 is seen to be about 230 kg/m^3 . The calculated Moho structure for this model is shown in Figure B.7. For this model, the depth to the Moho exceeds 60 km in the mountains. Much more relief is apparent on the Moho for this discrete layer model than for the previous model in which the intermediate layers were parallel to the Moho. It is evident that the structure on the intermediate layers is of paramount importance to the interpretation of the gravity field.

Other possible crustal models are based on a continuous decrease in crustal density with vertical distance from the Moho surface. Here, the crust is considered to consist of a large number of thin laminae all parallel to the Moho surface. Once again, the overall mean density of this standard crust is 2900 kg/m^3 . The rate of increase with depth of density below the RielM discontinuity is set at 16 kg/m^3 per km. This value was obtained by combining the depth versus velocity curve of Goodacre (1972) with the velocity versus density curve of Nafe and Drake. At the Moho, the velocity contrast is only 150 kg/m^3 . However, each of the laminae above the Moho will also have a small density contrast as well.

The method of determining the fraction of gravity anomaly due to the Moho structure for this model has been discussed in a previous section. The Parker-Oldenburg algorithm is then used on this fraction of the gravity to find the Moho structure. The result is shown in Figure B.8. The relief on the Moho is very small, the thickest crust being only 39 km beneath the mountains. Apparently, the thin laminae above the Moho contribute much more to the gravity anomaly than the Moho does itself.

While the four types of crustal model previously considered differ in so far as the vertical distribution of crustal density is concerned, they produce very similarly shaped topographies on the Moho though the amplitudes are

quite different as is evident from the profiles of the derived Moho structures shown in Figure B.9. As more and more of the anomalous density contrast is shifted up into the crust, less relief is required on the Moho itself to explain the anomalies present.

APPENDIX C: DERIVATION OF THE PARKER ALGORITHM

The coordinate system used in this derivation is shown in Figure 2.1. The gravitational potential for a point in free space is given by

$$U(\vec{r}_0) = Gd \int_D dA \int_{z=0}^{z=h(\vec{r})} dz / |\vec{r}_0 - \vec{r}|; \quad [54]$$

where U is the potential function; G is the universal gravitational constant; d is the density of the anomalous mass; and D is the finite domain in which all the anomalous mass must exist.

After performing a two dimensional Fourier transform of the above equation and interchanging the order of integration, one obtains

$$F[U] = Gd \int_D dA \int_0^{z=h(\vec{r})} dz \int_x [dA_0 \exp(i\vec{K} \cdot \vec{r}_0)] / |\vec{r}_0 - \vec{r}|. \quad [55]$$

The last integral in the above equation can be expressed as

$$2\pi \exp(i\vec{K} \cdot \vec{r}) \int_0^\infty u du J_0(|\vec{K}| u) / (u^2 + B^2)^{1/2} \quad [56]$$

where $J_0(|\vec{K}| u) = 1/2\pi \int_0^{2\pi} [\exp(i|\vec{K}| u \cos \theta)] d\theta$

$$B = z_0 - z \quad u = |\vec{r}_0 - \vec{r}| \quad [57]$$

The above integral can be shown analytically to be

$$[2\pi / |\vec{K}|] [\exp(i\vec{K} \cdot \vec{r} - |\vec{K}|(z_0 - z))] \quad [58]$$

After substitution back into the potential equation, one obtains

$$F[U] = 2\pi G d \int_D dA \int_0^{h(\vec{r})} dz [\exp(i\vec{K} \cdot \vec{r} - |\vec{K}|(z_0 - z))] / |\vec{K}| \quad [59]$$

Upon integration with respect to z , this becomes

$$F[U] = 2\pi G d \int_D dA [\exp(i\vec{K} \cdot \vec{r} - |\vec{K}|z_0)] [\exp(i\vec{K} h(\vec{r}) - |\vec{K}|h(\vec{r})) - 1] / |\vec{K}|^2 \quad [60]$$

Now the following Taylor Series expansion can be used.

$$\frac{\exp(i\vec{K} h(\vec{r}) - |\vec{K}|h(\vec{r})) - 1}{|\vec{K}|^2} = \sum_{n=1}^{\infty} [|\vec{K}|^{n-2} h^n(\vec{r})] / n! \quad [61]$$

The potential function becomes with some rearrangement

$$F[U] = 2\pi G d [\exp(-|\vec{K}|z_0)] \sum_{n=1}^{\infty} |\vec{K}|^{n-2} / n! \int_D dA h^n(\vec{r}) \exp(i\vec{K} \cdot \vec{r}) \quad [62]$$

The integral in the above equation is simply a Fourier transform, therefore

$$F[U] = 2\pi G d \exp(-|\vec{K}|z_0) \sum_{n=1}^{\infty} |\vec{K}|^{n-2} / n! F[h^n(\vec{r})] \quad [63]$$

By definition, the gravity anomaly is the vertical attraction of the anomalous mass.

$$\Delta g = + \partial U / \partial z.$$

[64]

$$F[\Delta g] = -|\vec{K}| F[U]$$

Therefore, the Parker algorithm is obtained as follows

$$F[\Delta g] = -2\pi G d_0 \left[\exp(-|\vec{K}| z_0) \right] \sum_{n=1}^{\infty} |\vec{K}|^{n-1} F[h^n(\vec{z})] / n! \quad [65]$$

APPENDIX D: COMPUTER PROGRAMS

INTRODUCTION

The purpose of this appendix is describe and list some of the computer programs used to produce the results given in this thesis. Much of the information given here is machine dependent, that is, it may be of interest only to those persons who have access to the University of Alberta Computing System. This comment applies most particularly to the programs written for the FPS AP-190L ARRAY PROCESSOR.

USE OF THE ARRAY PROCESSOR FOR SCIENTIFIC PROGRAMS

The FPS AP-190L is a high speed peripheral floating point arithmetic computing device which, at the University of Alberta, works in parallel with an Amdahl 470V8 host computer. Its internal organization is very appropriate for performing the large number of reiterative multiplication and addition operations inherent in potential field calculations of the type performed for this thesis. In fact, the fast Fourier transform calculations used throughout this thesis form an almost ideal application for the array processor since most of the computation time is overlapped with data memory access time, a result of the highly parallel architecture of the device.

There are various ways of programming the AP-190L. It is important to realize in this regard that a programmer writing code for scientific research purposes has different needs than someone writing code for production purposes. A research programmer needs the ability to easily revise and develop his code which is by definition experimental in nature. A production programmer, on the other hand, generally has to code an algorithm only once since it is meant to be used over and over again without revision. Hence compile time is generally insignificant to a production programmer, but to a research programmer, compile time is very important. The following is the author's experience with using the array processor for developing and

implementing new scientific subroutines. Many programmers, particularly production programmers, will not necessarily agree with the following observations.

Methods of programming which were not found to be particularly satisfactory are outlined below.

1. The AP-FORTRAN language was found to be awkward to use and incredibly expensive to compile. Furthermore, since the AP-190L is really designed to be programmed by the APAL language, programs written in AP-FORTRAN without due consideration given to the nature of the computer device tend to be very inefficient.
2. Programming the AP-190L through the use of calls to the ADCLIB library was also found to be quite inefficient since this method requires a great deal of redundant data movement between the host and the array processor.
3. Programming directly in APAL was found to be far too machine dependent. The algorithms scientific programmers deal with are already sufficiently complex without adding the complications due to machine cycles and pipeline code.

The method of coding the array processor which was found to best suit the needs of a scientific programmer is through the use of multitudinous calls to the HSRLIB. This library of subroutines is easy to use and it produces extremely efficient code. A range of subroutines is available in this library to perform computations as simple

as adding two scalars to as complex as solving linear equations.

If one wants the satisfaction of knowing that an entire computational process is being processed in the array processor, then the host loop overhead can be eliminated or minimized by linking the many subroutine calls together by invoking the Vector Function Chainer (VFC). This last step is really not necessary in the development stage of scientific programs since the savings are so minimal due to the fact that the Amdahl host is itself a very fast and efficient machine. The great savings involved in using the array processor lie in getting all the numerical data and all the number crunching of that data into the array processor. The source itself can reside in the host without much affect on the above savings.

The compile time using this method is comparable to a host FORTRAN program and several orders of magnitude faster than AP-FORTRAN. Programming is in the form of very straightforward FORTRAN, and the math library calls result in very tidy subroutines which are written in terms of complete arrays and which are easy to debug. All the code is directly translated via HSRLIB into routines written in the optimum language, APAL.

Many of the above advantages are offset if one has an existing FORTRAN program which one wants to convert for use

on the array processor since the transformation of most of the operations into call statements can be a tedious and error prone task. Nonetheless, if one is planning to further develop a program at a later date, then recoding into HSRLIB form is not a bad idea. The programmer will then have an easy to compile and debug program to work with and will generally have a feeling of control over the computing procedure.

THE FORWARD ALGORITHM

The following FORTRAN subroutine calculates the gravity anomaly, $g(x,y)$ at $z=Z_0$ due to a subsurface layer of variable density, $d(x,y)$, bounded by $z=0$ and $z=h(x,y)$. This subroutine calls PARKAP and LPAP which are VFC language subroutines coded for the AP-190L ARRAY PROCESSOR. The other subroutines referenced are in HSRLIB at the UNIVERSITY OF ALBERTA COMPUTING CENTRE, and are described in various FPS manuals.


```

      SUBROUTINE PARKER(MS,MSS,ZZERO,DENSTY,SPKN,SPKE,H,
1A,MSSS,IW,G,SUM,HH,NITS)
C
C THIS ROUTINE CALCULATES EQUATION (2) OF SPRENKE'S (1982) THESIS.
C EQUATION(2) IS THE FORWARD PARKER ALGORITHM FOR A SINGLE LAYER.
C
C THE INFORMATION WHICH MUST BE PASSED IN THE SUBROUTINE ARGUMENT
C IS AS FOLLOWS BELOW...ALL ARRAYS MUST BE PROPERLY DIMENSIONED IN THE
C MAIN PROGRAM ACCORDING TO THE SIZE PARAMETER, MS.
C
C
C MS SIZE OF ONE SIDE OF SQUARE MAP (2**INTEGRAL POWER)
C MS IS LIMITED TO 64 OR 128 DUE TO CORE LIMITATIONS
C IN THE AP (ARRAY PROCESSOR).
C
C
C MSS # OF POINTS IN FFT'S =MS*MS
C ZZERO DEPTH TO INVERSION SURFACE
C ZZERO MUST BE A POSITIVE NUMBER IN UNITS OF KM'S.
C
C DENSTY(MS,MS) DIGITIZED DENSITY VALUES FOR MAP
C DENSITY VALUES MUST BE IN GM/CC
C
C SPKN, SPKE ----SAMPLES PER KM NORTH AND EAST
C THIS MEANS ONE OVER THE SAMPLE INTERVAL.
C IE ... IF SAMPLE INTERVAL IS 5 KM, SPK IS 0.2/KM.
C
C H(MS,MS) SUBSURFACE TOPOGRAPHY RELATIVE TO INVERSION SURFACE
C SUBSURFACE TOPOGRAPHY VALUES MUST BE IN KM.
C
C
C A(MSSS) IS NOT USED AT PRESENT. SET MSSS=1 IN MAIN PROGRAM.
C
C MSSS IS NOT USED AT PRESENT...SET EQUAL TO 1 IN MAIN PROGRAM.
C
C IW...SWITCH FOR VARIABLE DENSITY.
C IF IW=1, DENSITY IS NOT CONSTANT WITH X AND Y.
C IF IW=0, DENSITY IS CONSTANT.
C
C
C G(MS,MS)...ARRAY OF RESULTING GRAVITY ANOMALY VALUES.
C
C NITS...NUMBER OF TERMS DESIRED IN SUMMATION OF FORWARD ALGORITHM.
C NITS=10 IS MORE THAN ADEQUATE FOR MOST PROBLEMS.
C IW EQUALS 1 IF DENSITY IS VARIABLE WITH X,Y
C
C
C SPECIFICATIONS
C
C WARNING: WV IS A WORKSPACE WHICH MUST BE OF DIMENSION MS BY MS.
C THE DIMENSION OF WV MUST BE ALTERED IF MS NOT EQUAL TO 64.
C
C HHR AND SUMR ARE ARTIFACTS WHICH ARE NOT USED AT PRESENT.
C
      COMPLEX HH
      COMPLEX*8 G,SUM
      DIMENSION A(MSSS)
      DIMENSION DENSTY(MS,MS),H(MS,MS)
1  ,G(MS,MS),SUM(MS,MS)
      DIMENSION HH(MS,MS)

```



```

        DIMENSION WV(64,64),HHR(64,64),SUMR(64,64)
        REAL NF(30),NV(30)
        INTEGER SPO0,SPO1,SPO3,SPO4,SPO5
        INTEGER SPO8,SPO9

```

```

C
C THE FOLLOWING STATEMENTS DEFINE THE STORAGE LOCATIONS OF REAL VARIABLES
C IN THE AP.

```

```

C
C EG   ARRAY H IS STORED IN THE AP AT LOCATION IH, WV IS AT IWV ETC.
C

```

```

C NOTE THAT THE SP NUMBERS ARE SIMPLE INTEGERS.
C

```

```

        MSS=MS*MS
        SPO9=6*MSS
        SPO8=SPO9+62
        IZZ=SPO8
        IPIG=SPO8+1
        IHMAX=SPO8+2
        IHMIN=SPO8+3
        IHM=SPO8+4
        IHALF=SPO8+5
        IDELG=SPO8+6
        IG=SPO8+7
        SPO9=IG
        SPO8=SPO9+MSS
        ISCALE=SPO8
        IGOV=SPO8+1
        IG1=SPO8+2
        IG2=SPO8+3
        IG3=SPO8+4
        IG4=SPO8+5
        IHMAXS=SPO8+6
        ISIGN=SPO8+7
        MSS=MS*MS
        ISUM=0
        SPO3=MS*MS
        MSS=SPO3
        SPO2=2
        IONE=SPO3
        IZERO=SPO3+1
        IHH=SPO3+SPO2
        SPO4=2*SPO3
        NEND=NITS
        IH=SPO2+SPO4
        SPO4=3*SPO3
        IDEN=SPO2+SPO4
        SPO4=4*SPO3
        IWN=SPO2+SPO4
        SPO4=5*SPO3
        INF=SPO2+SPO4
        IST=INF+30
        INV=IST+SPO3

```

```

C
C
C THE FOLLOWING CONSTANTS ARE REQUIRED IN THE AP FOR THE COMPUTATION, SO THEY
C ARE CALCULATED HERE FOR LATER TRANSFER TO THE AP.
C

```

```

        ONE=1.

```



```

ZERO=0.
PIG=2.*3.14159*6.67
HALF=.5
SCALE=1./(2.*MS*MS)
NF(1)=1
NV(1)=0.
C
C NF IS AN ARRAY OF FACTORIALS, NV IS SIMPLY AN ARRAY OF INTEGERS.
C
C
      DO 3 I=1,29
      NF(I+1)=NF(I)*I
3     NV(I+1)=I
      DO 4 I=1,30
4     NF(I)=1./NF(I)
C IT IS AWKWARD TO CALCULATE WAVENUMBERS IN THE AP, SO THEY ARE DONE IN THE
C HOST BY SUBROUTINE WNNU FOR SUBSEQUENT TRANSFER INTO THE AP.
C
      CALL WNNU(MS,SPKE,SPKN,WV)
C THE FOLLOWING STATEMENTS ARE ARTIFACTS NOT USED AT PRESENT.
102    FORMAT(1X,32F5.2)
987    CONTINUE
C
C
C INITILIZE THE AP
C ISTAT IS AN ERROR RETURN CODE...
C
      CALL APINIT(1,0,ISTAT)
C
C
C TRANSFER DATA TO AP
C E.G. REAL ARRAY H IS STORED IN THE AP BEGINNING AT LOCATION IH.
C THERE ARE MSS VALUES IN ARRAY H, AND THE VARIABLE TYPE IS 2 (REAL*4).
C
      CALL APPUT(ONE,IONE,1,2)
      CALL APPUT(ZERO,IZERO,1,2)
      CALL APPUT(H,IH,MSS,2)
      CALL APPUT(OENSTY,IDEN,MSS,2)
      CALL APPUT(WV,IWN,MSS,2)
      CALL APPUT(NF,INF,30,2)
      CALL APPUT(ST,IST,MSS,2)
      CALL APPUT(NV,INV,30,2)
      CALL APPUT(ZZERO,IZZ,1,2)
      CALL APPUT(PIG,IPIG,1,2)
      CALL APPUT(HALF,IHALF,1,2)
      CALL APPUT(SCALE,ISCALE,1,2)
C
C WAIT FOR DATA TRANSFER.
C
      CALL APWD
C
C CALL THE SUBROUTINE WHICH DOES THE WORK IN THE AP.
C
      CALL PARKAP(NEND,MS,IW)
C
C WAIT FOR RESULTS FROM THE AP.
C
      CALL APWR
C
C TRANSFER THE RESULTING GRAVITY ANOMALY FROM THE AP BACK TO THE HOST.

```



```

C STORE THE RESULTS IN ARRAY G.
  CALL APGET(G,IG,MSS,2)
  CALL APWD
C
C RELEASE THE AP.
C
  CALL APRLSE
  RETURN
END
  SUBROUTINE WNNU(MS,SPKE,SPKN,WN)
C
C THIS ROUTINE CALCULATES WAVENUMBERS.
C NOTE FOURIER SYMMETRY.
C
C
  DIMENSION WN(MS,MS)
  MSH=MS/2+1
  DO 1 K=1,MS,2
    DO 2 L=1,MS
      KKX=(K+1)/2
      KKY=L
      CALL WVN(KKX,KKY,W,MS,SPKE,SPKN)
      WN(K,L)=W
      WN(K+1,L)=W
2    CONTINUE
      KKX=1
      KKY=(K+1)/2
      CALL WVN(KKX,KKY,W,MS,SPKE,SPKN)
      WN(1,K)=W
      WN(1,K+1)=W
      KKX=MS/2+1
      KKY=(K+1)/2
      CALL WVN(KKX,KKY,W,MS,SPKE,SPKN)
      WN(2,K)=W
      WN(2,K+1)=W
1    CONTINUE
      KKX=1
      KKY=MSH
      CALL WVN(KKX,KKY,W,MS,SPKE,SPKN)
      WN(1,2)=W
      KKX=MSH
      KKY=1
      CALL WVN(KKX,KKY,W,MS,SPKE,SPKN)
      WN(2,1)=W
      KKX=MSH
      KKY=MSH
      CALL WVN(KKX,KKY,W,MS,SPKE,SPKN)
      WN(2,2)=W
      WN(1,1)=.00001
      RETURN
    END
  SUBROUTINE WVN(KKX,KKY,W,MS,SPKE,SPKN)
C
C THIS ROUTINE IS REQUIRED FOR WAVENUMBER CALCULATIONS
C IT IS CALLED BY SUBROUTINE WNNU REPEATABLY.
C
  PI=3.14159
  MSH=MS/2+1
  IF(KKY.GT.MSH) KKY=KKY-MS
  WX=SPKN*PI*(KKX-1)/(MSH-1)

```



```
      WY=SPKE*PI*(KKY-1)/(MSH-1)
      W=SQRT(WX*WX+WY*WY)
      RETURN
      END
      SUBROUTINE GET(IN,NP)
C
C THIS ROUTINE IS USEFUL FOR ERROR CHECKING.
C IT CAN BE USED TO RETRIEVE THE NP REAL NUMBERS STORED IN THE AP
C BEGINNING AT LOCATION, IN.
      DIMENSION Z(128)
      CALL APWR
      CALL APGET(Z,IN,NP,2)
      CALL APWD
      WRITE(11,201) IN,NP
201      FORMAT(1X,2I10)
      WRITE(11,203)(Z(I),I=1,NP)
203      FORMAT(1X,8F11.3)
      RETURN
      END
```



```

DEFINE PARKAP(NEND,MS,IW)
  LDCAL IZZ,IPIG,IHMAX,IHMIN,IHM,IHALF,IDELG,IG,ISCALE,IGOV
  LDCAL IG1,IG2,IG3,IG4,IHMAXS,ISIGN,IGL
  LOCAL NSTART,IST,IWN,ISUM
LOCAL MSS,IH,IDEN
  LOCAL K,N,IDNE,IZERD,IHH,INF,INV
  LDCAL NV,NF
  MSS=MS*MS
  SPO9=6*MSS
  SPO8=SPO9+62
  IZZ=SPO8
  IPIG=SPO8+1
  IHMAX=SPO8+2
  IHMIN=SPO8+3
  IHM=SPO8+4
  IHALF=SPO8+5
  IDELG=SPO8+6
  IG=SPO8+7
  SPO9=IG
  SPO8=SPO9+MSS
  ISCALE=SPO8
  IGDV=SPO8+1
  IG1=SPO8+2
  IG2=SPO8+3
  IG3=SPO8+4
  IG4=SPO8+5
  IHMAXS=SPO8+6
  ISIGN=SPO8+7
  ISUM=0
  SPO3=MS*MS
  MSS=SPO3
  SPO2=2
  IDNE=SPO3
  IZERD=SPO3+1
  IHH=SPO3+SPO2
  SPO4=2*SPO3
  IH=SPO2+SPO4
  SPO4=3*SPO3
  IDEN=SPO2+SPO4
  SPO4=4*SPO3
  IWN=SPO2+SPO4
  SPO4=5*SPO3
  INF=SPO2+SPO4
  IST=INF+30
  INV=IST+SPO3
  IDEN=IH+MSS
  CALL MAXV(IH,1,IHMAX,MSS)
  CALL MINV(IH,1,IHMIN,MSS)
  CALL VSUB(IHMIN,1,IHMAX,1,IHM,1,1)
  CALL VSMUL(IHM,1,IHALF,IHM,1,1)
  CALL VADD(IHM,1,IHMIN,1,IHM,1,1)
  CALL VSUB(IHM,1,IZZ,1,IZZ,1,1)
  CALL VMUL(IPIG,1,IDEN,1,IDELG,1,1)
  CALL VMUL(IDELG,1,IHM,1,IDELG,1,1)
  CALL VNEG(IHM,1,IHM,1,1)
  CALL VSADD(IH,1,IHM,IH,1,MSS)
  CALL VNEG(IHM,1,IHM,1,1)
  NSTART=1
  CALL VCLR(ISUM,1,MSS)

```



```

N=NSTART
AAAA:  CALL VFILL(IONE,IHH,1,MSS)
      K=1
BBBB:  CALL VMUL(IHH,1,IH,1,IHH,1,MSS)
      K=K+1
      IF K <= N GOTO BBBB
      CALL VMUL(IHH,1,IOEN,1,IHH,1,MSS)
      CALL RFFT2D(IHH,MS,MS,1)
      CALL VLOG(IWN,1,IST,1,MSS)
      SPO5=INV+N
      NV=SPO5-1
      CALL VSMUL(IST,1,NV,IST,1,MSS)
      CALL VALOG(IST,1,IST,1,MSS)
      CALL VMUL(IHH,1,IST,1,IHH,1,MSS)
      NF=INF+N
      CALL VSMUL(IHH,1,NF,IHH,1,MSS)
      CALL VADD(ISUM,1,IHH,1,ISUM,1,MSS)
N=N+1
      IF N <= NENO GOTO AAAA
      CALL VSMUL(IWN,1,IZZ,IST,1,MSS)
      CALL VNEG(IST,1,IST,1,MSS)
      CALL VEXP(IST,1,IST,1,MSS)
      CALL VSMUL(IST,1,IPIG,IST,1,MSS)
      CALL VMUL(ISUM,1,IST,1,IG,1,MSS)
      CALL RFFT2D(IG,MS,MS,-1)
      CALL VSMUL(IG,1,ISCALE,IG,1,MSS)
      IF IW = 0 GOTO CCCC
      CALL VNEG(IHM,1,IHMAXS,1,1)
      CALL VLIM(IHMAXS,1,IZERO,IONE,ISIGN,1,1)
      CALL RFFT2D(IDEN,MS,MS,1)
      CALL VCLR(ISUM,1,MSS)
      CALL VCLR(IHH,1,MSS)
      CALL VSMUL(IWN,1,IHMAXS,IHH,1,MSS)
      CALL VEXP(IHH,1,IHH,1,MSS)
      CALL VNEG(IONE,1,IONE,1,1)
      CALL VSAOD(IHH,1,IONE,IHH,1,MSS)
      CALL VNEG(IONE,1,IONE,1,1)
      CALL VDIV(IWN,1,IHH,1,IHH,1,MSS)
      CALL VSMUL(IWN,1,IZZ,ISUM,1,MSS)
      CALL VNEG(ISUM,1,ISUM,1,MSS)
      CALL VEXP(ISUM,1,ISUM,1,MSS)
      CALL VMUL(ISUM,1,IHH,1,ISUM,1,MSS)
      CALL VSMUL(ISUM,1,IPIG,ISUM,1,MSS)
      CALL VSMUL(ISUM,1,ISIGN,ISUM,1,MSS)
      CALL VMUL(IOEN,1,ISUM,1,ISUM,1,MSS)
      CALL VCLR(ISUM,1,ISUM,1,1)
      CALL RFFT2D(IDEN,MS,MS,-1)
      CALL VSMUL(IOEN,1,ISCALE,IOEN,1,MSS)
      CALL RFFT2D(ISUM,MS,MS,-1)
      CALL VSMUL(ISUM,1,ISCALE,ISUM,1,MSS)
      CALL VMOV(ISUM,1,IGOV,1,1)
      CALL VNEG(IGOV,1,IGOV,1,1)
      CALL VSAOD(ISUM,1,IGOV,ISUM,1,MSS)
      CALL VSUB(ISUM,1,IG,1,IG,1,MSS)
CCCC:  CALL VSAOD(IG,1,IOELG,IG,1,MSS)
      CALL VSADO(IH,1,IHM,IH,1,MSS)
      CALL VADD(IZZ,1,IHM,1,IZZ,1,1)
      IG1=IG
      SPO8=MS-1
      IG2=IG+SPO8

```



```
SPO8=MSS-MS
IG3=IG+SPO8
SPO8=MSS-1
IG4=IG+SPO8
  CALL VAOD(IG1,1,IG2,1,IGOV,1,1)
  CALL VADD(IGOV,1,IG3,1,IGOV,1,1)
  CALL VADD(IGOV,1,IG4,1,IGOV,1,1)
  CALL VMUL(IGOV,1,IHALF,1,IGOV,1,1)
  CALL VMUL(IGOV,1,IHALF,1,IGOV,1,1)
  CALL VNEG(IGOV,1,IGOV,1,1)
  CALL VSAOD(IG,1,IGOV,IG,1,MSS)
  CALL VNEG(IGOV,1,IGOV,1,1)
  ENO
```



```

      DEFINE LPAP(MS)
      SUBROUTINE LPAP(MS)
      LOCAL MSS,IFLOW,IFHIGH,ITWO,IPI,IWN,IPC,ISUM,IONE,IHALF,IHOLD,ITERM
      MSS=MS*MS
      SPO2=2*MSS
      SPO3=3*MSS
      SPO4=4*MSS
      SPO5=5*MSS
      SPO6=6*MSS
      SPO7=7*MSS
      SPO8=8*MSS
      SPO9=9*MSS
      SP10=10*MSS
      SP11=11*MSS
      IFLOW=SP10+107
      IFHIGH=SP10+108
      ITWO=SPO7+83
      IPI=SPO7+82
      IWN=SPO4+2
      IPC=SPO7+81
      ISUM=0
      IONE=MSS
      IHALF=SPO6+67
      IHOLD=SPO8+105
      ITERM=SP11+108
      CALL VNEG(IFLOW,1,IFLOW,1,1)
      CALL VSADO(IWN,1,IFLOW,ISUM,1,MSS)
      CALL VAOD(IFLOW,1,IFHIGH,1,IPC,1,1)
      CALL VNEG(IFLOW,1,IFLOW,1,1)
      CALL VDIV(IPC,1,IPI,1,IPC,1,1)
      CALL VSMUL(ISUM,1,IPC,ISUM,1,MSS)
      CALL VCOS(ISUM,1,ISUM,1,MSS)
      CALL VSADD(ISUM,1,IONE,ISUM,1,MSS)
      CALL VSMUL(ISUM,1,IHALF,ISUM,1,MSS)
      CALL VNEG(IHALF,1,IHALF,1,1)
      CALL VLIM(IWN,1,IFHIGH,IHALF,IHOLD,1,MSS)
      CALL VNEG(IHALF,1,IHALF,1,1)
      CALL VSAOD(IHOLD,1,IHALF,IHOLD,1,MSS)
      CALL VNEG(IONE,1,IONE,1,1)
      CALL VMSA(ISUM,1,IHOLD,1,IONE,ISUM,1,MSS)
      CALL VNEG(IONE,1,IONE,1,1)
      CALL VLIM(IWN,1,IFLOW,IHALF,IHOLD,1,MSS)
      CALL VSADD(IHOLD,1,IHALF,IHOLD,1,MSS)
      CALL VMSA(IHOLD,1,ISUM,1,IONE,ISUM,1,MSS)
      CALL VMUL(ITERM,1,ISUM,1,ITERM,1,MSS)
      CALL VCLR(ISUM,1,MSS)
      CALL VCLR(IHOLD,1,MSS)
      ENO

```


THE INVERSE ALGORITHM

The following FORTRAN subroutine computes the subsurface topography, $h(x,y)$, of a layer of density, $d(x,y)$, with its base at $z=0$ using the gravity anomaly at $z=Z_0$ as input. This routine calls the VFC subroutines OLDAP and LPAP as well as various subroutines in HSRLIB.


```

      SUBROUTINE OLOBRG(H,FRAC,ZZERO,MS,G,OENSTY,WV,SPKE,SPKN,
      INTRIES,NEND)
C
C THIS ROUTINE CALCULATES EQUATION (12) OF SPRENKE'S (1982) THESIS.
C EQUATION (12) IS THE INVERSE ALGORITHM FOR A SINGLE LAYER OF
C KNOWN DENSITY.
C
C THE INFORMATION WHICH MUST BE PASSED IN THE SUBROUTINE ARGUMENT
C IS AS FOLLOWS BELOW..ALL ARRAYS MUST BE CAREFULLY DIMENSIONED IN
C THE MAIN PROGRAM ACCORDING TO THE SIZE PARAMETER MS.
C
C MS... SIZE OF ONE SIDE OF SQUARE MAP-GRID.
C MS IS LIMITED TO 64 AT PRESENT DUE TO CORE LIMITS IN THE AP.
C
C H(MS,MS)...SUBSURFACE TOPOGRAPHY TO BE DETERMINED BY THIS ROUTINE.
C
C FRAC....FRACTION OF GRAVITY ANOMALY DUE ONLY TO INVERSION SURFACE.
C FRAC(MS,MS) IS A K-SPACE ARRAY AND IS GIVEN BY EQUATION(9) OF SPRENKE (1982).
C FOR A SINGLE LAYER, SET FRAC(I,J)=1 FOR ALL I AND J.
C
C ZZERO...DEPTH TO ORIGIN IN KM
C
C G(MS,MS)...GRAVITY ANOMALY TO BE INVERTEO IN MGAL.
C
C OENSTY(MS,MS)...DENSITY VALUES FOR THE INVERSION LAYER IN GM/CC.
C
C WV(MS,MS)...WORKSPACE TO BE OCCUPIED BY WAVENUMBERS.
C
C SPKE, SPKN....SAMPLE INTERVALS PER KM EAST AND NORTH.
C
C NTRIES...NUMBER OF ITERATIONS TO BE ATTEMPTED...PROGRAM WILL AUTOMATICALLY
C TERMINATE WHEN DIVERGENCE OCCURS, OR WHEN THE RMS CRITERIA FOR CONVERGENCE
C IS ACCOMPLISHED.
C
C NEND...NUMBER OF TERMS IN EACH SUMMATION....TEN IS GENERALLY MORE THAN ENOUGH.
C
C
C
C SPECIFICATIONS

```



```

C
    DIMENSION H(MS,MS)
    DIMENSION WV(MS,MS),G(MS,MS),OENSTY(MS,MS)
    DIMENSION FRAC(MS,MS)
    REAL NV(30),NF(30),METER,MONE,ERROR(21)
C
C COMPUTE ADDRESSES OF VARIABLES IN AP
    MSS=MS*MS
    SPO2=2*MSS
    SPO3=3*MSS
    SPO4=4*MSS
    SPO5=5*MSS
    SPO6=6*MSS
    SPO7=7*MSS
    SPO8=8*MSS
    SPO9=9*MSS
    SP10=10*MSS
    SP11=11*MSS
    IONE=MSS
    IZERO=MSS+1
    IH=SPO2+2
    IOEN=SPO3+2
    IWN=SPO4+2
    INF=SPO5+2
    INV=SPO6+32
    IZZ=SPO6+62
    IPIG=SPO6+63
    IHALF=SPO6+67
    IG=SPO6+69
    ISCALE=SPO7+69
    IMETER=SPO7+79
    IPI=SPO7+82
    ITWO=SPO7+83
    IERROR=SPO7+84
    IFRAC=SPO9+105
    IMONE=SP10+106
    IFLOW=SP10+107
    IFHIGH=SP10+108
C AT THIS POINT, PROGRAM PAUSES TO ALLOW INPUT OF FILTER PARAMETERS.
C THE HIGH CUT FILTER MUST BE SPECIFIED IN UNITS OF CYCLES PER DATA INTERVAL.
C
C THE LOW CUT IS AUTOMATICALLY SET AT 0.75 OF THE HIGH CUT.
C
    WRITE(6,103)
103    FORMAT(' INPUT HICUT')
    READ(5,106) FHIGH
106    FORMAT(F10.4)
    FLOW=.75 *FHIGH
105    WRITE(6,104) FLOW,FHIGH
104    FORMAT(' FILTER IS',2F10.3)
    FHIGH=FHIGH*2.*3.141592*(SPKE+SPKN)/2.
    FLOW=.75*FHIGH
C
C CALCULATE VARIOUS CONSTANTS FOR LATER TRANSFER TO THE AP.
C
C NF ARE FACTORIALS. NV ARE SIMPLY INTEGERS.
C
    ONE=1.
    ZERO=0.
    TWO=2.

```



```

    PI=3.141592
    METER=.001
    ONE=1.
    HALF=.5
    MONE=-1.
    PIG=2.*3.14159*6.67
    HALF=.5
    SCALE=1./(2.*MS*MS)
    NF(1)=1
    NV(1)=0.
    DO 3 I=1,29
    NF(I+1)=NF(I)*I
3    NV(I+1)=I
    DO 4 I=1,30
4    NF(I)=1./NF(I)
C CALL WNNU TO COMPUTE WAVENUMBERS FOR LATER TRANSFER TO THE AP.
C
    CALL WNNU(MS,SPKE,SPKN,WV)
C THE FOLLOWING TWO STATEMENTS ARE NOT USED AT PRESENT.
102    FORMAT(1X,32F5.2)
987    CONTINUE
C
C INITIALISE THE AP
C
    CALL APINIT(1,0,ISTAT)
C
C TRANSFER THE ARRAYS AND CONSTANTS INTO THE AP
C
    CALL APPUT(ONE,IONE,1,2)
    CALL APPUT(ZERO,IZERO,1,2)
    CALL APPUT(DENSTY,IDEN,MSS,2)
    CALL APPUT(WV,IWN,MSS,2)
    CALL APPUT(NF,INF,30,2)
    CALL APPUT(NV,INV,30,2)
    CALL APPUT(ZZERO,IZZ,1,2)
    CALL APPUT(PIG,IPIG,1,2)
    CALL APPUT(HALF,IHALF,1,2)
    CALL APPUT(FRAC,IFRAC,MSS,2)
    CALL APPUT(METER,IMETER,1,2)
    CALL APPUT(G,IG,MSS,2)
    CALL APPUT(SCALE,ISCALE,1,2)
    CALL APPUT(FLOW,IFLOW,1,2)
    CALL APPUT(FHIGH,IFHIGH,1,2)
    CALL APPUT(TWO,ITWO,1,2)
    CALL APPUT(PI,IPI,1,2)
    CALL APPUT(HALF,IHALF,1,2)
C
C WAIT FOR THE DATA TRANSFER
C
    CALL APWD
C
C CALL THE VFC SUBROUTINE WHICH DOES THE WORK IN THE AP.
C
    CALL OLDAP(NTRIES,NEND,MS)
C
C WAIT FOR THE RESULTS.
C
    CALL APWR
C
C TRANSFER THE RESULTING TOPOGRAPHY AND RMS ERROR BACK INTO THE HOST

```



```
      CALL APGET(H,IH,MSS,2)
      CALL APGET(ERROR,IERROR,21,2)
      CALL APWD
C  RELEASE THE AP
      CALL APRLSE
      WRITE(6,107)
107   FORMAT(' ITERATION      ERROR (KM) ')
      DO 108 K=1,NTRIES
      WRITE(6,109) K,ERROR(K+1)
109   FORMAT(I5,10X,F10.5)
108   CONTINUE
      RETURN
      END
```



```

"      SUBROUTINE OLDAP(NTRIES,NEND,MS)
      DEFINE OLDAP(NTRIES,NEND,MS)
        LOCAL IZZ,IPIG,IHMAX,IHMIN,IHM,IHALF,IDELG,IG,ISCALE,IGOV
        LOCAL IG1,IG2,IG3,IG4,IHMAXS,ISIGN,IGL
        LOCAL NSTART,IST,IWN,ISUM
LOCAL MSS,IH,IDEN
        LOCAL K,N,IONE,IZERO,IHH,INF,INV
        LOCAL IG11,IZO,IMETER,IZZ1,IPC,IPI,ITWO,IERROR,ID1H1,IHOLD,IFRA
LOCAL IT,ICONV,ILIM
        LOCAL KERR
        LOCAL KKK
LOCAL IPC1,IMONE,IFLOW,IFHIGH,ITERM,NV,NF
        MSS=MS*MS
        SPO2=2*MSS
        SPO3=3*MSS
        SPO4=4*MSS
        SPO5=5*MSS
        SPO6=6*MSS
        SPO7=7*MSS
        SPO8=8*MSS
        SPO9=9*MSS
        SP10=10*MSS
        SP11=11*MSS
        ISUM=0
        IONE=MSS
        IZERO=MSS+1
        IHH=MSS+2
        IH=SPO2+2
        IDEN=SPO3+2
        IWN=SPO4+2
        INF=SPO5+2
        IST=SPO5+32
        INV=SPO6+32
        IZZ=SPO6+62
        IPIG=SPO6+63
        IHMAX=SPO6+64
        IHMIN=SPO6+65
        IHM=SPO6+66
        IHALF=SPO6+67
        IDELG=SPO6+68
        IG=SPO6+69
        ISCALE=SPO7+69
        IGOV=SPO7+70
        IG1=SPO7+71
        IG2=SPO7+72
        IG3=SPO7+73
        IG4=SPO7+74
        IHMAXS=SPO7+75
        IG11=SPO7+76
        ISIGN=SPO7+77
        IZO=SPO7+78
        IMETER=SPO7+79
        IZZ1=SPO7+80
        IPC=SPO7+81
        IPI=SPO7+82
        ITWO=SPO7+83
        IERROR=SPO7+84
        ID1H1=SPO7+105
        IHOLD=SPO8+105

```



```

IFRAC=SPO9+105
IPC1=SP10+105
IMONE=SP10+106
IFLOW=SP10+107
IFHIGH=SP10+108
ITERM=SP11+108
KERR=IERROR
CALL RFFT2D(IG,MS,MS,1)
CALL VCLR(ISUM,1,MSS)
CALL VCLR(IHOLO,1,MSS)
CALL VCLR(IH,1,MSS)
CALL VMOV(IZZ,1,IZZ1,1,1)
CALL VSMUL(IWN,1,IZZ,ITERM,1,MSS)
CALL VEXP(ITERM,1,ITERM,1,MSS)
CALL VDIV(IPIG,1,IONE,1,IPIG,1,1)
CALL VSMUL(ITERM,1,IPIG,ITERM,1,MSS)
CALL VOIV(IPIG,1,IONE,1,IPIG,1,1)
CALL VMUL(ITERM,1,IFRAC,1,ITERM,1,MSS)
CALL VMUL(ITERM,1,IG,1,ITERM,1,MSS)
CALL VMOV(IG,1,IG11,1,1)
CALL LPAP(MS)
NSTART=2
IT=0
ODDD:  IT=IT+1
        IF IT=1 GOTO EEEE
        CALL VCLR(ISUM,1,MSS)
        N=NSTART
AAAA:  CALL VFILL(IONE,IHH,1,MSS)
        K=1
BBBB:  CALL VMUL(IHH,1,IH,1,IHH,1,MSS)
        K=K+1
        IF K<=N GOTO BBBB
        CALL VMUL(IHH,1,IOEN,1,IHH,1,MSS)
        CALL RFFT2D(IHH,MS,MS,1)
        CALL VLOG(IWN,1,IST,1,MSS)
        SPO5=INV+N
        NV=SPO5-1
        CALL VSMUL(IST,1,NV,IST,1,MSS)
        CALL VALOG(IST,1,IST,1,MSS)
        CALL VMUL(IHH,1,IST,1,IHH,1,MSS)
        NF=INF+N
        CALL VSMUL(IHH,1,NF,IHH,1,MSS)
        CALL VAOD(ISUM,1,IHH,1,ISUM,1,MSS)
        N=N+1
        IF N<=NEND GOTO AAAA
EEEE:  CALL VSUB(ISUM,1,ITERM,1,IO1H1,1,MSS)
        CALL RFFT2D(ID1H1,MS,MS,-1)
        CALL VSMUL(ID1H1,1,ISCALE,IO1H1,1,MSS)
        CALL VSUB(IZZ,1,IZZ1,1,IPC,1,1)
        CALL VDIV(IDEN,1,ID1H1,1,IH,1,MSS)
        CALL VSAOD(IH,1,IPC,IH,1,MSS)
        IF IT<3 GOTO GGGG
        CALL VSUB(IHOLO,1,IH,1,IH,1,MSS)
        CALL VSMUL(IH,1,IHALF,IH,1,MSS)
        CALL VAOD(IH,1,IHOLD,1,IH,1,MSS)
GGGG:  CALL VSUB(IHOLD,1,IH,1,IO1H1,1,MSS)
        IERROR=IERROR+1
        CALL RMSQV(IO1H1,1,IERROR,MSS)
        CALL VMOV(IH,1,IHOLD,1,MSS)
        CALL MAXV(IH,1,IHMAX,MSS)

```



```

CALL VNEG(IH,1,IH,1,MSS)
CALL MAXV(IH,1,IHMIN,MSS)
CALL VNEG(IHMIN,1,IHMIN,1,1)
CALL VNEG(IH,1,IH,1,MSS)
  CALL VSUB(IHMIN,1,IHMAX,1,IHM,1,1)
  CALL VSMUL(IHM,1,IHALF,IHM,1,1)
  CALL VADD(IHM,1,IHMIN,1,IHM,1,1)
CALL VMOV(IZZ,1,IZO,1,1)
CALL VSUB(IHM,1,IZZ1,1,IZZ,1,1)
CALL VMUL(IPIG,1,IDEN,1,IDELG,1,1)
  CALL VMUL(IDELG,1,IHM,1,IDELG,1,1)
CALL VDIV(ISCALE,1,IDELG,1,IDELG,1,1)
CALL VSUB(IDELG,1,IG1,1,IG,1,1)
CALL VSUB(IZO,1,IZZ,1,IPC,1,1)
CALL VSMUL(IWN,1,IPC,ID1H1,1,MSS)
CALL VEXP(ID1H1,1,ID1H1,1,MSS)
  CALL VMUL(ITERM,1,ID1H1,1,ITERM,1,MSS)
CALL VDIV(IPIG,1,IG,1,ITERM,1,1)
CALL VNEG(IHM,1,IHM,1,1)
CALL VSADD(IH,1,IHM,IH,1,MSS)
CALL VNEG(IHM,1,IHM,1,1)
  SPO3=IERROR-1
  SPO1=IERROR
  SPOO=SPO3
  CALL MDCOM
  ICONV=SP15
  SPO4=IERROR
  SPO3=IMETER
  SPO1=SPO4
  SPOO=SPO3
  CALL MDCOM
  ILIM=SP15
"  CALL APWR
"  KKK=IERROR-1
"  CALL APGET(OLDERR,KKK,1,2)
"  CALL APGET(ERROR,IERROR,1,2)
"  CALL APWD
"  ICONV=0
"  IF((OLDERR-ERROR).GT.0.) ICONV=1
"  ILIM=0
"  IF(ERROR.LT..001) ILIM=1
  IF IT<2 GOTO DDDD
  IF ILIM=1 GOTO HHHH
  IF ICONV<>1 GOTO HHHH
  IF IT<NTRIES GOTO DDDD
HHHH: CALL VSUB(IZO,1,IZZ,1,IPC,1,1)
CALL VMUL(IPIG,1,IZO,1,IPC,1,1)
CALL VDIV(ISCALE,1,IPC,1,IPC,1,1)
CALL VNEG(IPC,1,IPC,1,1)
CALL VADD(IG,1,IPC,1,IG,1,1)
CALL RFFT2D(IG,MS,MS,-1)
CALL VSMUL(IG,1,ISCALE,IG,1,MSS)
CALL VSUB(IZZ,1,IZZ1,1,IPC,1,1)
CALL VSADD(IH,1,IPC,IH,1,MSS)
  IG1=IH
  SPO8=MS-1
  IG2=IH+SPO8
  SPO8=MSS-MS
  IG3=IH+SPO8
  SPO8=MSS-1

```



```
IG4=IH+SPO8
  CALL VADD(IG1,1,IG2,1,IGOV,1,1)
  CALL VADD(IGOV,1,IG3,1,IGOV,1,1)
  CALL VADD(IGOV,1,IG4,1,IGOV,1,1)
  CALL VMUL(IGOV,1,IHALF,1,IGOV,1,1)
  CALL VMUL(IGOV,1,IHALF,1,IGOV,1,1)
  CALL VNEG(IGOV,1,IGOV,1,1)
  CALL VSADD(IH,1,IGOV,IH,1,MSS)
  CALL VNEG(IGOV,1,IGOV,1,1)
  CALL VMOV(IZZ1,1,IZZ,1,1)
END
```


FILTER

The following FORTRAN program designs and applies a filter which reduces a 256 by 256 array to a 128 by 128 array without altering the original map area.

C THIS PRDGRAM DESIGNS AND APPLIES A DECIMATION FILTER WHICH RDUCES ARRAY G
 C TO ARRAY YWITHDUT ALTERING THE NET MAP AREA OCCUPIED BY THE ORIGINAL
 C GRID.

C
 C
 C

 DIMENSION G(256,256),W(12,12),Y(128,128)
 C CALCULATE FILTER CDEFFICIENTS

 DD 1 I=1,12
 DD 1 J=1,12
 RD=SQRT((6.5-I)*(6.5-I)+(6.5-J)*(6.5-J))
 A=2*SIN(RD*3.141592/2.)/RD
 W(I,J)=A*0.5*(1.+COS(RD*3.14159/7.))
 IF(RD.GT.7.) W(I,J)=0.0
 SUM=SUM+W(I,J)

1 CONTINUE

 DO 2 I=1,12

 DO 2 J=1,12

2 W(I,J)=W(I,J)/SUM

 WRITE(6,100) SUM

 WRITE(6,100) W

100 FORMAT(12F10.4)

 READ(2) G

 CALL FOLD2D(G,W,Y,256,12,128)

 WRITE(8) Y

 CALL PMAP(Y,128)

 STOP

 END

 SUBROUTINE FOLD2D(G,W,Y,LG,LW,LY)

 DIMENSION G(LG,LG),W(LW,LW),Y(LY,LY)

 LY=128

 LG=256

 LW=12

C 2 D CDNVOLUTION DF G AND W TD PRODUCE Y

 DO 10 I2=1,LY

 DD 10 I1=1,LY

10 Y(I1,I2)=0.

 JST2=2

 JST1=2

 IT2=1

 IT1=1

 DO 20 I2=1,LG

 WRITE(6,120) I2

 IT2=-IT2

 JST2=JST2+IT2

 DO 20 I1=1,LG

 IT1=-IT1

 JST1=JST1+IT1

 DO 20 J2=JST2,LW,2

 DO 20 J1=JST1,LW,2

 K1=(I1+J1)/2-3

 K2=(I2+J2)/2-3

 IF(K1.LT.1.OR.K1.GT.128) GO TO 20

 IF(K2.LT.1.OR.K2.GT.128) GO TO 20

 Y(K1,K2)=Y(K1,K2)+G(I1,I2)*W(J1,J2)

120 FORMAT(6I4)

20 CONTINUE

 RETURN

 END

 SUBROUTINE PMAP(TV,NPTS)


```

      DIMENSION TV(NPTS,NPTS)
      INTEGER LINE(128)
      JST=1
      JEND=128
      IF(NPTS.EQ.128) GO TO 11
      OO 23 JST=1,129,128
      WRITE(7,119)
119      FORMAT(1H1)
      JEND=JST+127
11      OO 21 II=1,NPTS,5
      IE=II+4
      IF(IE.GT.NPTS) IE=NPTS
      OO 21 III=II,IE,2
      OO 22 JJ=JST,JEND
      J=JJ
      IF(JJ.GT.128) J=JJ-128
      LINE(J)=-TV(III,JJ)/(-500./3280.)
      IF(LINE(J).LT.0) LINE(J)=9
      IF(LINE(J).GT.9) LINE(J)=LINE(J)-10
      IF(LINE(J).GT.9) LINE(J)=0
22      CONTINUE
      WRITE(7,113) LINE
113      FORMAT(1H9,128I1)
21      CONTINUE
      IF(NPTS.EQ.128) RETURN
23      CONTINUE
      RETURN
      END

```


LAMBERT CONIC CONFORMAL PROJECTION

The following FORTRAN routine performs a Lambert Conic Conformal Projection of latitude-longitude values onto a flat plane. Program LAMBERT computes the necessary parameters depending on the desired standard parallels. Subroutine LTOG converts the latitude-longitude location to the projected x-y location on a flat plane.


```

C      PROGRAM LAMBERT
C      COMPUTES PARAMETERS FOR LAMBERT PROJECTION
C      FOR STANDARD PARALLELS AT LATITUDES AL1 AND AL2.
      READ(5,100) AL1,AL2
100    FORMAT(F10.5)
      AL1=6.28318*AL1/360.
      AL2=6.28318*AL2/360.
      AA=ALOG10(COS(AL1))
      BB=+ALOG10(COS(AL2))
      A=6378206.4
      B=6356583.8
      ETA=SQRT((A*A-B*B)/(A*A))
      EN1=A/SQRT(1.-ETA*ETA*SIN(AL1)*SIN(AL1))
      EN2=A/SQRT(1.-ETA*ETA*SIN(AL1)*SIN(AL2))
      SINM=SIN((1./3600.)*6.28318/360.)
      A1=1./(EN1*SINM)
      A2=1./(EN2*SINM)
      ETF1=(1.+ETA*SIN(AL1))/(1.-ETA*SIN(AL1))
      ETF2=(1.+ETA*SIN(AL2))/(1.-ETA*SIN(AL2))
      CC=ALOG10(A1)
      DD=ALOG10(A2)
      TANZ1=TAN((1.57079-AL1)/2.)*(ETF1**(ETA/2.))
      TANZ2=TAN((1.57079-AL2)/2.)*(ETF2**(ETA/2.))
      EE=ALOG10(TANZ1)
      FF=ALOG10(TANZ2)
      EL=(AA-BB-CC+DD)/(EE-FF)
      AK1=COS(AL1)/(A1*SINM*EL*TANZ1**EL)
      AK2=COS(AL2)/(A2*SINM*EL*TANZ2**EL)
      WRITE(6,101) EL,AK1,AK2
101    FORMAT(1X,F10.5,2E12.5)
      STOP
      END
      SUBROUTINE LTOG(ALAT,ALONG,X,Y)
C GENUINE LAMBERT CONFORMAL CONIC PROJECTION
C USES VALUES OF EL AND AK COMPUTED BY PROGRAM LAMBERT
C FOR STANDARD LATS OF 49 AND 77 DEGREES N.
      AK=2248
      EL=.9014
      ETA=.006768
      ALAT=ALAT*.0174
      S=ETA*SIN(ALAT)
      ETF=(1.+S)/(1.-S)
      TANZ=TAN((1.57079-ALAT)/2.)*(ETF**.0033834)
      R=AK*TANZ**EL
      THETA=6.28318*(108-ALONG)/360.
      THETA=THETA*EL
      Y=R*SIN(THETA)+178.
      X=934.742-R*COS(THETA)
      X=356-X
      X=10*X+220.
      Y=10*Y+220.
      ALAT=ALAT/.0174
      RETURN
      END

```


B30360